

# DEVELOPMENT OF A SIMPLE TRIAXIAL TEST FOR CHARACTERISING BITUMEN STABILISED MATERIALS

By

**William Kapya Mulusa** BEng, REng

Thesis submitted in partial fulfilment of the requirements for the degree of

**MASTER OF SCIENCE IN ENGINEERING (MScEng)**

In the

Faculty of Engineering, Department of Civil Engineering

University of Stellenbosch



Supervisor:

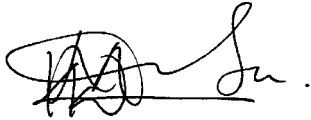
**Professor KIM J. JENKINS**

SANRAL Chair of Pavement Engineering at Stellenbosch University

January, 2009

## DECLARATION

By submitting this thesis electronically, I declare that the entirety of the work contained therein is my own, original work, that I am the owner of the copyright thereof (unless to the extent explicitly otherwise stated) and that I have not previously in its entirety or in part submitted it for obtaining any qualification.

A handwritten signature in black ink, appearing to read 'W. K. Mulusa', with a horizontal line underneath the name.

Signature:

William K. Mulusa

Date: 25<sup>th</sup> February, 2009

*'It's unbelievable what is achievable when one takes a step of faith,  
determination and belief in his own abilities to succeed'*

Inspirational quote by William K. Mulusa.

## SUMMARY

The need for a more reliable testing procedure for the characterisation and Quality Assurance/Control of Bitumen Stabilised Materials (BSMs), besides UCS and ITS testing, has long been recognised by the roads industry. In fact, at CAPSA 2004 and CAPSA 2007, discussions of improved test methods for granular materials, i.e. possible replacement tests for CBR procedures, were conducted in workshops. Triaxial testing for the evaluation of shear parameters is widely recognised as a reliable method of measuring these critical performance properties of granular and Bitumen Stabilised Materials (BSMs). However, the triaxial test in its current state as a research test has little chance of extensive use by practitioners and commercial laboratories, because of complexity, cost and time issues. Major adaptations to the research triaxial test are necessary, before this useful test can have a chance of being accepted by road practitioners.

The main aim of this study is to investigate possibilities of developing a simple, affordable, reliable and robust test for characterizing granular and bitumen stabilized materials thus linking test outcome with in-situ performance. This is achieved through the innovative design and manufacture of a prototype triaxial cell capable of accommodating 150 mm diameter by 300 mm deep specimens. The cell is simpler than the research (geotechnical) triaxial cell and the operational protocols have been streamlined, thereby reducing the time and steps required in assembling specimens and testing them.

In order to ensure the development of an appropriate triaxial cell for industry, a survey was conducted aimed at investigating currently available facilities, testing capacity and resources within civil engineering laboratories in South Africa. Findings of the survey (Appendix 4) have provided guidance with regard to the nature and sophistication of any new tests to be developed. The survey highlighted some of the limitations and lack of sophistication of the current loading frames used for CBR and UCS testing such as lack of electronic LVDTs, limited overhead space, limited loading capacity and others. Most laboratories would need to invest in new loading facilities to carry out triaxial tests.

A review of the test procedure for monotonic triaxial test showed that two main factors contribute to the complexity of the research (geotechnical) triaxial cell namely, time taken to assemble the specimen accurately in the cell and secondly the inherent design of the cell which makes it water and/or air tight at relatively high pressures.

The design of the Simple Triaxial Test, therefore, was aimed at overcoming the drawbacks of research triaxial test e.g. fitting a membrane to each specimen to be tested, through considerable simplification by means of a new structure design and procedure of assembly of specimen into the cell. The advantage of addressing these issues would be reduction in the number of steps required in

the test procedure and therefore reduction in testing time. The design of the cell particularly was preceded by a conceptualization process that involved investigation of numerous options. Concepts such as the bottle, encapsulated-tube, bottle and sandwich concepts were considered and given reality checks. In addition, available triaxial procedures of a similar nature e.g. Texas Triaxial, were evaluated and analyzed.

Ultimately, with some trials and innovation, a design was developed for a simple triaxial cell comprising a steel casing with a latex tube which is then introduced around the specimen sitting on a base plate. It is based on the 'tube concept' in which the specimen acts like a 'rim' and the cell acts like a 'tyre' providing confinement to the triaxial specimens for testing, within the tube. This approach eliminates the use of O-rings and membranes for the specimen and tie-rods for the triaxial cell, thus reducing testing time considerably. The overall dimensions of the cell are 244 mm diameter by 372 mm height (Appendix 5).

The cell was manufactured at Stellenbosch University Civil Engineering workshop and preliminary tests were conducted under this study. Parallel tests were also conducted with the Research Triaxial Test setup at Stellenbosch University in order to determine if preliminary results obtained with the Simple Triaxial Test setup were comparable therefore providing a means of validating the data.

Results of analysis of variance (ANOVA) show that variability between Simple Triaxial Test (STT) and Research Triaxial Test (RTT) results is less significant whilst that within samples of STT and RTT results is quite significant. Comparisons also show that good correlation were obtained from Reclaimed Asphalt Pavement (RAP) Hornfels + 3.3 % Emulsion + 0 % Cement mix and mixes with the G2 base course aggregate whilst completely different correlation was obtained from RAP + 3.3 % Emulsion + 1% Cement. It is evident however that the differences observed stem from material variability i.e. random variability to one degree or the other and not to the STT apparatus. It is recommended for future research that more STT versus RTT testing be done especially on a mix with known mechanical properties when compacted to a specified dry density, e.g. graded crushed stone (G1) compacted to 100% mod. AASHTO.

In summary, a locally made, low cost, relatively durable triaxial cell with relatively easy and quick specimen assembly procedures has been developed. It is now possible to perform triaxial tests on 150 mm diameter by 300 mm high specimen relatively easily and quickly. However, the challenge of validating results obtained, as well as improving the manufacture process of its main component, the tube, still remains.

## OPSOMMING

Die behoefte aan 'n meer betroubare toetsprosedure vir die karakterisering en QA/QC van Bitumen Gestabiliseerde materiale (BSMe), behalwe EDS en ITS toetse, word reeds lank deur die pad industrie erken. Daar was reeds by CAPSA 2004 en CAPSA 2007 besprekings van verbeterde toetsmetodes vir granulêre materiale, o.a. moontlike vervangingstoetse vir KDV prosedures, in die vorm van werkwinkels gedoen. Die kans dat die drie-assige toets, in sy huidige toestand as 'n navorsingstoets, algemeen deur praktiserende en kommersiële laboratoriums gebruik sal word, is baie skraal, as gevolg van kompleksiteit, koste en tyd aspekte. Om hierdie redes word grootskaalse aanpassings aan die navorsings drie-assige toets benodig voordat so 'n nuttige toets 'n kans staan om deur padpraktisyns aanvaar gaan word.

Die hoofdoel van hierdie studie is om die moontlikhede van 'n eenvoudige, ekonomiese, betroubare en robuuste toets vir karakterisering van granulêre en bitumen gestabiliseerde materiale te ondersoek, gekoppel aan werkverrigting. Dit sal bereik word deur die innoverende ontwerp en vervaardiging van 'n prototipe drie-assige sel wat 150mm x 300mm hoë monsters kan akkommodeer. Die sel is eenvoudiger as die navorsings (geotegnies) drie-assige sel en die operasionele protokol is verfyn, waardeur die stappe en tyd wat benodig word om die monsters te monteer en te toets, verminder.

Om te verseker dat 'n geskikte drie-assige sel vir die industrie ontwerp word, is 'n projek geloods om die huidige beskikbare fasiliteite te ondersoek, om kapasiteit te toets, asook fasiliteite binne siviele ingenieurswese laboratoria in Suid-Afrika. Bevindinge uit die ondersoek (sien Aangangsel 4 van hierdie verslag) het rigting gegee met betrekking tot die tipe en ingewikkeldheid van enige nuwe toetse wat ontwikkel is. Die ondersoek het sommige van die beperkinge en gebrek aan verfyning van die huidige lasrame wat gebruik word vir KDV en EDS toetse, bv. gebrek aan elektroniese LVDTs, beperkte oorhoofse spasie, onvoldoende laskapasiteit, ens. beklemtoon. Die meeste laboratoria sal in nuwe lasrame moet belê om sodoende drie-assige toetse te kan uitvoer.

'n Oorsig van die toetsprosedure vir monotoniese drie-assige toets/e, het gewys dat daar twee belangrike faktore is wat bydra tot die kompleksiteit van die navorsings (geotegniese) drie-assige sel, nl. die tyd wat dit neem om die monster akkuraat in die sel te monteer, en tweedens, die inherente ontwerp van die sel, wat dit water- en lugdig teen relatief hoë druk maak.

Die ontwerp van die Eenvoudige Drie-assige Toets was dus gemik om die tekortkomings van navorsings drie-assige toets te oorkom, bv. om 'n membraan om elke toetsmonster te plaas, deur aansienlike vereenvoudiging d.m.v. 'n nuwe struktuurontwerp en prosedure van montering van die monster in die sel. Die voordeel om hierdie uitdagings aan te spreek sou wees die vermindering van die aantal stappe wat in die toets benodig word en dus 'n vermindering in die toetstyd. Die ontwerp van die sel was spesifiek voorgegaan deur 'n konsepsualiseringsproses wat 'n ondersoek na

verskillende opsies ingesluit het. Konsepte soos die bottel, “ombullende” buis, bottel en “sandwich” konsep, was oorweeg en is aan realiteitstoetse onderwerp. Om hierby aan te sluit was dit nodig om soortgelyke huidige beskikbare drie-assige prosedures, bv. Texas Drie-assige apparaat, te evalueer en die voor- en nadele te analiseer.

Met 'n paar toetslopiëe en innovasie, was 'n ontwerp uiteindelik ontwikkel vir 'n eenvoudige drie-assige sel, wat bestaan uit 'n staal omhulsel met 'n lateks buis wat dan om die monsters, wat op die basisplaat staan, gemonteer word. Dit is gebaseer op die “buis konsep” waarin die monster soos 'n velling optree en die sel soos 'n buiteband – hierdeur voorsien dit “confinement” aan die drie-assige monsters vir toetse binne die buis. Hierdie benadering elimineer die gebruik van O-ringe en membrane vir die monster en “tie-rods” vir die drie-assige sel, dus word die toetsperiode aansienlik verminder. Die algehele dimensies van die sel is 244 mm omtrek x 372 mm hoogte (Aanhangsel 5)

Die sel is vervaardig by die Siviele Ingenieurswese Werkswinkel van die Universiteit van Stellenbosch en voorlopige toetse was onder hierdie studie gedoen. Paralleltoetse was ook met die Navorsing drie-assige opstelling by die Universiteit van Stellenbosch gedoen om vas te stel of voorlopige resultate met die eenvoudige drie-assige toetsopstelling vergelykbaar was, en dus 'n manier voorsien om data te bevestig.

Vergelykings het bewys dat goeie korrelasie verkry was vanaf een mengsel (RAP + Emulsie + 0%C) en 'n heeltemal verskillende korrelasie vanaf 'n ander mengsel (RAP + Emulsie = 1%C). Dit is dus duidelik dat die verskil wat waargeneem was, spruit uit variasies in die meganiese eienskappe van die monsters a.g.v. vermeende variasies in monster voorbereiding, en variasies aan die RAP (Hornfels) mineraal aggregate wat gebruik was. Daar word dus aanbeveel dat, vir die doel van die korrelasie, verdere toetse uitgevoer word op 'n mengsel met bekende meganiese eienskappe en wat gekompakteer is tot 'n spesifieke droë digtheid, bv. gegradeerde vergruisde klip (G1) gekompakteer tot 100% Gew. AASHTO.

Gevolgtrekking: 'n tuisgemaakte, lae koste, relatief duursame drie-assige sel met relatief maklik en vinnige monster montering prosedure is ontwikkel. Dit is nou moontlik om drie-assige toetse op 150mm Ø by 300mm hoë monsters relatief maklik en vinnig uit te voer. Dit is egter steeds 'n uitdaging om die resultate verkry geldig te verklaar, en om die vervaardiging van die hoofkomponent, die buis, te verbeter

## ACKNOWLEDGEMENTS

I would like to express my sincere gratitude and appreciation to the under listed persons and institutions:

- First and foremost the Lord God Almighty for making all things possible, giving me strength, good health and ability to complete the work.
- Prof. Kim Jonathan Jenkins, for mentoring, good guidance and counsel. Furthermore for facilitating financial support. I am greatly indebted to Prof Jenkins for the opportunity given to me to take up such a significant task on the TGx Project. The pressure endured on this project is the reason for the timely completion of this study.
- Special thanks to all lecturers involved in my studies, Prof André A.A. Molenaar from Delft University, Prof Christo Bester, Prof Chris Brown, Prof Fred Hugo, Dr Marius de wet, Mr Johann Engelbrecht and practising engineers who complemented lecturers' efforts in moulding us into better engineers. The wealth of experience and knowledge they shared with us is invaluable.
- Many thanks to Prof D. G. Nel of Statistical Consultancy Unit at Stellenbosch University for assisting with statistical analysis and for the shared knowledge on statistics.
- SABITA and Gauteng Department of Transport and Public works South Africa, for sponsoring this research work.
- My wife Bwalya for the support, love and encouragement. My son Kine and daughter Sante for cheering me all the way despite having to be without Dad for long hours. My father and mother Mr & Mrs John T. Mulusa for being there, encouraging me and always assuring me of their prayers.
- Ulli and Heide Lehmann of Stellenbosch Baptist Church for the spiritual support and helping me and my family settle down in Stellenbosch.
- Messer's BCHOD & Partners Consulting Engineers Zambia for their support.
- Workshop personnel Dion Viljoen, assisted by Louis Fredericks, for their tireless effort in machining the simple triaxial cell.
- Members of the TGx Research team, Lucas Ebels, Elias Twangira, Percy Moloto and Rex Kelfkens for the interaction and knowledge shared.

- The laboratory technicians Gavin Williams and Colin Isaacs, for helping with material preparation and general assistance with experimental work
- Janine Myburgh, Alett Slabbert and Amanda de Wet for kind and tireless assistance.
- Course mates and friends too numerous to mention, I thank you all for the interaction.

# Table of Contents

SUMMARY .....	i
OPSOMMING .....	iii
ACKNOWLEDGEMENTS.....	v
Table of Contents.....	vii
List of Tables .....	xi
List of Figures.....	xii
Definitions of Terms.....	xvi
List of Abbreviations.....	xviii
List of Symbols .....	xix
1. INTRODUCTION .....	1
1.1. General Introduction .....	1
1.2. Background .....	1
1.3. Rationale.....	2
1.4. Project Main Aim.....	3
1.5. Project Main Objectives .....	3
1.6. Project Scope .....	3
1.7. Study Outline.....	3
2. LITERATURE STUDY OF BITUMEN STABILISED MATERIALS .....	5
2.1. Introduction.....	5
2.2. Stabilising with bitumen emulsion .....	6
2.2.1. Brief history of bitumen emulsion.....	6
2.2.2. Bitumen emulsion technology .....	7
2.2.3. Manufacture of bitumen emulsion .....	10
2.2.4. Stability levels of bitumen emulsion.....	11
2.2.5. Setting (or breaking) of bitumen emulsion.....	12
2.2.6. Working with bitumen emulsion .....	13
2.2.6.1. Mix design .....	13
2.2.6.2. Formulation and handling .....	14
2.2.6.3. Total Fluid Content (TFC) and density .....	14
2.2.6.4. Curing .....	15
2.3. Stabilising with foamed bitumen .....	16
2.3.1. What is foamed bitumen?.....	16
2.3.2. Characterisation of foamed bitumen.....	17
2.3.3. Factors influencing foamed bitumen properties .....	18
2.3.3.1. Water addition .....	18
2.3.3.2. Bitumen type and source .....	18
2.3.3.3. Temperature and pressure .....	19

2.3.3.4.	Additives .....	19
2.3.4.	Suitability of material for foamed bitumen .....	19
2.3.5.	Working with foamed bitumen .....	20
2.4.	Application in cold recycling .....	22
2.4.1.	Cold recycling methods .....	23
2.5.	Comparison between stabilising agents .....	24
2.6.	UCS and ITS Tests .....	25
2.7.	Summary.....	26
	References .....	27
3.	LITERATURE STUDY ON TRIAXIAL TESTING .....	29
3.1.	General introduction.....	29
3.2.	Triaxial testing .....	29
3.2.1.	Introduction.....	29
3.2.2.	Principles of triaxial testing .....	31
3.2.3.	Types of triaxial tests .....	33
3.2.3.1.	Monotonic triaxial test .....	33
3.2.3.2.	Short duration dynamic loading triaxial test .....	34
3.2.3.3.	Long duration dynamic loading triaxial test .....	34
3.2.4.	Standard triaxial test apparatus .....	34
3.2.4.1.	Triaxial cell .....	35
3.2.4.2.	Testing system .....	36
3.2.4.3.	Measuring devices.....	36
3.2.4.4.	Specimen size .....	37
3.3.	Application of triaxial data .....	37
3.3.1.	Material Classification .....	37
3.3.2.	Other material properties .....	40
3.3.3.	Pavement design, modelling and performance prediction.....	41
3.4.	Quality Control/Assurance .....	44
3.5.	Current state of the art .....	46
3.5.1.	The K-Mould .....	46
3.5.2.	Rapid Triaxial Test (RaTT) .....	46
3.5.3.	Simple Performance Test (SPT).....	47
3.5.4.	Summary.....	49
3.6.	Conclusion.....	49
	References .....	51
4.	METHODOLOGY.....	53
4.1.	Introduction.....	53
4.2.	Civil engineering laboratory survey.....	53

4.3.	Design approach .....	53
4.4.	Conceptualisation.....	54
4.4.1.	The tube concept.....	54
4.4.2.	Other concepts .....	55
4.4.2.1.	The bottle concept .....	55
4.4.2.2.	The bottle and sandwich concept .....	56
4.4.2.3.	Encapsulated tube concept .....	57
4.5.	The break through .....	57
4.5.1.	Trials.....	57
4.5.2.	Latex membrane drum and tube making .....	59
4.5.2.1.	Latex membrane drum design .....	59
4.5.2.2.	Tube making process .....	59
4.6.	The simple triaxial cell design .....	60
4.6.1.	Design aim .....	60
4.6.2.	Design and modelling.....	60
4.7.	Manufacture of the simple triaxial cell .....	61
4.8.	Assembly of parts .....	62
4.9.	Closure.....	62
5.	EXPERIMENTAL PROGRAM .....	63
5.1.	Introduction.....	63
5.2.	Materials and specimen preparation .....	63
5.2.1.	Mineral aggregates .....	63
5.2.1.1.	Hornfels (RAP).....	63
5.2.1.2.	Base-course aggregate (G2) .....	64
5.2.2.	Binder .....	67
5.2.3.	Moisture content and mixing process.....	68
5.2.4.	Compaction .....	68
5.2.5.	Curing .....	72
5.2.5.1.	BSM-emulsion mixes .....	72
5.2.5.2.	G2 material mixes .....	72
5.3.	Simple triaxial test (STT) equipment and procedure .....	72
5.3.1.	Triaxial cell .....	72
5.3.2.	Testing system .....	72
5.3.3.	Test procedure .....	73
5.3.4.	Calculation.....	76
5.4.	Research triaxial test (RTT) equipment and procedure .....	77
5.4.1.	Calculation.....	78
5.5.	Closure.....	78

6.	TEST RESULTS AND FINDINGS.....	79
6.1.	Test specimens.....	79
6.1.1.	Specimen characteristics for STT.....	79
6.1.2.	Specimen characteristics for RTT .....	80
6.2.	Triaxial test results.....	81
6.2.1.	STT results .....	81
6.2.2.	RTT results.....	84
6.3.	Closure.....	88
7.	ANALYSIS AND INTERPRETATION OF RESULTS.....	89
7.1.	STT vs RTT results on Hornfels + 3.3% Emulsion+0% Cement mix .....	89
7.1.1.	Discussion .....	91
7.2.	STT vs RTT results on Hornfels + 3.3% Emulsion+1% Cement mix .....	92
7.2.1.	Discussion .....	98
7.3.	STT vs RTT results on G2 + 0% Cement mix .....	98
7.3.1.	Discussion .....	101
7.4.	STT vs RTT results on G2 + 1% Cement mix .....	101
7.4.1.	Material Classification .....	104
7.4.2.	Example calculation.....	105
7.4.3.	Discussion .....	105
7.5.	Analysis of variance (ANOVA) .....	106
7.5.1.	Introduction.....	106
7.5.2.	ANOVA Calculation .....	106
7.5.3.	ANOVA results where applied stress at failure (kPa) is the response variable .....	108
7.5.4.	ANOVA results where major principal stress at failure is the response variable.....	110
7.5.5.	ANOVA results where tangent modulus is the response variable.....	112
7.6.	Closure.....	114
8.	CONCLUSIONS AND RECOMMENDATIONS.....	116
8.1.	Conclusions .....	116
8.1.1.	Advantages .....	116
8.1.2.	Disadvantages .....	118
8.2.	Recommendations.....	119
8.3.	Closure.....	119
	References .....	119
	Appendices	

## List of Tables

Table 1: Bitumen emulsion type/aggregate type compatibility (Wirtgen, 2004) .....	9
Table 2: Comparison of stabilising agents .....	24
Table 3: Types of stress – deformation tests (Rodriguez et al, 1988) .....	30
Table 4: Shear properties of granular materials (Theyse et al, 1996).....	39
Table 5: Summary of comparisons of test set-ups .....	49
Table 6: Summary of comparison of different triaxial tests .....	49
Table 7: Grading constitutions per 12 kg sample.....	63
Table 8: Testing matrix for Hornfels (RAP) .....	64
Table 9: Grading constitutions per 13.5 kg sample.....	66
Table 10: Testing matrix for G2 material .....	67
Table 11: Summary of OMC and MDD of blends.....	68
Table 12: BSM-emulsion specimens for STT.....	79
Table 13: G2 material specimens for STT .....	79
Table 14: BSM-emulsion specimens for RTT .....	80
Table 15: G2 specimens for RTT .....	80
Table 16: Summary of STT results on 3.3% Emulsion + 0% Cement mix .....	81
Table 17: Summary of STT results on 3.3% Emulsion + 1% Cement mix .....	82
Table 18: Summary of STT results on G2 + 0% Cement mix .....	83
Table 19: Summary of STT results on G2+1% Cement mix .....	83
Table 20: Summary of RTT results on 3.3% Emulsion + 0% Cement mix .....	84
Table 21: Summary of RTT results on 3.3% Emulsion + 1% Cement mix .....	85
Table 22: Summary of RTT results on G2 + 0% Cement mix .....	86
Table 23: Summary of RTT results on G2 + 1% Cement mix .....	87
Table 24: Summary of material properties from STT and RTT on Hornfels (RAP) + Emulsion + 0% Cement mix .....	91
Table 25: Summary of material properties from STT and RTT on Hornfels (RAP) + Emulsion + 1% Cement mix .....	98
Table 26: Summary of material properties from STT and RTT on G2 + 0% Cement mix.....	101
Table 27: Summary of material properties from STT and RTT on G2 + 1% Cement mix.....	104
Table 28: BSM material classification system (Jooste, et al 2007).....	105
Table 29: Summary frequency table for STT (same as for RTT) .....	107
Table 30: Target summary frequency table.....	108
Table 31: Repeated measures ANOVA table with $\sigma_{a,f}$ as DV_1 .....	108
Table 32: Repeated measures ANOVA table with $\sigma_{1,f}$ as DV_1.....	110
Table 33: Repeated measured ANOVA table with $E_{tan}$ as DV_1 .....	112
Table 35: Summary of comparison between STT and RTT .....	117

## List of Figures

Figure 1: Type of emulsions (Akzo Nobel 2000) .....	7
Figure 2: Particle size distribution of bitumen emulsion droplets (Akzo Nobel, 2000) .....	8
Figure 3: Strong electrostatic attraction between aggregate and bitumen droplet .....	9
Figure 4: Mechanical dispersion of bitumen in water (after Louw, 2006).....	10
Figure 5: Colloid mill for bitumen emulsion production (After Louw, 2006).....	10
Figure 6: Stability levels of bitumen emulsion (Louw, 2006).....	11
Figure 7: Fluid consideration for stabilisation with bitumen emulsion (Wirtgen, 2004) .....	15
Figure 8: Schematic nozzle for foamed bitumen production (Wirtgen, 2004).....	17
Figure 9: Characteristics of foamed bitumen (Wirtgen, 2004) .....	17
Figure 10: Relationship between foaming properties (Wirgen, 2002) .....	18
Figure 11: Gradation limits for foamed bitumen treatment (Wirtgen, 2002) .....	20
Figure 12: Schematic CIPR process with foam (Wirtgen, 2004) .....	23
Figure 13: UCS set up (Malubila, 2005) .....	25
Figure 14: ITS set up (Malubila, 2005) .....	25
Figure 15: Principle of triaxial test .....	31
Figure 16: Stress scenario at particle level .....	31
Figure 17: Schematic representation of triaxial test results .....	32
Figure 18: Mohr-Coulomb plots of monotonic triaxial tests (Jenkins, 2008) .....	33
Figure 19: Schematic representation of triaxial equipment (Molenaar, 2005) .....	35
Figure 20: Specimen size .....	37
Figure 21: Texas triaxial cell (Crockford et al, 2002).....	38
Figure 22: Chart for classification subgrade and flexible base material (UWP, 2004).....	39
Figure 23: Schematic stress-strain diagram showing Tangent and Secant Modulus, Maximum Stress and Strain at Failure.....	40
Figure 24: $M_r$ - $\theta$ Model of Resilient Modulus for coarse grained granular materials (Jenkins, 2008)....	43
Figure 25: Typical permanent deformation triaxial test result for granular materials (Jenkins, 2008)	44
Figure 26: Typical permanent deformation model (Jenkins, 2008).....	44
Figure 27: K-Mould apparatus (Dynatest, 2008) .....	46
Figure 28: The RaTT Cell (Crockford et al 2002) .....	47
Figure 29: Simple Performance Tester (IPC Global, 2008).....	48
Figure 30: Illustration of tube concept.....	54
Figure 31: Torus - shape of common tube (Wikipedia, 2007) .....	55
Figure 32: Elliptical tube (Wikipedia, 2007) .....	55
Figure 33: Sketch of the bottle concept .....	56
Figure 34: Sketch of the bottle and sandwich concept .....	56
Figure 35: Encapsulated tube concept .....	57
Figure 36: Valve fitted on membrane .....	58

Figure 37: Top view of trial set-up .....	58
Figure 38: All round confinement .....	58
Figure 39: Trial cell pressure testing.....	58
Figure 40: Membrane making .....	60
Figure 41: Produced membrane (700x320) .....	60
Figure 42: Valve fitted on tube.....	60
Figure 43: STT tube .....	60
Figure 44: STT 3-D models.....	61
Figure 45: Steel case machining.....	61
Figure 46: STT components.....	62
Figure 47: Assembled STT cell .....	62
Figure 48: Grading curve for Hornfels (RAP) mineral aggregates relative to suitable limits for the BSMs.....	64
Figure 49: G2 grading curve relative to Lafarge grading and TRH 14 limits.....	65
Figure 50: Adjusted G2 grading .....	65
Figure 51: Mod AASHTO Density - Moisture relationship for G2 material.....	66
Figure 52: Bitumen emulsion (ANiB SS-60) .....	67
Figure 53: Laboratory vertical shaft drum mixer .....	68
Figure 54: Mounted vibratory Bosch Hammer (Kelfkens, 2008) .....	69
Figure 55: Marking off Zero line (Kelfkens, 2008) .....	70
Figure 56: Indicating target dry density - 100 % Mod AASHTO (Kelfkens, 2008).....	71
Figure 57: Photos showing extension collar attachment on mould .....	71
Figure 58: Height extension of the RTT .....	77
Figure 59: Bolting of the pipe extension .....	77
Figure 60: Applied stress vs strain for STT on 3.3% Emulsion + 0% Cement mix.....	81
Figure 61: Applied stress vs strain for STT on 3.3% Emulsion + 1% Cement mix.....	82
Figure 62: Applied stress vs strain for STT on G2+0% Cement .....	83
Figure 63: Applied stress vs strain for STT on G2+ 1% Cement mix.....	84
Figure 64: Applied stress vs strain for RTT on 3.3% Emulsion + 0% Cement mix .....	85
Figure 65: Applied stress vs strain for RTT on 3.3% Emulsion + 1% Cement mix .....	86
Figure 66: Applied stress vs strain for RTT on G2 + 0% Cement mix.....	87
Figure 67: Applied stress vs strain for RTT on G2 + 1% Cement mix.....	88
Figure 68: Stress vs Strain diagram on Hornfels (RAP) + 3.3% Emulsion + 0% Cement mix by STT and RTT tested at 50 kPa .....	89
Figure 69: Stress vs Strain diagram on Hornfels (RAP) + 3.3% Emulsion + 0% Cement mix by STT and RTT tested at 100 kPa .....	89
Figure 70: Stress vs Strain diagram on Hornfels (RAP) + 3.3% Emulsion + 0% Cement mix by STT and RTT tested at 200 kPa .....	90

Figure 71: Mohr-Coulomb diagram on Hornfels (RAP) + 3.3% Emulsion + 0% Cement using STT ...	90
Figure 72: Mohr-Coulomb diagram on Hornfels (RAP) + 3.3% Emulsion + 0% Cement using RTT ...	91
Figure 73: Stress vs Strain diagram on Hornfels (RAP) + 3.3% Emulsion + 1% Cement by STT and RTT at 50 kPa.....	92
Figure 74: Stress vs Strain diagram on Hornfels (RAP) + 3.3% Emulsion + 1% Cement by STT and RTT at 100 kPa (repeat 1) .....	92
Figure 75: Stress vs Strain on Hornfels (RAP) + 3.3% Emulsion + 1% Cement by STT and RTT at 100 kPa (repeat 2) .....	93
Figure 76: Stress vs Strain on Hornfels (RAP) + 3.3% Emulsion + 1% Cement by STT and RTT at 100 kPa (repeat 3) .....	93
Figure 77: Stress vs Strain on Hornfels (RAP) + 3.3% Emulsion + 1% Cement by STT and RTT at 200 kPa .....	94
Figure 78: $\sigma_{1,f}$ versus $\sigma_3$ from STT on Hornfels (RAP)+3.3% Emulsion+1% Cement mix .....	94
Figure 79: $\sigma_{1,f}$ versus $\sigma_3$ from RTT on Hornfels (RAP)+3.3% Emulsion+1% Cement mix.....	95
Figure 80: $\sigma_{1,f}$ versus $\sigma_3$ from STT (adjusted) .....	95
Figure 81: Mohr-Coulomb diagram on Hornfels (RAP) + 3.3% Emulsion + 1% Cement using STT ...	96
Figure 82: $\sigma_{1,f}$ versus $\sigma_3$ from RTT (adjusted).....	97
Figure 83: Mohr-Coulomb diagram on Hornfels (RAP) + 3.3% Emulsion + 1% Cement mix using RTT .....	97
Figure 84: Stress vs Strain on G2 + 0% Cement mix by STT and RTT at 50 kPa .....	99
Figure 85: Stress vs Strain on G2 + 0% Cement mix by STT and RTT at 100 kPa .....	99
Figure 86: Stress vs Strain on G2 + 0% Cement mix by STT and RTT at 200 kPa .....	99
Figure 87: Mohr-Coulomb diagram on G2 + 0% Cement mix using STT .....	100
Figure 88: Mohr-Coulomb diagram on G2 + 0% Cement mix using RTT .....	100
Figure 89: Stress vs Strain on G2 + 1% Cement mix by STT and RTT .....	102
Figure 90: Stress vs Strain on G2 + 1% Cement mix by STT and RTT at 100 kPa .....	102
Figure 91: Stress vs Strain on G2 + 1% cement mix by STT and RTT at 200 kPa.....	103
Figure 92: Mohr-Coulomb diagram on G2 + 1% Cement mix, using STT .....	103
Figure 93: Mohr-Coulomb diagram on G2 + 1% Cement mix, using RTT .....	104
Figure 94: Variation of applied stress at failure between STT and RTT .....	109
Figure 95: Variation within STT and RTT samples .....	109
Figure 96: Principal stress at failure vs confining pressure for STT and RTT .....	110
Figure 97: Variation of major principal stress at failure between STT and RTT .....	111
Figure 98: Variation of major principal stress at failure within STT and RTT.....	111
Figure 99: Principal stress at failure vs confining pressure for STT and RTT.....	112
Figure 100: Variation of tangent modulus between STT and RTT .....	113
Figure 101: Variation of tangent modulus within STT and RTT.....	113
Figure 102: Variation of principal stress at failure within STT and RTT.....	114

Figure 103: Variation of tangent modulus within STT and RTT ..... 114  
Figure 104: Weight comparison of STT against RTT ..... 117

## Definitions of Terms

<b>Term</b>	<b>Definition</b>
Anti-foaming agent	A chemical additive that inhibits the foaming of foam
Axial Load	Sum of the applied load and the dead load (including the weight of the top disk) applied along the vertical axis of the test specimen.
Binder	General term for asphalt cement which includes bitumen, coal tar or polymer modified bitumens.
Bitumen	Dark viscous liquid, residue of the vacuum distillation of petroleum. Predominately aliphatic or cycloaliphatic. Known as asphalt in the USA.
Bitumen Emulsion, Anionic	Bitumen Emulsion produced using negatively charged emulsifiers such as fatty acids, containing droplets of bitumen carrying a negative charge.
Bitumen Emulsion, Cationic	Bitumen Emulsion produced using positively charged emulsifiers such as amines, containing droplets of bitumen carrying a positive charge.
BSM-emulsion	Bitumen Stabilised Material with emulsion as binder.
BSM-foam	Bitumen Stabilised Material with foamed bitumen as binder.
Cohesion	This is a force tending to hold particles of the soil together as a solid mass without the application of any external forces. This force is mainly due to molecular attraction and surface tension of water between the grains. It is also influenced by grain size, density and water content.
Conditioning	Placing of specimens and loading plates overnight in a climate chamber at 25 °C the day before testing.
Curing	This is the maintenance of appropriate moisture and temperature conditions to permit hydration or pozzolanic reaction. Curing of BSMs is characterised by loss of water (primarily through evaporation) and increase in stiffness and strength of a compacted mix.
Electrophoresis	Electrophoresis is a separation technique that is based on the mobility of ions in an electric field. Positively charged ions migrate towards a negative electrode and negatively-charged ions migrate toward a positive electrode.
Expansion Ratio	The expansion ratio is the ratio between the maximum expanded volume of the foamed bitumen and the original volume of the base bitumen (before foaming).
Foaming agent	A chemical additive which when present in small amounts facilitates the formation of a foam
Gradation	A general term used to describe the aggregate composition of a bituminous mix. Exact percentages of all aggregate essential to a good mix are controlled through the percentage of each size aggregate used.

Half-life Time	The period (in seconds) during which the volume of the foamed bitumen has reduced to half of its maximum expanded volume (at $t = 0$ ).
Internal angle of friction or friction angle	This is the resistance to movement between sliding particles of the material. The resistance is as result of friction force between sliding particles caused by particle interlock. It is measured in degrees and is influence by grain size and shape, soil structure, density and water.
Inverted Emulsion	Water-in-oil emulsion prepared from cut back bitumen and typically used for priming or tack coats.
Latex	Natural or synthetic dispersion of rubber particles in water. Usually based on natural rubber, SBR, polychloroprene or acrylates.
Major Principal Stress	Is the axial load divided by the average area of the cylindrical specimen.
Maximum Density	This is highest density of a material at a specific compactive effort achieved when compaction is carried out on the material at various moisture/fluid contents.
Minor principal stress (lateral pressure)	Pressure supplied by air in the triaxial cell, applied in a radial or horizontal direction.
Mohr's Diagram	A graphical construction of combined principal stresses in static equilibrium.
Mohr's Failure Circle	A stress circle constructed from major and minor principal stresses of the specimen at failure.
Mohr-Coulomb Failure Envelope	A common tangent to a series of failure circles constructed from different pairs of principal stresses required to fail the material. The envelope is related to the mechanical characteristics of the material $C$ and $\phi$ .
Outlier	A statistical term of an observation that is numerically distant from the rest of the data.
Surfactants	Wetting agents that lower the surface tension of a liquid, allowing easier spreading, and lower the interfacial tension between two liquids.
Triaxial Test	A test in which stresses are measured in three mutually perpendicular directions. It is used to determine the shear strength of aggregate samples enclosed in a pressurised chamber (Triaxial cell), which subjects the sample to three compressive stresses at right angles to each other. The vertical compressive stress is then increased in excess of horizontal (lateral) stress untill sample fails in shear or strain to such an extent that excessive deformation results.

## List of Abbreviations

<b>Abbreviations</b>	<b>Description</b>
AASHTO	American Association of Highway and Transportation Officials
ANiB SS-60	Stable grade, Slow setting Anionic Bitumen Emulsion with 60% Residual Binder
BSM	Bitumen Stabilised Materials
CBR	Californian Bearing Ratio
CIPR	Cold In-Place Recycling
CSIR	Council for Scientific and Industrial Research; based in Pretoria, South Africa
HMA	Hot Mix Asphalt
ITS	Indirect Tensile Strength
kPa	Kilo Pascal = $10^3$ Pascals = 1000 N/m <sup>2</sup>
LVDT	Linear Variable Differential Transducer
MC	Moisture Content
MDD	Maximum Dry Density
MPa	Mega Pascal = $10^6$ Pascals = 1 N/mm <sup>2</sup>
MTS	Material Testing System
OMC	Optimum Moisture Content
OTFC	Optimum Total Fluid Content
QA/QC	Quality Assurance/Quality Control
RAP	Reclaimed Asphalt Pavement
RTT	Research Triaxial Test at Stellenbosch University
SABITA	South African Bitumen Association
SANS	South African National Standards, formerly SABS, South African Bureau of Standards
STT	Simple Triaxial Test Developed in this Study
SU	Stellenbosch University

TFC	Total Fluid Content
TG2	Technical Guideline No. 2, published by the Asphalt Academy (2002)
TMH	Technical Methods for Highways
UCS	Unconfined Compressive Stress

## List of Symbols

Symbol	Description
C	Cohesion (kPa)
E	Elastic stiffness (kPa)
$E_{sec}$	Secant Modulus (MPa)
$E_{tan}$	Tangent Modulus (MPa)
$M_r$	Resilient Modulus or Elastic Stiffness (MPa)
N	Amount or number of load repetitions
$\epsilon$	Strain
$\epsilon_f$	Strain at failure
$\epsilon_p$	Permanent strain
$\theta$	Bulk stress (kPa) = $\sigma_1 + \sigma_2 + \sigma_3$
$\rho_b$	Bulk density (kg/m <sup>3</sup> )
$\rho_d$	Dry density (kg/m <sup>3</sup> )
$\sigma$	Normal Stress (kPa)
$\sigma_1, \sigma_2, \sigma_3$	Major, intermediate and minor principal stress. All in kPa
$\sigma_{1,f}$	Major principal stress at failure (kPa)
$\sigma_{a,f}$	Applied stress at failure (kPa)
$\sigma_d$	Deviator stress (kPa) = $\sigma_1 - \sigma_3$
$\sigma_{dw}$	Dead weight pressure (kPa)
$\tau$	Shear stress (kPa)
$\phi$	Angle of internal friction (°)

# **1. INTRODUCTION**

## **1.1. General Introduction**

One of the global challenges facing the road construction industry and South Africa in particular, is the need to incorporate the principles of soil mechanics more effectively in design, construction and evaluation of pavements. The continued extensive use of the CBR method has been questioned the world over by researchers over the years and therefore, the need to use more relevant parameters such as shear, resilient and plastic behaviour in design, construction and evaluation of pavements and especially in quality control/quality assurance (QC/QA), is increasingly becoming important. Despite real achievements through high quality research locally and internationally in terms of the mechanical characterization of road materials and development of tests, there still remains a big gap between research and practice. The answer to reducing this 'gap' locally, lies in a blend of innovation and steady attention to implementing more fundamentals known to soil mechanics testing while communicating effectively between researchers and road practitioners.

The major challenge is to develop a suitable test that can be carried out by accredited commercial laboratories to reliably determine the relevant material properties. In this vein, the development of a Simple Triaxial Test (STT) therefore, represents a step towards closing of the 'gap' locally. The study will endeavour to investigate the possibilities of developing a simple, affordable, reliable and robust test for characterizing granular and bitumen stabilized materials, with a link to performance.

## **1.2. Background**

A triaxial test is a recognised method used to measure the mechanical properties such as shear, resilient and plastic behaviour of many deformable solids, especially soil, sand, clay, and other granular materials. The use of triaxial testing has its origin in geotechnical engineering. However, for pavement engineering the use of triaxial testing is less common. It is mostly limited to research projects.

Some standard triaxial test methods for pavement engineering exist internationally. There are only two institutions in South Africa that are known to undertake triaxial testing of granular road building materials, namely the Council for Scientific and Industrial Research (CSIR) and Stellenbosch University (Jenkins et al, 2007). The main reason for this situation is that the equipment for standard triaxial test, designed to accommodate granular road building material specimens of 150 mm diameter and 300 mm deep, is costly and time consuming as it is not easy to assemble specimens in the cell. For instance, the Material Testing System (MTS 810, model 318.10) and the triaxial cell or

pressure chamber used in the standard triaxial test at the University of Stellenbosch are not manufactured locally and even when imported, procedures for assembly of specimens in the triaxial cell take more time and attention to detail than would be required in a production pavement testing, especially for the QC/QA of granular and bitumen stabilized materials. Additionally, technicians required to handle and interact with instrumentation effectively, are supposed to have high skill levels with a high level of computer literacy. This therefore, generally limits the test to research applications only.

In spite of the limitations, the triaxial test remains one of the better tests available to characterize flexible pavement materials, especially granular and bitumen stabilized materials. Many of the available methods such as CBR produce “index” or “empirical” properties instead of engineering material properties. The monotonic failure triaxial test on the other hand can be used to determine the shear parameters; cohesion ( $C$ ) and angle of internal friction ( $\phi$ ) while elastic resilient stiffness behaviour (Resilient Modulus,  $M_r$ ) and permanent deformation are determined by short duration dynamic loading and long duration dynamic loading triaxial tests respectively. These parameters can be used for material classification and pavement design in combination with mechanistic-empirical design methods, linear-elastic multi layer pavement analysis using design and finite element softwares. Other applications can include use in QA/QC and performance prediction.

The triaxial approach in determining material properties is useful for a variety of reasons. One of the more important reasons for this utility is the ability to properly handle the characterization of different types of materials, including those materials with low cohesion or bonding (e.g. unbound base and subgrade materials and asphalt concrete at high temperature) or those that are anisotropic (e.g. composites). Further Crockford et al (2002) concluded that the characterizations attainable with proper conduct of this testing approach are generally considered to be more closely associated with true engineering properties than many other tests.

### **1.3. Rationale**

In QA/QC for pavement engineering, results must be available relatively rapidly, leaving no room for time consuming repeated load tests that might be needed to characterize the materials. Therefore, with ever increasing demand on projects to deliver on time and within budget, the triaxial test in its state as a research test has little chance of breaking through to road practitioners. What can be done then in order to use triaxial test as a standard to characterize granular and bitumen stabilized materials for road construction?

This study will endeavour to answer the above question.

## 1.4. Project Main Aim

The main aim of this study is to investigate possibilities of developing a simple, economical, reliable and robust test for characterizing granular and bitumen stabilized materials, linking test outcome with in-situ performance.

## 1.5. Project Main Objectives

In order to achieve the above aim, the following objectives were identified:

- To carry out a detailed analysis of what is available in the road construction industry in South Africa in terms of equipment, tests and testing procedures, especially those used to characterize granular and bitumen stabilized materials.
- To innovate, design and manufacture a prototype triaxial cell (adequate to accommodate 150 mm diameter by 300 mm deep specimen) that will be simpler than the standard (geotechnical) triaxial cell, thereby reducing the time and steps required in assembling specimen in the triaxial cell.
- Validate whether the new test procedure provides reasonable results by carrying out triaxial tests with the prototype triaxial cell and correlating these results with those obtained using a standard (research) triaxial cell.

## 1.6. Project Scope

This study is limited to the monotonic failure test type of triaxial test and therefore, determination of shear parameters; cohesion (C) and angle of internal friction ( $\phi$ ) will be the primary focus. The study does not focus on dynamically loaded triaxial tests due to expected limitations of space around the specimen, restricting the use of LVDT's on specimen; however, these types of tests can still be done by introducing cyclic loading and measuring vertical deformation over the full specimen height.

The study is also limited to modifications to the triaxial cell. Therefore, the loading and measuring devices used in this research will be those of the Research Triaxial Test (RTT) at Stellenbosch University including the hydraulic testing system (MTS 810, Model 318.10).

## 1.7. Study Outline

Chapter 2 presents the background of bitumen emulsion and foam bitumen as stabilizing agents for cold mixes. Included in this background is brief historic developments, technology, manufacture and main aspects relating to optimal utilization of these technologies. Good understanding of these

technologies is of paramount importance when dealing with BSMs and especially where it involves its main application, cold recycling.

The literature study continues in Chapter 3 focusing on the main item of this study, triaxial testing. It presents an overview on the philosophy and fundamentals of standard triaxial testing. The Chapter goes on to give a review on standard test apparatus, procedure, data collection and analysis and applications of experimental data especially in characterizing road building materials. Since the main aim of this study is to simplify the standard (research) triaxial test, the literature study has also included a review of the work done elsewhere in simplifying triaxial testing for use in both laboratory and field work.

Chapter 4 presents the research methodology employed for the development of a simple triaxial test. It includes an analysis of what is available in South Africa in terms of road material testing equipment in commercial laboratories and procedures being followed. It discusses conceptualization, design, manufacture and test procedures of the simple triaxial cell. Chapter 5 describes the experimental program for both Simple Triaxial and Research Triaxial Testing. It describes the materials and procedures used in the preparation of the specimens. Chapter 6 presents the exposition of the results and findings of both types of triaxial tests proposed in Chapter 4. Results presented in Chapter 6 are synthesized and interpreted in Chapter 7. The thesis is concluded and recommendations made in Chapter 8.

## 2. LITERATURE STUDY OF BITUMEN STABILISED MATERIALS

### 2.1. Introduction

A wide variety of stabilising agents are currently in use in the road construction industry around the world. These include chemical compounds, such as calcium chloride, long-chain polymers and sulphonated petroleum products, other proprietary products and the more conventional binding agents such as cement and bitumen. All these, aim to achieve the same objective of binding the individual aggregate particles together to increase strength and durability, improve workability and/or make material more water-resistant. Clearly, some are more effective than others on specific materials, while others have clear cost advantages, but all have a place in the road construction industry.

To the pavement engineer of today, due largely to technological advances, the use of bitumen stabilising agents applied both in an emulsion form and in a foaming state, is becoming increasingly popular. Stabilising with bitumen is a cost-effective way of improving the strength of a material whilst reducing the detrimental effects of water. Bitumen stabilisation produces a relatively flexible layer compared to the same material treated with cement. Wirtgen (2004) reports that material stabilised with bitumen and less than 1.5% (by mass) cement does not suffer from the shrinkage cracking phenomenon associated with cement treatment and may be trafficked immediately due to the initial binding (strength) of the surface particles which prevents ravelling under action of traffic.

Bitumen is a very viscous liquid that is not workable at ambient temperature. How then is it utilised as a stabilising agent? One may ask. Well, to make bitumen workable, it is subjected to any of the following processes:

- Heating (increasing the temperature);
- blending with petroleum solvents (cutback);
- emulsifying in water to form bitumen emulsion; or
- foaming (creating foamed bitumen in a temporary state of low viscosity)

The first alternative is the hot-mix asphalt process, which requires the aggregate to be preheated and dried. The second alternative includes expensive solvents that are hazardous pollutants and therefore undesirable in this day of sustainable development. The last two processes, applicable to cold mixes are the only two viable bituminous stabilising agents and form the focus of this literature study.

With clear cut environmental, economic and practical benefits, there has been an increased use of cold mixes of bitumen emulsion and foamed bitumen worldwide. This increased use however, presents the challenge of the need for more reliable testing procedures such as triaxial testing for

characterising BSMs besides the UCS and the ITS. The first step to tackling this challenge is to gain sound understanding of the material behaviour to be characterised, as such the rest of this Chapter is devoted to understanding the background, technology, manufacture, characterisation and applications of bitumen stabilising agents.

## **2.2. Stabilising with bitumen emulsion**

### **2.2.1. Brief history of bitumen emulsion**

Bitumen emulsions were originally developed to overcome the difficulties of working with hot bitumen, initially intended as sprays in dust palliative applications. In 1902 Ernest Guglielminetti, a Swiss physical doctor, established the French Anti-Dust Association for the purpose of reducing dust generation by traffic on roads along the Mediterranean shoreline of Monaco. The association promoted the coating of road surfaces with hydrocarbons. The hydrocarbons were emulsified using ammonium based soap. During 1905 the first dedicated bitumen emulsion plant was commissioned in Lutterbach, Germany, by a chemist named Emile Feigel.

During the 1920's Hugh Mackay, an English chemist, developed bitumen emulsions further and filed a patent on anionic bitumen emulsion in 1922. The trade mark was "Cold Spray" which was a few years later changed into "Cold Asphalt". This was later abbreviated into "COLAS" (Le Corroller, 2005). The use of bitumen emulsion for road works increased rapidly and within four years five countries had manufacturing plants; viz England, Germany, Denmark, Australia and India. The combined annual production of these five countries was estimated at 150,000 tons in 1926.

In South Africa, the company COLAS established the first bitumen emulsion manufacturing plant in 1928 in Bellville (Louw *et al.*, 2004). The incentive for reduction in energy consumption in the 1970's fuel crisis boosted the use of emulsions world wide in stabilisation of mineral aggregate, including mixing with damp material at ambient temperatures.

Great success has been achieved by road engineers over the past 40 years in South Africa with the technique of adding small quantities of bitumen emulsion to gravels of fair to good quality. One case worth noting occurred in 1981 (SABITA, 1999), a cracked cement-treated base (CTB) pavement on Main Road 37, near Cape Town, was rehabilitated by using a milling and recycling procedure. As part of this project, two experimental sections were built using a technique of milling and recycling half depth of the cracked CTB. On Section 1, the material was treated with a low percentage of emulsion (1.4%), while the other section (Section 2) was recompacted without any emulsion added. Heavy Vehicle Simulator (HVS) tests conducted on both sections yielded the following conclusions according to observations made by Horak et al, 1984:

- Benkelman beam deflections and radii of curvature on section 1 were respectively lower and higher than those on section 2;
- Less permanent deformation was measured in the HVS test on Section 1 (this was also reflected in DCP results, where greater bearing capacity and greater resistance to shear forces were measured); and
- The emulsion treatment of Section 1 resulted in a considerable reduction in the moisture sensitivity of the treated layer as a result of lower permeabilities and binding of fines.

Taking into account differences in treatment of the two sections above, the predicted lives for Section 1 and Section 2 were estimated to be 3 and 12 years, and between 0.8 and 3 million equivalent 80 kN axle loads respectively.

### 2.2.2. Bitumen emulsion technology

An emulsion is a dispersion of small droplets of liquid in another. It consists of two immiscible liquids, the one in the dispersed phase (small globules or droplets of 0.001 to 0.01 mm) and the other in the continuous phase. In the case of a bitumen emulsion the two fluids are bitumen and water. One can distinguish between three main types of emulsions (see Figure 1):

- Oil-in-water (O/W);
- Water-in-oil (W/O), also called inverted emulsion; and
- Multiple emulsions (W/O/W).

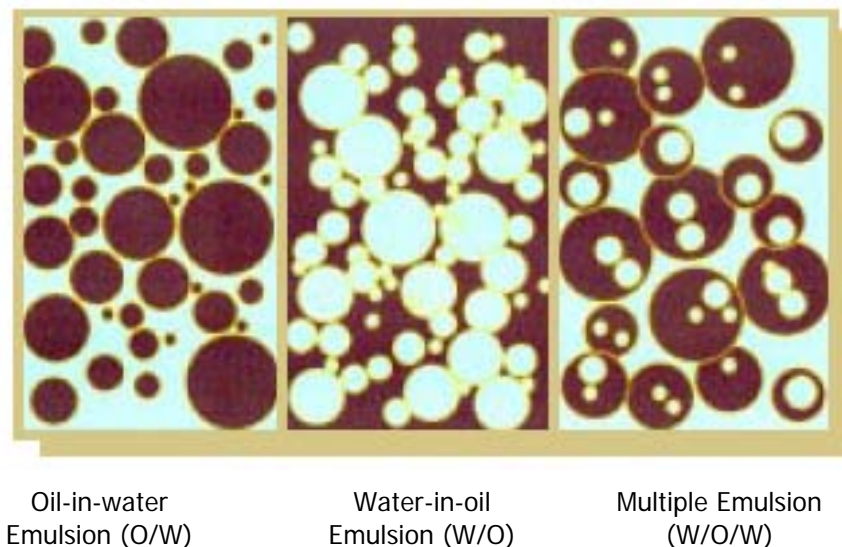


**Figure 1: Type of emulsions** (Akzo Nobel 2000)

As illustrated in Figure 1, Oil-in-water (O/W) emulsions are those in which the continuous phase is water and the disperse (droplet) phase is an 'oily' water – insoluble liquid, in this case bitumen. Water-in-oil (W/O) emulsions are those in which the continuous phase is oil and the disperse phase water. W/O emulsions are sometimes called inverted emulsions. Multiple phase emulsions can be

formed in which the dispersed droplets themselves contain smaller droplets of a third phase, usually the same liquid as the continuous phase.

Oil and water may form an emulsion if mixed but will quickly separate when mixing is stopped. To prevent this happening, a third component, the emulsifier, is introduced which prevents or retards the separation of the phases forming stable emulsions.

Bitumen emulsions are normally of the O/W type although inverted emulsions based on cut-back bitumens have special applications. There is evidence that bitumen can form multiple W/O/W emulsions. Emulsions containing from 40 to 80% bitumen are brown liquids with consistencies ranging from that of milk to heavy cream. The droplets range from 0.1 to 20 micron in diameter. Akzo Nobel (2000) shows the particle size distribution of most bitumen emulsions with the microscopic image as illustrated in Figure 2.

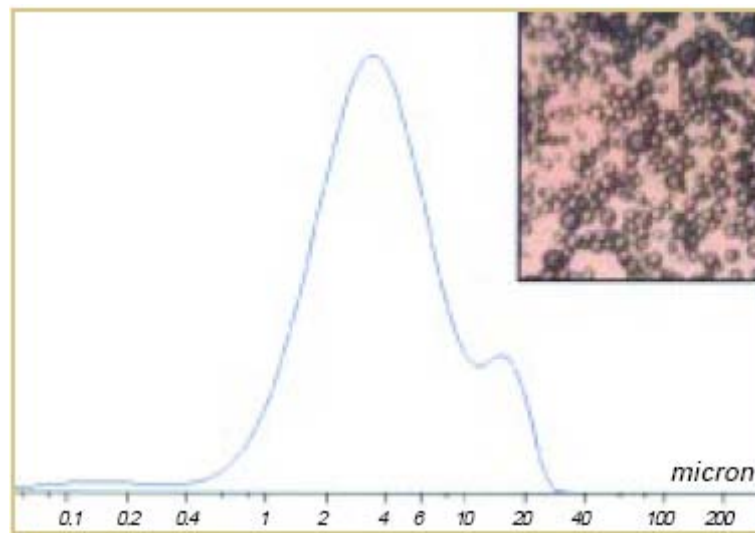


**Figure 2: Particle size distribution of bitumen emulsion droplets** (Akzo Nobel, 2000)

The bitumen emulsion used in this study for example, had a residual bitumen component of 60%, which means that 60% of the volume of emulsion was made up of bitumen dispersed in 40% of the volume of water. For most emulsions used as stabilising agents in the road industry, the percentage of bitumen ranges between 30 to 70%. However, bitumen percentages higher than 60% are not recommended for recycling as the emulsion becomes viscous and therefore more difficult to pump and coat the aggregate.

The bitumen droplets in the emulsion are either positively (cationic) or negatively (anionic) charged. This electrostatic charge is caused by the emulsifier that is active on the surface of the bitumen droplet. Anionic emulsions are produced using negatively charged emulsifiers such as fatty acids. The

emulsifiers are reacted with sodium hydroxide to release the ions into solution in a saponification process. In the case of cationic emulsion, positively charged emulsifiers such as amines are used. These emulsifiers need to be reacted with an acid, commonly hydrochloric acid, before they function.

In both anionic and cationic emulsions, the emulsifiers are chemically controlled to stabilise or speed up rate of break. Wirtgen (2004) reports that emulsions with extended break times of between 30 minutes to 1.5 hours and sometimes longer are called stable grade or slow setting and are used for stabilisation whilst those that set quickly are referred to as spray or rapid setting.

The ionic charge on the bitumen emulsion droplets has an influence on emulsion interaction with the aggregate, depending on the chemistry of the aggregate. An alkaline aggregate such as limestone and an acidic aggregate such as granite or quartzite, interacts differently with emulsion depending on emulsion's ionic charge. Cationic emulsifiers adsorb much more strongly on acidic (siliceous) minerals than anionic or nonionic emulsifiers, which explains the usefulness of cationic emulsions with acidic aggregates, as illustrated in Figure 3 below.

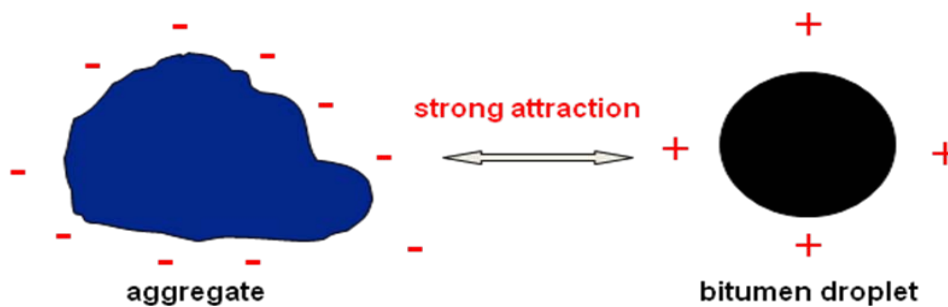


**Figure 3: Strong electrostatic attraction between aggregate and bitumen droplet**

Wirtgen (2004), further reports the influence of the interaction between bitumen emulsion and aggregate as summarised in Table 1 below.

**Table 1: Bitumen emulsion type/aggregate type compatibility** (Wirtgen, 2004)

Emulsion Type	Aggregate (Rock) Type	Trends	
		Breaking rate	Adhesion
Anionic	Acidic	Slow	Poor
Anionic	Alkaline	Medium	Good
Cationic	Acidic	Fast	Excellent
Cationic	Alkaline	Fast	Good

### 2.2.3. Manufacture of bitumen emulsion

Emulsions in principle are produced by applying energy to a mixture of two immiscible (unblendable) liquids by means of shaking, stirring, homogenising, or spray processes as illustrated in Figure 4. The amount of energy required can be significantly reduced by the adsorption of emulsifiers, the choice of which affects the particle size and charge obtained. Because the emulsion is not formed spontaneously, it is unstable and over time it will tend to revert back to the stable state of phases comprising the emulsion. Therefore, to prevent the revert back process, surface active substances (surfactants) are also added to increase the kinetic mobility of emulsions so that once formed the emulsion does not change significantly over time of storage.

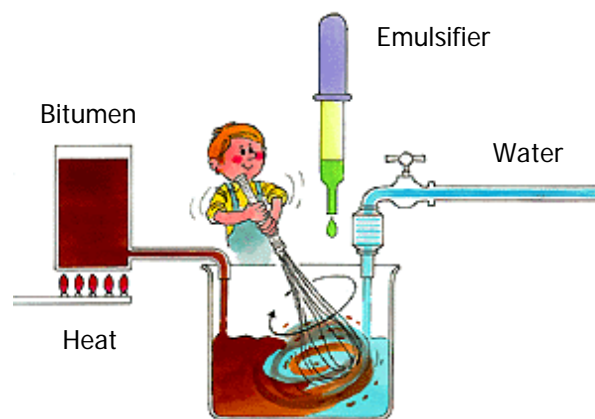


**Figure 4: Mechanical dispersion of bitumen in water** (after Louw, 2006)

Bitumen emulsions for use in stabilizing road construction materials are usually made using a colloid mill as shown in schematic diagram in Figure 5. In the colloid mill energy is applied to the system by passing the mixture of hot bitumen and water phase between a rotating disc, cone or flywheel and a stator. The rotor as well as stator may be grooved or have teeth in order to create a turbulent flow. Bitumen emulsion can be produced either in a batch or an in-line process plant.

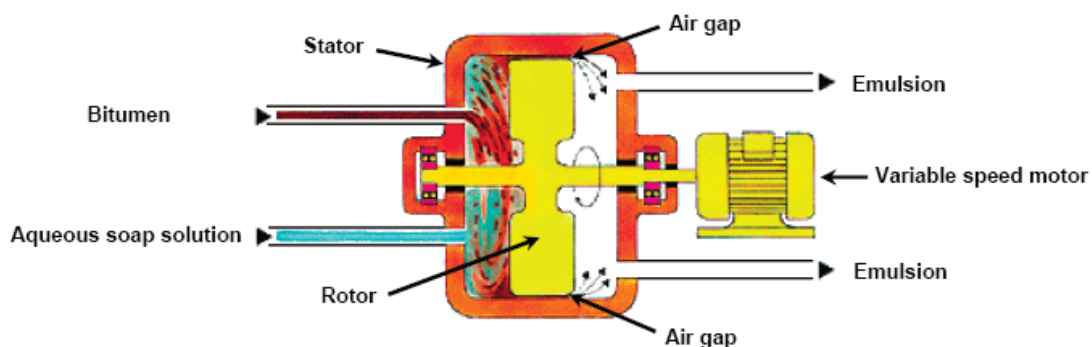


**Figure 5: Colloid mill for bitumen emulsion production** (After Louw, 2006)

The batch process involves at least two process steps namely water phase (soap) preparation and the actual emulsion production. The water phase is prepared in a tank into which heated water, emulsifier and other emulsion chemicals are metered and the solution properly mixed. In the emulsion production process the bitumen and the ready-made water phase are dosed to the colloid mill. If solvent is to be added to the bitumen then a batch tank is needed for bitumen as well, or the solvent must be dosed in-line.

In the batch plant the emulsion production itself involves only a few material flows, which allows manual process control. However, proper metering of the various components are decisive for the quality of the emulsion and automatic or semiautomatic control will make the manufacturing more efficient and reduce human error. Furthermore, the chemicals used may be hazardous as well as corrosive, which means closed dosage systems rather than open tanks and portable pumps are preferable in order to ensure safe work and environmental conditions.

In the in-line process the water heating and all material dosage are done continuously using individual dosage pumps for each material. No batch tanks are used. Instead, the water phase system must further be designed to provide sufficient reaction time for the chemicals so that adequate neutralization and solution take place before the water phase meets the bitumen. The process needs to be automatically controlled using flow meters for all material dosage except acid, which is controlled by the pH in the water phase.

#### 2.2.4. Stability levels of bitumen emulsion

Levels of bitumen emulsion stability vary from stable emulsion, flocculation, and densification to coalescence, depending on the volume fraction of the phases and on the type of emulsifier.

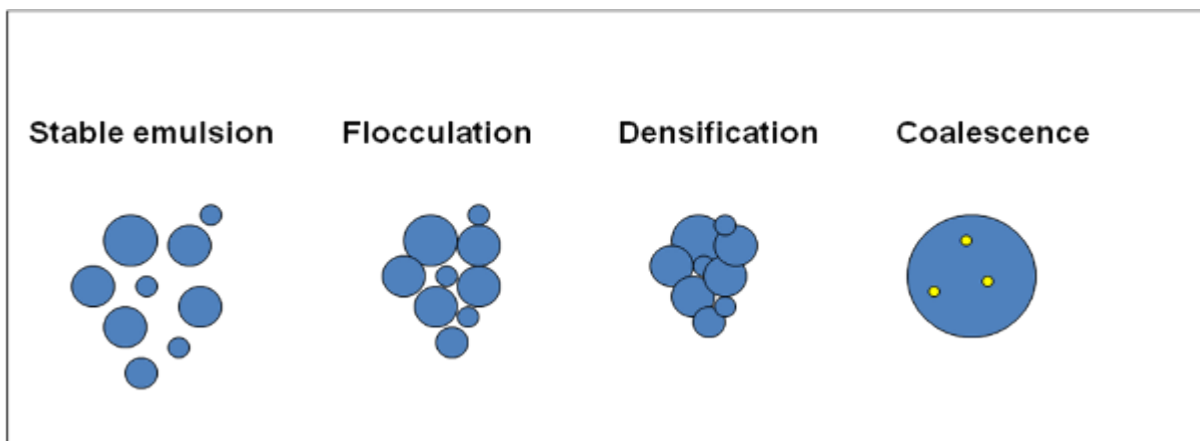


**Figure 6: Stability levels of bitumen emulsion** (Louw, 2006)

As can be seen in Figure 6, the emulsion is said to be stable when the distance between the dispersed droplets is sufficient to prevent contact or possible coalescence. Flocculation occurs when following the destabilization of the emulsifier, evaporation of the water phase or mechanical action

causes droplets to form clumps. Densification also referred to as creaming in other types of emulsion, occurs where the droplets concentrate towards the surface (or the bottom, depending on relative density of the two phases) of the mixture whilst staying separated. The final state, coalescence occurs due to close proximity of the bitumen droplets, resulting in the droplets fusing and flowing together. The coalescence of the droplets results in a continuous film of binder, with some minute water droplets initially being trapped in the coalesced layer.

Flocculation and coalescence may also be initiated by contact with minerals and are important stages in the eventual setting and curing of the emulsion explained in detail in Section 2.2.5 below.

### **2.2.5. Setting (or breaking) of bitumen emulsion**

In order for bitumen emulsion to fulfil its role as a stabilising agent for road materials, it must revert back to a continuous bitumen film. This is achieved through the process of 'breaking', which is the separation of the bitumen from the water phase and the coalescence of the bitumen droplets to produce a continuous film of bitumen on the aggregate. Excess water from the emulsion is deposited into the mix. The time lapse from mixing to when the bitumen globules separate from the water phase is referred to as breaking time.

The break process is followed by curing, which is the loss of water from the mix (primarily through evaporation) and increase in stiffness and tensile strength of the stabilised pavement layer.

As explained in Section 2.2.2 below, the speed of this setting and curing process depends on the reactivity of the emulsion, the reactivity of the aggregate and the environmental conditions such as temperature and humidity. Bitumen emulsions for road use are classified depending on their reactivity. Akzo Nobel (2000) reports that Rapid-setting emulsions set quickly in contact with clean aggregates of low surface area such as the chippings used in chipseals (surface dressings). Medium-setting emulsions set sufficiently less quickly that they can be mixed with aggregates of low surface area such as those used in open-graded mixes. Slow-setting emulsions will mix with aggregates of high surface area.

According to most of the literature reviewed, the setting of an emulsion is a complex process which is not fully understood, and more than one factor is responsible for the break. The following process steps are however understood to take place leading to breaking of the emulsion (Nobel, 2000):

#### **(i) Adsorption of the emulsifier onto the aggregate surface**

There is always free (reservoir) emulsifier present in the bitumen emulsion to take care of stability during transportation and storage of the emulsion. Once the bitumen emulsion is mixed with the aggregate, the free emulsifier adsorbs rapidly onto the aggregate surface. The rapid removal of the reservoir of stabilizing emulsifier makes the emulsion liable to coalesce leading to breaking of the

emulsion. However, this effect can also work to reduce or even reverse the surface charge on the aggregate, which can delay setting.

Figure 3 illustrates how cationic emulsifiers adsorb much more strongly on siliceous minerals than anionic or non-ionic emulsifiers, which explains the usefulness of cationic emulsions with acidic aggregates.

(ii) Movement of the emulsion drops to the aggregate surface

The droplets of bitumen in the emulsion have a small charge and move towards an aggregate surface with the opposite charge by the process called electrophoresis. When the droplets concentrate at the aggregate surface they flocculate leading to coalescence and spreading over the surface.

(iii) Changes in pH

Some aggregates like limestones or fillers like lime or cement may actually neutralize the acid in a cationic emulsion causing the pH to rise and the emulsion to be destabilized. In other cases, the aggregates may adsorb hydrogen ions leading to a less marked rise in pH, but still sufficient to destabilize the bitumen emulsion. Some soluble aggregates like limestones can provide calcium or magnesium ions to the solution which tend to neutralize the charge on anionic emulsions.

(iv) Evaporation of water

The final process step is evaporation of water. As water leaves the system by evaporation, the droplets become concentrated, leading to coalescence. Evaporation may be the main breaking mechanism for very slow-setting emulsions.

### **2.2.6. Working with bitumen emulsion**

As has been discussed in earlier sections of this Chapter, bitumen emulsions provide an alternative approach to making bitumen workable at ambient temperatures by dispersing it in water. As such emulsions can be used with cold and wet aggregates, with the final strength of the road material developing as the emulsion sets i.e. reverts to a continuous bitumen phase and water is removed. In many road construction applications emulsions provide a safer and environmental-friendly system than hot bitumen since the risks of fire, burns and emissions are avoided and the processes use less energy.

When stabilizing with bitumen emulsion it is important to note the following factors, if desired results are to be obtained:

#### **2.2.6.1. Mix design**

A proper mix design should be carried out before any stabilisation attempt is undertaken in order to assist in identifying optimal formulation, blending and production of material. Not only optimization in

terms of volumetrics and compaction characteristics is important but also consideration of engineering properties of the mix, durability and long term performance. In addition, economic considerations are paramount in the selection of mix designs for BSMs, where the binder has a significant influence on the cost for the overall material.

For stabilization with bitumen emulsion the reader can refer to published South Africa guideline, the ETB Manual (SABITA, 1999) and an international guideline, Cold Recycling Manual (Wirtgen, 2004).

#### 2.2.6.2. Formulation and handling

Emulsifier type and concentration, choice and concentration of additives determine the reactivity of the bitumen emulsion from rapid setting to slow setting. This formulation is usually tailored for a specific application since the type of material that is mixed with the emulsion has a major influence on stability (breaking time) of the emulsion. Therefore as Wirtgen (2004) notes, it is important that the manufacturer be given a representative sample of the material that is to be stabilised with details of any active filler to be added.

Handling of the bitumen emulsion including transportation, storage and pumping should be given paramount consideration as bitumen emulsion is susceptible to temperature and pressure changes. Therefore the conditions that will promote separation of the bitumen out of suspension must be clearly understood to prevent this happening on site. Similarly, the manufacturer must know prevailing conditions on site to allow for correct formulation including details of all pumps that will be used for transferring the emulsion between tankers and in case of recycling for supplying spraybar on the recycler. Labelling and storing emulsions carefully and ensuring that distribution systems are clear of residual from previous use is important. It will be disastrous on site if blending of anionic and cationic emulsions occurred, as this would result in an instantaneous break and blockage of pumps and pipes with viscous bitumen.

#### 2.2.6.3. Total Fluid Content (TFC) and density

TFC in bitumen emulsion stabilisation refers to the total quantity of fluid in the mix, including hygroscopic (in-situ) moisture, bitumen and water within the emulsion and moisture added for compaction. When working with bitumen emulsion it is important to use TFC in place of MC in defining the moisture/density relationship. Therefore, maximum density is achieved at the Optimum Total Fluid Content (OTFC), which is the combined mass of moisture and bitumen emulsion in the mix. The mass of bitumen emulsion is accounted for because both bitumen and water components of an emulsion act as a lubricant in assisting compaction.

Figure 7 (Wirtgen, 2004) below illustrates the consideration of fluids for bitumen emulsion stabilisation. It is shown that the in-situ moisture content is 2.5 % with 3.5 % bitumen emulsion applied. The material has an OTFC of 7 % under standard compaction. Additional 1.0 % of water may

be added to bring the TFC to the OTFC, alternatively additional compactive effort could be applied to achieve maximum density. Like in any moisture/density relationship of the material, if the TFC of the material approaches saturation level (as indicated by the zero air voids line in Figure 7), then hydraulic pressures will develop, making it impossible to compact the material.

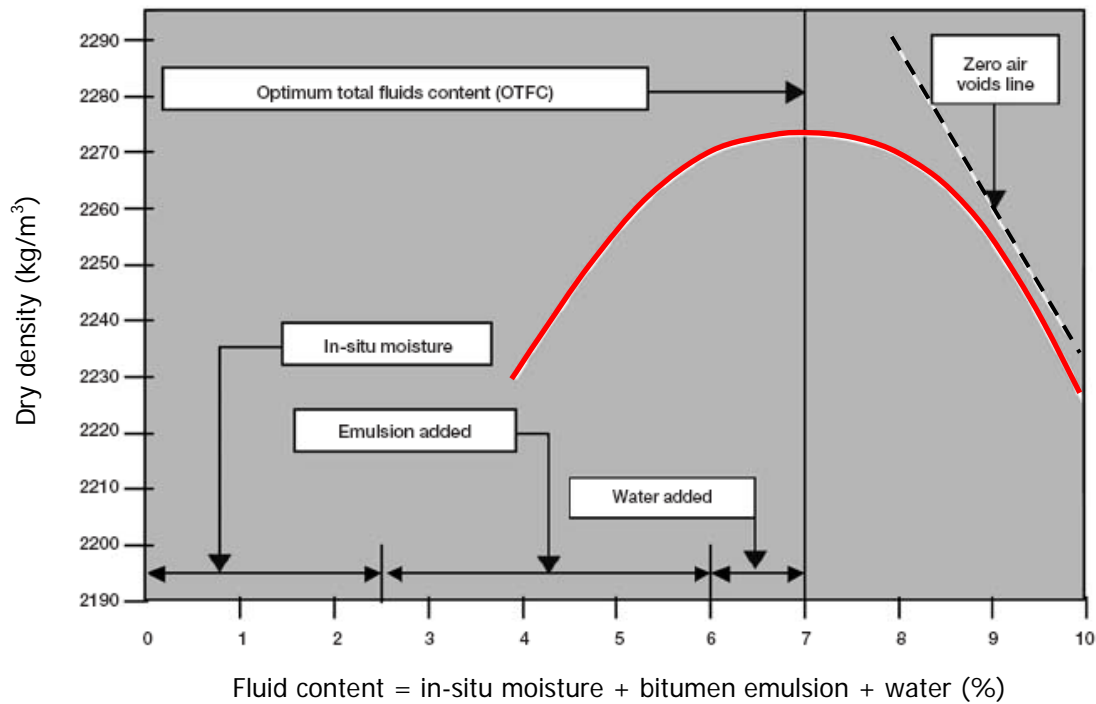


**Figure 7: Fluid consideration for stabilisation with bitumen emulsion** (Wirtgen, 2004)

Where the in-situ field moisture is high, the addition of bitumen emulsion can increase the total fluid content beyond the saturation point. Wirtgen (2004) notes that this situation cannot be addressed by reducing the amount of bitumen emulsion added as doing so will compromise the quality of the stabilized material. Neither can the addition of cement to the mix in order to adsorb the surplus moisture be considered as such a practice introduces rigidity and changes the nature of the product. The manual recommends that high in-situ moisture contents are best addressed by prepulverising the existing pavement thereby exposing the material and allowing it to dry sufficiently before stabilizing.

#### 2.2.6.4. Curing

As stated in Section 2.1, the reason for stabilizing with bitumen emulsion is that, the bitumen component of the emulsion is required to strengthen the material and reduce detrimental effects of water. The bitumen is applied through in an emulsion form since in its pure form it is not workable at ambient temperatures. Therefore, the objective of stabilizing with bitumen emulsion is realized if the emulsion breaks and dispels excess water, a process collectively known as curing.

Materials stabilized with bitumen emulsion vary in how long they take to achieve their full strength. Some materials achieve full strength within a short period of time (one month) whilst with others curing can take longer than a year. How long it takes depends on various factors including field moisture, emulsion/aggregate interaction, climate (temperature, precipitation and humidity) and voids in the mix.

Cement addition, limited to preferably 1.5 %, has a significant impact on the rate of gain of strength. This amount of cement is enough to neutralize the acid in a cationic emulsion causing the pH to rise and the emulsion to be destabilized. This reaction explains why early trafficking is accommodated on a recycled layer shortly after treatment.

## **2.3. Stabilising with foamed bitumen**

### **2.3.1. What is foamed bitumen?**

Foam generally is a substance that is formed by trapping many gas bubbles in a liquid or solid. With this general definition foam is so common that it is difficult to notice how odd it is or the physics behind its formation. It can be seen on top of sea water from the action of waves, on dishes as they are being washed, on top of glasses of fizzy drinks or beer, leavened bread is another example of solid foam; the list of examples in our daily lives is endless.

Similarly, foamed bitumen is a type of foam that is produced by adding small amount of water (approximately 2 to 3 % by weight of bitumen) to hot bitumen (160 – 180 °C) in a special purpose expansion chamber. When injected into the hot bitumen, the water evaporates abruptly thus causing explosive foaming of the bitumen in the saturated stream. The bitumen therefore, expands between 15 to 20 times its original volume (Wirtgen, 2002). The bitumen used for this process is ordinary penetration grade bitumen which is used for standard hot mix asphalt road construction applications. In this foamed state, which is a temporary state of low viscosity, bitumen is workable at ambient temperatures and in-situ moisture conditions and can easily be mixed with aggregates.

The foaming process of bitumen is dependent on the water changing state from liquid to vapour. When water particles come into contact with hot bitumen, heat energy from the bitumen is transferred to the water. Almost immediately the water temperature reaches the boiling point and changes state, thereby creating a thin-filmed bitumen bubble filled with water vapour.

The potential of using foamed bitumen as a stabilising agent was first realised over fifty years ago by Prof. Ladis Csanyi at the Engineering Experiment Station of the Iowa State University (Csanyi, 1957 and 1959). The technology was later refined by the Mobil Oil organisation that developed the first

expansion chamber for mixing water with bitumen to make foam. Several decades later in the mid-1990's, Wirtgen developed a system which injects both air and water in an expansion chamber, as shown in Figure 8. It can be seen that the nozzle includes an expansion chamber to accommodate the foaming of the bitumen before it is released into mixing chamber.

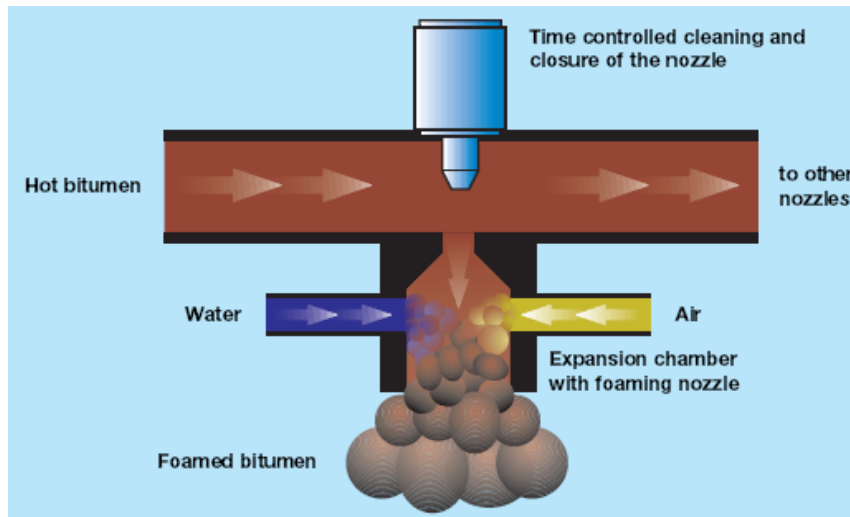


**Figure 8: Schematic nozzle for foamed bitumen production (Wirtgen, 2004)**

### 2.3.2. Characterisation of foamed bitumen

Foamed bitumen is characterised by two primary properties, namely expansion ratio which is a measure of viscosity of the foam and will determine how well it will disperse in the mix and half-life which is a measure of the stability of the foam and provides an indication of the rate of collapse of the foam. As illustrated in Figure 9, half-life is calculated as the time taken in seconds for the foam to collapse to half of its maximum volume.

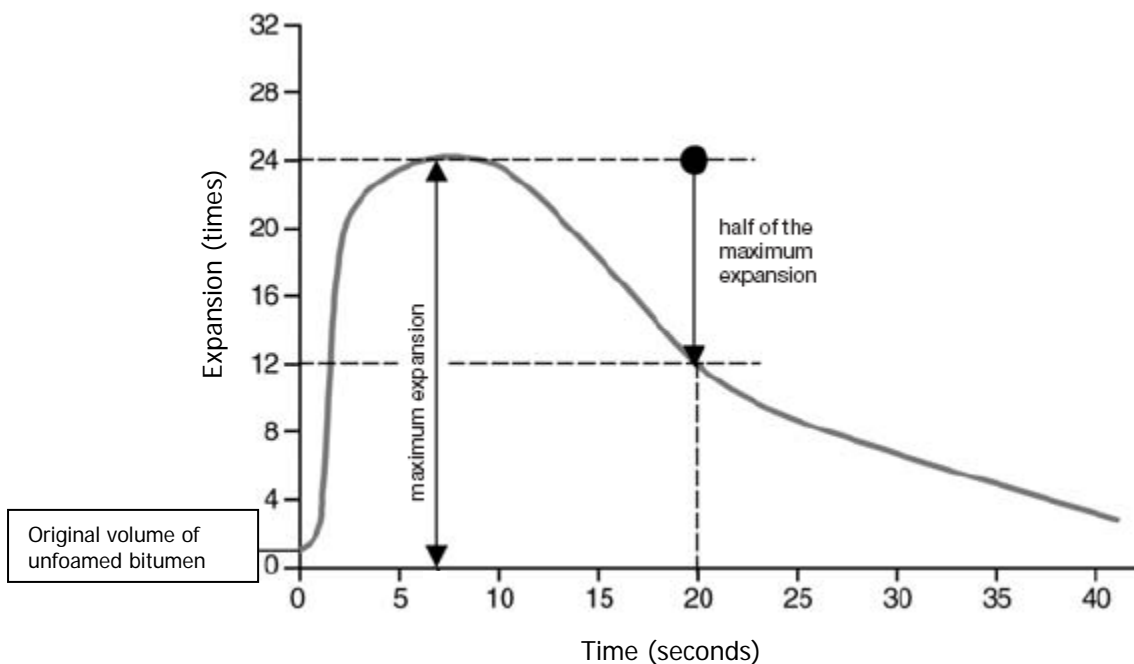


**Figure 9: Characteristics of foamed bitumen (Wirtgen, 2004)**

The two foam properties are influenced by several factors described below. However, the best foam is generally considered to be the one that optimises both expansion and half-life.

### 2.3.3. Factors influencing foamed bitumen properties

The expansion of the bitumen and the half-life time are dependent on a large number of factors, some of which are briefly described below:

#### 2.3.3.1. Water addition

Water addition has the effect of increasing the volume of foam. Therefore, the more water is added the bigger the size of bubbles created, the higher the expansion ratio. However, increasing the size of the individual bubbles reduces the film thickness of the surrounding bitumen, making it less stable and resulting in a reduction in half-life.

Figure 10 shows this inverse relationship of the expansion ratio and half-life to the amount of water that is added.

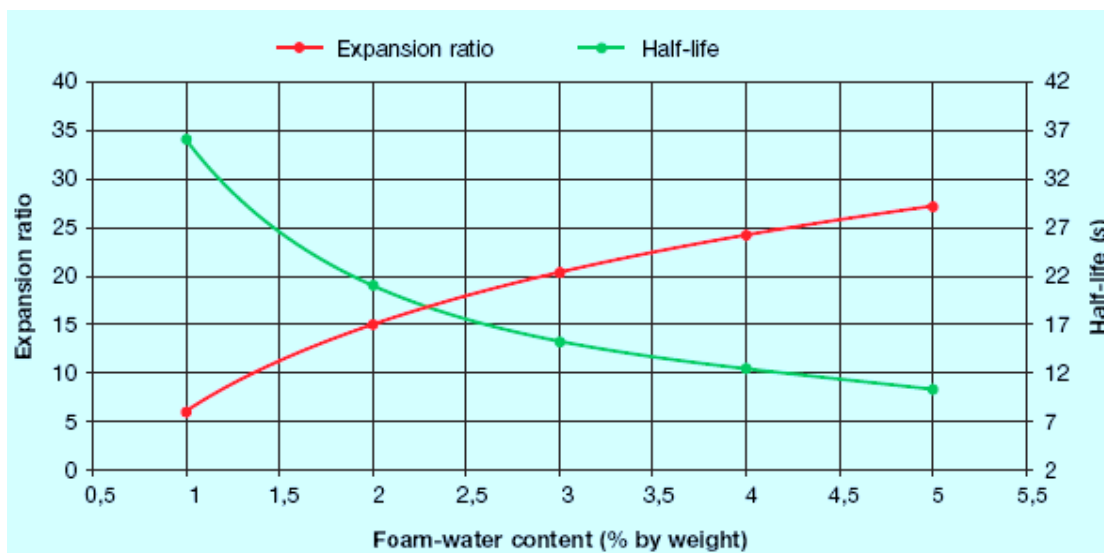


**Figure 10: Relationship between foaming properties** (Wirgen, 2002)

#### 2.3.3.2. Bitumen type and source

Bitumen with penetration values between 80 and 150 are generally used for foaming, although harder bitumens meeting minimum foaming requirements have been successfully used in the past. Wirtgen (2004) notes that for practical reasons harder bitumens should generally be avoided as they produce poorer quality foam, leading to poorer dispersion.

The manual also notes that some bitumens foam better than others because of their composition. It gives an example of the foaming properties of bitumens from Venezuela far exceeding those from other sources.

#### 2.3.3.3. Temperature and pressure

It is a property of bitumen that when temperature is increased, its viscosity reduces and the lower the viscosity the bigger the size of bubbles that will form when the water changes state in the foaming process. This change of state of water from liquid to vapour draws heat energy from bitumen therefore, the temperature of bitumen needs to be high enough (160 – 180 °C) to achieve a satisfactory product.

Bitumen and water are injected into the expansion chamber through small diameter openings. Increasing the pressure in the supply lines causes the flow through these openings to disperse (atomise). The smaller the individual particles, the larger the contact area available, thereby improving the uniformity of the foam.

#### 2.3.3.4. Additives

Foaming properties of bitumen can be influenced both negatively by anti-foaming agents and positively by foamants. Foamants are usually only required where bitumen has been treated with an anti-foaming agent (normally during refining process). Most foamants are added to the bitumen prior to heating to application temperatures and tend to be heat-sensitive, implying that their effect is short lived. To reap the benefits of adding a foamant, the bitumen must therefore be used within a few hours. However, these products are generally expensive and are usually only considered as a last resort to improving the foaming properties of a stubborn bitumen.

#### **2.3.4. Suitability of material for foamed bitumen**

One of the advantages of stabilising with foam bitumen is its suitability for treating a wide range of materials, from sands, weathered gravels to crushed stone and RAP. However, a well graded material with a satisfactory distribution from fine to large grained aggregates is recommended for the treatment with foamed bitumen. The material that is deficient in fines (percentage passing 0.075 mm sieve) will not mix well with foamed bitumen as the fines assist the bitumen to disperse.

What happens when foamed bitumen comes into contact with aggregate is that the bitumen bubbles burst into millions of tiny bitumen droplets that seek out and adhere to the fine particles, specifically the fraction smaller than 0.075 mm. The foamed mix then results in a bitumen-bound filler that acts as a mortar between the coarse particles. Wirtgen (2004) sets a minimum requirement of 5 % passing the 0.075 mm (No. 200) sieve as depicted in Figure 11.

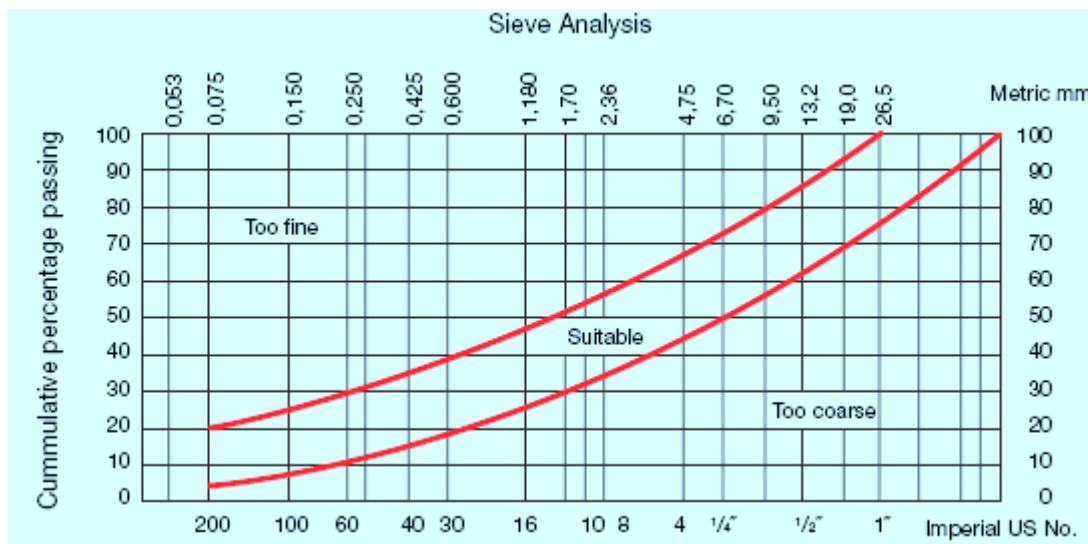


**Figure 11: Gradation limits for foamed bitumen treatment** (Wirtgen, 2002)

When treating a material that is deficient in fines with foam bitumen, improvement of the fines content by the addition of cement, lime or other such material with 100 % passing the 0.075 mm sieve is necessary. However, the use of cement in excess of 1.5 % by mass should be avoided due to the negative effect on the flexibility of the stabilised layer.

### 2.3.5. Working with foamed bitumen

As discussed in earlier sections of this Chapter, foamed bitumen is a versatile binding agent which can be used for a large variety of mineral aggregates of different types and origins. Milled asphalt, crushed tar contaminated road material or natural gravels can be treated with foamed bitumen and used for road construction or road rehabilitation. Roads consisting of unbound gravel surfaces, impairing traffic due to considerable dust development and becoming sodden with moisture during wet season, can successfully be treated with foamed bitumen.

When stabilizing with foam bitumen it is important to note the following factors, if desired results are to be obtained:

- (i) Safety - At the high temperatures (160 – 180 °C) needed for the water reaction to produce acceptable foam, bitumen is a lethal substance and if not handled properly, it can kill. Asphalt manufacturers know this too well and the same safety rules as those documented for hot mix asphalt are applicable to foam.
- (ii) Mix design - Same as working with bitumen emulsion, a proper mix design should be carried out before any stabilisation attempt is undertaken in order to optimize the foam properties. Not only optimization in terms of foam properties, volumetrics and compaction characteristics is

important but also consideration of engineering properties of the mix, durability and long term performance.

For stabilization with foamed bitumen the reader can refer to the TG2 Interim Guideline for Foamed Bitumen Treated Materials (Asphalt cademy, 2002) and an international guideline, Cold Recycling Manual (Wirtgen, 2004).

- (iii) Mixing technique – Foamed bitumen has a short life, measurable in seconds. Thus, the type of mixer used directly influences the characteristics of the mix. A variety of mixing techniques exist for manufacture of foamed mixes including twin-shaft pugmills, in-situ recyclers and free-fall mixers each of which has a different mixing energy.
- (iv) Aggregate gradation – See Section 2.3.4
- (v) Aggregate moisture – Jenkins, et al (2000) noted that the moisture in the mix is the medium for the distribution of the foamed binder. Without moisture, lumps of fine aggregate and binder are formed, and the mortar of the mix i.e. sand, filler and binder, behaves in the same manner as HMA mortar. The inclusion of moisture in the filler-foamed binder component i.e. mastic, makes it stiffer than that of HMA at the same filler-binder ratio. Although the moisture content at which the aggregate has its maximum volume (fluff point) is recommended for cold mixes i.e. 65 % to 85 % of Modified AASHTO OMC. However, this is not applicable to absorptive and half-warm mixes.
- (vi) Aggregate temperature – The temperature of the aggregate before mixing has an overwhelming influence on the equilibrium mix temperature. The transfer of the heat from the foam at just over 100 °C to the aggregate at less than 30 °C will influence the rate of collapse of the foam i.e. the rate of viscosity increase of the binder during mixing. The overall temperature of the mix will increase by less than 10 °C with the addition of the foam bitumen (Jenkins, et al 2000).

Wirtgen (2004) recommends that when the temperature of the aggregate drops below 10 °C, foamed bitumen treatment should not be considered. This recommendation is based on work done by Jenkins (2000) where he showed that the Foam Index and aggregate temperature (at the time of mixing) were important factors in the dispersion achieved.

## 2.4. Application in cold recycling

One of the major applications of bitumen stabilized materials using bitumen emulsion and foam is in cold recycling of existing pavements as a means of road rehabilitation for existing high-level facilities through to upgrading of unpaved roads. Cold recycling is increasingly becoming popular due to the following environmental, economic and practical benefits (Wirtgen, 2004):

- Environmental factors - Full use is made of the material in the existing pavement. Spoil sites do not have to be found and the volume of new material that has to be imported from quarries is minimised. This reduces scars in the countryside that are inevitable when opening quarries and borrowpits. Haulage is drastically reduced. The overall energy consumption is thus significantly reduced, as is the damaging effect of haulage vehicles on the road network.
- Quality of the recycled layer - Consistent, high quality mixing of the in-situ materials with water and stabilising agents is achieved. The addition of fluids is accurate due to micro-processor controlled pumping systems. The recycled material and additives are rigorously mixed together in the mixing chamber.
- Structural integrity - The cold recycling process produces thick bound layers that are homogeneous and do not contain weak interfaces between thinner pavement layers
- Subgrade disturbance is minimized - Disturbance of the underlying pavement structure is minimal compared to pavement rehabilitation using conventional construction equipment. Cold recycling is typically a single-pass operation. When using a track-mounted recycler, the rear tracks pass only once on the exposed underlying material. Tyre-mounted recyclers spread the material behind the machine avoiding any contact between the tyres and the exposed underlying pavement structure. (Reworking pavement material with conventional construction equipment often results in the subgrade being subjected to repeated high stress loading, causing "heaving" conditions that have to be excavated and backfilled with fresh imported material.)
- Shorter construction time - Modern recyclers are capable of high production rates that significantly reduce construction times compared to alternative rehabilitation methods. Shorter construction times reduce project costs as well as providing a largely intangible benefit for the road user in the reduced time that traffic is disrupted.
- Safety - One of the most important benefits of this process is the high level of traffic safety that can be achieved. The full recycling train can be accommodated within the width of one traffic lane. For example, on roads with two traffic lanes, recycling can be carried out along one half of

the road-width during the day and the full-road width, including the completed recycled lane, can be opened to traffic by nightfall.

- Cost effectiveness - The above benefits all combine to make cold recycling a most attractive process for pavement rehabilitation in terms of cost effectiveness.

#### 2.4.1. Cold recycling methods

Cold recycling can be achieved by two basic methods namely cold plant (in-plant) mix recycling and cold in-place recycling (CIPR). Cold plant mix recycling, the less common of the two methods, involves mixing RAP with bitumen emulsion or foamed bitumen at a central or mobile plant facility. A rejuvenating agent can also be added to improve the recycled bitumen binder viscosity and new aggregate can also be added to improve overall performance. The resulting cold mix is then typically used as a stabilized base course.

In-plant processing is generally a slightly more expensive option in terms of cost per cubic meter of material processed, primarily due to haulage costs that are absent from in-place recycling. However, where high control of input materials, quality of mixing and stockpiling capabilities are required, in-plant mix recycling remains an option that should be considered when recycling is applicable particularly where a blend of recycled and virgin materials is to be treated, and especially when treating with foamed bitumen and stockpiling for later use.

The second method, cold in-place recycling (CIPR) involves the same process of cold plant mix recycling except that it is done in-situ by a train of equipment.

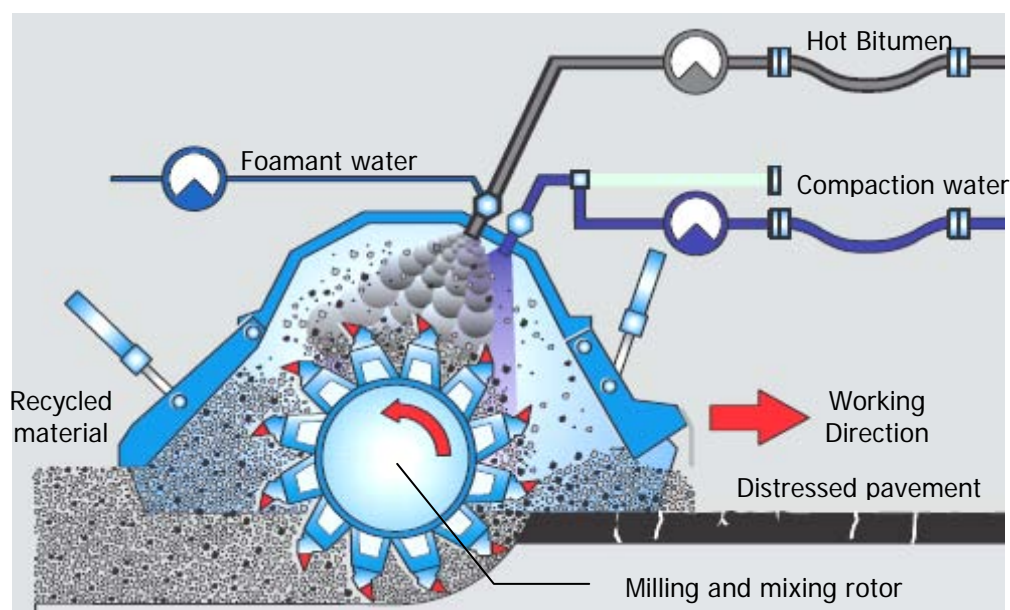


Figure 12: Schematic CIPR process with foam (Wirtgen, 2004)

CIPR can be done at either partial depth (25 - 50 mm deep) or full depth such as the entire HMA pavement depth plus a predetermined depth of the base material (NAPA, 2002). This type of recycling is becoming popular with improving technology in the capabilities of modern recyclers (see Figure 12) which can mill to depths of up to 300 mm, apply treatment and compaction water, and replace the mix in a single pass.

## 2.5. Comparison between stabilising agents

This Section presents a summarised comparison between bitumen stabilising agents discussed in this Chapter and cement, a more widely used stabilising agent.

**Table 2: Comparison of stabilising agents**

<b>Type of Stabilising Agent</b>	<b>Advantages</b>	<b>Disadvantages</b>
Cement stabilisation	<ul style="list-style-type: none"> <li>• Readily available worldwide</li> <li>• Cheaper relative to bitumen.</li> <li>• Easy application can be spread by hand.</li> <li>• Well known. Standard test methods and specification exists.</li> </ul>	<ul style="list-style-type: none"> <li>• Shrinkage cracking is unavoidable though it can be minimised.</li> <li>• Cement increases rigidity in flexible pavements.</li> <li>• Proper curing and protection from early traffic.</li> </ul>
Bitumen Emulsion Stabilisation	<ul style="list-style-type: none"> <li>• Improved flexibility and resistance to deformation.</li> <li>• Easy of application. Bulk tanker is coupled to recycler and bitumen emulsion injected through spray bar.</li> <li>• Relatively well known. Standard tests and specifications are available</li> <li>• Can be trafficked immediately after, though not sealable immediately</li> </ul>	<ul style="list-style-type: none"> <li>• High cost of manufacturing requiring strict control, expensive emulsifiers and transport costs inflated by hauling the component of water, not only bitumen.</li> <li>• Risk of saturation if in-situ MC is close to OMC</li> <li>• Long curing time as strength gain is dictated by moisture loss</li> <li>• Required formulation may not always be available</li> </ul>
Foam Bitumen Stabilisation	<ul style="list-style-type: none"> <li>• Improved flexibility and resistance to deformation.</li> <li>• Easy of application. Bulk tanker is coupled to recycler and bitumen emulsion injected through spray bar.</li> <li>• Uses standard pen-grade bitumen thus, no additional manufacturing costs</li> <li>• Material can be trafficked immediately after placing and compaction</li> <li>• Can be stockpiled and reworked if problems are encountered</li> </ul>	<ul style="list-style-type: none"> <li>• Requires special heating facilities and safety precautions as bitumen is required to be above 160 °C</li> <li>• Material deficient in fraction smaller than 0.075 mm cannot be treated without pre-treatment or addition of new material.</li> <li>• High level skill required for mix design</li> <li>• Structural and mix design procedures are not well formulated</li> </ul>

## 2.6. UCS and ITS Tests

Ongoing research has indicated that materials stabilized with bitumen emulsion generally have strength and stiffness similar to those of foamed bitumen mixes. Traditional methods such as CBR and UCS borrowed from soil stabilization (Cement) design were used to determine engineering properties of cold mixes. Since the 1990's the ITS test also known as splitting test has been used to determine the flexibility behaviour of the mixes (Jenkins et al., 2004).



**Figure 13: UCS set up** (Malubila, 2005)

As can be seen in Figure 13 above, the UCS test is much like the triaxial test at zero confinement, its main limitations as a test for mix design of BSMs are:

- Lack of confinement means the test is not capable of determining the stress-dependent behaviour of the material, i.e. the material response at different levels of confinement; and
- Geometry (height to diameter ratio) of the specimen being tested. For most UCS tests the ratio is 0.85 which is considered too low to provide reliable shear strength parameters. A ratio in the order of 2 is preferred to eliminate edge effect, which is the generation of additional confinement due to the friction at the specimen loading plate interfaces.



**Figure 14: ITS set up** (Malubila, 2005)

The ITS test as implied by the term is an indirect way of determining tensile strength, see set up in Figure 14. Although the ITS test is considered to be a 'simple test' (because it can be performed with relative ease), the interpretations of the results are very complex since internal stress distribution in the test is extremely complicated. There exist no direct relation between the applied force and the stress at the centre of the specimen, Erkens, (2002).

## **2.7. Summary**

It is clear from the sections presented in this Chapter that Bitumen Stabilised Materials require proper mix design to give a good performance. Mix design procedures that are available for BSMs are not well formulated especially for BSM-foam. Almost all existing mix design procedures for BSMs use ITS and UCS to evaluate the strength of BSMs. However, BSMs are stress dependant materials with little or no tensile strength. Shearing resistance of BSM (influenced by gradation, moisture, density, fines, particle geometry and confining pressure) is used to develop a load distributing quality that reduces the stresses transmitted to the underlying layers. Therefore, as discussed in Section 2.6, ITS and UCS are not well suited for characterising BSMs and a more suited test such as triaxial test that can simulate more accurately the stress scenario under which BSMs function has long been recognised by the road construction industry.

The next chapter, Chapter 3 will explore the theory, fundamentals, apparatus, procedure, data collection and analysis methods of triaxial testing.

## References

- Akzo Nobel. 2008. **Bitumen Emulsion**. Technical Bulletin. Akzo Nobel Asphalt Applications Stockholm, Sweden, 2008/11/03 Downloaded from: [http://www.surface.akzonobel.com/asphalt\\_russian/publications/tb/tb.htm](http://www.surface.akzonobel.com/asphalt_russian/publications/tb/tb.htm)
- Asphalt Academy. 2002. **The Design and Use of Foamed Bitumen Treated Materials**. Interim Technical Guideline No. 2, Pretoria, South Africa, 2002.
- Crockford W. W., Berthelot C., Tritt B. and Sinadinos C. 2002. **Rapid Triaxial Test**. Association of Asphalt Paving Technologists AAPT Volume 71, Colorado, Pp 712-724.
- Csanyi, L. H. 1957. **Foamed Asphalt in Bituminous Paving Mixtures**, Bulletin No. 160, Vol. 10, Highway Research Board, Washington D.C., USA, 1957
- Csanyi, L. H. 1959. **Foamed Asphalt**, Technical Bulletin Vol. 240, American Road Builders' Association, USA, 1959
- Erkens, S. M. J. G. 2002. **Asphalt Concrete Response (ACRe) – Determination, modelling and prediction**. PhD dissertation Delft University, the Netherlands, 2002.
- Horak, E., Myburgh, P.A. and Rose, D.A. 1984. **Rehabilitation of a cement treated base pavement**. In Proceedings of the 4<sup>th</sup> Conference on Asphalt Pavements for Southern Africa, Cape Town, South Africa, Volume 1, pp 316-326.
- Jenkins K.J., 2000. **Mix Design Considerations for Cold and Half-Warm Bituminous Mixes with Emphasis on Foamed Bitumen**. PhD Dissertation, Department of Civil Engineering, Faculty of Engineering, University of Stellenbosch, South Africa
- Jenkins KJ, Robroch S, Henderson M.G., Wilkinson J, Molenaar A.A.A., 2004. **Advanced testing for cold recycling treatment selection on N7 near Cape Town**. 8<sup>th</sup> conference on asphalt pavements for Southern Africa.
- Jenkins, K.J. and Ebels, L.J, 2007. **Determination of Shear Parameters, Resilient Modulus and Permanent Deformation Behaviour of Unbound and Bound Granular Materials Using Tri-Axial Testing on 150mm Ø x 300mm High Specimens**. Technical Memorandum. Stellenbosch, South Africa, 2007.
- Jenkins, K.J., Molenaar, A.A.A., de Groot, J.L.A., and van de ven, M.F.C. 2000. **Developments in the uses of foamed bitumen in road pavements**. Heron, Vol. 45, No. 3, 2000
- Le Corroler. 2008. **The use of bitumen emulsion in Europe**.[www.eapa.org/START/positionprs\\_publications/paper/bitumen.html](http://www.eapa.org/START/positionprs_publications/paper/bitumen.html). Accessed on 2008/11/24
- Louw, K., Spence, K. and Kuun, P., **The Use of Bitumen Emulsions as a Cost Effective Solution for Constructing Seals during Winter**, 8th Conference on Asphalt Pavements for Southern Africa (CAPSA), Sun City, South Africa, 2004
- Louw, K. 2006. **Technical presentation on seals**. Colas Group Presentation. Lusaka, Zambia, 08 June 2006.
- Malubila, S. M. 2005. **Curing of foamed bitumen mixes**. M.Eng thesis Stellenbosch University, South Africa, 2005
- NAPA. 2002. **Guide for Hot Mix Asphalt Pavement**. National Asphalt Pavement Association, NAPA Building, 5100 Forbes Blvd, Lanham MD. Information series 131. 2002

SABITA. Manual 21. 1999: **ETB – The design and use of emulsion-treated bases**. Published by Sabita Ltd, South Africa, 1999

Wirtgen GmbH. 2002. **Foamed Bitumen – The Innovative Binding Agent for Road Construction**, published by Wirtgen GmbH, Windhagen, Germany, 2002

Wirtgen GmbH. 2004. **Cold Recycling Manual**, 2nd edition published by Wirtgen GmbH, Windhagen, Germany, 2004

### **3. LITERATURE STUDY ON TRIAXIAL TESTING**

#### **3.1. General introduction**

A brief overview on the philosophy and fundamentals of standard triaxial testing is presented in this chapter. Literature study of the triaxial test principles, apparatus, procedure, data collection and analysis has been included. The Technical Memorandum (Jenkins et al, 2007) provides details on types of triaxial tests and procedures. Applications of experimental data, especially in characterizing pavement materials and in mechanistic-empirical design, have also been presented. What is obviously interesting to the reader is to know what work has been done to simplify triaxial testing for use to test road materials especially in the field for quality control purposes.

The primary objectives of the literature study on triaxial testing are to illustrate:

- The general theory and principles of triaxial testing;
- The role that triaxial testing fulfil in the material classification, mechanistic-empirical design and modelling of pavements;
- The appropriateness of the triaxial test in quality control/assurance and performance prediction of flexible pavement materials; and
- The current state of the art regarding simplification of the standard triaxial test.

#### **3.2. Triaxial testing**

##### **3.2.1. Introduction**

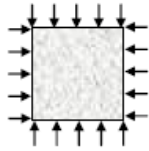
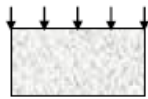
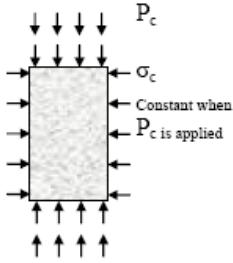
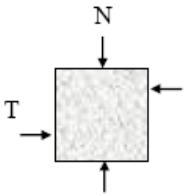
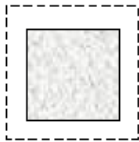
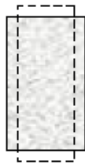
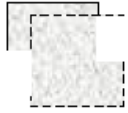
With the increased use of bitumen stabilized materials, of crushed stone, RAP and even gravel, as bases, subbases and even surface layers heard in Chapter 2, the load-deformation response of Bitumen Stabilized Materials is therefore increasingly becoming an important pavement design consideration. Both permanent and resilient deformation characteristics are important. The shear strength of bitumen stabilized materials is also important relative to the behaviour and performance of the material as a pavement layer. Since bitumen stabilized materials have little or no tensile strength, shearing resistance of the material is used to develop a load-distributing quality that greatly reduces the stresses transmitted to the underlying layers. Some important factors influencing the shear strength of Bitumen Stabilized Materials are gradation, moisture and density, maximum particle size, amount and plasticity of fines, particle geometric properties, and confining pressure. Thus shearing strength of road materials is the result of the resistance to movement at interparticle contacts due to particle interlocking, physical bonds formed across the contact areas and chemical bonds (i.e. cementation) and is reduced by any pore pressure or lubrication that develops or exists

during particle movement. It is measured in terms of two parameters namely cohesion and angle of internal friction.

Several laboratory tests for determining the parameters of shear strength exist in geotechnical engineering. They include direct shear test, triaxial shear test, simple shear test, using different drainage conditions (drained or undrained), rate of loading, range of confining pressures, and stress history. In pavement engineering however, these tests are not common, their use is limited only for research purposes. CBR is the commonly used test in pavement engineering for evaluating the strength of road materials. This test however is purely an empirical-phenomenological test method whose results cannot be used in a mechanistic road modeling framework.

From different types of tests used to determine the shear strength parameters, triaxial test in principle (with or without adaptations) effectively simulates the stress-deformation behaviour of road materials. This is supported by various stress-deformation tests reported by (Rodriguez et al, 1988) and illustrated in Table 3 below.

**Table 3: Types of stress – deformation tests** (Rodriguez et al, 1988)

Test	Isotropic Compression	Confined compression (Consolidometer)	Triaxial Compression	Direct Shear Test
Basic Conditions	 <p><math>\sigma_1 = \sigma_3</math></p>	 <p>No horizontal Movement</p>	 <p><math>P_c</math> <math>\sigma_c</math> Constant when <math>P_c</math> is applied</p>	 <p>N T N-constant when T is applied</p>
Type of Strain	Volumetric 	Mainly volumetric, but with some distortion 	Distortion and volumetric 	Mainly distortion, but with some volumetric 
Uses	For volumetric deformation studies	To reproduce certain real field conditions	The most commonly used test for studying soil strength	For studying soil strength

### 3.2.2. Principles of triaxial testing

Triaxial test is defined by the Texas Department of Transport (TXDOT, 2002) as a test in which stresses are measured in three mutually perpendicular directions. It is used to determine the shear strength of the material (e.g. BSMS) using samples enclosed in a pressurised chamber (Triaxial cell), which subjects the sample to three compressive stresses at right angles to each other. The vertical compressive stress is then increased in excess of horizontal (lateral) stress until the sample fails in shear or strain to such an extent that excessive deformation occurs. Figure 15 illustrates the principle of triaxial test on a material sample.

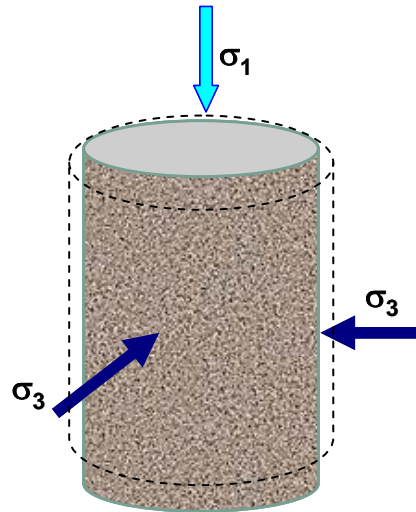


Figure 15: Principle of triaxial test

The stress scenario at failure on a particulate of the sample depicted in Figure 15 is as shown in Figure 16

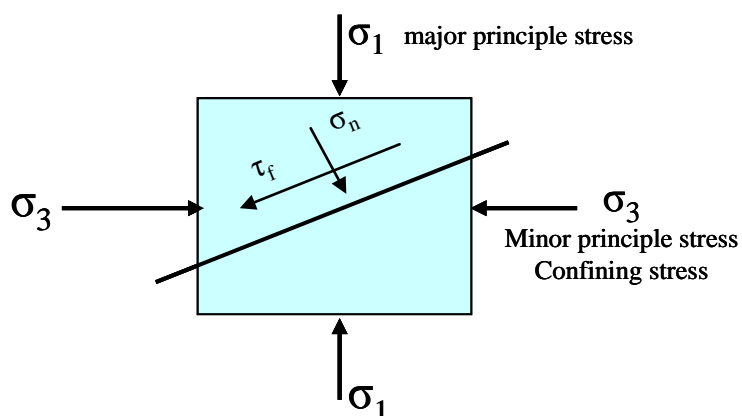


Figure 16: Stress scenario at particle level

The shear strength of the material is obtained using a Mohr-Coulomb failure criterion represented by the following mathematical relationship:

$$\tau_f = C + \sigma \tan \varphi \quad \text{Eq. 1}$$

Where,

$\tau_f$  = shear strength;  $C$  = cohesion;  $\sigma$  = normal stress acting on failure plane; and  $\varphi$  = angle of internal friction.

The shear parameters (cohesion  $C$  and angle of internal friction  $\varphi$ ) of a material can be determined by conducting a series of monotonic triaxial tests to failure on comparable specimens but over a range of different confining pressures (minor principal stresses,  $\sigma_3$ ). This requires at least three different specimens of the same material to be tested at different confining pressures in a triaxial cell. For each test a plot of the load (or applied stress) versus the induced displacement (strain) is made as is schematically represented in Figure 17 below.

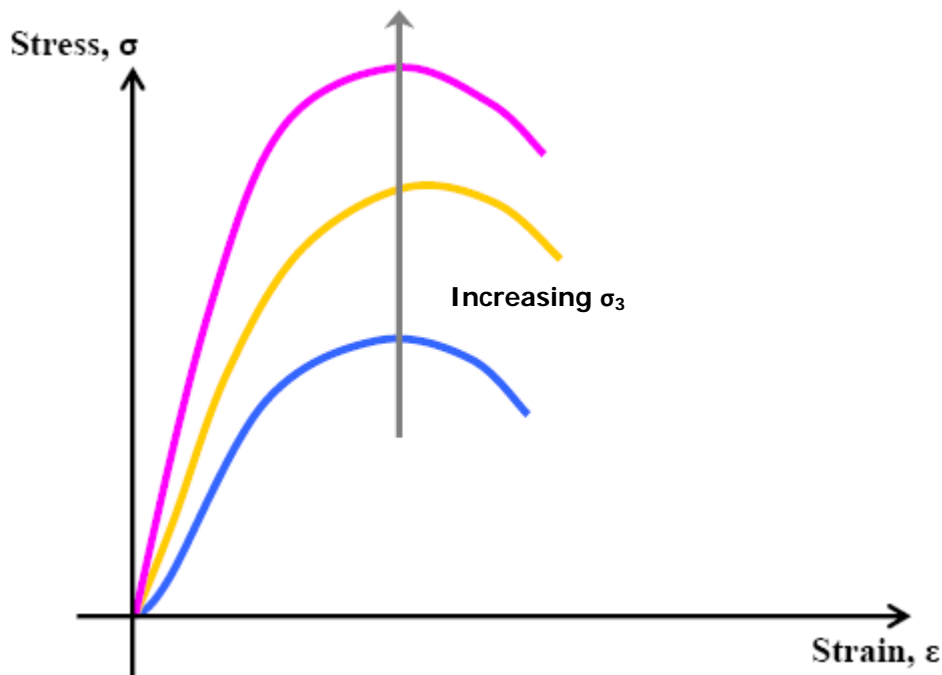


**Figure 17: Schematic representation of triaxial test results**

The stress conditions at which (shear) failure occurs can be represented by means of Mohr circles. An example of the set of those is shown in Figure 18. The tangent line to all circles is called the Mohr-Coulomb failure criterion. It is represented by Equation 1 above. Each stress circle is represented by the minor principal stress  $\sigma_3$  and the major principal stress  $\sigma_1$ . At a given  $\sigma_3$  there is one  $\sigma_1$  that makes the stress circle touching the failure criterion. The major principal stress at which failure occurs,  $\sigma_{1,f}$  can be calculated using Equation 2:

$$\sigma_{1,f} = \left[ (1 + \sin \varphi) \cdot \sigma_3 + 2C \cdot \cos \varphi \right] / (1 - \sin \varphi) \quad \text{Eq. 2}$$

Where  $\sigma_3$  = minor principal stress equal to confining pressure during test

$\varphi$  = angle of internal friction

$C$  = cohesion

Experimentally, the major principle stress at failure for each tested specimen can be determined from Equation 3 as:

$$\sigma_{1,f} = \sigma_{a,f} + \sigma_3 + \sigma_{dw} \quad \text{Eq. 3}$$

Where  $\sigma_{a,f}$  = Applied stress at failure (kPa) obtained by dividing applied failure load (N) by the end area (m<sup>2</sup>) of the specimen at the beginning of the test.

$\sigma_3$  = Confining pressure during the test (kPa)

$\sigma_{dw}$  = pressure (kPa) resulting from dead weight of top cap and loading ram.

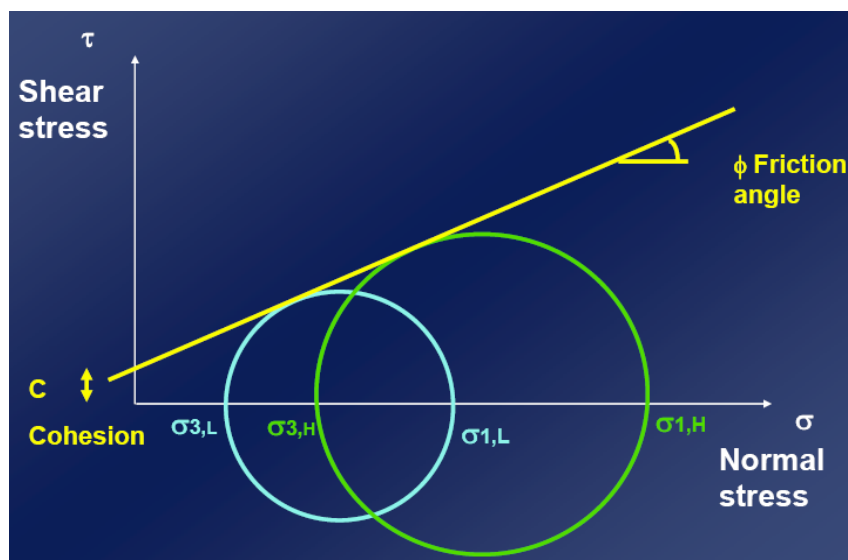


Figure 18: Mohr-Coulomb plots of monotonic triaxial tests (Jenkins, 2008)

### 3.2.3. Types of triaxial tests

In pavement engineering three types of triaxial tests are described on compacted undrained specimens with constant confining pressure (Jenkins et al, 2007), these are:

#### 3.2.3.1. Monotonic triaxial test

This test also known as monotonic failure test is performed in order to determine shear parameters; cohesion  $C$  and angle of internal friction  $\varphi$ . The monotonic triaxial test is carried out at 25°C. This is believed to be a representative temperature for BSM's in base layers in South Africa. Investigations by

Moloto (2009) have shown that during the coldest month (July) the base temperature varies between 10 and 20 °C, while during November (summer) temperatures between 20 and 35 °C were found.

The test is performed with a controlled constant displacement rate of 2.1-2.6% strain per minute. For a specimen height of 300mm at a rate of 2.1% this would result in 6.3 mm per minute. Confining pressure is provided by increasing the air pressure in the cell. A set of at least three monotonic triaxial tests is carried out, all at different pressures ranging from 25 to 200 kPa. The load and displacement data is captured on the computer as the test is running.

#### 3.2.3.2. Short duration dynamic loading triaxial test

This test is performed in order to determine elastic resilient stiffness behaviour (Resilient Modulus  $M_r$ ). During the short duration dynamic triaxial test the response of the specimen to different levels of loading at a range of confining pressures is measured. These confining pressures are the same as used during the monotonic testing. The load level during the short duration dynamic test is described by the deviator stress ratio. This is the ratio between the applied deviator stress and the deviator stress at failure  $\left(\sigma_{d,applied} / \sigma_{d,failure}\right)$ . The latter is determined during the monotonic triaxial testing.

#### 3.2.3.3. Long duration dynamic loading triaxial test

This test is performed in order to determine permanent deformation behaviour of the material. In this test the load signal is the same as for the short duration dynamic testing, i.e. a haversine load with a pre-load of 20 kPa applied at a frequency of 2 Hz. Four tests are performed, each at a different deviator stress ratio. One of the objectives of this test is to determine which deviator stress ratio is the critical stress ratio. Specimens subjected to higher stress ratio than the critical one tend to show accelerated rate plastic strain accumulation towards the end of the test (>4% plastic strain), while specimens subjected to a lower stress ratio than the critical one will show an ever decreasing rate of plastic strain accumulation resulting in a stable condition until the end of the test (1 million load repetitions).

The first type, monotonic triaxial test is the focus of this study.

#### **3.2.4. Standard triaxial test apparatus**

Various set-ups of triaxial testing apparatus exists both in geotechnical and pavement engineering depending on among other factors, sample type and size, type of confining fluid, type of test (monotonic or dynamic), type of loading frame, measuring system and accessories used. In all set-ups common features of a triaxial testing are described below. A schematic representation of a common triaxial equipment set-up in pavement engineering is shown in Figure 19.

### 3.2.4.1. Triaxial cell

The triaxial cell is a fluid-tight container with hydraulic connections at the base and a sliding load piston in the top. The cell can be readily opened to allow the positioning of specimens and cell accessories. The pedestal (base disc) on which the specimen sits is interchangeable with discs of different diameter provided that these are compatible with the cell itself. The cell must be able to safely withstand the confining pressures required. Both air and water may be used as confining agents. Normally, the confining pressure around the specimen is furnished by pressurized fluid, thus the triaxial cell must be connected to a system capable of providing pressurized air or water. This system must also be capable of compensating for eventual volume changes of the specimen by providing or receiving the corresponding volume of fluid without change in fluid pressure. The system must also be capable of controlling the fluid pressure to a high degree of accuracy. These systems are commonly known as Constant Pressure Sources and are available in various forms based on different working principles and thus have differing characteristics.

The internal dimensions of the cell should be large enough to accommodate the specimen size to be tested. The clearance between the specimen and the cell wall should be sufficient to allow for the installation of on-specimen displacement transducers. The specimen is enclosed in a latex membrane which is sealed with rubber O-rings on the base disc and top cap.

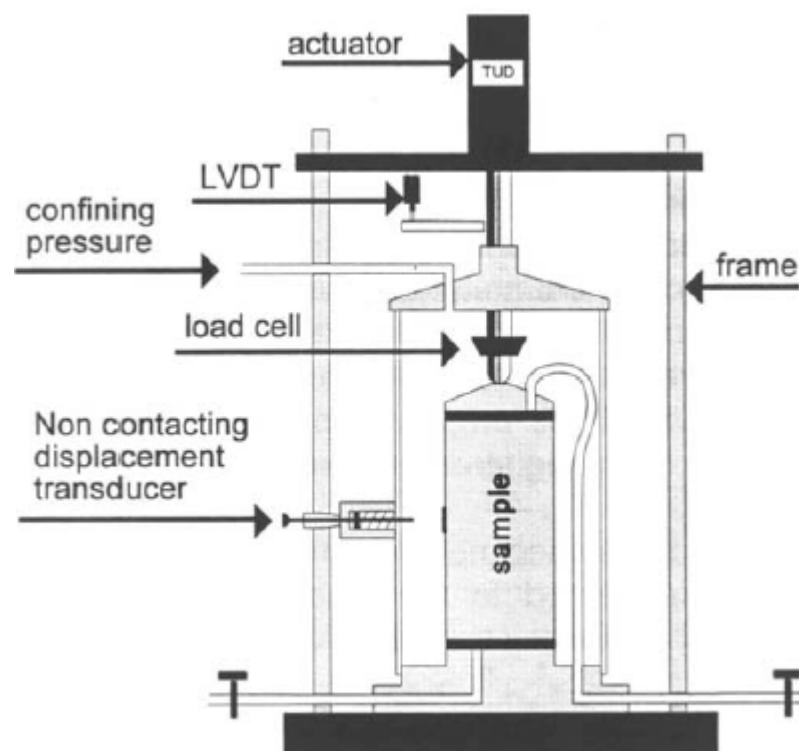


Figure 19: Schematic representation of triaxial equipment (Molenaar, 2005)

#### 3.2.4.2. Testing system

The triaxial testing is carried out in a testing system that must at least comprise of an actuator, a reaction (load) frame, a control panel and a data acquisition system. In modern systems, the actuator is operated by a servo-controlled hydraulic pressure system which exerts either a ramp or cyclic motion on the loading frame depending on the test setting. This servo-controlled hydraulic system is a closed loop feedback system that is capable of both displacement and load controlled testing if required. The preferred geometry of testing system is such that the moving actuator is situated above the triaxial cell with the fixed reaction point situated below the triaxial cell. Inverted set-ups result in limitations on the maximum frequency of the dynamic load testing.

The reaction frame has the function of applying ramp or cyclic loads on the specimen. It is necessary to be able to regulate the rate of strain applied to the specimen within a very large range and, ideally, fully variable so as to allow the correct selection of strain for each particular test. Another requisite of the reaction frame is the accuracy and continuity of strain rate independent of the forces encountered. A minimum loading capacity of 100 kN and a minimum stroke of 40 mm is recommended for testing 150 mm diameter specimens (Jenkins, et al 2007). The data acquisition systems must capture the following:

- Load
- Displacement of the actuator
- Displacement of the on-specimen transducers
- Cell pressure (optional)
- Temperature (optional)

#### 3.2.4.3. Measuring devices

Measuring devices in triaxial testing mainly refer to instruments for measuring load, strain and pressure. They include load cells, actuator displacement transducers and on-specimen displacement transducers. Other measuring instruments that may be connected to the triaxial cell include; pressure, volume change and temperature sensors.

The capacity of the load measuring instrument should be compatible with the loads to be measured which will depend upon the resistance and diameter of the specimen. It may well be necessary to have available various capacity load measuring instruments. The highest loads are generated during the monotonic failure test while dynamic tests require much lower loads. A smaller load cell of capacity 20 kN must be used when the magnitude of the dynamic load is below 10% of the capacity of a larger load cell (Jenkins et al, 2007).

Testing systems capable of generating large loads of up to 100 kN usually have actuator strokes in excess of what is required for triaxial testing. The accuracy of the displacement transducer that

measures the actuator movement is therefore too low for dynamic triaxial testing. The actuator displacement data can therefore only be used for monotonic triaxial testing and permanent deformation testing. Therefore, for measuring displacement during the dynamic testing for resilient modulus, on-specimen displacement transducers (LVDTs) with the accuracy of within 2 micron are required. These displacements are measured over the middle third of the specimen and the total stroke must be at least 4 mm.

#### 3.2.4.4. Specimen size

In geotechnical engineering, the diameter of specimens commonly used in triaxial tests range from 35mm up to 100mm. However, in pavement engineering because of the relatively large particle size of granular road building materials (compared to soils and clays in the geotechnical field) the diameter of specimens made from these materials need to be increased to 150mm or even 300mm. In order to have a  $d_{specimen} / d_{max-particle}$  ratio high enough to prevent effects stemming from particle size, the  $d_{max-particle}$  for 150mm diameter specimen is limited to 19.0mm. This results in a  $d_{specimen} / d_{max-particle}$  ratio of 7.9.

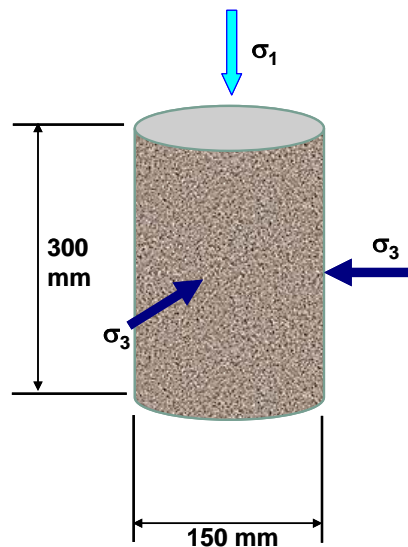


Figure 20: Specimen size

### 3.3. Application of triaxial data

#### 3.3.1. Material Classification

The use of triaxial test data in material classification is not common in pavement engineering. However, successful use of triaxial test data in material classification is evidenced by the Texas Triaxial Classification Procedure over the years. The Texas Department of Transportation has been using this procedure for over 50 years for the evaluation of unbound materials for pavement construction. Although the classification system was developed empirically it evaluates the material based on its strength and gives important pavement design input by estimating the subgrade

modulus which is used in pavement design. This triaxial procedure characterizes the subgrade and base layers using laboratory test results on specimens of 152.4 mm (6 in.) diameter and 203.2 mm (8 in.) in height, representing a height to diameter ratio of 1.3. The specimens are tested at a rate of compression of  $2.0 \pm 0.3\%$  strain per minute over 0 to 103.4 kPa range of confining pressures. Curing of specimens is according to the type of material to avoid excessive cracking. Details of the Texas Triaxial Test Procedure are appended in Appendix 1 of this report.



**Figure 21: Texas triaxial cell** (Crockford et al, 2002)

The classification procedure entails the plotting of the Mohr circles and failure envelope for the material to be classified. Once the failure envelope is constructed it is carried over to the classification chart (Figure 22) from where the class of material is determined to the nearest  $1/10^{\text{th}}$  of the class. The figure obtained is known as the Texas – Classification of the material.

From the chart in Figure 22 below, it can be seen that there are six strength classes into which a material can be classified. Materials classified as Class 1 ( $T = 1.0$ ) have the highest shear strength and materials classified as Class 6 ( $T = 6.0$ ) have the lowest shear strength.

A case, in which this classification system was used locally in South Africa, was in the comparison of possible base course materials for the reconstruction of the MR 201 between National Route 1 (N1) and traffic circle in the Market Street (Paarl), by UWP Consulting (PTY) Ltd for Western Cape Provincial Administration Department of Transport and Public Works in the year 2004. The Consultant in his draft report recommended among other things the development of the criteria for triaxial classes for South African conditions.

Pavement materials can therefore be classified according to their friction angle and cohesion. This is also shown by work carried out by Maree (Theyse et al, 1996) on many triaxial tests on different materials, Table 4 below.

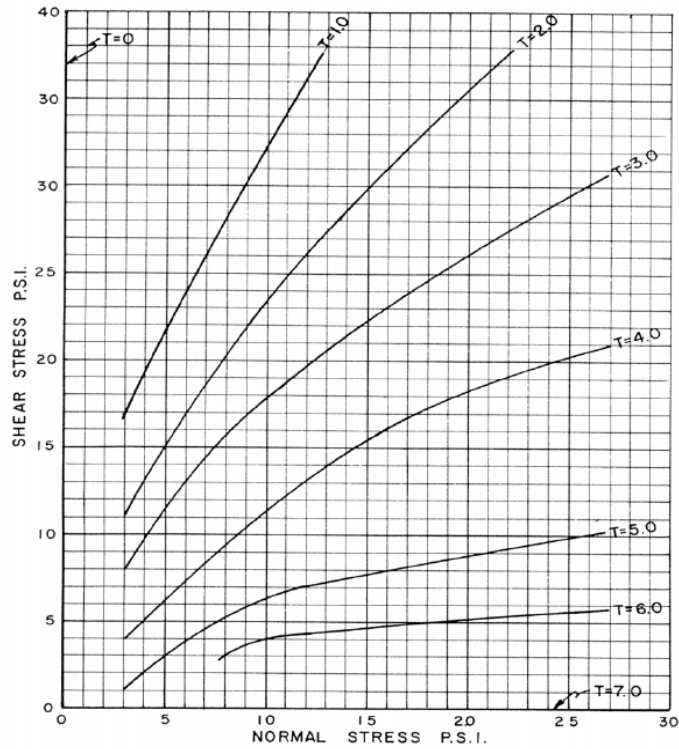


Figure 22: Chart for classification subgrade and flexible base material (UWP, 2004)

Table 4: Shear properties of granular materials (Theyse et al, 1996)

Material	Moisture state	Cohesion C [kPa]	Internal Friction [°]
High density crushed stone <b>G1</b>	Dry	65	55
	Wet	45	55
Moderate density crushed stone <b>G2</b>	Dry	55	52
	Wet	40	52
Crushed stone and soil binder <b>G3</b>	Dry	50	50
	Wet	35	50
Base quality gravel <b>G4</b>	Dry	45	48
	Wet	35	48
Subbase quality gravel <b>G5</b>	Moderate	40	43
	Wet	30	43
Low quality subbase gravel <b>G6</b>	Moderate	30	40
	Wet	25	40
Good Selected subgrade <b>G7</b>	Dry	25	35
	Wet	20	35
Moderate selected subgrade <b>G8</b>	Dry	30	30
	Wet	20	30
Weaker selected subgrade <b>G9</b>	Dry	30	28
	Wet	20	28
Soil fill <b>G10</b>	Dry	35	25
	Wet	20	25

### 3.3.2. Other material properties

Owing to the relatively big sizes of specimens (150 mm  $\varnothing$  by 300 mm height) required for triaxial tests on BSMs, the need to obtain more information from the monotonic triaxial test than just load (stress) versus strain (deformation) at failure leading to the determination of shear strength parameters ( $C$  and  $\phi$ ) is increasingly becoming justified. This other information defined in Figure 23 includes the strain at failure, tangent and secant moduli.

The tangent modulus ( $E_{tan}$ ) can be defined as the slope of the tangent at the linear part of the stress-strain curve. The tangent modulus therefore, provides an indication of the elastic stiffness modulus of the material. In his dissertation Ebels (2008) showed that bituminous stabilised mixes with active filler (1% cement) tended to show high tangent modulus values whilst similar mixes with high percentage of RAP (75%) showed low tangent modulus values. He further showed in his work that tangent modulus exhibited a stress dependent behaviour.

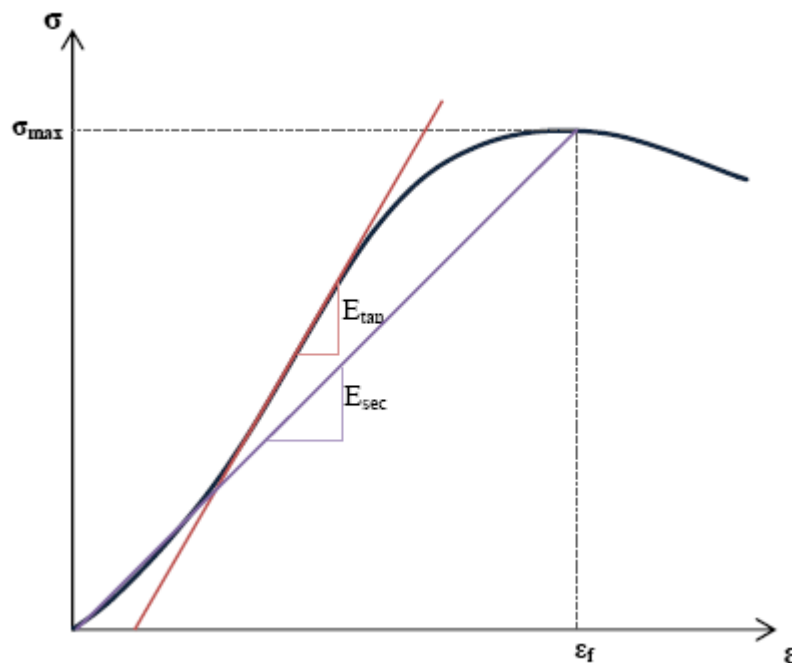


**Figure 23: Schematic stress-strain diagram showing Tangent and Secant Modulus, Maximum Stress and Strain at Failure**

Also from Figure 23, the secant modulus ( $E_{sec}$ ) is illustrated as the slope of the line drawn from the origin of the stress-strain diagram to the point on the curve where the maximum stress occurs whilst the strain-at-failure ( $\epsilon_f$ ) being the strain at which the maximum stress occurs. Ebels, (2008) reported from his experimental observations that the strain at failure increases with increasing confining pressure rendering it a stress dependent parameter.

### 3.3.3. Pavement design, modelling and performance prediction

Triaxial tests can be used to determine the fundamental strength characteristics of materials used in the construction of flexible pavements. By determining the strength properties of surface, base course, subbase, and subgrade materials by this means, an opportunity is available to utilize these materials on the basis of resistance to strain and shear, comparable to the methods used for other structural materials, such as steel, concrete and timber. The theoretical required thicknesses of pavement layers, as determined by the results of triaxial tests on soil-aggregate mixtures can therefore be obtained through a mechanistic-empirical design method. Equation 2 in Section 3.2.2 represents a formula that is of importance in the determination of the stress ratio.

Stress ratio,  $SR = \frac{\sigma_1}{\sigma_{1,f}}$  in mechanistic design of flexible pavements provides a means of limiting

permanent deformation by allowing stress levels which are only a moderate percentage of stress level at failure. Work by van Niekerk, (2002) has shown that if the stress ratio stays below 0.4, no excessive deformation will occur. This ratio is valid for compaction levels of 97 – 103%. Jenkins

(2000) modified the stress ratio equation to the deviator stress ratio  $\left( SR = \frac{\sigma_d}{\sigma_{d,f}} \right)$  as opposed to the

principal stress ratio to account for the damage that occurs in a granular or BSM that is stressed relatively close to the failure stresses (see Equation 4):

$$SR = \frac{\sigma_d}{\sigma_{d,f}} = \frac{\sigma_1 - \sigma_3}{\sigma_{1,f} - \sigma_3} = \frac{\sigma_1 - \sigma_3}{\sigma_3 \left( \tan^2 \left( 45^\circ + \frac{\varphi}{2} \right) - 1 \right) + 2C \tan \left( 45^\circ + \frac{\varphi}{2} \right)} \quad \text{Eq.4}$$

Where,  $\sigma_d$  = deviator stress

$\sigma_{d,f}$  = deviator stress at failure

$\sigma_1$  = principal stress

$\sigma_{1,f}$  = principal stress at failure

$\sigma_3$  = confining pressure

$\varphi$  = angle of internal friction

$C$  = cohesion

The advantage of using deviator stress ratio over principal stress ratio is that the deviator stress ratio is not influenced by the confining pressure levels, while the principal stress ratio is. At decreasing friction angles  $\varphi$ , this difference becomes more evident (Jenkins, 2000). A material subjected to two different stress levels can have a significantly different principal stress ratio, but relatively to its shear capacity be in a similar stress state. In such a scenario the deviator stress ratio of the two different stress levels would be the same.

Stress ratio is also useful in predicting the development of permanent deformation as a function of the number of load repetitions, stress conditions and material characteristics. It is apparent in Equations 2 and 4 that cohesion and friction angle are important parameters in determining this ratio.

Another good example of the utilisation of triaxial test parameters and results of cohesion and angle of friction can be traced in the South African Mechanistic-Empirical Design Method. This design procedure defines a safety factor against shear failure for granular materials by Equations 5 and 6 (Theyse et al, 1996). The safety factor concept was developed from Mohr-Coulomb theory and represents the ratio of the material shear strength divided by applied stress causing shear.

$$F = \frac{\sigma_3 \left[ K \left( \tan^2 \left( 45 + \varphi/2 \right) - 1 \right) \right] + 2KC \tan \left( 45 + \varphi/2 \right)}{\left( \sigma_1 - \sigma_3 \right)} \quad \text{Eq. 5}$$

Alternatively:

$$F = \frac{\sigma_3 \varphi_{term} + C_{term}}{\left( \sigma_1 - \sigma_3 \right)} \quad \text{Eq. 6}$$

Where,

$\sigma_1$  and  $\sigma_3$  = major and minor principle stresses acting at a point in the granular layer (compressive stress positive and tensile stress negative);

C = cohesion;  $\varphi$  = angle of internal friction; and

K = constant = 0.65 for saturated conditions, 0.8 for moderate moisture conditions and 0.95 for normal moisture conditions.

The F factor is in fact the inverse of principal stress ratio. The only difference is that in the F equation, the factor K is introduced which takes care of the effect of the moisture conditions in the layer.

Triaxial testing using dynamic loading at applied vertical different stress levels and at different deviator stresses, can be used to determine the resilient modulus of granular material. The results of the dynamic triaxial tests can be analysed best by plotting Resilient Modulus versus the total stress, both on a logarithmic scale as shown in Figure 24 representing a typical model of resilient modulus for coarse grained granular materials.

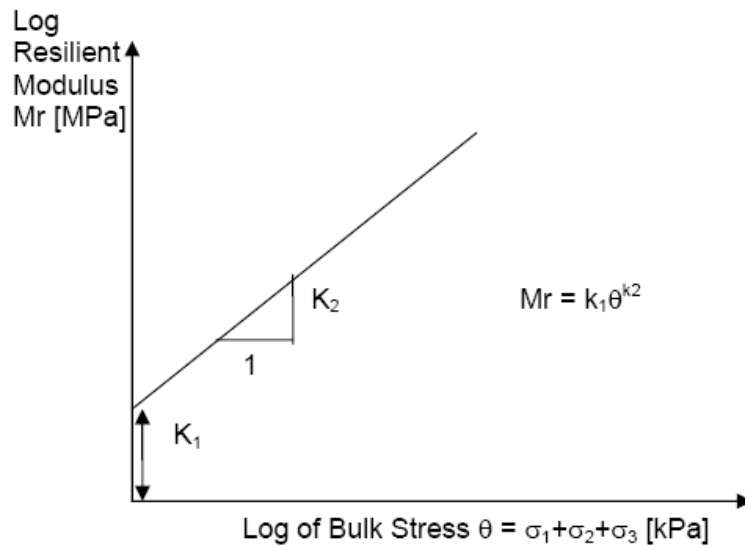


**Figure 24:  $M_r$ - $\theta$  Model of Resilient Modulus for coarse grained granular materials** (Jenkins, 2008)

This model is defined mathematically by Equation 7 below:

$$M_r = k_1 \cdot \theta^{k_2} \quad \text{Eq. 7}$$

Where  $M_r$  = Resilient Modulus [MPa]

$k_1$  and  $k_2$  = material coefficients

$\theta$  = bulk stress =  $\sigma_1 + \sigma_2 + \sigma_3$  [kPa]

Material coefficients  $k_1$  and  $k_2$  can therefore be derived from triaxial tests. In South Africa however, Maree reported that for crushed stone bases, the applicable values are 9.7 and 0.66 respectively.

Another important application of the triaxial test is in the modelling of granular materials for permanent deformation. This is achieved by the use of the third type of triaxial test described in Section 3.2.3. In this type of test dynamic triaxial test is carried out on several separate specimens at different applied deviator stress levels. The permanent deformation experienced by the specimen is monitored over an extended period, sometimes to more than 1 million load repetitions. Figure 25 below shows typical permanent deformation triaxial test results for granular materials.

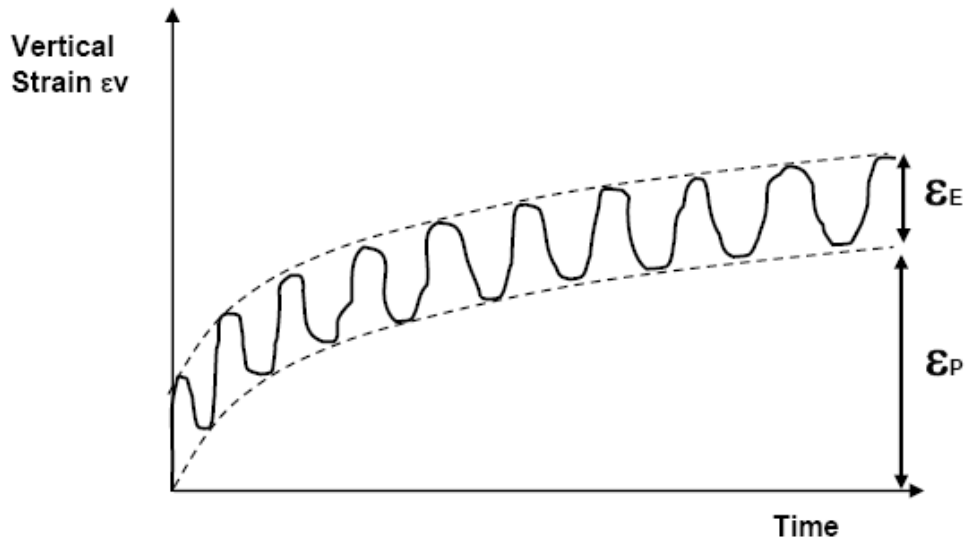


**Figure 25: Typical permanent deformation triaxial test result for granular materials** (Jenkins, 2008)

A general formula for the permanent deformation provided by (Huurman, 1997), (Jenkins, 2000) and (van Niekerk, 2000):

$$\varepsilon_p = A \cdot N^B \quad \text{Eq. 8}$$

Where N = number of load repetitions

A, B = material constants

The formula can be graphically represented on a log scale as shown in Figure 26 below and the formula rewritten as:

$$\log \varepsilon_p = \log A + B \cdot \log N \quad \text{Eq. 9}$$

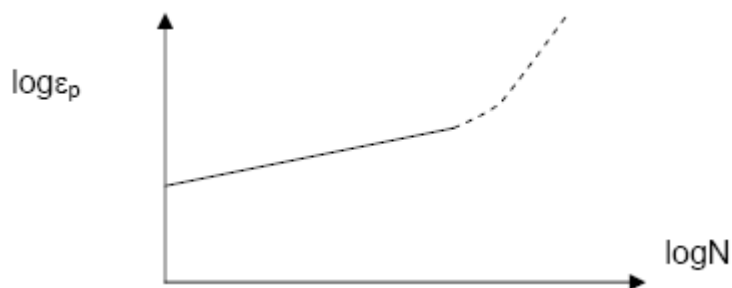


**Figure 26: Typical permanent deformation model** (Jenkins, 2008)

### 3.4. Quality Control/Assurance

The objectives of this section are to explore the appropriateness of the triaxial test on 150 mm diameter x 300 mm high specimens in quality control/assurance of flexible pavement construction. In

order to appreciate the complexity of the standard triaxial testing method, it is necessary to briefly review the operation of one of the triaxial testing procedures currently being used at University of Stellenbosch by use of the Material Testing System (MTS 810, model 318.10). The review is in the context of assembly of specimen in the triaxial cell when conducting a monotonic failure test to determine the shear parameters; cohesion (C) and angle of internal friction ( $\phi$ ). Details of procedures for conducting other types of trial tests can be obtained in the Technical Memorandum (Jenkins et al, 2007).

The following steps describe the procedure for assembly of specimen in the triaxial cell:

- The specimen to be tested is placed in a climate chamber and conditioned overnight at 25°C. The triaxial cell including the base disk and top cap are also subjected to the same conditioning.
- The sides of the base disk and top cap are lightly greased to ensure an air or water tight seal with the membrane.
- The base disk is placed on the cell base and the specimen positioned in the middle of the base disk.
- A latex membrane is carefully placed around the specimen and around the base disk. Care is taken not to damage the edges of the specimens during this procedure. It is recommended to use a membrane expander for the placement of the membrane. The top part of the membrane is folded back to expose the top of the specimen.
- The first rubber O-ring is placed around the bottom end of the membrane over the base disk. The top cap is placed on the specimen and the top part of the membrane is pulled over the top cap. The second rubber O-ring is placed around the top end of the membrane over the top cap.
- The top cap drain is then connected to the top cap drainage port in the cell base with a plastic tube. The valve on the top cap drainage port in the cell base is then closed. Care is taken to ensure that the specimen is positioned in the middle of the base plate and that the centre of the top cap is aligned with the centre of the specimen.
- The loading ram is lubricated with silicon oil and the triaxial chamber is lowered over the specimen and onto the cell base. Care is taken not to make contact with the specimen.
- The tip of the loading ram is checked to ensure that it is aligned with the locating dent in the centre of the top cap. Finally the chamber tie rods are tightened firmly after ensuring that the cell chamber is correctly aligned with the cell base.

This procedure takes more time and attention to detail than would be required especially for quality control purposes. In that case the results must be available relatively quickly leaving no room for time consuming repeated load tests that might be needed to characterize the materials. Therefore, major adaptations to the standard triaxial test are necessary if such a useful test can have a chance of being accepted by road practitioners.

### 3.5. Current state of the art

Various innovative approaches to adapting triaxial testing for a research laboratory involved in design, construction and maintenance of flexible pavement systems have been noted locally and internationally.

#### 3.5.1. The K-Mould

The K-mould shown in Figure 27 is such an example. It is used to determine the elastic (i.e.  $M_r$ ,  $v$ ) and shear properties ( $c$  and  $\phi$ ) of road building materials at similar conditions to those anticipated in the pavement (i.e. dry density, moisture or binder content, and vertical stress level), this assists in optimal design of the pavement structure.



**Figure 27: K-Mould apparatus** (Dynatest, 2008)

The K-mould can also be used to determine the material's resistance to permanent deformation. It uses samples with height: diameter ratio of less than one. Botha et al (2005) investigated the early trafficking of emulsion treated bases (ETB) and foamed bitumen (FB) bases treated in combination with cement (OPC) in South Africa using the K-mould.

However, because it uses height: diameter ratio of less than one, its suitability for samples with 300mm height and 150mm diameter having a ratio of two is therefore questioned. Furthermore, Vuong et al, (2003) has argued that the South African K-mould requires further simplification and standardization before it would be suitable for practical use.

#### 3.5.2. Rapid Triaxial Test (RaTT)

The Rapid Triaxial Test (RaTT) is another invention worth noting. The cell is depicted in Figure 28, as a modified geotechnical cell with automation. The prototype rapid triaxial testing system was developed by Tritt, of Industrial Process Controls (IPC), on the basis of conceptual designs by Crockford and theoretical considerations put forth by Lytton, of Texas Transportation Institute, as part of the NCHRP Project 9-7 research program.



**Figure 28: The RaTT Cell** (Crockford et al 2002)

In his evaluation of the Rapid Triaxial Test, Gould et al (2004) described the basic philosophy behind the test as based on triaxial testing of construction and geomaterials as conducted for many years by the Texas Department of Transportation and the California Department of Transportation. He further stated that the newly developed testing system was much easier to use than a conventional geotechnical cell triaxial system and was fully automated and software controlled. Testing using the RaTT can be conducted using a wide range of stress, states of stress, and confinement conditions. Gould concluded that the equipment has the potential to be used as a rational and practical tool for effective QC of HMA production. However, there was a need to conduct a study with properly controlled mixes to evaluate the equipment's sensitivity to key mix components.

The RaTT is another example of real achievements through high quality research on the international scene however; the apparatus was developed for Hot Mix Asphalt and not for Bitumen Stabilized or granular materials which require specimen dimensions of 150 mm diameter x 300 mm deep.

### **3.5.3. Simple Performance Test (SPT)**

The IPC Simple Performance Tester (SPT) is another state of the art invention by the Australians. This test set up as depicted in Figure 29 is a fully integrated package comprising a triaxial cell, environmental chamber, hydraulic actuator and pump, refrigeration and heating unit with heat exchanger and a control and data acquisition system.



**Figure 29: Simple Performance Tester** (IPC Global, 2008)

The triaxial test cell is mounted on the top left of the unit. There is space for the operators PC on the top at the right hand side if required, or it can be remotely located. A quiet (built-in) hydraulic pump provides pressure for the vertical loading system. Compressed air is used for confining pressure and to raise and lower the triaxial cell.

IPC highly modified a geotechnical triaxial cell, to double as an environmental chamber. The test cell allows viewing of the sample at all times during a test without the need for special lighting or illumination. Prior to installation in the test cell, samples are fitted with three surface mounted transducers.

The triaxial cell itself is raised and lowered by an inbuilt control system, which meets required operator safety standards and avoids the need for the operator to dismantle and move the heavy cell assembly when changing test specimens. The temperature of the confining medium (re-circulated air) is regulated by a heat exchanger assembly and controlled by a temperature sensor within the cell. Thermal equilibrium can be obtained within a three-minute time limit.

This apparatus is another example of a set-up developed for hot mix asphalt samples of 100 mm  $\varnothing$  x 150 mm deep and not granular material. For instance it is difficult to core out the inner 100 mm diameter specimen from a granular layer for use in SPT. Moreover the current set up cannot accommodate 150mm  $\varnothing$  x 300mm deep bitumen stabilized or granular materials.

### 3.5.4. Summary

A summary of comparisons of state of the art triaxial test set-ups considered in this study has been included in Table 5 below:

**Table 5: Summary of comparisons of test set-ups**

Test Set-up	Applicable material	Specimen Size (mm)	height/diameter ratio	Max aggregate size (mm)
K-Mould	Granular, BSM	variable	< 1	37.5
RaTT	Asphalt	100 x variable	Variable	12.5
SPT	Asphalt	100 x 150	1.5	37.5

### 3.6. Conclusion

In concluding this chapter, a summarised comparison of different triaxial tests common in Pavement Engineering has been included in tabular form (see Table 6 below). It compares features including common apparatus used, test conditions, loading conditions, test results, models used in analysis and parameters of materials determined.

**Table 6: Summary of comparison of different triaxial tests**

Feature	Types of Triaxial Tests in Pavement Engineering		
	Monotonic	Dynamic (Short Duration)	Dynamic (Long Duration)
<b>Apparatus</b>	Air tight triaxial Cell  Testing System <ul style="list-style-type: none"> <li>• Actuator</li> <li>• Reaction Frame</li> <li>• Control Panel</li> <li>• Data Acquisition</li> </ul> Measuring Devices <ul style="list-style-type: none"> <li>• Load Cell</li> <li>• Actuator Displacement Transducer</li> <li>• Pressure gauge</li> <li>• Temperature sensor (optional)</li> </ul>	Air tight triaxial Cell  Testing System <ul style="list-style-type: none"> <li>• Actuator</li> <li>• Reaction Frame</li> <li>• Control Panel</li> <li>• Data Acquisition</li> </ul> Measuring Devices <ul style="list-style-type: none"> <li>• Load Cell</li> <li>• Actuator Displacement Transducer</li> <li>• Pressure gauge</li> <li>• LVDTs</li> <li>• Temperature sensor</li> </ul>	Air tight triaxial Cell  Testing System <ul style="list-style-type: none"> <li>• Actuator</li> <li>• Reaction Frame</li> <li>• Control Panel</li> <li>• Data Acquisition</li> </ul> Measuring Devices <ul style="list-style-type: none"> <li>• Load Cell</li> <li>• Actuator Displacement Transducer</li> <li>• LVDTs</li> <li>• Pressure gauge</li> <li>• Temperature sensor</li> </ul>
<b>Test Conditions</b>	<ul style="list-style-type: none"> <li>• Temperature 25 °C</li> <li>• Varying Confinement Pressure, <math>\sigma_3 = 50, 100, 200</math> kPa</li> </ul>	<ul style="list-style-type: none"> <li>• Temperature 25 °C</li> <li>• Varying Confinement Pressure, <math>\sigma_3 = 50, 100, 200</math> kPa</li> </ul>	<ul style="list-style-type: none"> <li>• Temperature 25 °C</li> <li>• Constant Confinement Pressure, <math>\sigma_3</math></li> </ul>
<b>Loading</b>	Static or Ramp load applied at a 2.1% mm/min displacement	Dynamic or Cyclic haversine load with	Dynamic or Cyclic haversine load with

Feature	Types of Triaxial Tests in Pavement Engineering		
	Monotonic	Dynamic (Short Duration)	Dynamic (Long Duration)
Conditions		preload of 20kPa applied at 2 Hz frequency	preload of 20kPa applied at 2 Hz frequency
Test Results	Load (Stress) Vs Displacement (Strain)	Load (stress) vs Time and Displacement (Strain) vs Time	Permanent Axial Strain vs No. of Load Repetitions or Time
Models Used	$\tau_f = c + \sigma \tan \phi$	$M_r = k_1 \cdot \theta^{k_2}$	$\epsilon_p = A \cdot N^B$
Parameters Determined	Shear Strength of Material (cohesion, C and angle of internal friction $\phi$ )	Elastic Resilient Stiffness Behaviour of a material, $M_r$	Permanent Deformation Behaviour of a Material, $\epsilon_p$

It can also be stated that in order to make reliable designs that accurately estimate the performance of the pavement, it is necessary to have the following information on the mechanical properties of the pavement materials used:

- Shear strength (C and  $\phi$ )
- Resilient modulus ( $M_r$ ); and
- Permanent deformation (N- $\epsilon_p$ )

This therefore, puts the triaxial test at the centre stage of any mechanistic approach to pavement design. However, the challenge remains and is that the triaxial test with all its types should meet the requirements of a practical tool i.e. simple, low cost, easily standardized, reliable and reproducible, like the CBR test if it is to be of any relevance to the pavement production industry.

The next chapter outlines the methodology for the development of a simple triaxial test.

## References

- Botha, et al. (2005). **Investigation into the early trafficking of emulsion treated (ETB) foamed bitumen (FB) bases treated in combination with cement and cement (OPC) only.** TREMTI 2005: Treatment and Recycling of Materials for Transport Infrastructure. 2nd International Symposium, Paris, France, 24-26 October, 2005, pp. 1-10
- Crockford W.W., Berthelot C., Tritt B. and Sinadinos C., 2002. **Rapid Triaxial Test.** Journal of the Association of Paving Technologies, Volume 71. Colorado Springs, Colorado. March, 2002
- Dynatest, 2008. [www.dynatest.com/hardware/CSIR/k-mould.html](http://www.dynatest.com/hardware/CSIR/k-mould.html). Accessed on 2008/07/21
- Ebels L.J., 2008. **Characterisation of Material Properties and Behaviour of Cold Bituminous Mixtures for Road Pavements.** PhD Dissertation, Department of Civil Engineering, Faculty of Engineering, University of Stellenbosch, South Africa.
- Ebels, L.J. and Jenkins, K.J., 2006. **Performance Models of Bitumen Emulsion Treated Materials for Semmaterials.** Institute for Transport Technology University of Stellenbosch, 2006.
- Gould J.S., Nanagiri Y.V., Mallick R.B., Petruccelli J. D. and Crockford W.C., 2002. **Evaluation of Rapid Triaxial Test in Quality Control of Hot Mix Asphalt,** TRB 1832. Pp 191-200.
- Huurm M., 1997. **Permanent Deformation in Concrete Block Pavements.** PhD Dissertation. Delft University of Technology, Netherlands
- IPC Global, 2008. [www.ipcglobal.com.au/pavement.html](http://www.ipcglobal.com.au/pavement.html). Accessed on 2008/07/21
- Jenkins K.J., 2000. **Mix Design Considerations for Cold and Half-Warm Bituminous Mixes with Emphasis on Foamed Bitumen.** PhD Dissertation, Department of Civil Engineering, Faculty of Engineering, University of Stellenbosch, South Africa.
- Jenkins, K.J. and Ebels, L.J., 2007. **Determination of Shear Parameters, Resilient Modulus and Permanent Deformation Behaviour of Unbound and Bound Granular Materials Using Tri-Axial Testing on 150mm Ø x 300mm High Specimens.** Technical Memorandum. Stellenbosch, South Africa, 2007.
- Jenkins K.J., 2008. **Lecture Notes on Hitchhiker's Guide to Pavement Engineering.** Flexible Pavement Design Course University of Stellenbosch, February 2008.
- Molenaar AAA, 2005. **Cohesive and Non-cohesive Soils and Unbound Granular Materials for Bases and Sub-bases in Roads.** Lecture Notes Delft University of Technology presented during Flexible Pavement Design at Stellenbosch University, February 2008.
- Rico Rodriguez A., del Castillo H., Sowers G. F., 1988. **Soil Mechanics in Highway Engineering.** *Trans Tech Publications.* ISBN 0-87849-072-8. Pp 15
- Texas Department of Transport, 2002. **Triaxial Compression for disturbed soils and base materials,** TxDOT Designation: Tex-117-E, August 2002.
- Theyse, H. L. M. de Beer, and F. C. Rust. **Overview of the South African Mechanistic Pavement Design Method.** *Transportation Research Record 1539,* TRB, National Research Council, Washington, D.C., 1996, pp. 6–17.
- UWP Consulting (PTY) Ltd, 2004. **Draft Report on Comparison of Base Course Materials Using Texas Triaxial Test Method.** Western Cape Provincial Administration Department of Transport and Public Works. 2004

- Vuong, Binh T, Hazell, David, 2003. **Development of performance-based specifications for unbound granular materials: Issues and recommendations.** Road and Transport Research, Dec 2003
- Van Niekerk, A.A. van Scheers J. and Galjaard P.J., 2000a. **Resilient Deformation Behaviour of Coarse Grained Mix Granulate Base Course materials from Testing Scaled Gradings at Smaller Specimen Sizes.** UNBAR 5 Conference, University of Nottingham
- Van Niekerk, A.A. van Scheers J., Muraya P. and Kisimbi A., 2000b. **The Effect of Compaction on the Mechanical Behaviour of Mix Granulate Base Course Materials and on Pavement Performance.** UNBAR 5 Conference, University of Nottingham.
- Van Niekerk, A.A., 2002. **Mechanical Behaviour and Performance of Granular Bases and Subbases.** PhD Dissertation. Delft University of Technology. Delft, 2002.

## **4. METHODOLOGY**

### **4.1. Introduction**

This chapter describes the research methodology for the development of a simple triaxial cell. It includes analysis of survey findings regarding facilities, testing capacity and available resources at civil engineering laboratories in South Africa. The chapter describes in detail the conceptualization part of the development phase. It discusses various options considered building to the final design, manufacture and assembly of the simple triaxial test.

### **4.2. Civil engineering laboratory survey**

In a bid to develop a simple triaxial test relevant to the local road construction industry, the author conducted a survey aimed at investigating facilities, testing capacity and resources that are currently available with civil engineering laboratories in the South Africa. A questionnaire (Appendix 2) was therefore distributed to sixteen (16) SANAS (South African National Accreditation System) accredited civil engineering laboratories commercially operating in the country. The targeted laboratories and their contact details are listed in Appendix 3.

Eight out of sixteen targeted responses were received representing a 50% response rate. The findings from the survey (Appendix 4) had provided guidance with regard to the nature and sophistication of any new tests to be developed.

The survey also highlighted some of the limitations and lack of sophistication of the current loading frames used for CBR and UCS testing such as lack of electronic LVDTs, limited overhead space, limited loading capacity etc. Most laboratories would need to invest in new loading facilities to carry out triaxial tests.

### **4.3. Design approach**

After analysing the specimen assembly procedures of the Texas triaxial test procedure (TxDOT, 2002) and the monotonic triaxial test procedure obtained in the Technical Memorandum (Jenkins et al, 2007), it was concluded that two main factors contribute to the complexity of the geotechnical triaxial cell namely the time it takes to assemble the specimen accurately in the cell resulting from paying attention to many details such as placing membrane with its O-rings on the specimen and on platen disks. Secondly the inherent design of the cell which makes it water and/or air tight at relatively high pressures. Therefore, the general approach of the simple triaxial cell development was aimed at finding simple solutions to these factors.

## 4.4. Conceptualisation

To achieve simple solutions to the general approach of the simple triaxial cell development, several ideas were considered and given reality checks including:

### 4.4.1. The tube concept

The tube concept is an idea which originated from personal discussions between Prof M.F.C. Van de ven and Prof K. J. Jenkins in the 1990's. With this concept the specimen acts like a 'rim' and the cell acts like a 'tyre' providing confinement to the tube as illustrated in Figure 30. This concept eliminates the need for the cell to be air tight as pressurized air is contained in the tube. It also eliminates the need to fit membrane and O-ring on the specimen.



**Figure 30: Illustration of tube concept**

However, the challenge with this concept was to find the tube that could meet the dimensional requirement for the specimen (150mm  $\varnothing$  x 300mm height). The initial thought was that this tube would be obtainable off the shelf from tyre and tube suppliers. However, this later proved to be impossible in the tyre industry where tubes take a geometric shape of a torus (Figure 31), which is a surface of revolution generated by revolving a circle in three dimensional space about an axis coplanar with the circle. The size of tube is most commonly described by suppliers using two pieces of information in the size number format of xxx – yy. The first number, 'xxx', is related to the size of the tube across the width of the tyre in millimetres. The second, 'yy' is the diameter across the rim in inches. For example, a 750 – 20 tube is for a 20" rim.

Therefore, if a specimen size of 150 mm  $\varnothing$  x 300 mm is taken as a rim, allowing for maximum total deformation of 30 mm in diameter, the rim size for the tube would be 7 inches. The depth of the tube should be adequate to cover the specimen height and can be taken to be minimum of 300 mm. The profile or aspect ratio should be as low as possible in order for the casing to be of reasonable size in diameter. Calculations resulted in the size of the tube too odd to be available on the market, moreover it was doubtful whether the circular tube designed to wrap around a rim would interact evenly in the vertical direction of the cylindrical edge of the specimen even under rigid confinement.

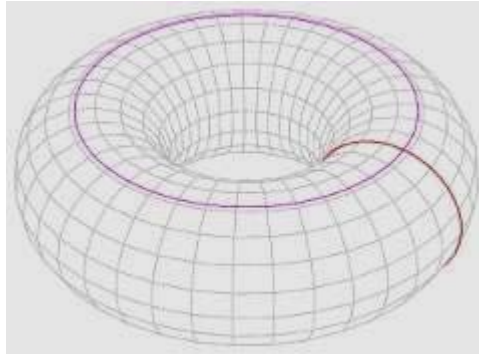


**Figure 31: Torus - shape of common tube** (Wikipedia, 2007)

If the tube concept was to work, it required the making of a special tube like an elliptical tube shown below in Figure 32. This type of tube would fit more evenly around the cylindrical specimen and the aspect ratio would not be too big. However, the machinery required to manufacture/mould a tube of this type could not be obtained locally and even if importing a mould was to be considered as an option, it would require a special order from mould manufacturers in China. It became apparent that the 'tube concept' had hit a serious setback.

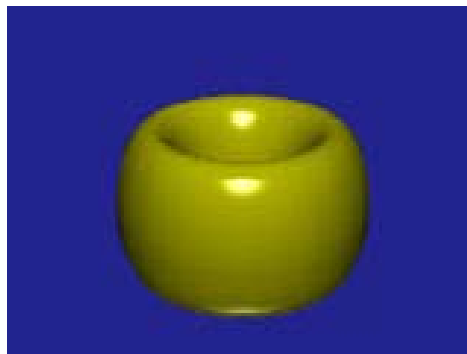


**Figure 32: Elliptical tube** (Wikipedia, 2007)

#### **4.4.2. Other concepts**

The subsections below describe some other concepts which were considered and were given a reality check especially when the tube concept proved impractical.

##### **4.4.2.1. The bottle concept**

This concept illustrated in Figure 33 was based on the simple approach of getting the specimen in an impermeable membrane like sack, tying it to the top by a mechanical clamp, and there after pressurize the cell and apply the loading. Though indeed very simple, a practical consideration showed that the membrane in the Detail A would not last under pressure and it was not clear whether such a mechanical clamp would clamp down the membrane to the casing at high pressures. It is also not the best idea to have to extract the specimen from the casing/cell using a membrane.

#### 4.4.2.2. The bottle and sandwich concept

The Bottle and Sandwich Concept shown in Figure 34 was a modification of the Bottle Concept by introducing bolt and nut connection to sandwich the membrane between hollow cylinders of the cell. The reality check indicated that the bolt and nut provided an added complication that defeated the purpose of a simple triaxial test.

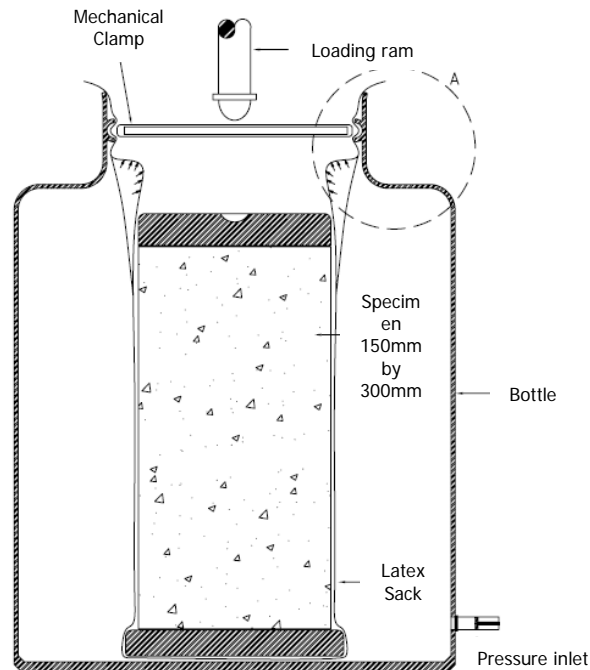


**Figure 33: Sketch of the bottle concept**

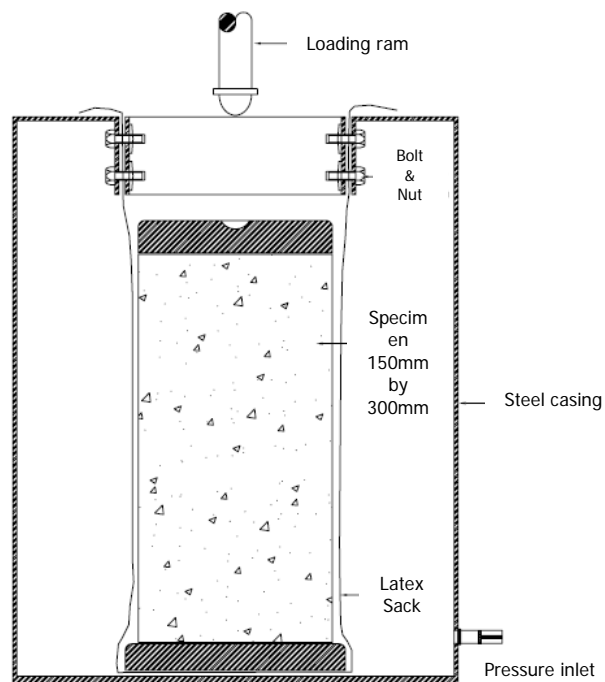


**Figure 34: Sketch of the bottle and sandwich concept**

#### 4.4.2.3. Encapsulated tube concept

More concepts were investigated the other one, the Encapsulated tube concept illustrated in Figure 35 below. The reality check on this one eliminated the concept on the basis of availability of right tube and on how the tube would behave whilst containing pressurized air in the corner spaces between the specimen, platen disks and tube. The tube would obviously tend to be squeezed into the space and with the movement of the specimen under loading, it would be pinched and fail.

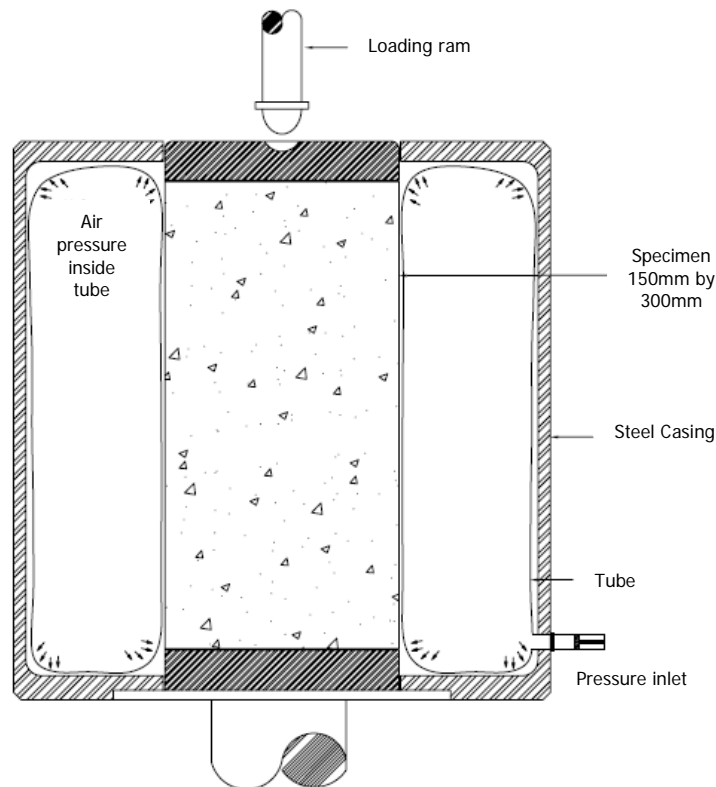


**Figure 35: Encapsulated tube concept**

### 4.5. The break through

Following difficulties encountered in acquiring a tube of standard size from the market and with other concepts considered in this study, the tube concept was revisited this time with increased efforts to improvise the needed odd sized tube. This resulted in the focus of manufacturing the latex membrane at the University of Stellenbosch Civil Engineering Laboratory, which could be used as the tube fitting the 150mm diameter by 300mm height specimen.

#### 4.5.1. Trials

To put the idea to test, a large scale triaxial membrane was used in the trials aimed at establishing the possibility of making the membrane into a tube by joining the two ends of the membrane and to find out what pressure the tube can withstand, while fitted around the specimen and in a

confinement similar to what can be obtained in a simple Triaxial setup. The following was the procedure which was undertaken in the trial test:

- The ends of the membrane were washed and sanded as a preparation measure to make a solid joint with the adhesive. The two ends were joined carefully to make a tube, 435 mm deep and just fitting around a 150 mm diameter specimen as shown in Figure 36 through to Figure 39.
- Confinement to simulate what would happen in the triaxial cell, with the exclusion at this stage of the dilating effect of axial loading on the specimen, was provided by 8mm thick PVC pipe with height equal to that of the tube was prepared. PVC disks were also screwed on each end after setting up the specimen and tube in the pipe. This ensured an all round confinement as illustrated below.



**Figure 36: Valve fitted on membrane**



**Figure 37: Top view of trial set-up**



**Figure 38: All round confinement**



**Figure 39: Trial cell pressure testing**

Compressed air was gradually applied to the cell as seen in Figure 39. The cell withstood a pressure of 260 kPa. The fact that latex membranes could be made at US laboratories and that it could be joined using contact adhesive to make a tube that fits the required specimen size and could withstand a pressure of over 200 kPa under confinement showed that a simple triaxial testing using a 'tube concept' was practical.

#### 4.5.2. Latex membrane drum and tube making

An investigation was therefore, undertaken which took the concept in the trial further. It included taking the latex material to an adhesive manufacturer (Bondstick of 18 Benbow Avenue, Epping, Cape Town) to conduct experiment on the material and design glue that will be durable. Secondly, designing and manufacturing of a drum that would be used to produce the required size of the tube.

##### 4.5.2.1. Latex membrane drum design

After studying the relationship between the size of the membrane and the tube size required to fit the specimen size, the following relationship was established to exist between the latex drum used to make the membrane and the tube made thereof:

The height (h) of the tube is approximately equal to half the circumference (C) of the drum less 5% of tube height, expressed simply as in Equation 10.

$$h = \frac{\pi r}{1.05} \quad \text{Eq. 10}$$

Where, h is the height of the tube; and  
r is the radius of the drum size.

From Equation 10 and given the depth of the required tube as approximately **320 mm**, the diameter of the drum was found to be **214 mm**. The drum was then made and used in the membrane making device (see Figure 40) to produce 700 mm x 320 mm membrane shown in Figure 41. The membrane was then joined on both ends using the procedure described below and glue supplied by Bondstick to produce a latex tube for the STT shown in Figure 43.

##### 4.5.2.2. Tube making process

The following details the procedure and glue used to glue to ends of the membrane into a tube as supplied by Bondstick of Cape Town:

- Wipe all areas to be glued with BL561 and leave for 1 hour;
- Wipe the same areas with the HS112 mix and leave for a minimum of 30 min. Note that the HS112 must be mixed with Chlorine 902 (1 teaspoon of 902 to 1 litre of HS112) to activate before it is applied;
- Apply 738 adhesive to both sides to be glued and allow drying for minimum 30 minutes. Note also that to the 738 adhesive, add VAT 070 (approximately 5 % of the amount to be glued) to activate it before it is applied;
- Apply heat on both surfaces to be glued by means of heat gun or hair drier; and
- Put the two surfaces pressed together and leave overnight.



Figure 40: Membrane making



Figure 41: Produced membrane (700x320)



Figure 42: Valve fitted on tube



Figure 43: STT tube

## 4.6. The simple triaxial cell design

The design of a Simple Triaxial Cell (STC) for this project had taken into consideration the drawbacks of a long and inconvenient procedure of assembly of specimen in the triaxial cell that is associated with the standard (geotechnical) triaxial test. It is not always simple to place a latex membrane and rubber O-rings around specimen and platen disks and later on fastening six tie rods to the base plate. This takes time and a lot of attention to details is required, especially that care has to be taken not to damage the edges of the specimen and that the specimen must be centrally positioned on the base plate and the centre of the top cap must be aligned with the centre of the specimen.

### 4.6.1. Design aim

The purpose of the simple triaxial cell design was then to overcome the drawbacks of standard triaxial testing cell through considerable simplification by means of a new structure and procedure of assembly of specimen into the cell. This is aimed at specifically reducing time and steps required in the procedure.

### 4.6.2. Design and modelling

The basic concept of the simple triaxial cell is to use a steel casing comprising a latex tube which is then introduced around the specimen sitting on a base plate. This approach eliminates the use of

membrane, O-rings on the specimen and tie rods, as shown in Figure 44. The overall dimensions of the cell are 244mm diameter by 372mm height (see detailed drawings in Appendix 5). The cell comprises the base, hollow cylindrical steel casing, latex tube and top disk. The casing is introduced, with the tube in it, onto the base and held into position by simple mechanical clamps. Regulated air pressure is applied through pressure inlet valve.

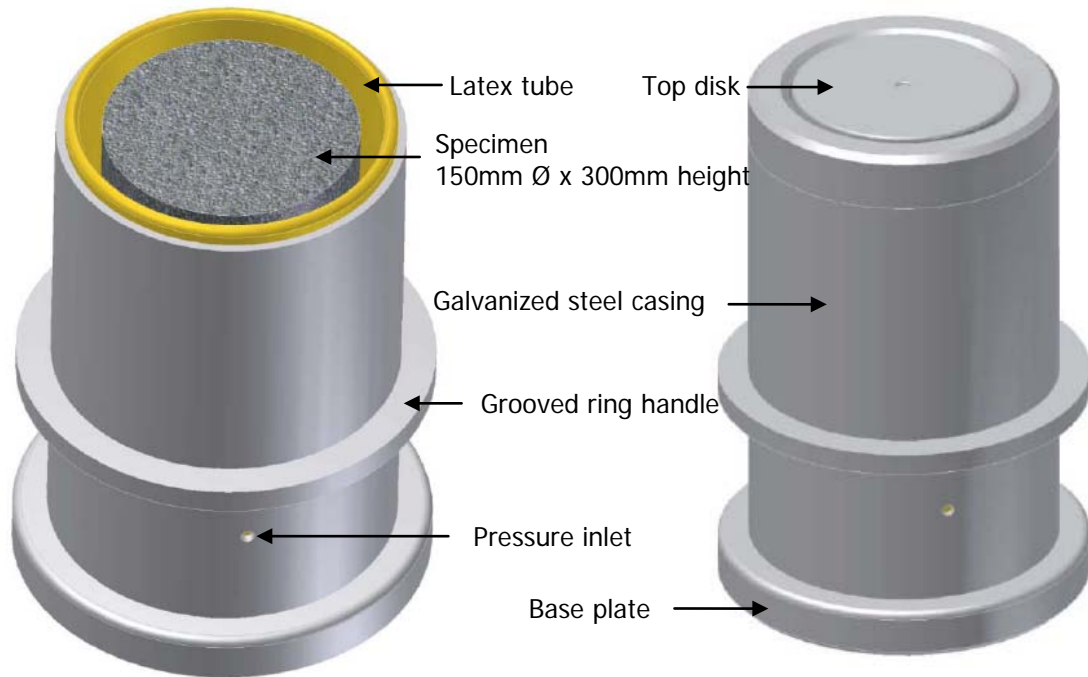


**Figure 44: STT 3-D models**

#### 4.7. Manufacture of the simple triaxial cell

Following a complete design, modelling and acquisition of materials required, the manufacture of a Simple Triaxial Cell parts was carried out in the Civil Engineering workshop at Stellenbosch University as can be seen on Figure 45 below (photos taken for quality control purposes).



**Figure 45: Steel case machining**

All machined parts were electro galvanised to give them good resistance against rusting. The following parts were machined including:

- Base;
- Top disk; and
- Casing including grooved ring handle.



**Figure 46: STT components**

#### **4.8. Assembly of parts**

Following successful machining, all parts were assembled to make the Simple Triaxial Cell. Trial tests were conducted to ensure the apparatus was working properly.



**Figure 47: Assembled STT cell**

#### **4.9. Closure**

This chapter presented the successful development process of the STT cell. From conceptualisation, design and modelling, through to manufacturing and assembly. Thereafter successful trial tests of the STT were conducted on 150 mm diameter by 300 mm high specimens. The next chapter, Chapter 5 on experimental program will detail the methodology employed in specimen preparation describing in detail the material, compaction and curing procedures used to prepare specimens. The next chapter will also describe the test equipment and procedure used for both STT and RTT.

## 5. EXPERIMENTAL PROGRAM

### 5.1. Introduction

This chapter presents a detailed discussion of the materials, equipment, test procedures and data collection and analysis techniques deployed under this research. The test program was limited to the monotonic failure test type of triaxial test conducted with the Simple Triaxial Test (STT) and parallel monotonic failure tests conducted with the Research Triaxial Test (RTT).

### 5.2. Materials and specimen preparation

#### 5.2.1. Mineral aggregates

Two types of materials were identified for specimen preparation in this study. They included Reclaimed Asphalt Pavement (RAP) and a hornfels blended material obtained from N7 rehabilitation project site, and base-course aggregate (G2) obtained from Lafarge Tygerberg Quarry.

##### 5.2.1.1. Hornfels (RAP)

Reclaimed asphalt pavement (RAP) Hornfels with maximum aggregate size of 19 mm was used with grading as shown in Figure 48 below. Selected materials were stabilized with bitumen emulsion (ANiB SS-60). The residual binder content for Hornfels was 2%. Stabilised materials were tested with both 0% and 1% active filler (i.e. cement).

The target sample mass for a specimen was determined based on the grading shown in Figure 48 and materials target MDD. The correct proportions of fraction were then weighed off to reconstitute a sample thus ensuring a consistent grading across all samples. Grading constitution per sample is tabulated in Table 7.

**Table 7: Grading constitutions per 12 kg sample**

<b>Hornfels (RAP)</b>		
MDD =	2177.3	(kg/m <sup>3</sup> )
OMC =	5.12	(%)
Stockpile	Ratio in Blend	Mass in Blend (Kg)
19.0 - 13.2	6.90%	0.828
13.2 – 4.75	40.60%	4.872
4.75 - 2.36	16.00%	1.920
(0.075 – 2.36)	36.49%	4.379
<b>Total</b>	<b>100.0%</b>	<b>12.00</b>

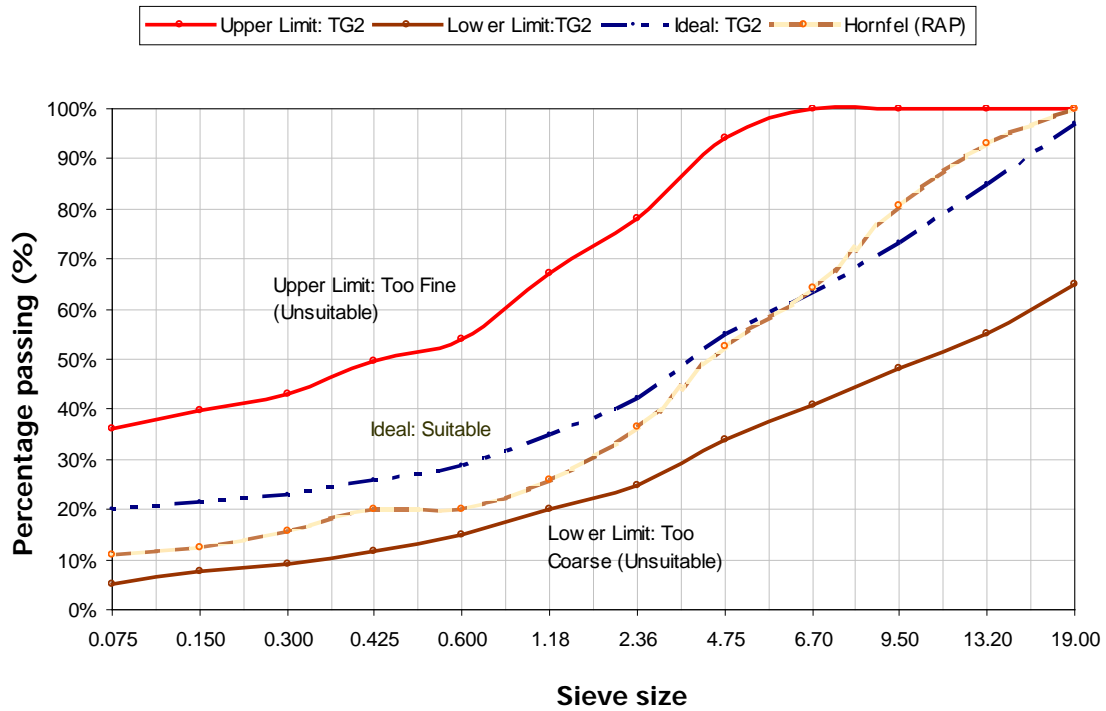


**Figure 48: Grading curve for Hornfels (RAP) mineral aggregates relative to suitable limits for the BSMs.**

The test matrix with Hornfels (RAP) involved two mixes namely emulsion + 0% cement and emulsion + 1% cement, producing 16 specimens for both STT and RTT tests. Table 8 below shows the matrix of the tested mixes with Hornfels (RAP) as aggregate.

**Table 8: Testing matrix for Hornfels (RAP)**

Item	Simple Triaxial Test (STT)		Research Triaxial Test (RTT)	
	Emulsion + 0% Cement	Emulsion + 1% Cement	Emulsion + 0% Cement	Emulsion + 1% Cement
Hornfels (RAP) + 2% Residual Binder				
Total No. of Specimens	3	5	3	5
Confining Pressure, $\sigma_3$ (kPa) x no. of specimens	50 x 1 specimen	50 x 1 specimen	50 x 1 specimen	50 x 1 specimen
	100 x 1 specimen	100 x 3 specimen	100 x 1 specimen	100 x 3 specimen
	200 x 1 specimen	200 x 1 specimen	200 x 1 specimen	200 x 1 specimen

5.2.1.2. Base-course aggregate (G2)

Base-course aggregate (G2) material with maximum aggregate size of 37.5 mm was obtained from the quarry. A comparative grading analysis was performed to investigate any discrepancies on

selected sample in comparison with the grading analysis obtained with the material from Lafarge Tygerberg Quarry. According to the grading analysis (see Figure 49), the material's grading was well within TRH 14 limits set for G2 materials.

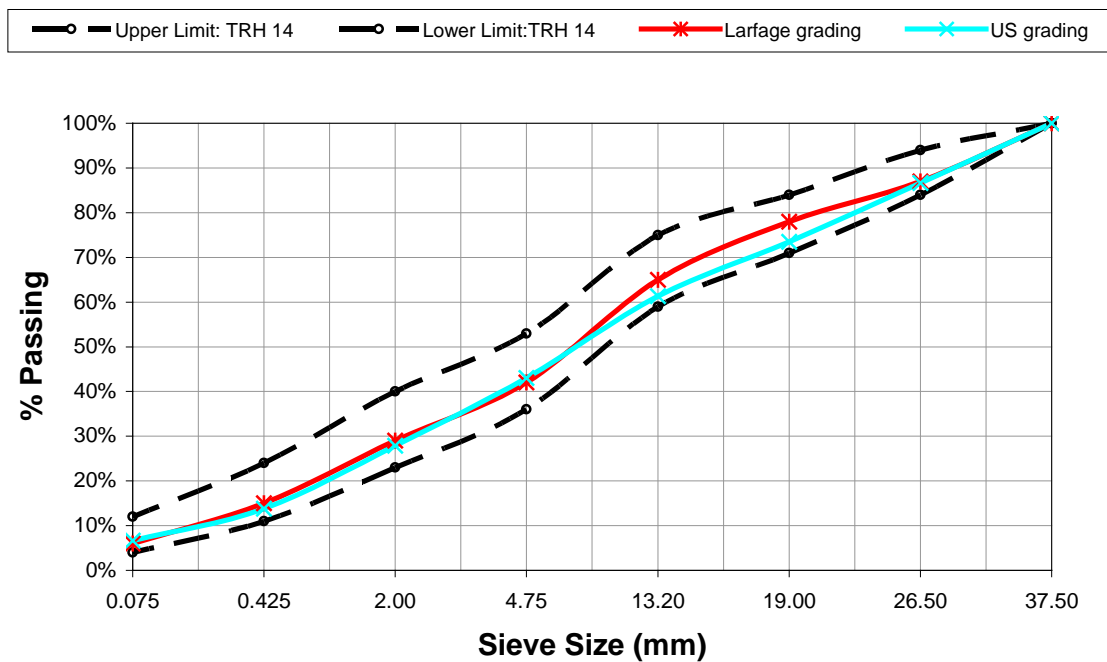


**Figure 49: G2 grading curve relative to Lafarge grading and TRH 14 limits**

Because aggregate sizes greater than 19 mm are considered too large for specimen diameter of 150 mm, all aggregates retained on the 19 mm sieve in the initial grading were crushed and then re-added to the sample for another grading analysis as shown in Figure 50.

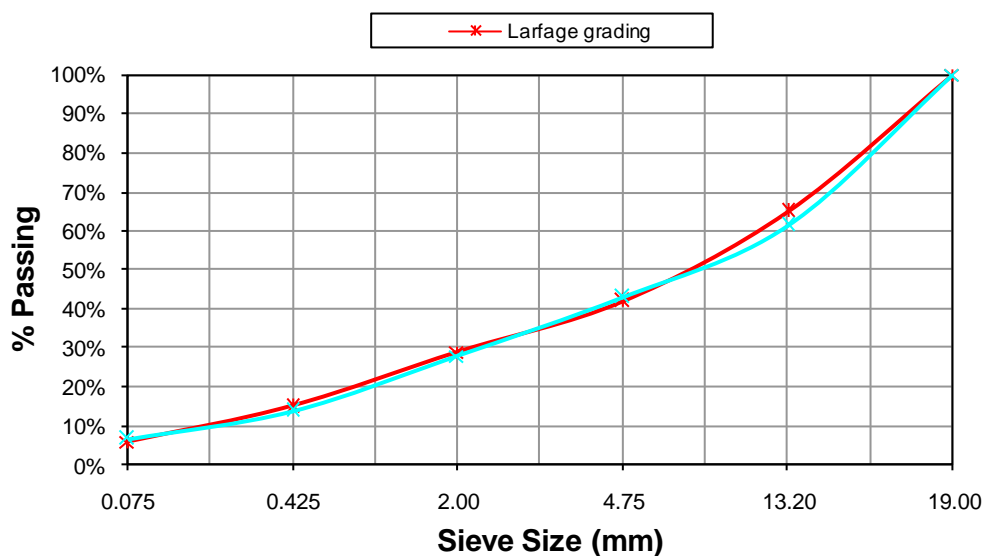


**Figure 50: Adjusted G2 grading**

As with Hornfels (RAP), the target sample mass for a specimen was determined based on the grading shown in Figure 50 and the MDD obtained by Mod AASHTO compaction (see Figure 51). The correct proportions of fraction were then weighed off to reconstitute a sample thus ensuring a consistent grading across all samples. Grading constitution per sample is tabulated in Table 9 below.

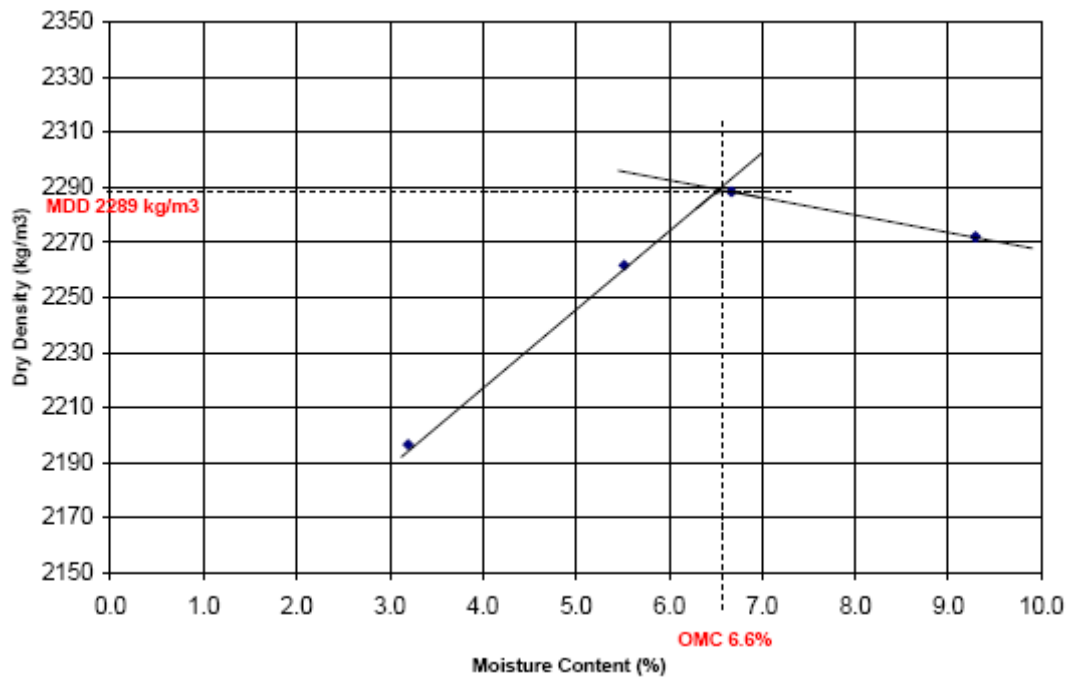


Figure 51: Mod AASHTO Density - Moisture relationship for G2 material

Table 9: Grading constitutions per 13.5 kg sample

G2 Material		
MDD =	2289	(kg/m <sup>3</sup> )
OMC =	6.6	(%)
Stockpile	Ratio in Blend	Mass in Blend (Kg)
19.0 - 13.2	32.11%	4.33
13.2 - 4.75	26.71%	3.61
4.75 - 2.36	14.75%	1.99
(0.075 - 2.36)	26.43%	3.57
<b>Total</b>	<b>100.0%</b>	<b>13.5</b>

It can be noted that the sample mass for a G2 material specimen is higher (13.5 kg) than that of the Hornfels (RAP) specimen (12.0 kg) despite having the same diameter (150 mm) and height (300 mm). The reason for this discrepancy is due to different target densities which meant that more material is needed to meet the MDD with G2 material than for RAP Hornfels with lower MDD. It was

also observed initially with the Hornfels (RAP) mineral aggregates that producing a 150 mm by 300 mm specimen from 12 kg of material left little material to work with for the purpose of moisture at mixing determination thus it was decided to increase the sample mass per specimen.

The test matrix with G2 material involved two mixes namely G2 + 0% cement and G2 + 1% cement, producing 12 specimens for both STT and RTT tests. Table 10 below shows the matrix of the tested mixes with G2 material as aggregate.

**Table 10: Testing matrix for G2 material**

Item	Simple Triaxial Test (STT)		Resear ch Triaxial Test (RTT)	
	G2 + 0% Cement	G2 + 1% Cement	G2 + 0% Cement	G2 + 1% Cement
Total No. of Specimens	3	3	3	3
Confining Pressure, $\sigma_3$ (kPa) x no. of specimens	50 x 1 specimen	50 x 1 specimen	50 x 1 specimen	50 x 1 specimen
	100 x 1 specimen	100 x 1 specimen	100 x 1 specimen	100 x 1 specimen
	200 x 1 specimen	200 x 1 specimen	200 x 1 specimen	200 x 1 specimen

Therefore in total four mixes were investigated using 28 specimens (150 mm by 300 mm diameter). Additional specimens were also prepared for STT trials but these have been excluded from this report.

### 5.2.2. Binder

The binder used in this study was bitumen emulsion (ANiB SS-60) which is type B stable grade Anionic emulsion with 60% residual binder. The bitumen emulsion content of 3.3 % representing 2 % residual binder was used for the treatment of the Hornfels RAP blends.



**Figure 52: Bitumen emulsion (ANiB SS-60)**

### 5.2.3. Moisture content and mixing process

The optimum moisture content (OMC) and maximum dry density of the selected materials were determined by Modified AASHTO compaction as summarised in Table 11 for the two selected blends. The hygroscopic moisture in the mineral aggregates was 0.5 % for RAP and 0.3 % for G2 material.

**Table 11: Summary of OMC and MDD of blends**

Blend	Compaction	OMC (%)	MDD (kg/m <sup>3</sup> )
Hornfels RAP	Mod AASHTO	5.1	2177.3 (field comp)
G2 material	Mod AASHTO	6.6	2289

All the mixes performed in this study were mixed in a standard laboratory vertical shaft mixer, shown in Figure 53.



**Figure 53: Laboratory vertical shaft drum mixer**

The moisture content of the aggregate during mixing with the bitumen emulsion was 65% of OMC and 70% of OMC for the G2 material. The mixing moisture was initially added and mixed for one minute. Then the aggregate was sealed in a bag and left for three hours to allow absorption of the moisture.

In the case of emulsion mixes with 1% cement, addition of cement took place before adding emulsion and mixing for one minute, followed by addition of emulsion and again mixing for another minute. After stabilization the mixture was sealed in a bag. The emulsion mixture was placed in an oven at 40°C for 30 minutes to assist initial breaking of emulsion before compaction.

### 5.2.4. Compaction

Compaction is a process by which mechanical energy is used to increase the density of a given material. The density is increased by removing air from the pores of the material aimed at improving material strength (and stiffness), reducing voids in the material, decreasing permeability and producing a consistent product.

The degree of compaction is measured in dry density which refers to the mass of solids per unit volume of material. If the bulk density of a material  $\rho_b$  and the water content  $MC$  (% of dry mass) are known, then the dry density  $\rho_d$  is given by:

$$\rho_d = \frac{\rho_b}{1 + MC} \quad \text{Eq. 11}$$

The density of a given material therefore, depends on the type of material, its grading, water or moisture content and energy applied. After using a certain compaction technique, the bulk density and OMC is determined from which the MDD is calculated. For a given material, the compaction is repeated at least five times for different moisture contents to obtain a density – moisture curve; see Figure 51.

The compaction of a 150 mm X 300 mm sample of BSM-emulsion and G2 material was carried out using a vibratory hammer, the Bosch GSH 11E® (see Figure 54), with a surcharge of 10 kg mounted in a frame. Compaction of the material was performed with the aggregate at room temperature.

The sample was compacted in 5 layers in a mould 300 mm high with a diameter of 150 mm. From the target dry density information, the mass of material required per 60mm layer thickness was determined. Spot drilling (10-15 mm deep) on underlying layer was carried out in order to scarify the layer so as to create an interlocked joint.

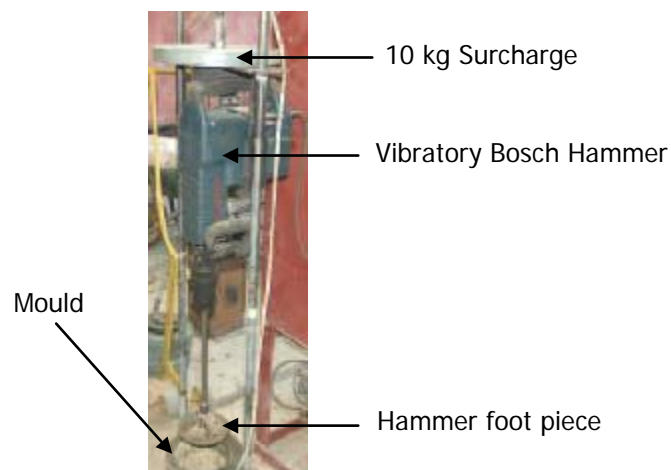


**Figure 54: Mounted vibratory Bosch Hammer** (Kelfkens, 2008)

The following compaction procedure for using vibratory hammer was followed based on work done by Kelfkens, (2008):

Step 1: The moisture density relationship of the untreated (non-stabilised) sample to be tested was determined according to the THM 1 Method A7 procedure (see Figure 51 obtained for G2 material);

Step 2: The target moisture content was calculated as a percentage of OMC determined in Step 1 (65 % and 70 % was used for emulsion and G2 mixes respectively).

Step 3: Using the relationship developed in Step 2 and the target moisture content of Step 3, the target dry density was determined based on Equation 10;

Step 4: From the target dry density of Step 3, the mass of the final compacted specimen was calculated, using Equation 12 below:

$$M_{sp} = \frac{\rho \cdot V}{1 + MC} \quad \text{Eq. 12}$$

Where;

$M_{sp}$  = Mass of compacted specimen;

$\rho$  = Target dry density;

$V$  = Volume of the mould; and

$MC$  = Target moisture content.

**Note** that to  $M_{sp}$  add approximately (1-2) kg of material to allow for moisture content determination by means of standard oven drying method (TMH 1);

Step 5: The final mass derived in Step 4 is divided by 5 to obtain that mass of material to be compacted per layer (called the "layer mass"). Five layer mass samples for either BSM-emulsion or G2 material are then accurately weighed and placed in plastic bags;

Step 6: The mounted vibratory hammer is lowered into the empty mould and the hammer foot piece allowed to rest on the base of the mould. The position of the base on the right sleeve of the mounting head on the guide rod is clearly marked as 'zero line' (See Figure 55).

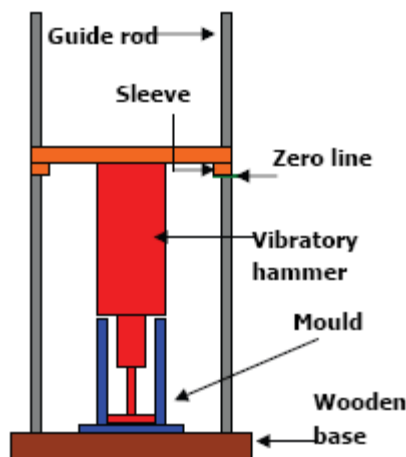


**Figure 55: Marking off Zero line** (Kelfkens, 2008)

Step 7: The mounted vibratory hammer is then raised, a distance of 60 mm measured from the zero line (using a 150 mm steel rule) and is clearly marked (using a permanent marker pen). This line denotes the target Dry Density.

Step 8: One of the five bags from Step 5 is taken and the material is poured into the mould;

Step 9: The mounted vibratory hammer is lowered into the mould until the foot piece rests on the surface of the material. The mounted vibratory hammer is switched on and the material is compacted until the base of the right sleeve reaches the marked point, indicating that the target density has been achieved for that layer (see Figure 56).

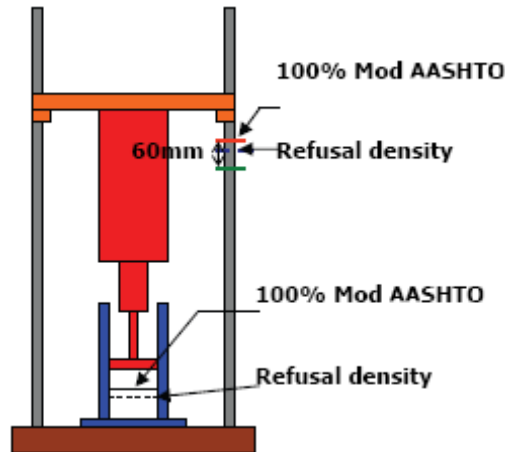


**Figure 56: Indicating target dry density - 100 % Mod AASHTO** (Kelfkens, 2008)

This procedure is repeated for the rest of the layers. The surface of each compacted layer is scarified by spot drilling (10 -15 mm) to ensure interlocking of layers.

The mould is 300 mm high and the required height of specimen is 300 mm therefore, to accommodate the loose material of the final layer mass an extension collar was attached by means of G-clamps as depicted in Figure 57 below.



**Figure 57: Photos showing extension collar attachment on mould**

### **5.2.5. Curing**

After specimens were compacted accelerated curing was performed on them. The curing procedure followed for BSM-emulsion was different from that followed for G2 material mixes as described in following sections.

#### **5.2.5.1. BSM-emulsion mixes**

The curing procedure used for BSM-emulsion mixes (with or without cement) involved placing compacted specimens in the draft oven at 30 °C for 24 hrs unsealed, followed by sealing and raising the temperature to 40 °C for 48 hrs. After curing the specimen was sealed in a different bag and left to cool at ambient temperature prior to the conditioning and triaxial testing.

#### **5.2.5.2. G2 material mixes**

Specimens made of G2 material mix with 0 % cement were not cured as such. After compaction the specimens were sealed at ambient temperature for 24 hrs to allow moisture distribution before triaxial testing was conducted on them.

Specimens of G2 material mix with 1 % cement were cured for seven days at a relative humidity of 95 to 100 % and a temperature of 25 °C in the concrete laboratory curing room, according to TMH1 method A14 procedure. After seven days the specimens were removed and conditioned before triaxial testing was conducted.

## **5.3. Simple triaxial test (STT) equipment and procedure**

### **5.3.1. Triaxial cell**

The Simple Triaxial Cell described in Section 4.6 of this report was used. The cell is designed to withstand confinement pressures required for a monotonic triaxial test with air as a confining agent.

The internal dimensions of the cell are large enough to accommodate a specimen with a maximum diameter of 150 mm and a height of 300 mm. The clearance between the specimen and the cell wall is sufficient to accommodate lateral deformation of the specimen and allow withdrawal of the cell casing with tube.

The cell prototype used was designed and manufactured at US under this study.

### **5.3.2. Testing system**

Triaxial testing was carried out using a testing system comprising an actuator, a reaction frame, a control panel and a data acquisition system. The Material Testing System (MTS 810, Model 318.10), which is a closed loop servo-hydraulic testing press system was used in this experiment for both STT

and RTT monotonic failure tests. The system uses MTS model 506.03 hydraulic power unit with high pressure supply of approximately 70,000 kPa. It has a 100 kN actuator with 80 mm stroke (up and down). The University's MTS was upgraded in February 2004 and is now operated by a MTS controller 407.

Data from the tests (load cell and MTS LVDT) can be captured on computer while the tests are in progress. The load and displacement measurements are adjusted by the MTS controller to a  $\pm 10.0$  V scale. This data is sent to the computer in binary format. The analogue-digital converter used is a 12 bit converter, which means that the load and displacement data is captured on a  $\pm 2048$  scale (-2048 is -10.0 V and +2048 is +10.0 V). The data is captured by a personal computer using a Pascal written program and stores the data on the computer in a file text format (.txt). This text format can be further analysed using spreadsheets.

For monotonic triaxial testing the load cell gain would be set to measure over the full capacity (98.1 kN).

### 5.3.3. Test procedure

The triaxial testing of the specimens was planned to take place within 48 – 72 hours after completion of the curing procedure. This delay was kept as constant as possible.

The following steps describe the procedure taken to assemble specimen in the simple triaxial cell and the cell in the loading frame:

- (i) Place the specimens, casing with tube, top disk and base plate in a climate chamber and condition them overnight at 25°C.
- (ii) Lightly grease the sides of the top disk and base plate to reduce friction as much as possible.



- (iii) Place the specimen in the middle of the base plate.



- (iv) Carefully introduce the casing, comprising the tube, around the specimen. Take care not to damage the edges of the specimen during this procedure.



- (v) Clamp the casing in position on to the base plate using simple mechanical clamps on the casing.



- (vi) Put the top disk on top of the specimen.



(vii) Place the cell in the hydraulic loading frame; adjust actuator position until visual contact is made with the loading ram.

(viii) Connect the air supply to the cell; open the regulator and valve on the cell pressure port until the cell pressure is stable at the desired level.



(ix) Set monotonic test parameters on the MTS controller including displacement rate of strain (2.1%), full-scale for the loading (10.0V = 98.1 kN) and half-scale for the displacement (10.0V = 40mm)



(x) Ready to run test.

At least three specimens of comparable density and moisture content were selected. The specimens to be tested were assembled in the triaxial cell according to the procedure above.

The testing system was operated in displacement control mode. The cell pressures for a series of monotonic tests performed are 50kPa, 100 kPa and 200 kPa. Monotonic triaxial testing was carried out by compressing the specimen at a constant rate of displacement of 2.1 mm/min. The load versus displacement was recorded during the test with a minimum sampling rate of 10 Hz, as well as the cell pressure, temperature and specimen identifier.

Testing and recording cease when the total displacement exceeds 18 mm (6% strain) or when the specimen bulges excessively before the end displacement is reached.

The procedure was repeated for the rest of the specimens until all specimens have been tested at the three levels of confining pressures.

After completion of a test, the specimen was removed by first holding the actuator to its current position, then closing the valve on the cell pressure port and releasing the cell pressure by

disconnecting the pressure supply tube to the cell. The actuator is then turned to a position whereby the cell can easily be removed from the loading frame.

A sample between 500 and 1000 g of material is taken from the middle of the tested specimen for moisture determination during testing according to the procedure given in TMH1 Method A7.

#### 5.3.4. Calculation

- (i) Determine the applied failure load  $P_{a,f}$  for each specimen tested. The applied failure load is defined as the maximum applied load during the test. Calculate the applied failure stress  $\sigma_{a,f}$ :

$$\sigma_{a,f} = \frac{P_{a,f}}{A} \cdot 10^{-3} \quad \text{Eq. 13}$$

Where,

$\sigma_{a,f}$  = applied failure stress [kPa]

$P_{a,f}$  = applied failure load [N]

$A$  = end area of a cylindrical specimen at beginning of test [m<sup>2</sup>]

- (ii) Calculate the major principle stress at failure ( $\sigma_{1,f}$ ) for each tested specimen:

$$\sigma_{1,f} = \sigma_{a,f} + \sigma_{dw} \quad \text{Eq. 14}$$

Where,

$\sigma_{1,f}$  = major principle stress at failure [kPa]

$\sigma_{a,f}$  = applied failure stress [kPa]

$\sigma_{d,w}$  = pressure resulting from dead weight of top disk and loading ram [kPa]

- (iii) According to Jenkins et al (2007), the relationship between  $\sigma_{1,f}$  and confining stress ( $\sigma_3$ ) is described by:

$$\sigma_{1,f} = A \cdot \sigma_3 + B \quad \text{Eq. 15}$$

Where,

$$A = \frac{1 + \sin \varphi}{1 - \sin \varphi} \quad \text{And} \quad B = \frac{2 \cdot C \cdot \cos \varphi}{1 - \sin \varphi}$$

Values of A and B can be determined by performing a linear regression analysis on the combinations of  $\sigma_{1,f}$  and  $\sigma_3$  per mix.

- (iv) Values of  $\varphi$  [°] and C [kPa] can be calculated as follows:

$$\varphi = \sin^{-1} \left( \frac{A-1}{A+1} \right) \quad \text{And} \quad C = \frac{B(1 - \sin \varphi)}{2 \cdot \cos \varphi}$$

## 5.4. Research triaxial test (RTT) equipment and procedure

Parallel monotonic failure testing with the RTT was carried out on specimens of comparable density and moisture to determine if the results obtained from the STT on similar specimens are comparable thus providing a means of validating data obtained from the Simple Triaxial Test. Parallel testing with the Research Triaxial Test was conducted according to the triaxial testing protocol that was developed at Stellenbosch University (Jenkins et al, 2007). Ideally a parallel test set-up is expected to be a 'perfect' benchmark set-up to provide ground for comparison. However, the situation was not always so for the particular parallel test used in this study, modifications to the research (geotechnical) triaxial cell had to be made in order for it to accommodate 150 mm diameter by 300 mm deep specimens which were tested with the STT. As depicted in Figure 58 below, a double flanged pipe was used to extend the height capacity of the research triaxial cell.



**Figure 58: Height extension of the RTT**

The introduction of a flanged pipe (extension) added an additional strain on the operator's effort to assemble specimen in the cell according to the test procedure obtained in the Technical Memorandum (Jenkins et al, 2007). As shown in Figure 59, the pipe extension is bolted down by six bolts which have to be screwed and unscrewed for each specimen tested, this is besides six other thumb screws to connect it to the rest of the cell.



**Figure 59: Bolting of the pipe extension**

The test system used and data capturing was the same as for the STT including displacement rate of strain of 2.1 mm/min, full-scale for the loading (10.0 V = 98.1 kN) and half-scale for the displacement (10.0 V = 40 mm).

#### 5.4.1. Calculation

- (i) Determination of the applied failure load  $P_{a,f}$  for each specimen tested and calculation of the applied failure stress  $\sigma_{a,f}$ . Equation 13 is used.
- (ii) Calculate the major principle stress at failure ( $\sigma_{1,f}$ ) for each tested specimen:

$$\sigma_{1,f} = \sigma_{a,f} + \sigma_3 + \sigma_{dw} \quad \text{Eq. 16}$$

Where,

$\sigma_3$  = confining pressure during the test [kPa]

$\sigma_{1,f}$  = major principle stress at failure [kPa]

$\sigma_{a,f}$  = applied failure stress [kPa]

$\sigma_{d,w}$  = pressure resulting from dead weight of top disk and loading ram [kPa]

- (iii) Linear regression analysis leading to the determination of mechanical properties C and  $\phi$  is performed according to the calculation method for STT described in 5.3.4 based on Equation 15.

#### 5.5. Closure

This chapter presented the type of materials and experimental methods used to make specimens and test them for both STT and RTT. The results obtained are presented in the next Chapter 6.

## 6. TEST RESULTS AND FINDINGS

### 6.1. Test specimens

Twenty eight (28) specimens in total were prepared from four mixes for monotonic triaxial tests of both STT and RTT. Characteristics of specimens prepared including mix, height, weight, moisture content and dry and relative density have been summarised in this section.

#### 6.1.1. Specimen characteristics for STT

**Table 12: BSM-emulsion specimens for STT**

Item No.	Specimen No.	Height [mm]	Cured Mass [g]	MC [%] After testing	Dry Density After curing [kg/m <sup>3</sup> ]	Relative Density*
1	E+0C_1	302	11650.1	3.1	2182.98	1.00
2	E+0C_2	302	11637.5	3.2	2180.62	1.00
3	E+0C_3	302	11668.5	2.8	2186.43	1.00
4	E+1C_1	304	11449.7	2.2	2131.32	0.98
5	E+1C_5	302	11352.7	2.4	2127.26	0.98
6	E+1C_6	302	11385.5	2.8	2133.40	0.98
7	E+1C_9	304	11639.7	2.0	2166.69	1.00
8	E+1C_10	299	11353.0	5.6	2148.66	0.99
Average		302	11517.1	3.0	2157.17	0.99
Standard deviation		1.6	144.4	1.1	24.97	0.01

\* Calculated as: Specimen dry density/MDD (2177.3 kg/m<sup>3</sup>) obtained in the field – N7 site; see Table 7 in Section 5.2

**Table 13: G2 material specimens for STT**

Item No.	Specimen No.	Height [mm]	Cured Mass [g]	MC [%] After testing	Dry Density After curing [kg/m <sup>3</sup> ]	Relative Density*
1	G2+0C_1R	305	12427.5	4.0	2305.75	1.01
2	G2+0C_4	305	12553.0	3.8	2329.03	1.02
3	G2+0C_5	306	12626.5	3.9	2335.01	1.02
4	G2+1C_3	308	12549.4	4.6	2305.68	1.01
5	G2+1C_5	304	12537.4	4.8	2333.79	1.02
6	G2+1C_6	307	12568.7	5.2	2316.75	1.01
Average		306	12543.8	4.4	2321.00	1.02
Standard deviation		1.5	65.0	0.6	13.5	0.01

\* Calculated as: Specimen dry density/MDD (2289 kg/m<sup>3</sup>) obtained from density – moisture relationship for G2 material; see Table 9 in Section 5.2

### 6.1.2. Specimen characteristics for RTT

**Table 14: BSM-emulsion specimens for RTT**

Item No.	Specimen No.	Height [mm]	Cured Mass [g]	MC [%] After testing	Dry Density After curing [kg/m <sup>3</sup> ]	Relative Density*
1	E+0C_4	302	11629.4	2.4	2179.10	1.00
2	E+0C_5	303	11623.7	2.5	2170.85	1.00
3	E+0C_6	302	11582.0	2.4	2170.22	1.00
4	E+1C_2	303	11498.2	2.8	2147.41	0.99
5	E+1C_3	303	11504.8	3.1	2141.57	0.99
6	E+1C_4	302	11354.7	2.6	2127.63	0.98
7	E+1C_7	301	11512.2	4.2	2164.31	0.99
8	E+1C_8	301	11509.8	3.9	2163.86	0.99
Average		302	11526.9	3.0	2158.12	0.99
Standard deviation		0.8	88.1	0.7	17.48	0.01

\* Calculated as: Specimen dry density/MDD (2177.3 kg/m<sup>3</sup>) obtained in the field – N7 site; see Table 7 in Section 5.2

**Table 15: G2 specimens for RTT**

Item No.	Specimen No.	Height [mm]	Cured Mass [g]	MC [%] After testing	Dry Density After curing [kg/m <sup>3</sup> ]	Relative Density*
1	G2+0C_2	301	12377.0	3.7	2326.89	1.02
2	G2+0C_3R	308	12474.0	4.0	2291.83	1.00
3	G2+0C_6	304	12601.0	3.9	2345.63	1.02
4	G2+1C_1	304	12561.2	3.6	2338.22	1.02
5	G2+1C_2	307	12487.1	4.7	2301.71	1.01
6	G2+1C_4	308	12837.8	4.6	2358.67	1.03
Average		305	12556.4	4.1	2327.16	1.02
Standard deviation		2.8	158.1	0.5	25.89	0.01

\* Calculated as: Specimen dry density/MDD (2289 kg/m<sup>3</sup>) obtained from density – moisture relationship for G2 material; see Table 9 in Section 5.2

## 6.2. Triaxial test results

### 6.2.1. STT results

Table 16: Summary of STT results on 3.3% Emulsion + 0% Cement mix

Specimen No.	$\sigma_3$ [kPa]	Max applied load [kN]	Displ. at failure [mm]	Corr. strain at failure [%]	$\sigma_{a,f}$ [kPa]	$\sigma_{1,f}$ [kPa]	$E_{tan}$ [MPa]	$E_{sec}$ [MPa]
E+0C_1	50	11.4	10.7	3.4	645	649	91	19
E+0C_2	100	16.6	17.6	5.6	937	941	103	17
E+0C_3	200	24.6	15.1	5.1	1390	1394	131	28

Stress development during STT on 3.3% Emulsion + 0% Cement mix is depicted in Figure 60

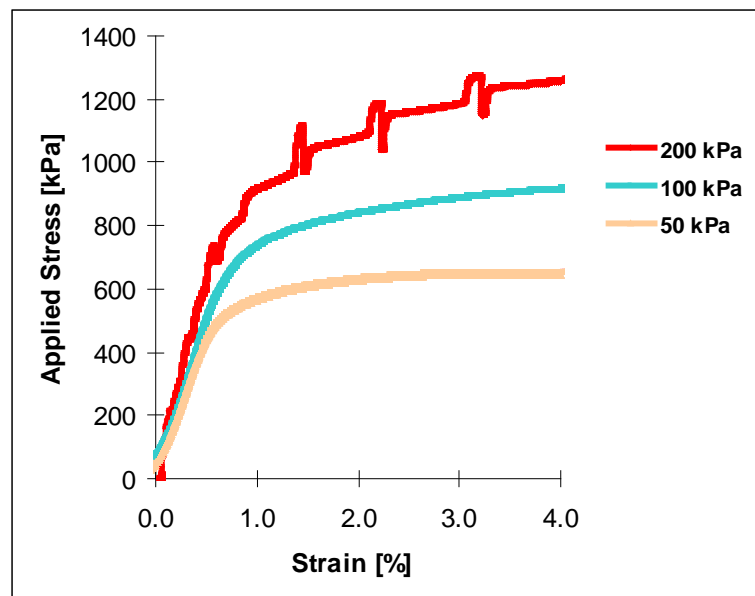
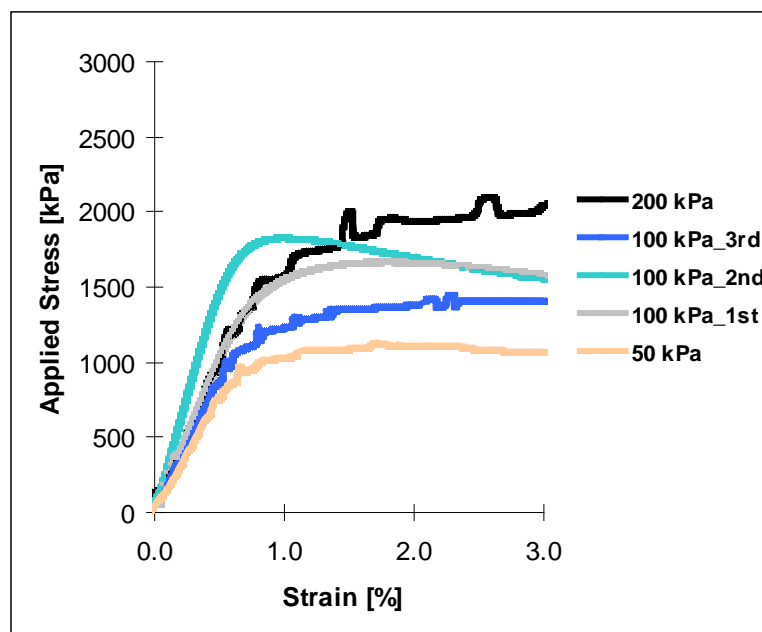


Figure 60: Applied stress vs strain for STT on 3.3% Emulsion + 0% Cement mix

**Table 17: Summary of STT results on 3.3% Emulsion + 1% Cement mix**

Specimen No.	$\sigma_3$ [kPa]	Max applied load [kN]	Displ. at failure [mm]	Corr. strain at failure [%]	$\sigma_{a,f}$ [kPa]	$\sigma_{1,f}$ [kPa]	$E_{tan}$ [MPa]	$E_{sec}$ [MPa]
E+1C_5	50	19.9	7.4	1.7	1126	1130	156	66
E+1C_10	100	29.5	5.4	1.8	1669	1673	211	91
E+1C_9	100	32.3	3.7	1.0	1829	1832	311	184
E+1C_6	100	25.5	8.3	2.3	1443	1447	172	63
E+1C_1	200	37.0	8.2	2.6	2096	2100	197	82

Stress development during STT on 3.3% Emulsion + 1% Cement mix is depicted in Figure 61



**Figure 61: Applied stress vs strain for STT on 3.3% Emulsion + 1% Cement mix**

**Table 18: Summary of STT results on G2 + 0% Cement mix**

Specimen No.	$\sigma_3$ [kPa]	Max applied load [kN]	Displ. at failure [mm]	Corr. strain at failure [%]	$\sigma_{a,f}$ [kPa]	$\sigma_{1,f}$ [kPa]	$E_{tan}$ [MPa]	$E_{sec}$ [MPa]
G2+0C_4	50	17.6	9.8	3.4	1010	1014	98	30
G2+0C_5	100	25.8	12.5	3.7	1461	1465	142	39
G2+0C_1R	200	35.0	11.1	3.8	1983	1987	260	53

Stress development during STT on G2 + 0% Cement mix is depicted in Figure 62

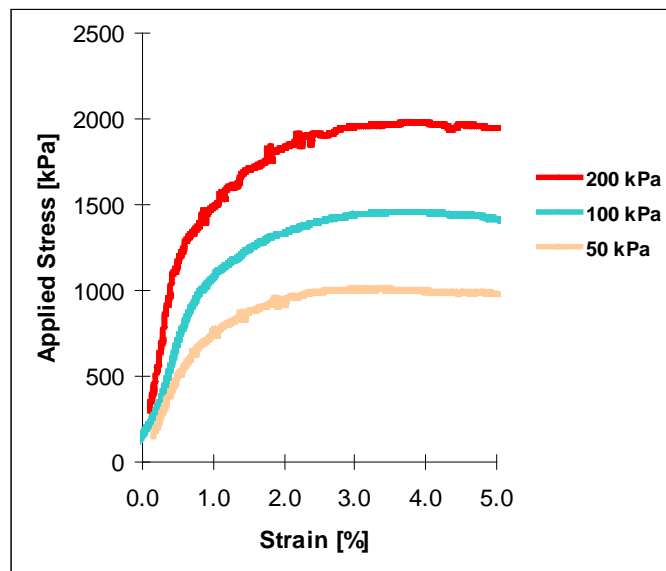


**Figure 62: Applied stress vs strain for STT on G2+0% Cement**

**Table 19: Summary of STT results on G2+1% Cement mix**

Specimen No.	$\sigma_3$ [kPa]	Max applied load [kN]	Displ. at failure [mm]	Corr. strain at failure [%]	$\sigma_{a,f}$ [kPa]	$\sigma_{1,f}$ [kPa]	$E_{tan}$ [MPa]	$E_{sec}$ [MPa]
G2+1C_6	50	27.9	6.1	1.6	1581	1584	279	99
G2+1C_3	100	34.3	6.9	1.6	1942	1946	278	119
G2+1C_5	200	50.5	9.6	2.8	2857	2861	329	103

Stress development during STT on G2 + 1% Cement mix is depicted in Figure 63

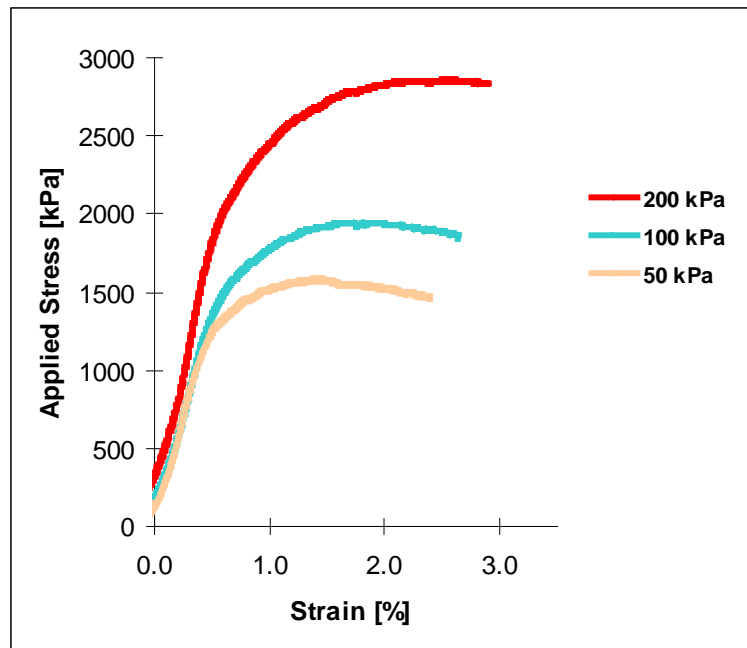


Figure 63: Applied stress vs strain for STT on G2+ 1% Cement mix

### 6.2.2. RTT results

Table 20: Summary of RTT results on 3.3% Emulsion + 0% Cement mix

Specimen No.	$\sigma_3$ [kPa]	Max applied load [kN]	Displ. at failure [mm]	Corr. strain at failure [%]	$\sigma_{a,f}$ [kPa]	$\sigma_{1,f}$ [kPa]	$E_{tan}$ [MPa]	$E_{sec}$ [MPa]
E+OC_4	50	12.3	12.1	3.8	696	748	115	20
E+OC_6	100	15.1	11.9	3.7	853	955	136	24
E+OC_5	200	21.4	16.4	5.5	1211	1413	134	24

Stress development during RTT on 3.3% Emulsion + 0% Cement mix is depicted in Figure 64

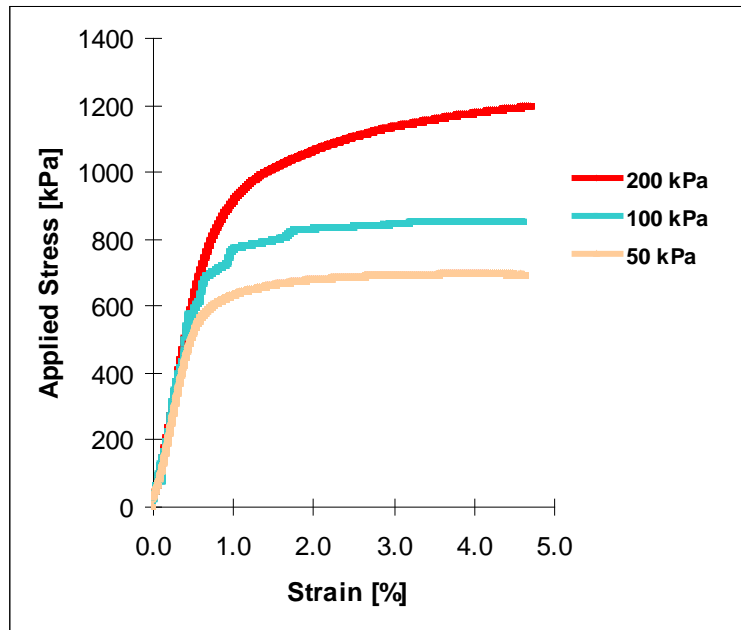


Figure 64: Applied stress vs strain for RTT on 3.3% Emulsion + 0% Cement mix

Table 21: Summary of RTT results on 3.3% Emulsion + 1% Cement mix

Specimen No.	$\sigma_3$ [kPa]	Max applied load [kN]	Displ. at failure [mm]	Corr. strain at failure [%]	$\sigma_{a,f}$ [kPa]	$\sigma_{1,f}$ [kPa]	$E_{tan}$ [MPa]	$E_{sec}$ [MPa]
E+1C_2	50	18.9	5.0	1.5	1070	1122	172	76
E+1C_4	100	18.1	6.8	1.8	1023	1125	158	63
E+1C_8	100	18.0	19.4	5.2	1019	1121	94	22
E+1C_7	100	16.0	13.8	3.8	904	1006	105	27
E+1C_3	200	28.9	12.7	3.2	1638	1840	188	57

Stress development during RTT on 3.3% Emulsion + 1% Cement mix is depicted in Figure 65

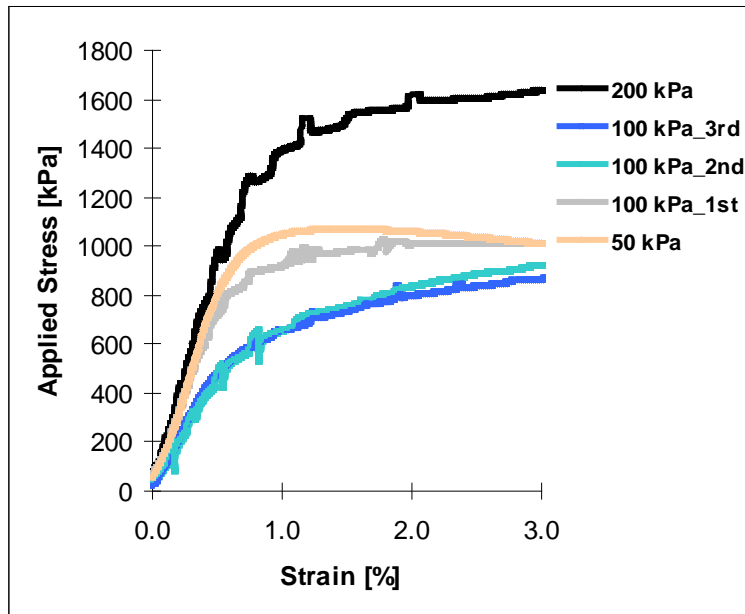


Figure 65: Applied stress vs strain for RTT on 3.3% Emulsion + 1% Cement mix

Table 22: Summary of RTT results on G2 + 0% Cement mix

Specimen No.	$\sigma_3$ [kPa]	Max applied load [kN]	Displ. at failure [mm]	Corr. strain at failure [%]	$\sigma_{a,f}$ [kPa]	$\sigma_{1,f}$ [kPa]	$E_{tan}$ [MPa]	$E_{sec}$ [MPa]
G2+0C_6	50	15.8	10.4	2.7	892	944	89	34
G2+0C_3R	100	18.1	12.7	3.9	1026	1128	94	26
G2+0C_2	200	30	14.8	4.5	1698	1899	204	38

Stress development during RTT on G2 + 0% Cement mix is depicted in Figure 66

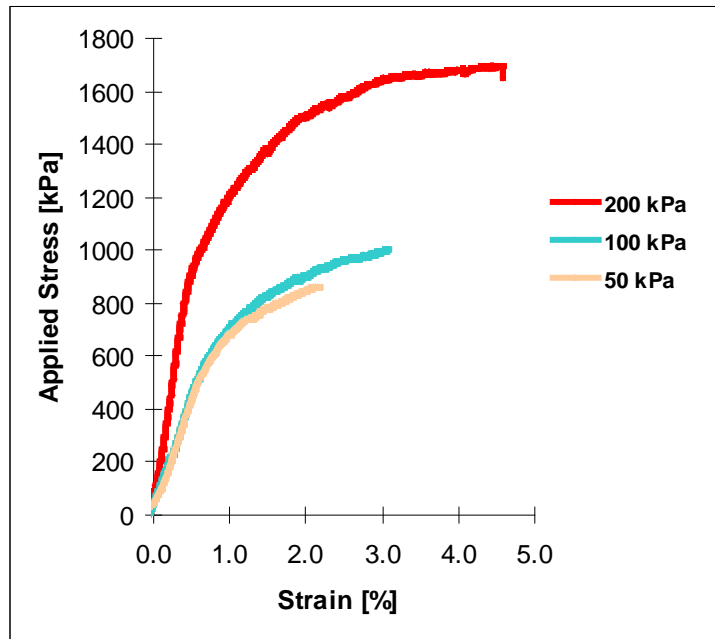


Figure 66: Applied stress vs strain for RTT on G2 + 0% Cement mix

Table 23: Summary of RTT results on G2 + 1% Cement mix

Specimen No.	$\sigma_3$ [kPa]	Max applied load [kN]	Displ. at failure [mm]	Corr. strain at failure [%]	$\sigma_{a,f}$ [kPa]	$\sigma_{1,f}$ [kPa]	$E_{tan}$ [MPa]	$E_{sec}$ [MPa]
G2+1C_4	50	27.9	6.1	1.7	1580	1631	203	91
G2+1C_2	100	33.9	6.6	1.9	1920	2021	268	101
G2+1C_1	200	45.1	9.5	2.4	2553	2755	185	114

Stress development during RTT on G2 + 1% Cement mix is depicted in Figure 67

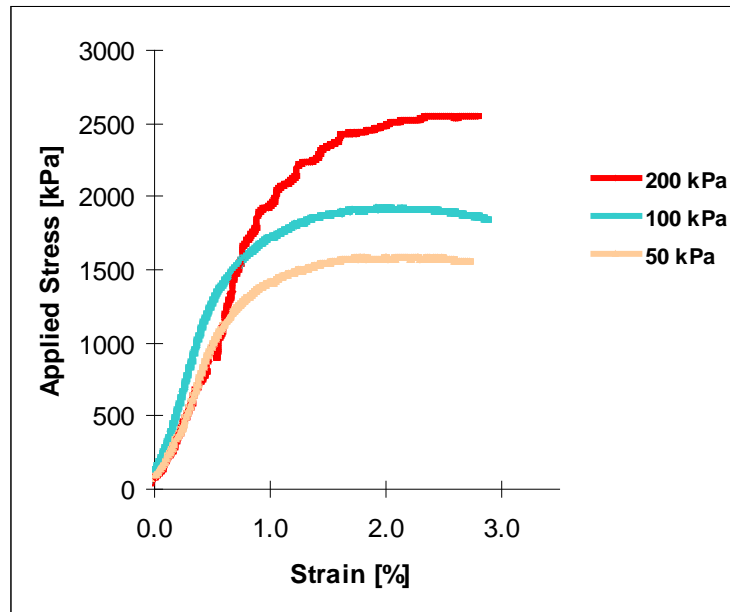


Figure 67: Applied stress vs strain for RTT on G2 + 1% Cement mix

### 6.3. Closure

The presented results and findings on specimens produced and subsequent triaxial tests performed, will be analysed and comparisons done between results obtained using STT against those for RTT in the next chapter. Mechanical properties of materials as determined by STT and RTT on same mixes will be compared also in Chapter 7.

## 7. ANALYSIS AND INTERPRETATION OF RESULTS

In this chapter the analysis of results obtained from both STT and RTT is presented as well as interpretation thereof. The synthesis is based on the comparison of triaxial results obtained using STT and RTT methods on comparable specimens from the same mix tested at same confining pressure. The synthesis will also include determination and presentation of mechanical properties (cohesion and angle of friction) using results from both STT and RTT methods on same mixes and comparison thereof. Discussions of correlations obtained will also be included in this chapter.

### 7.1. STT vs RTT results on Hornfels + 3.3% Emulsion+0% Cement mix

Comparison of stress-strain data at 50, 100 and 200 kPa confining pressure was plotted for both STT and RTT on the same graph in order to observe correlation in the stress-strain diagrams. As observed from the graphs below, good correlation in results obtained for 'Hornfels (RAP) + 3.3% Emulsion + 0% Cement' mix can be seen.

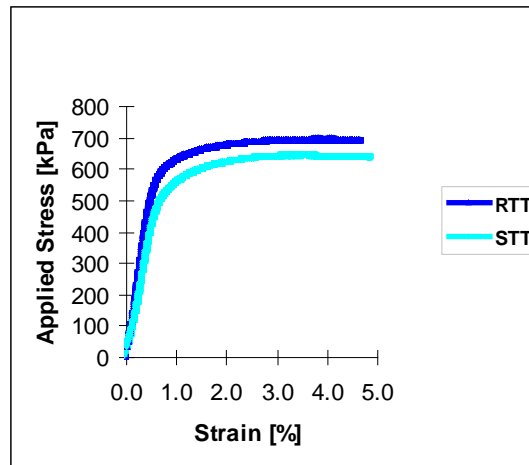


Figure 68: Stress vs Strain diagram on Hornfels (RAP) + 3.3% Emulsion + 0% Cement mix by STT and RTT tested at 50 kPa

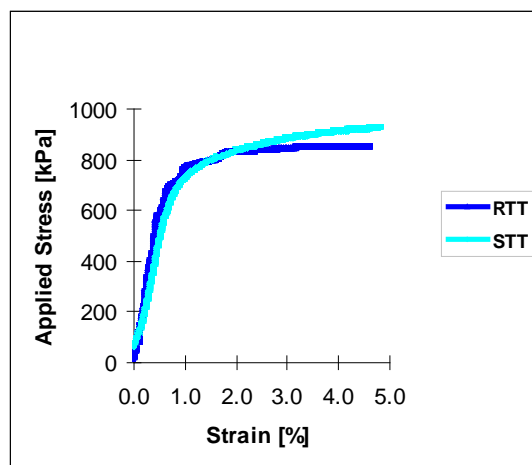
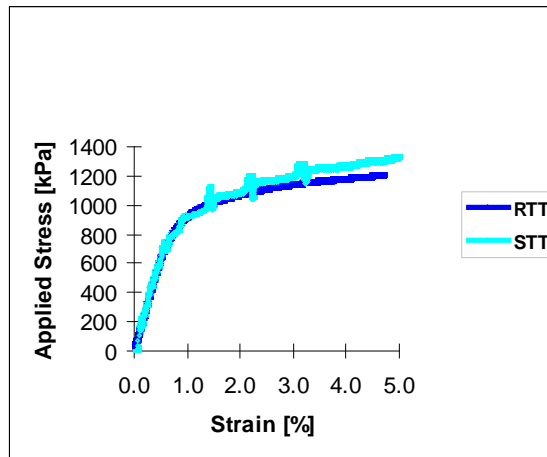
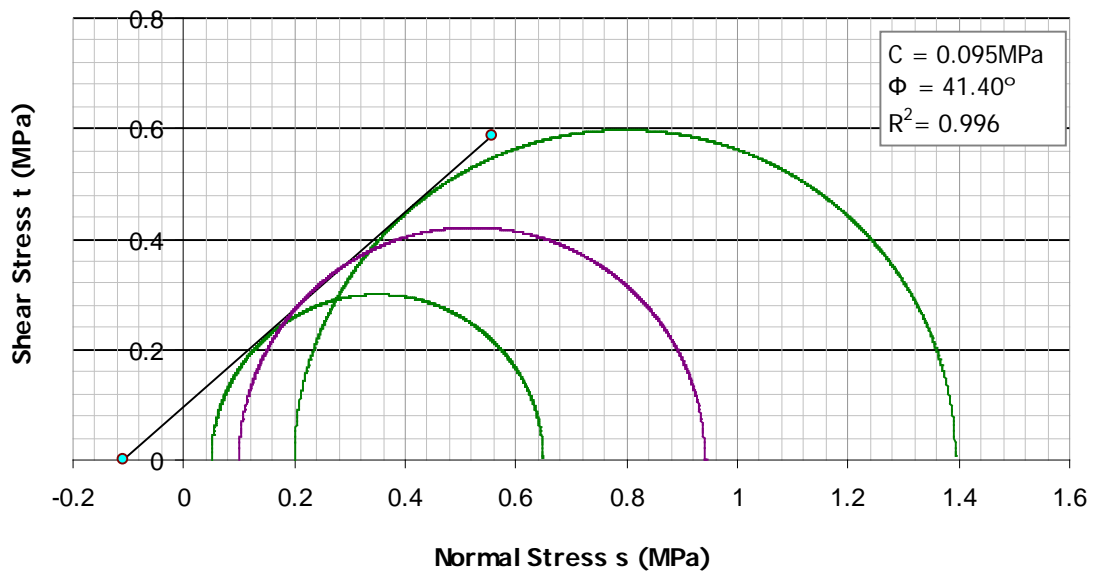


Figure 69: Stress vs Strain diagram on Hornfels (RAP) + 3.3% Emulsion + 0% Cement mix by STT and RTT tested at 100 kPa



**Figure 70: Stress vs Strain diagram on Hornfels (RAP) + 3.3% Emulsion + 0% Cement mix by STT and RTT tested at 200 kPa**

Linear regression analysis of results from both STT and RTT on 'Hornfels + 3.3% Emulsion + 0% Cement' mix was performed to obtain Mohr-Coulomb failure envelope lines as shown in Figure 71 and Figure 72 below.



**Figure 71: Mohr-Coulomb diagram on Hornfels (RAP) + 3.3% Emulsion + 0% Cement using STT**

A good correlation coefficient ( $R^2 = 0.996$ ) was obtained for the linear regression analysis performed to obtain the Mohr-Coulomb failure envelope line. This provides confidence that the results obtained from STT on 'Hornfels (RAP) + 3.3% Emulsion + 0% Cement' mix at different confining pressures, are almost in line with each other. In statistical analysis, correlation of coefficient above 0.95 is considered accurate enough.

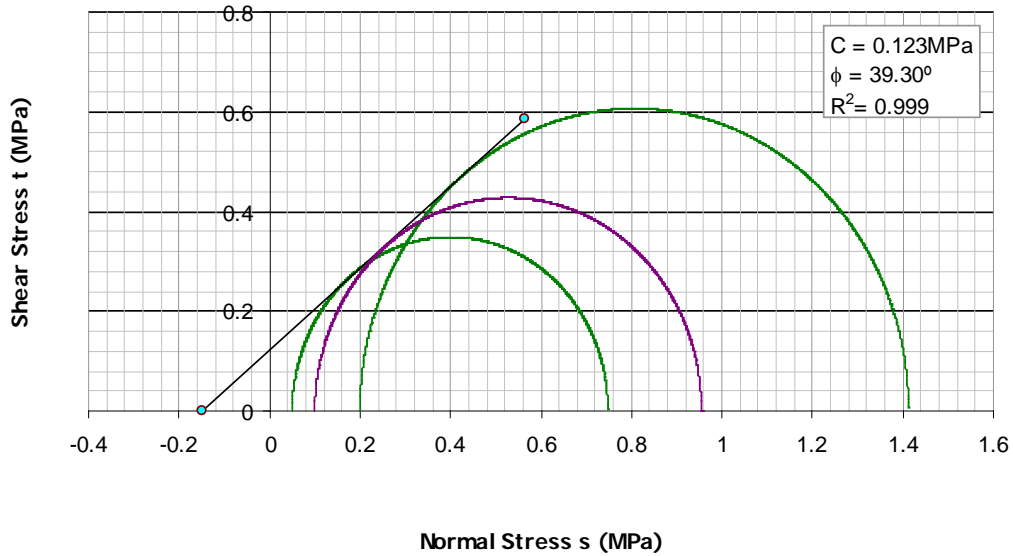


**Figure 72: Mohr-Coulomb diagram on Hornfels (RAP) + 3.3% Emulsion + 0% Cement using RTT**

Similarly regression analysis depicted in Figure 72 above shows a good correlation coefficient ( $R^2 = 0.999$ ), another good indication that results obtained from RTT on 'Hornfels (RAP) + 3.3% Emulsion + 0% Cement' mix at different confining pressures, were in line with each other.

Mechanical properties of cohesion and angle of internal friction determined by regression analysis of results from both STT and RTT on 'Hornfels (RAP) + 3.3% Emulsion + 0% Cement' mix, are summarised in Table 24.

**Table 24: Summary of material properties from STT and RTT on Hornfels (RAP) + Emulsion + 0% Cement mix**

Test	Specimen No.	$\sigma_3$ [kPa]	$\sigma_{a,f}$ [kPa]	$\sigma_{1,f}$ [kPa]	Cohesion [kPa]	Internal Friction Angle [°]	Correlation Coefficient [ $R^2$ ]
STT	E+0C_1	50	645	649	95	41.4	0.996
	E+0C_2	100	937	941			
	E+0C_3	200	1390	1394			
RTT	E+0C_4	50	696	748	123	39.3	0.999
	E+0C_6	100	853	955			
	E+0C_5	200	1211	1413			

### 7.1.1. Discussion

From Table 24, it can be seen that the mechanical properties (cohesion and internal angle of friction) determined from results using STT and RTT are comparable. Differences exist though represented by percentage increase of 5% in angle of internal friction and percentage decrease of 23% in cohesion, as obtained using STT results. These differences however, are due to the fact that specimens from

one mix are not exactly the same in characteristics (see Section 6.1), variations in density, moisture and particle orientation caused by segregation exist, which can alter the mechanical properties. Another contributing factor is the use of 100% RAP aggregates which have high probability of material variability.

## 7.2. STT vs RTT results on Hornfels + 3.3% Emulsion+1% Cement mix

Comparison of stress-strain data at 50, 100 and 200 kPa confining pressure was plotted for both STT and RTT on the same graph in order to observe correlation in the stress-strain diagrams. Three tests of STT and RTT were conducted at 100 kPa confinement in order to observe repeatability of results. As observed from the graphs below, no good correlation in results can be seen on 'Hornfels (RAP) + 3.3% Emulsion + 1% Cement' mix except for the one performed at 50 kPa confinement.

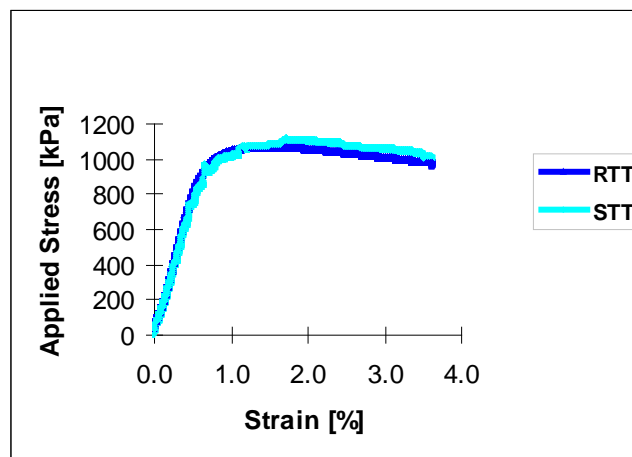


Figure 73: Stress vs Strain diagram on Hornfels (RAP) + 3.3% Emulsion + 1% Cement by STT and RTT at 50 kPa

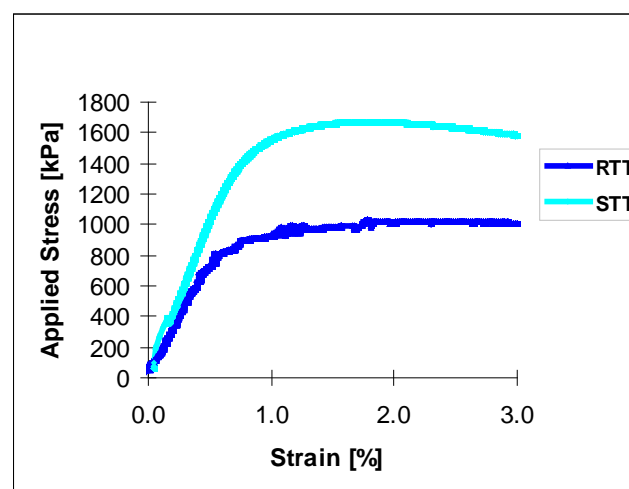


Figure 74: Stress vs Strain diagram on Hornfels (RAP) + 3.3% Emulsion + 1% Cement by STT and RTT at 100 kPa (repeat 1)

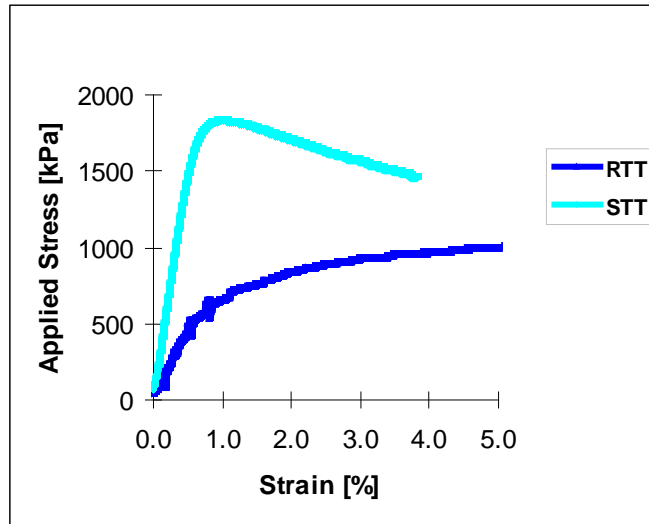


Figure 75: Stress vs Strain on Hornfels (RAP) + 3.3% Emulsion + 1% Cement by STT and RTT at 100 kPa (repeat 2)

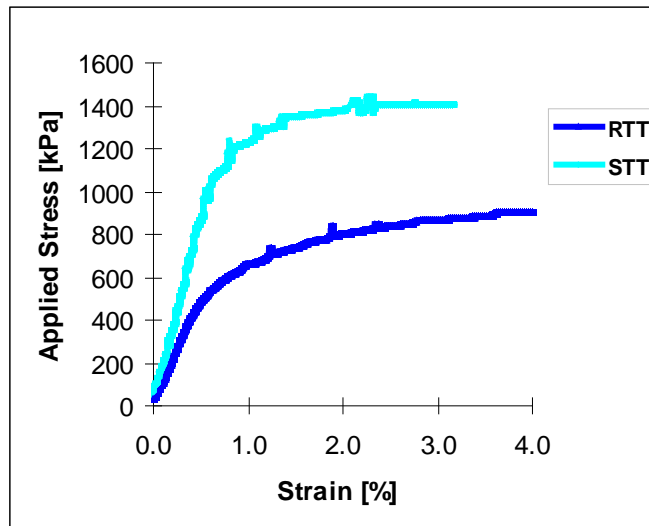
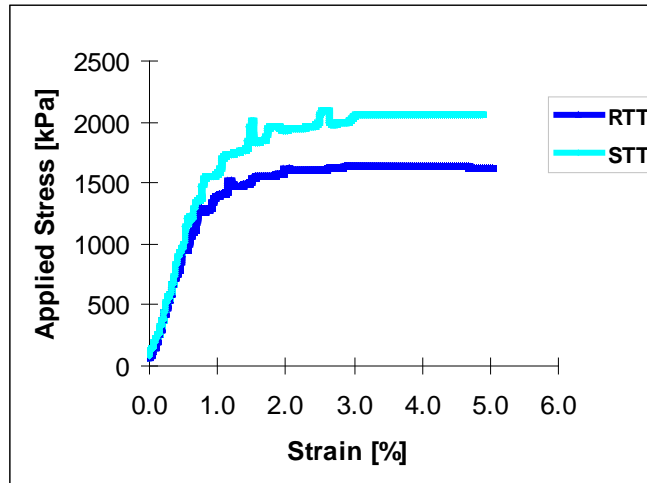
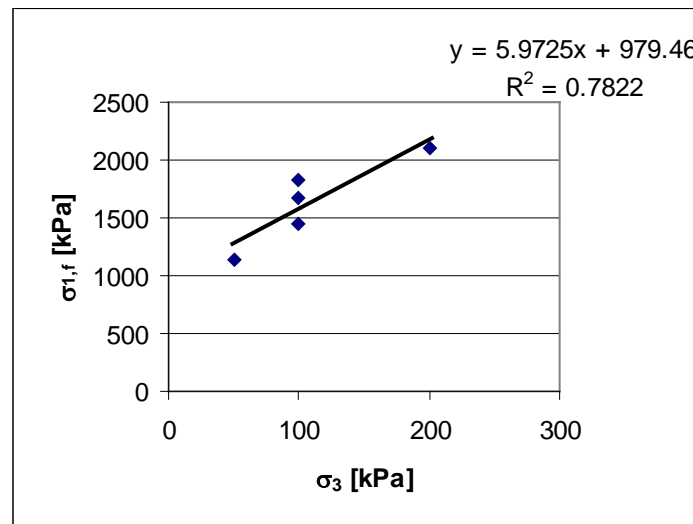


Figure 76: Stress vs Strain on Hornfels (RAP) + 3.3% Emulsion + 1% Cement by STT and RTT at 100 kPa (repeat 3)



**Figure 77: Stress vs Strain on Hornfels (RAP) + 3.3% Emulsion + 1% Cement by STT and RTT at 200 kPa**

Results obtained from both STT and RTT on 'Hornfels + 3.3% Emulsion + 1% Cement' mix at 100 kPa confinement, were not observed to be repeatable either (due to factors discussed in Section 7.1.1) as is depicted from the plots of principle stress at failure ( $\sigma_{1,f}$ ) versus confinement pressure ( $\sigma_3$ ); see Figures 78 and 79 below.



**Figure 78:  $\sigma_{1,f}$  versus  $\sigma_3$  from STT on Hornfels (RAP) + 3.3% Emulsion + 1% Cement mix**

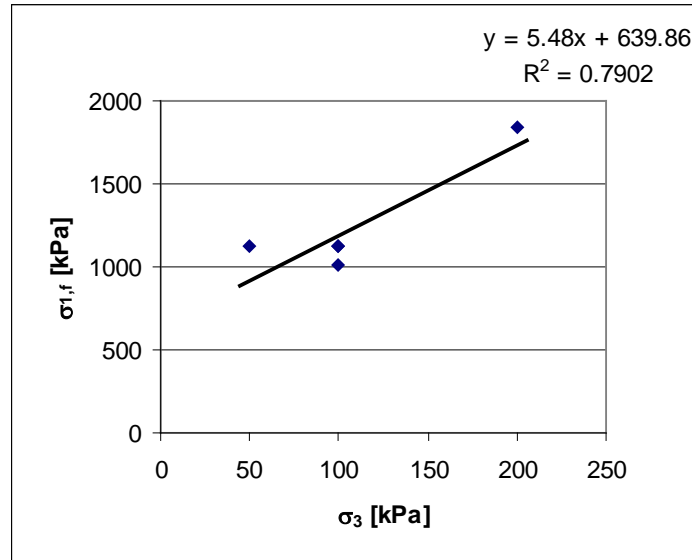


**Figure 79:  $\sigma_{1,f}$  versus  $\sigma_3$  from RTT on Hornfels (RAP) + 3.3% Emulsion + 1% Cement mix**

Correlation coefficients obtained considering all data points from both STT and RTT of  $R^2 = 0.782$  and  $R^2 = 0.790$  respectively, are not accurate enough for linear regression analysis to be performed in order to obtain the Mohr-Coulomb failure envelope line for 'Hornfels (RAP) + 3.3% Emulsion + 1% Cement' mix. However, review of both plots from STT and RTT of  $\sigma_{1,f}$  versus  $\sigma_3$  in Figures 78 and 79 indicate some outlier data points (laying further from the trendline) at 100 kPa confinement which when ignored yields more accurate correlation coefficients which gives confidence that remaining data points are in line with each other and can be used in regression analysis for the determination of shear parameters.

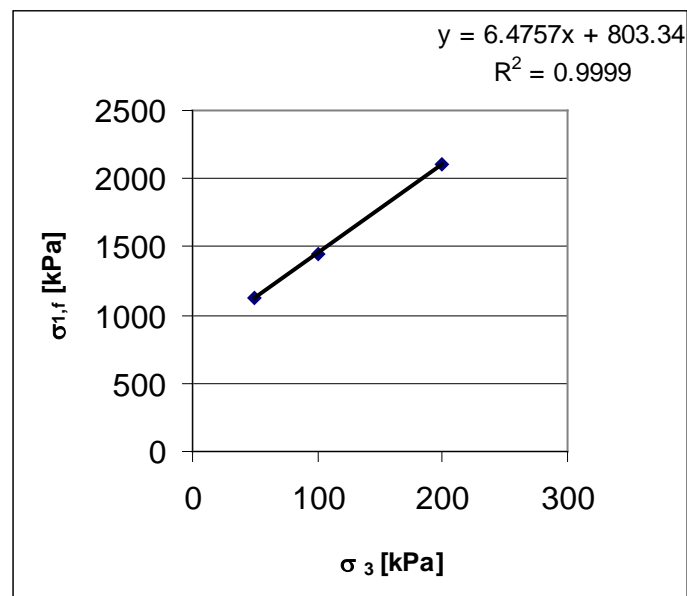


**Figure 80:  $\sigma_{1,f}$  versus  $\sigma_3$  from STT (adjusted)**

As can be seen in Figure 80, removing data points for E+1C\_9 and E+1C\_10 specimens tested at 100 kPa as outliers, leaves behind three data points at 50, 100, 200 kPa which are highly correlated as indicated by  $R^2 = 0.9999$ . Mohr-Coulomb failure envelope line obtained using data points in Figure 80 is as shown below in Figure 81.

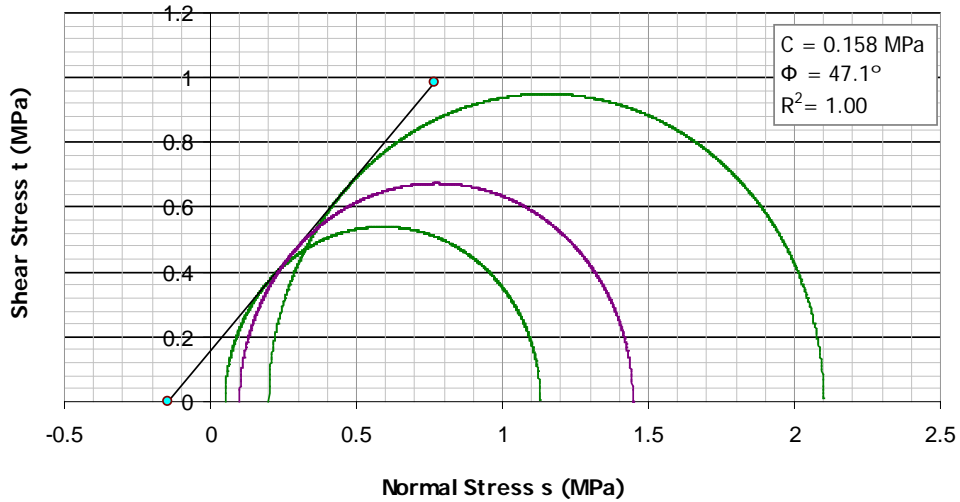


**Figure 81: Mohr-Coulomb diagram on Hornfels (RAP) + 3.3% Emulsion + 1% Cement using STT**

Similarly, the same approach can be taken for RTT results displayed in Figure 79 with a low  $R^2 = 0.790$ . However, it can be seen from Figure 79 that with fixed points at 50 and 200 kPa, and the scatter that can be observed in the data set which is mostly as a result of lower values of principle stress at failure obtained at 100 kPa than was obtained for a specimen at 50 kPa, a situation not ideal according to theory. Therefore, getting well correlated data points like in the case of STT (see Figure 80) is not possible even after removing outliers. This further justifies the statistical demand of the linear regression analysis of more data points at different confining pressure in order to get at least three well correlated data points at different confinement that can be used to determine the Mohr-Coulomb failure line for a mix. The best correlation coefficient that can be obtained from the data set from RTT after ignoring data points for E+1C\_7 and E+1C\_8 specimens (see Figure 82) is  $R^2 = 0.90$  which is slightly less than the desired 0.95 however, can still be used.

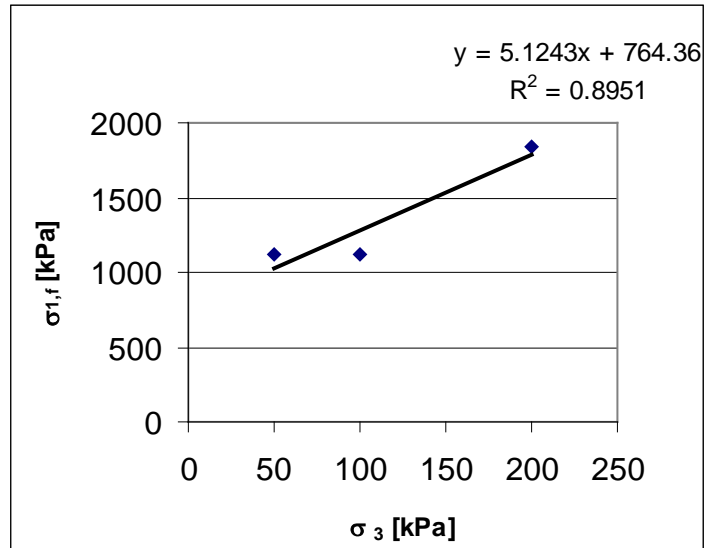


**Figure 82:  $\sigma_{1,f}$  versus  $\sigma_3$  from RTT (adjusted)**

Mohr-Coulomb envelope line obtained from RTT results displayed in Figure 82 on 'Hornfels (RAP) + 3.3% Emulsion + 1% Cement' mix is depicted from Figure 83 below.

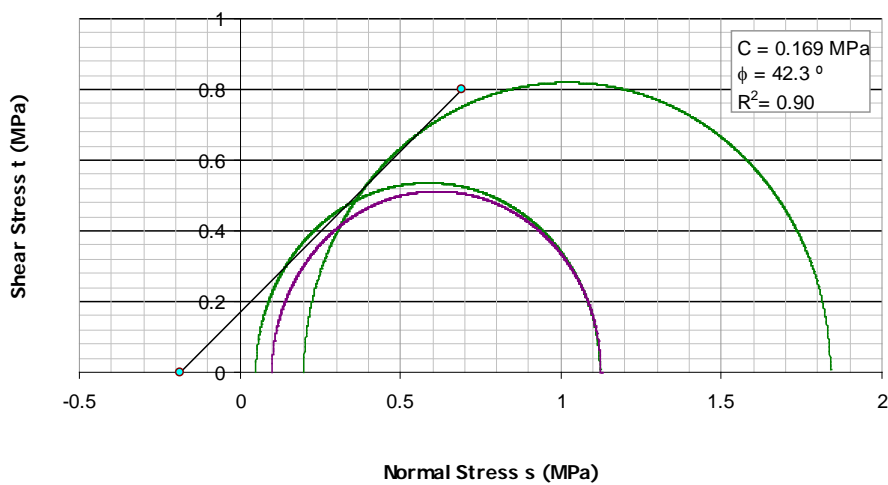


**Figure 83: Mohr-Coulomb diagram on Hornfels (RAP) + 3.3% Emulsion + 1% Cement mix using RTT**

Mechanical properties of cohesion and angle of internal friction determined by regression analysis of selected results from STT and RTT on 'Hornfels (RAP) + 3.3% Emulsion + 1% Cement' mix, are summarised in Table 25 below.

**Table 25: Summary of material properties from STT and RTT on Hornfels (RAP) + Emulsion + 1% Cement mix**

Test	Specimen No.	$\sigma_3$ [kPa]	$\sigma_{a,f}$ [kPa]	$\sigma_{1,f}$ [kPa]	Cohesion [kPa]	Internal Friction Angle [°]	Correlation Coefficient [R <sup>2</sup> ]
STT	E+1C_5	50	1126	1130	158	47.1	1.00
	E+1C_6	100	1443	1447			
	E+1C_1	200	2096	2100			
RTT	E+1C_2	50	1070	1122	169	42.3	0.90
	E+1C_4	100	1023	1125			
	E+1C_3	200	1638	1840			

### 7.2.1. Discussion

Despite irregularities in results obtained from both STT and RTT on ‘Hornfels (RAP) + Emulsion + 1% Cement’ mix, sorting out of outlier data points has aided the process of determining with confidence the mechanical properties of the mix which from Table 25 can be seen to be also comparable. Cohesion obtained using STT results is lower by 6.5% whilst angle of internal friction is higher by 11.3%, even though results from STT can be said to be more reliable because of higher correlation between results than those obtained from the RTT. These differences however, are due to reasons advanced already in Section 7.1.1.

In spite of the above mentioned differences, the effect of cement as active filler on cohesion of the mix can still be noticed by comparing Table 24 in which mix without cement has lower cohesion than the mix with 1% cement; see Table 25.

One of the reasons for the discrepancy in results advanced in Section 7.1.1 is the material variability of the 100% Hornfels (RAP) used in both mixes discussed above. Therefore, to test the effect of this factor, sensitivity analysis tests were stipulated which required the use of good grade crushed aggregate material (preferably G1) compacted to 100 % Mod AASHTO. However, due to non availability of the G1 material at the time of the research, a relatively good aggregate (base course G2 material) was used and two mixes were prepared from which twelve specimens for both STT and RTT were prepared and tested; see Sections 5.2 and 6.1. The results obtained are analysed in Sections 7.3 and 7.4 below.

### 7.3. STT vs RTT results on G2 + 0% Cement mix

Comparison of stress-strain data at 50, 100 and 200 kPa confining pressure was plotted for both STT and RTT on the same graph in order to observe correlation in the stress-strain diagrams, as can be observed on the graphs below:

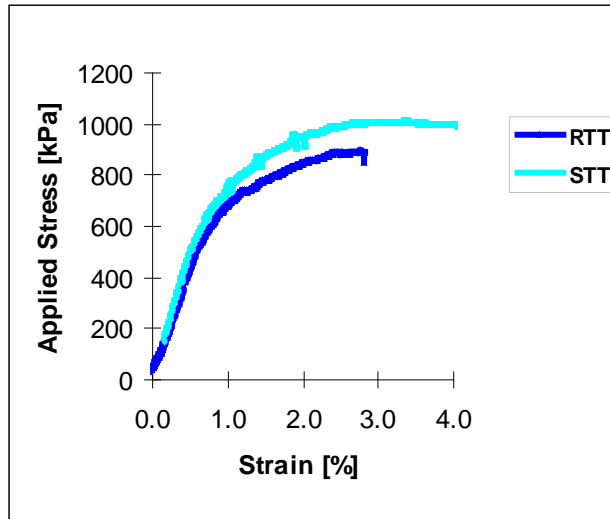


Figure 84: Stress vs Strain on G2 + 0% Cement mix by STT and RTT at 50 kPa

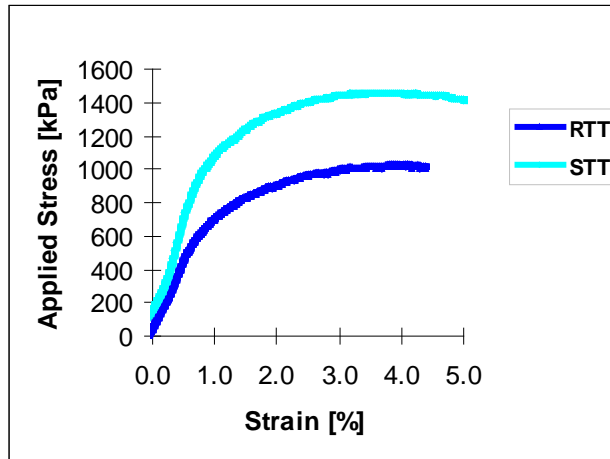


Figure 85: Stress vs Strain on G2 + 0% Cement mix by STT and RTT at 100 kPa

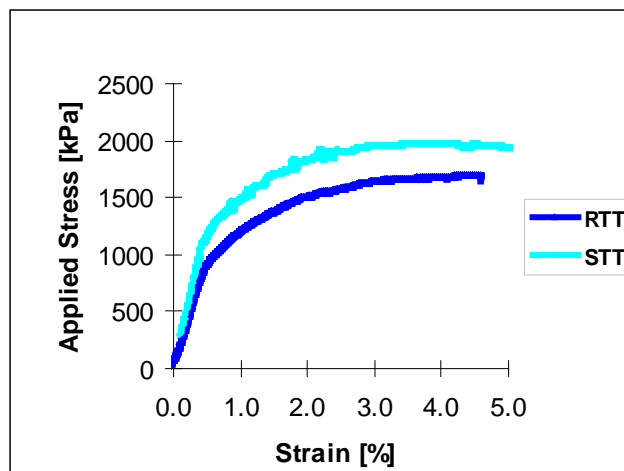
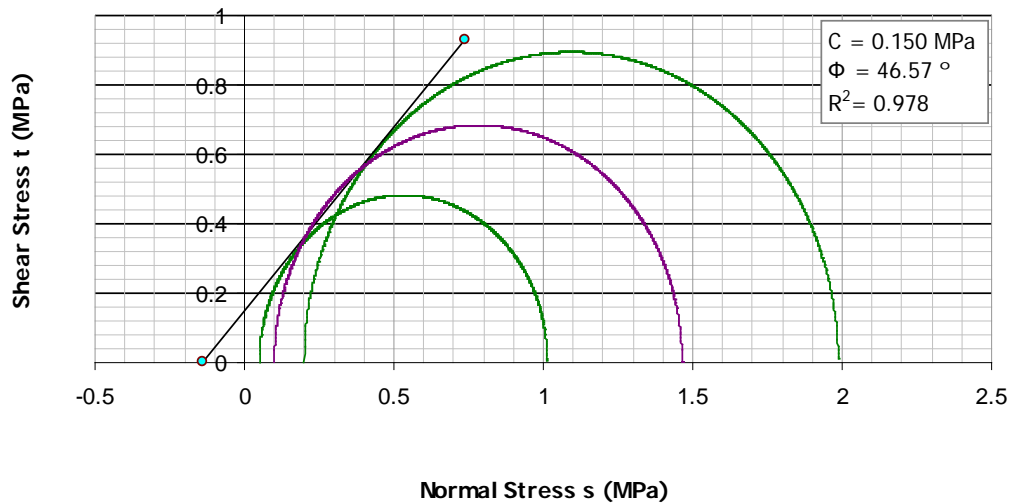


Figure 86: Stress vs Strain on G2 + 0% Cement mix by STT and RTT at 200 kPa

Linear regression analysis of results from both STT and RTT on 'G2 + 0% Cement' mix was performed to obtain Mohr-Coulomb failure envelope lines as shown in Figure 87 and Figure 88 below.



**Figure 87: Mohr-Coulomb diagram on G2 + 0% Cement mix using STT**

Good correlation coefficient ( $R^2 = 0.978$ ) was obtained for the linear regression analysis performed to obtain the Mohr-Coulomb failure envelope line. This provides confidence that the results obtained from STT on 'G2 + 0% Cement' mix at different confining pressures, were in line with each other.

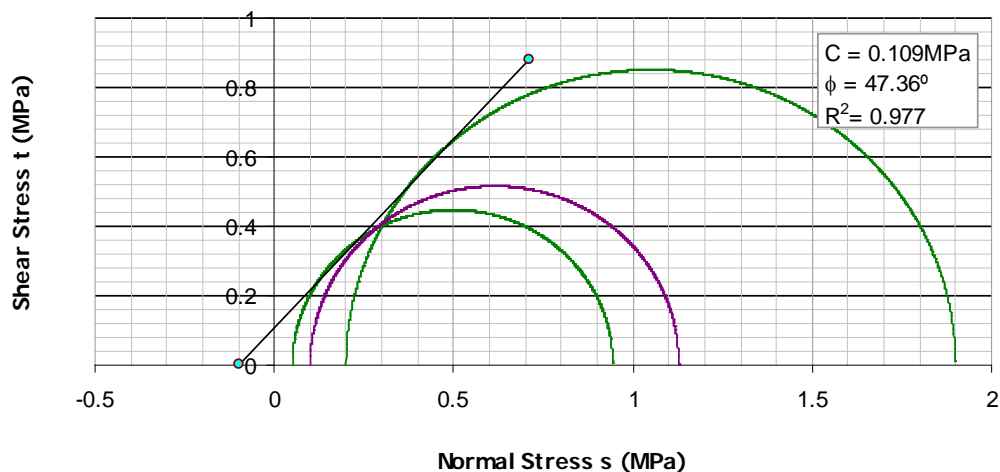


**Figure 88: Mohr-Coulomb diagram on G2 + 0% Cement mix using RTT**

Similarly, for the results from RTT on G2 + 0% Cement, accurate enough correlation coefficient ( $R^2 = 0.977$ ) was obtained for the linear regression analysis performed to obtain the Mohr-Coulomb failure envelope line. Mechanical properties of cohesion and angle of internal friction determined by

regression analysis of results from STT and RTT on 'G2 + 0% Cement' mix, are summarised in Table 26 below.

**Table 26: Summary of material properties from STT and RTT on G2 + 0% Cement mix**

Test	Specimen No.	$\sigma_3$ [kPa]	$\sigma_{a,f}$ [kPa]	$\sigma_{1,f}$ [kPa]	Cohesion [kPa]	Internal Friction Angle [°]	Correlation Coefficient [R <sup>2</sup> ]
STT	G2+0C_4	50	1010	1014	150	46.6	0.978
	G2+0C_5	100	1461	1464			
	G2+0C_1	200	1983	1987			
RTT	G2+0C_6	50	892	944	109	47.4	0.977
	G2+0C_3R	100	1026	1128			
	G2+0C_2	200	1698	1900			

### 7.3.1. Discussion

From Table 26, it can be seen that cohesion as determined using STT results is higher by 37.6% which is a complete contrast to internal angle of friction which compares very well with the one determined using RTT results being only 1.7% higher. There is also noticeable increase in the internal angle of friction compared to BSM-emulsion mixes justifying the crushed nature of the aggregate used in this case. These differences that exist between mechanical properties especially cohesion are due to the same reasons of differing specimen characteristics advanced in Section 7.1.1. In addition, the fact that specimens for this mix were not cured could have contributed to varying effect on cohesion.

Generally it can be observed from the plots of stress-strain for STT and RTT at same confining pressure that there is a trend, where the STT results tend to have higher stresses at failure than the RTT. The only reason that can explain this from literature is varying confining pressure as BSMS and granular materials are stress dependent materials. The STT is based on the assumption that the pressure in the tube is equal to the pressure exerted on the surface of the specimen, this makes scientific sense but some results like those obtained on 'G2 + 0% cement' mix are showing otherwise. Maybe as the specimen is failing there is an increase in pressure or the tube has an effect of additional confinement. The author can currently only speculate the reasons behind the anomalies, thus a further study to calibrate the pressure exerted on the specimen during the test can answer some of these questions and is highly recommended.

### 7.4. STT vs RTT results on G2 + 1% Cement mix

Comparison of stress-strain data at 50, 100 and 200 kPa confining pressure was plotted for both STT and RTT on the same graph in order to observe correlation in the stress-strain diagrams. As observed

from the graphs below and in contrast with results obtained on 'G2 + 0% cement' mix, very good correlation in results are obtained for 'G2 + 1% Cement' mix.

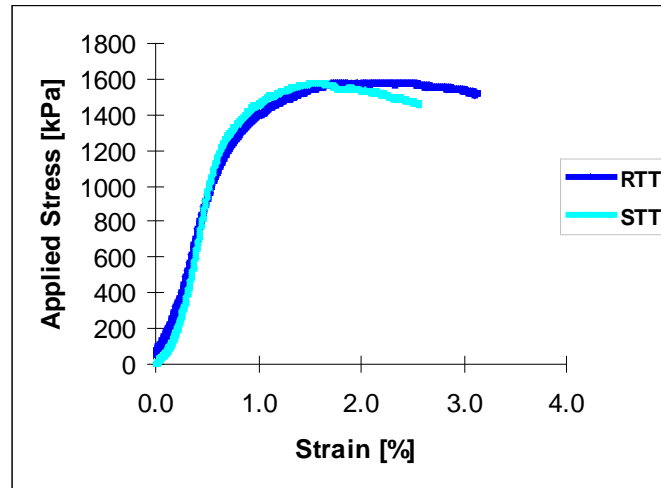


Figure 89: Stress vs Strain on G2 + 1% Cement mix by STT and RTT

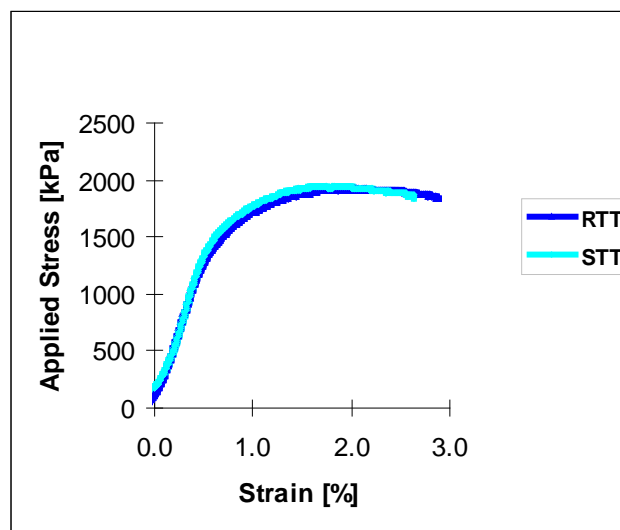


Figure 90: Stress vs Strain on G2 + 1% Cement mix by STT and RTT at 100 kPa

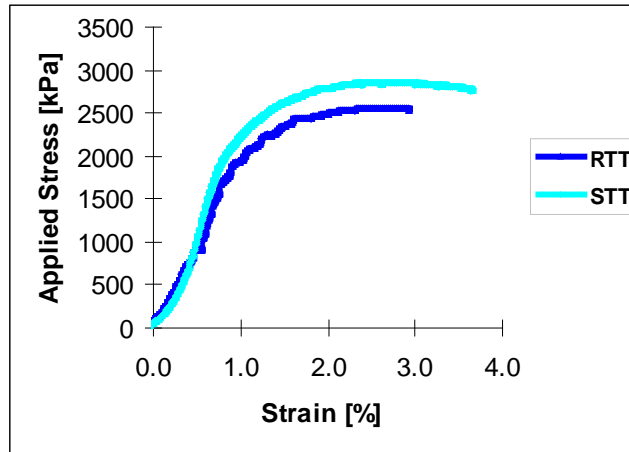


Figure 91: Stress vs Strain on G2 + 1% cement mix by STT and RTT at 200 kPa

Linear regression analysis of results from both STT and RTT on 'G2 + 1% Cement' mix was performed to obtain Mohr-Coulomb failure envelope lines as shown in Figure 92 and Figure 93. It can be seen from these graphs that the data used in both cases of linear regression had good correlation coefficients of  $R^2 = 0.997$  and  $R^2 = 1.00$  respectively.

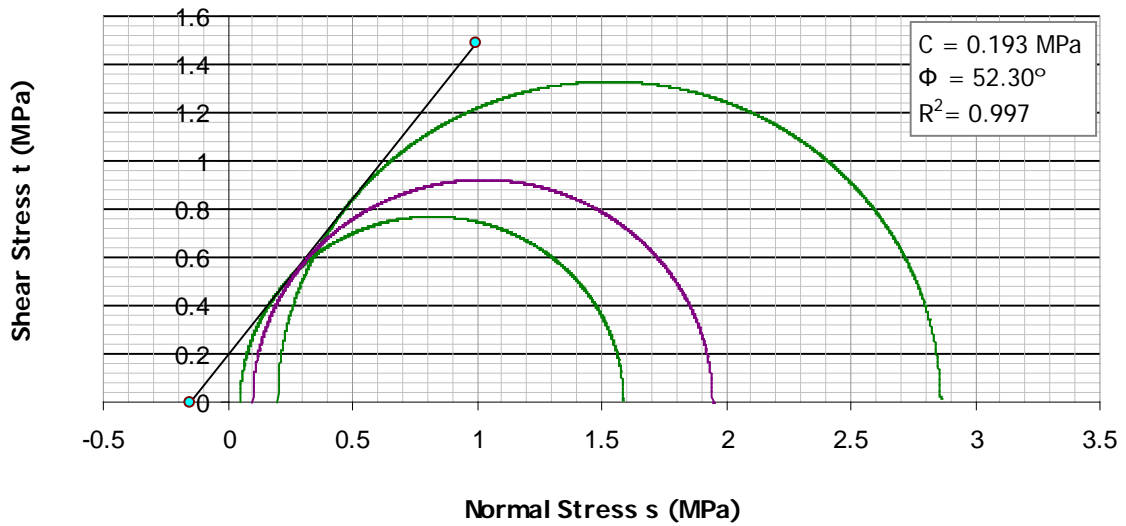
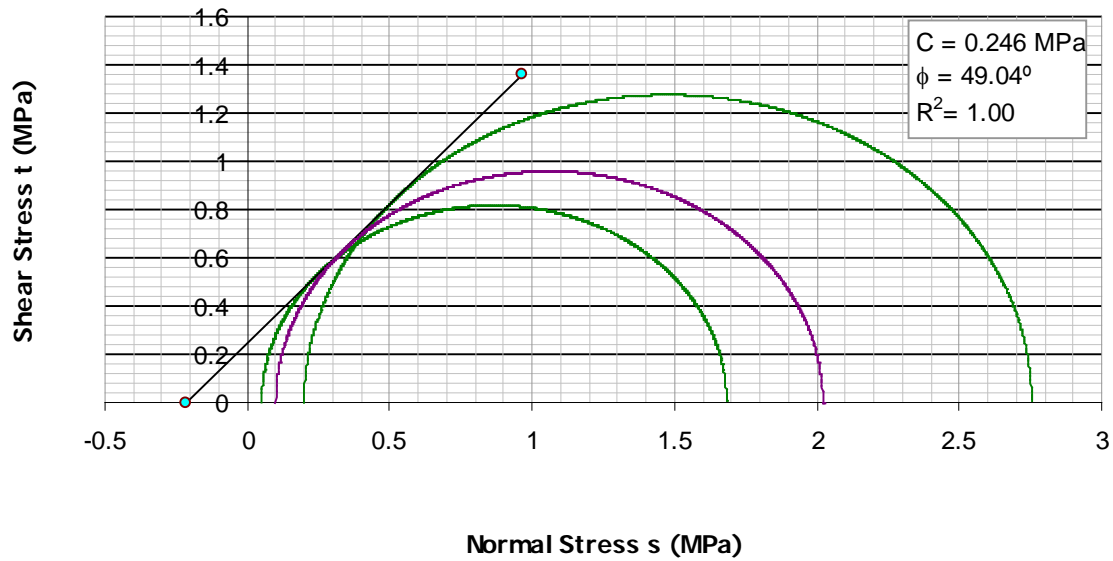


Figure 92: Mohr-Coulomb diagram on G2 + 1% Cement mix, using STT



**Figure 93: Mohr-Coulomb diagram on G2 + 1% Cement mix, using RTT**

Mechanical properties of cohesion and angle of internal friction determined by regression analysis of results from STT and RTT on 'G2 + 1% Cement' mix, are summarised in Table 27 below.

**Table 27: Summary of material properties from STT and RTT on G2 + 1% Cement mix**

Test	Specimen No.	$\sigma_3$ [kPa]	$\sigma_{a,f}$ [kPa]	$\sigma_{1,f}$ [kPa]	Cohesion [kPa]	Internal Friction Angle [°]	Correlation Coefficient [R <sup>2</sup> ]
STT	G2+1C_6	50	1584	1588	193	52.3	0.997
	G2+1C_3	100	1942	1946			
	G2+1C_5	200	2857	2861			
RTT	G2+1C_4	50	1632	1684	246	49.0	1.00
	G2+1C_2	100	1920	2022			
	G2+1C_1	200	2553	2755			

#### 7.4.1. Material Classification

According to classification system of BSMs in Table 28 (Jooste, et al 2007), and taking average  $E_{tan}$  values of 108 and 128 MPa for STT and RTT respectively, the material can be classified as BSM2. Using friction angles obtained from STT and RTT, the material can be classified as BSM1 and BSM2 respectively while cohesion criteria would put the material in BSM3 and BSM2. It can however be safely stated that the material is of a BSM2 category which would be typically used as a base layer for design traffic applications of less than 6 mesa.

**Table 28: BSM material classification system (Jooste, et al 2007)**

Test or Indicator	Material	Design Equivalent Material Classes			Not suitable for stabilisation
		BSM1	BSM2	BSM3	
Cohesion	All	> 250	100 to 250	50 to 100	< 50
Friction Angle	All	> 40	30 to 40	< 30	
Tangent Modulus	All	> 150	50 to 150	< 50	
ITS	100 mm <sup>2</sup>	> 225	175 to 225	125 to 175	< 125
	150 mm	> 175	135 to 175	95 to 135	< 95
ITS (wet)		> 150	100 to 150	60 to 100	< 60

#### 7.4.2. Example calculation

An example calculation is included in this section to determine the implication of the differences in results of STT and RTT. Equation 17 below represents a relationship used when determining deformation of granular materials in South African Mechanistic Empirical Pavement Design Method. This relationship will determine the effect in terms of number of load repetitions obtained using STT and RTT results.

$$\log N = 19.548 - 20.0564 \sigma_d / \sigma_{d,f} \quad \text{Eq. 17}$$

Where;

N = number of load repetitions to 20mm deformation (lateral wander included);

$\sigma_d$  = deviator stress =  $\sigma_1 - \sigma_3$ ; and

$\sigma_{d,f}$  = deviator stress at failure =  $\sigma_{1,f} - \sigma_3$

Note that  $\sigma_1 = \sigma_a + dw$  where  $\sigma_a$  is stress at 0.05% corrected strain and dw is stress due to dead weight loading effect of the disk.

Results of the calculation are tabulated in Table below and it can be noted that small differences in values of  $\sigma_1$  and  $\sigma_{1,f}$  lead to significant difference in the life of the granular layer.

Source Test	$\sigma_3$	$d_w$	$\sigma_a$ @ 0.05% strain	$\sigma_1$	$\sigma_{1,f}$	$\sigma_d$	$\sigma_{d,f}$	logN	N
STT	100	3.84	232.3	236.14	1945.67	136.14	1845.67	18.07	<b>1.17E+18</b>
RTT	100	1.86	202.08	203.94	2021.51	103.94	1921.51	18.46	<b>2.90E+18</b>

#### 7.4.3. Discussion

From Table 27, it can be seen that the mechanical properties are comparable and the effect of active filler (1% cement) on cohesion values obtained compared to those obtained with no cement added is noticeable. Cement has the effect of increasing the cohesion of the mix. Also evident is higher

internal angle of friction values obtained for G2 mixes compared to those obtained for Hornfels (RAP) justifying the crushed status of the aggregate.

The stress – strain plots for 'G2 + 1% cement' mix show good correlation between those for STT and RTT owing to the fact that the specimens used in this test were cured for seven days under 95 – 100 humidity at 25 °C and immediately after seven days they were tested within a day.

There is no significant difference between principal stresses at failure of the STT results compared to those of RTT on G2 + 1% cement mix except for the results at 200 kPa. This could be mainly due to the fact that specimens were cured and therefore, less sensitive to the effect of confinement except in cases where confinement is high i.e. 200 kPa.

## **7.5. Analysis of variance (ANOVA)**

### **7.5.1. Introduction**

Analysis of variance (ANOVA) was carried out to look for statistically significant relationship between results obtained from STT and those from RTT. ANOVA works by examining the difference between the samples as well as the difference within a sample. This difference is referred to as variance, defined as the average squared deviation from the mean. Variance (abbreviated as MS for mean of squares) is found by dividing the variation by the degree of freedom, df (see Equation 17);

$$\text{Variance (MS)} = \text{variation (SS)}/\text{degree of freedom (df)} \quad \text{Eq.18}$$

Where, variation (abbreviated as SS for sum of squares) is the sum of squares of the deviations of the values from the mean of those values; and degree of freedom (df) is the number of values that are free to vary once certain parameters have been established. Usually degree of freedom is taken as one less than the sample size but in general it is the number of values minus the number of parameters being estimated.

Therefore, as long as the data values are not identical, there is variation and the source of this variation can be the model or the factor. There is always the left over variation that cannot be explained by any other sources and is referred to as the error.

### **7.5.2. ANOVA Calculation**

Calculating an ANOVA means calculating the F test statistic which is the ratio of two sample variances (see Equation 18) and this F statistic is then used to determine the likelihood of obtaining such a score by chance.

F statistic = Mean Squared Between (MSB)/Mean Squared Within (MSW)

Eq.19

Where;

MSB = Sum of Squares Between/degrees of freedom between; and

MSW = Sum of Squares within/degrees of freedom within.

ANOVA calculations are best presented in table format (ANOVA table) composed of rows; each row representing one source of variation and five columns for variation (SS), degree of freedom (df), variance (MS), F statistic and the last column which presents the critical F value or the p value which finishes the hypothesis test. The hypothesis test for the ANOVA in this study is that if p value is less than 5 % then the variation is significant. The ANOVA in this study was performed using a statistical package, Statistica in consultation with Prof D. G. Nel of Statistical Consultation Unit of the US.

One of the assumptions made by ANOVA is that population is normally distributed. However, this is not always the case with most data as can be noted from normal probability plots in Appendix 6. Therefore, to go around this problem the Bootstrap statistical method (Efron & Tibshirani, 1993) was used. The bootstrap is a computationally intensive resampling method which is widely applicable and allows the treatment of situations in which the exact sampling distribution of the statistic of interest is unknown.

Due to many variables which included cement, aggregate type and confining pressure for the number of data points available, the ANOVA could not be carried out; see Table 29. The statistician consulted, advised that for ANOVA to be carried out, 4 to 5 minimum data points for each mix type and confining pressure need to be achieved to solidly conclude the variance analysis (Nel, 2008).

**Table 29: Summary frequency table for STT (same as for RTT)**

Cement	Aggregate	Pressure 50 kPa	Pressure 100 kPa	Pressure 200 kPa	Row Totals
0%	RAP	1	1	1	3
0%	G2	1	1	1	3
Total		2	2	2	6
1%	RAP	1	3	1	5
1%	G2	1	1	1	3
Total		2	4	2	8
Column Total		4	6	4	14

The target summary frequency table (see Table 30) for STT alone would require 48 specimens and another 48 for RTT as a minimum. This statistical demand could not be achieved in this study for the

available time and resources especially that a lot of time was spent developing the STT apparatus and making sure it was working properly. Therefore, the author recommends that future research on the evaluation of the STT be in line with this statistic design.

**Table 30: Target summary frequency table**

Cement	Aggregate	Pressure 50 kPa	Pressure 100 kPa	Pressure 200 kPa	Row Totals
0%	RAP	4	4	4	12
0%	G2	4	4	4	12
Total		8	8	8	24
1%	RAP	4	4	4	12
1%	G2	4	4	4	12
Total		8	8	8	24
Column Total		16	16	16	48

Nevertheless, in order to have a statistical feel for the data obtained so far, a repeated measures ANOVA is possible if the effect of cement can be ignored and assuming same aggregate. This was performed in order to compare how response variables (maximum applied load, displacement at failure, corrected strain at failure, applied stress at failure, major principal stress at failure, tangent modulus and secant modulus) for STT and RTT denoted as DV\_1 behave relative to different confining pressures. Where data was not normally distributed Bootstrap techniques were deployed in the analysis.

### 7.5.3. ANOVA results where applied stress at failure (kPa) is the response variable

**Table 31: Repeated measures ANOVA table with  $\sigma_{a,f}$  as DV\_1**

Effect	Repeated Measures Analysis of Variance (DATA STTRIT 20) Sigma-restricted parameterization Effective hypothesis decomposition				
	SS	Degr. of Freedom	MS	F	p
Intercept	56474255	1	56474255	152.6160	0.000000
PRESSURE	3101382	2	1550691	4.1906	0.044368
Error	4070458	11	370042		
REPEAT	433390	1	433390	17.5167	0.001523
REPEAT*PRESSURE	186427	2	93213	3.7675	0.056716
Error	272157	11	24742		

From Table 31, the p – value for repeated measures is 0.05672 which is greater than 5 % and thus the variation of applied stress at failure obtained between STT and RTT is not significant according to

the hypothesis. This is illustrated in Figure 94 below with the least variation obtained at 50 kPa confining pressure and STT values being higher than RTT at 100 and 200 kPa confining pressures.

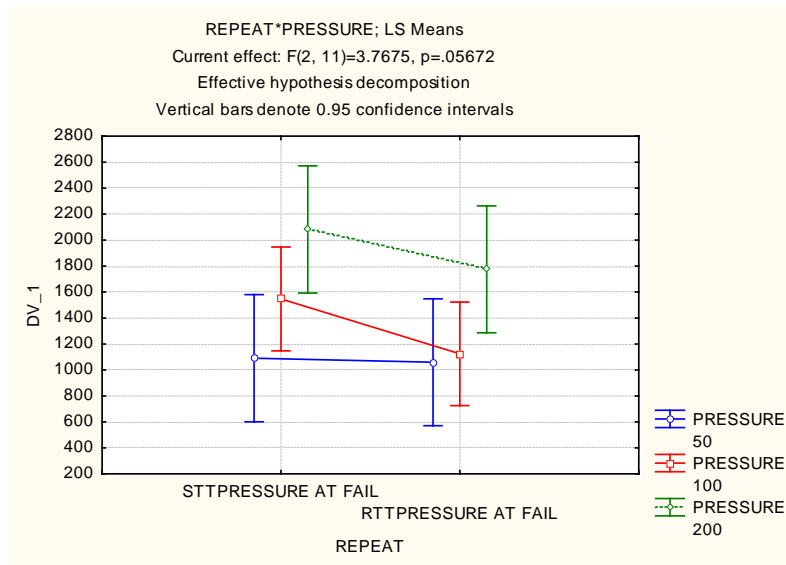


**Figure 94: Variation of applied stress at failure between STT and RTT**

Variation within samples of both STT and RTT is quite significant though, as indicated by a p – value of 0.00152 and illustrated in Figure 95.

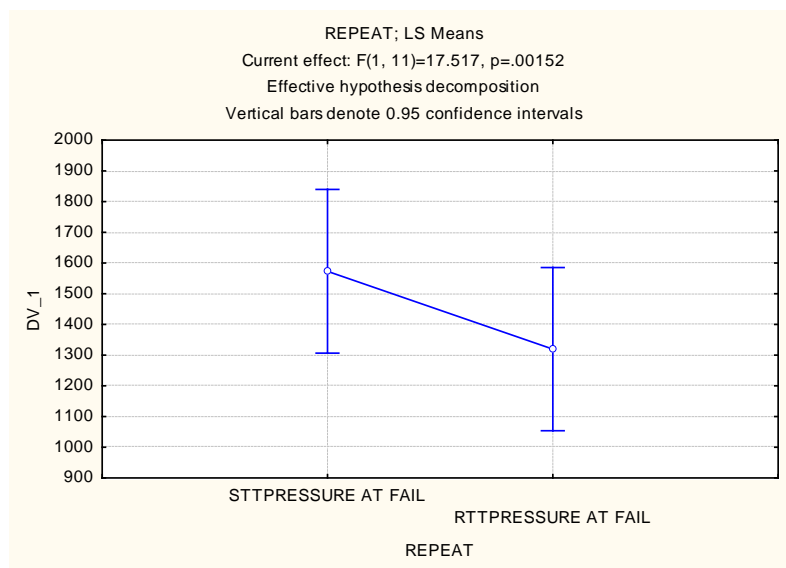


**Figure 95: Variation within STT and RTT samples**

From Figure 96, it can be noted that STT results of applied stresses at failure at different confining pressures are more consistent with theory than RTT results, with small differences between stress at failure at 50 and 100 kPa confining pressures.

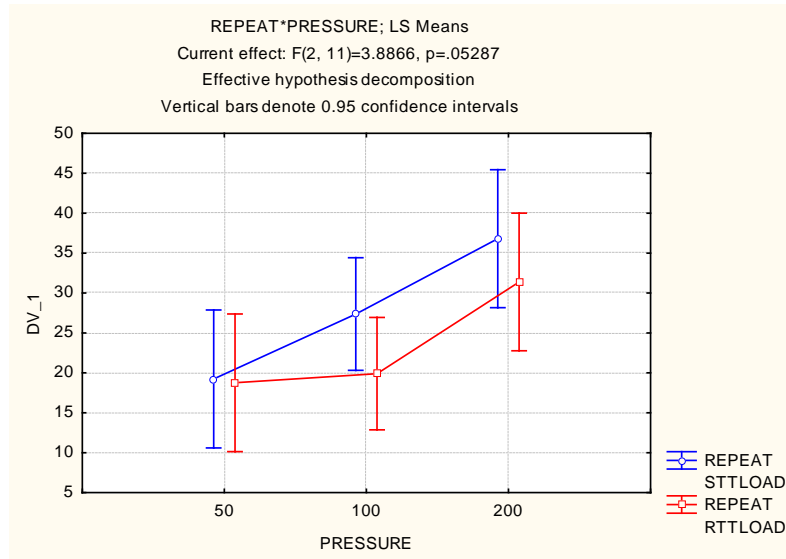


Figure 96: Principal stress at failure vs confining pressure for STT and RTT

#### 7.5.4. ANOVA results where major principal stress at failure is the response variable

Table 32: Repeated measures ANOVA table with  $\sigma_{1,f}$  as DV\_1

Repeated Measures Analysis of Variance (DATA STTRTT 20) Sigma-restricted parameterization Effective hypothesis decomposition					
Effect	SS	Degr. of Freedom	MS	F	p
Intercept	61351105	1	61351105	165.9261	0.000000
PRESSURE	3666260	2	1833130	4.9578	0.029180
Error	4067246	11	369750		
REPEAT	130052	1	130052	5.2721	0.042321
REPEAT*PRESSURE	149056	2	74528	3.0212	0.089998
Error	271349	11	24668		

From Table 32, the p – value for repeated measures is 0.0900 which is greater than 5 % and thus the variation of applied stress at failure obtained between STT and RTT is not significant according to the hypothesis. This is illustrated in Figure 97 with similar trend observed between STT and RTT results of principal stress at failure as for applied stress at failure in Section 7.5.3, except for this case less variation is observed for results at 50 and 200 kPa confining pressures.

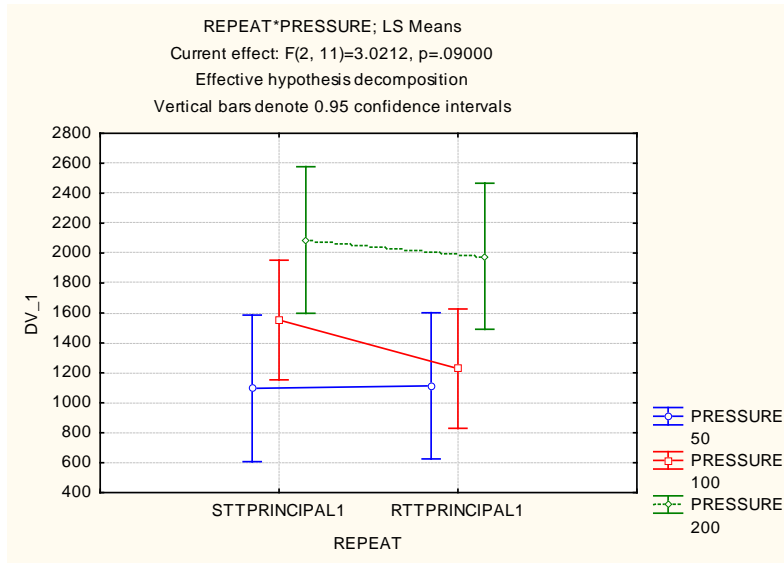


**Figure 97: Variation of major principal stress at failure between STT and RTT**

Variation of major principal stress at failure within samples of STT and RTT is still significant as indicated by the p – value of 0.04232 which is less than 5 % according to our hypothesis. This is illustrated in Figure 98 below.

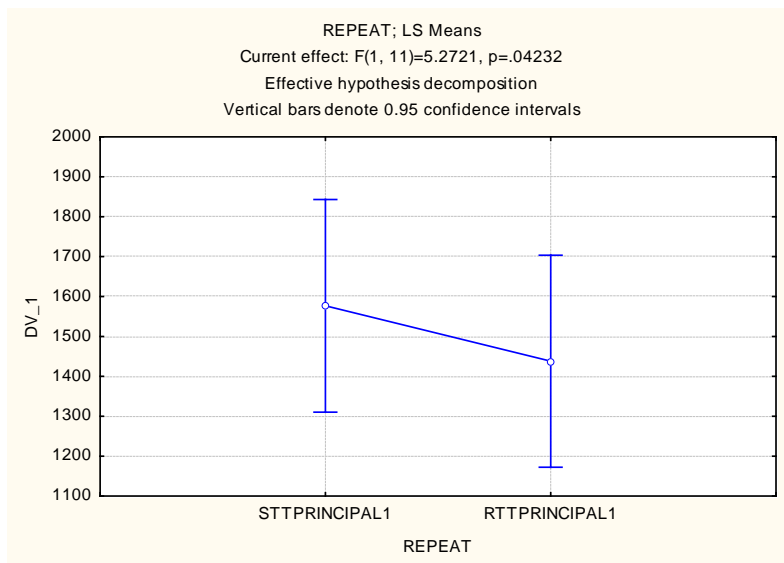


**Figure 98: Variation of major principal stress at failure within STT and RTT**

From Figure 99, it can still be noted that STT results at different confining pressures are more consistent with theory than RTT results.

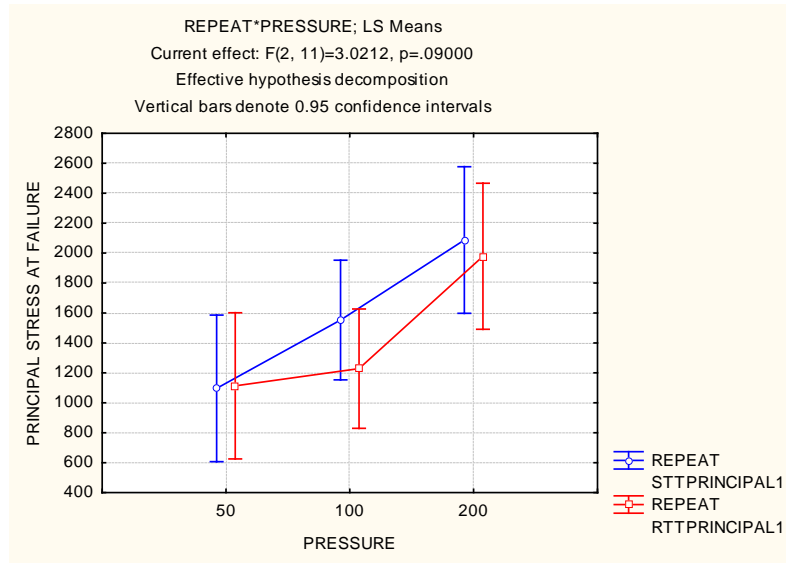


Figure 99: Principal stress at failure vs confining pressure for STT and RTT

#### 7.5.5. ANOVA results where tangent modulus is the response variable

Table 33: Repeated measured ANOVA table with  $E_{tan}$  as DV\_1

Effect	Repeated Measures Analysis of Variance (DATA STTRTT 2) Sigma-restricted parameterization Effective hypothesis decomposition				
	SS	Degr. of Freedom	MS	F	p
Intercept	831738.4	1	831738.4	112.1394	0.000000
PRESSURE	11414.1	2	5707.1	0.7695	0.486665
Error	81587.0	11	7417.0		
REPEAT	11362.1	1	11362.1	4.4978	0.057489
REPEAT*PRESSURE	3057.6	2	1528.8	0.6052	0.563178
Error	27787.5	11	2526.1		

From Table 33, the p – value for repeated measures is 0.563 which is greater than 5 % and thus the variation of tangent modulus obtained between samples of STT and RTT is not significant according to the hypothesis. Figure 100 also shows a similar trend where this variation is much less significant at 50 kPa confining pressure than at 100 and 200 kPa confining pressures. Variation of tangent modulus within samples of STT and RTT results is not significant as indicated by p-value of 0.0575 (see Figure 101) however, STT sample show more variability within than RTT.

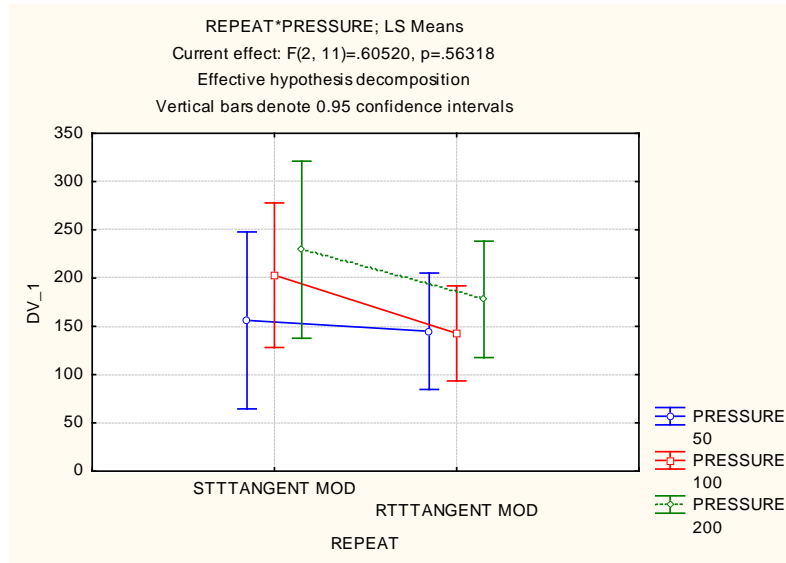


**Figure 100: Variation of tangent modulus between STT and RTT**

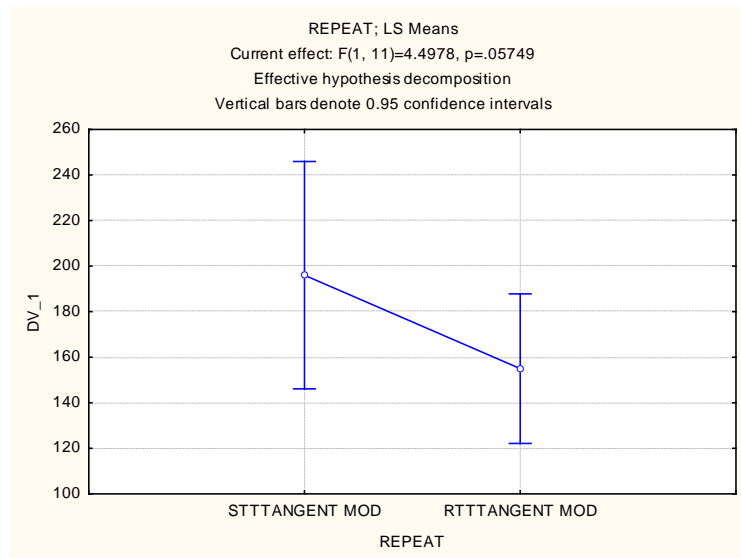


**Figure 101: Variation of tangent modulus within STT and RTT**

The relationship between STT and RTT results (characterised by less significant variation between and significant variation within samples) is more less the same for other response variables considered, details of ANOVA analysis for all response variables are appended in Appendix 6.

Also included in Appendix 6 is a Case 2 Repeated ANOVA based on repeated results on 'RAP (Hornfels) + 3.3 % Emulsion + 1 % Cement' mix at 100 kPa confinement. This analysis though with limited data shows less significant variation between STT and RTT samples, however STT samples show significant within sample variability, see Figures 102 and 103.

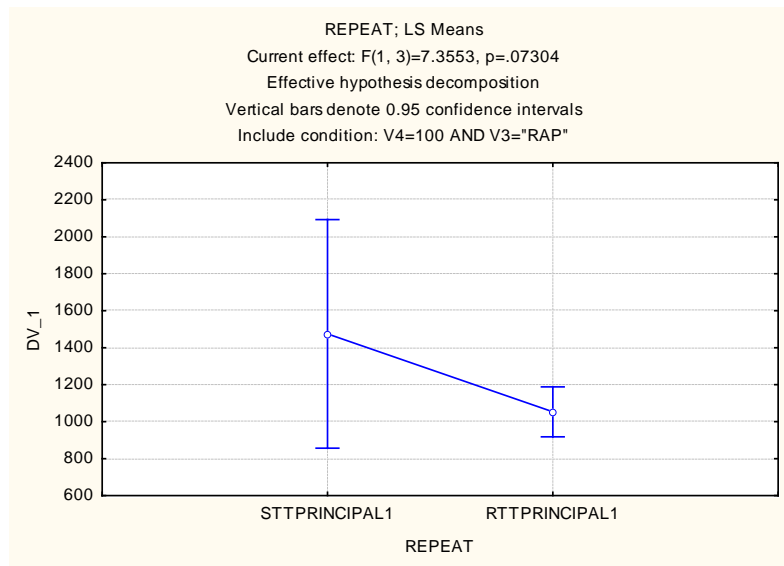


**Figure 102: Variation of principal stress at failure within STT and RTT**

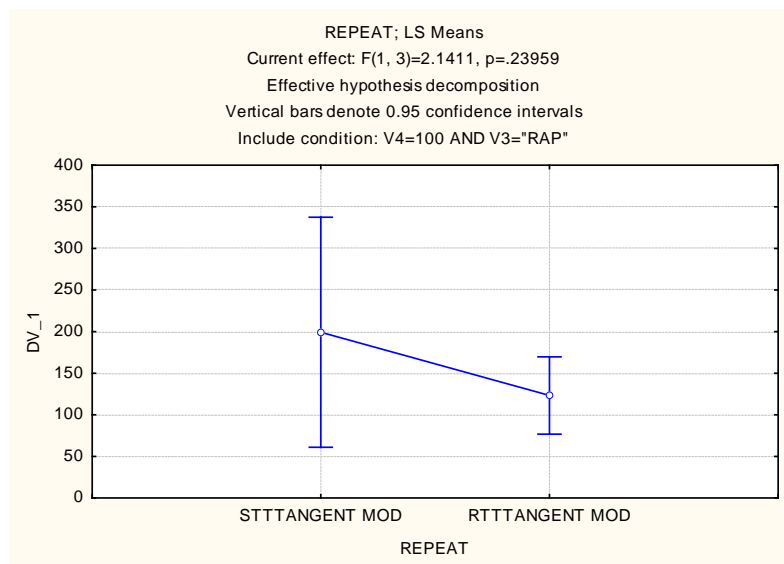


**Figure 103: Variation of tangent modulus within STT and RTT**

## 7.6. Closure

The analysis in general shows that the mechanical properties (cohesion and internal angle of friction) obtained using STT and RTT results are comparable and the differences noted could be attributed to material variability i.e. random variability to one degree or the other and not to the STT apparatus.

The ANOVA particularly shows that the variability that exists between STT and RTT results is less significant; what is significant though is the variability within the samples. However, this within sample variability could be attributed to material variability and to the assumptions made in order to perform the analysis which ignored the effect of cement and assumed same aggregate type.

Also from the analysis of variance performed, STT results at 100 and 200 kPa confining pressures are observed to be consistently higher than those of RTT, confirming the suspicion of additional confinement effect of the tube at confining pressures higher than 50 kPa. This however, can be investigated through further study (outside the scope of this study) on the STT such as pressure calibration.

Nonetheless, many researchers in this field can agree with the fact that different results are obtainable on comparable specimens of one mix, using the same equipment, at the same confinement as was the case with the RTT in Section 7.2. The only way to go round this is to meet the statistical demand of having more data points to work with (at least four at each confining pressure). However, this presents a challenge where RTT is a complex procedure and meeting such statistical demands is a daunting task therefore, efforts to simplify the procedure as much as possible like the STT are extremely welcome.

Conclusions drawn from the results presented and analysed as well as recommendations for future research and modifications to the STT are presented in the following chapter.

## 8. CONCLUSIONS AND RECOMMENDATIONS

This chapter is the culmination of the research study in conclusion of the presented work and makes recommendations for future research in this field.

### 8.1. Conclusions

From the development process of the STT which included situation analysis, conceptualisation, design, manufacture, assembly, testing and analysis of test results, it can be concluded in accordance with the main objective of this study that an effective and applicable Simple Triaxial test has been developed for characterising granular and bituminous stabilised materials.

#### 8.1.1. Advantages

The simplicity of the STT stems from the following features related to the simple triaxial cell developed:

- It is locally made at a low cost compared to the imported and expensive geotechnical triaxial cells;
- Assembly of specimen in the cell is relatively easy and quick compared to procedures of the research triaxial;
- Besides the latex tube the rest of the cell is made of steel; though you cannot see inside of the cell it is very durable comparably;
- The tube takes the air pressure and as long as the tube is air tight, one does not need to worry about making the whole cell air tight or preventing pressurised air from interacting with air in the specimen's voids;
- The tube may not last many tests but it can also be patched. This was observed after eight tests the tube was punched but after mending it lasted another six tests and it is still available for more tests.
- It can be carried around easily in and outside the laboratory.

Another aspect of the simplicity of the STT cell is its dead weight, even if it is made of steel the STT cell is much lighter than the RTT cells for measuring 300 mm high specimens (RTT<sub>300</sub>) and another type for measuring 250 mm specimens (RTT250). This finding was concluded by the weight analysis conducted in Appendix 7 and summarised as shown in Figure 104.

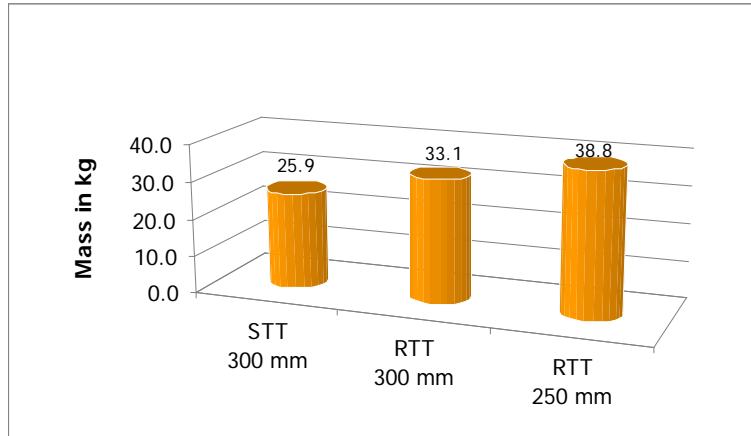


**Figure 104: Weight comparison of STT against RTT**

The weight of the triaxial cell is another aspect of complexity as current specimen assembly procedures require the operator to assemble a specimen of approximately 12 kg in the cell weighing 39 kg and lifting the whole assembled mass of about 51 kg to and from the testing frame over a four step distance. This is a strain on the operator and thus a reduction in weight capacity in excess of 12 kg is a welcome development.

Table 35 below summarises the comparison between the STT and RTT in terms of apparatus, test conditions, calculation of principle stress at failure, test results, models used and parameters obtained.

**Table 34: Summary of comparison between STT and RTT**

Feature	STT	RTT
<b>Apparatus</b>	<p><b>Triaxial Cell Features</b></p> <ul style="list-style-type: none"> <li>• Not transparent</li> <li>• Steel casing</li> <li>• Tube</li> <li>• Four simple mechanical clamps</li> <li>• Bottom platen belt in with base</li> <li>• No membrane on specimen required</li> <li>• No O rings required</li> </ul> <p><b>Testing System</b></p> <ul style="list-style-type: none"> <li>• MTS</li> </ul> <p><b>Measuring Devices</b></p> <ul style="list-style-type: none"> <li>• Same</li> </ul>	<p><b>Triaxial Cell Features</b></p> <ul style="list-style-type: none"> <li>• Transparent</li> <li>• Perspex casing</li> <li>• No Tube</li> <li>• Six thumb screws</li> <li>• Six bolts</li> <li>• Separate bottom platen and base</li> <li>• Membrane required</li> <li>• Two O rings required</li> </ul> <p><b>Testing System</b></p> <ul style="list-style-type: none"> <li>• MTS</li> </ul> <p><b>Measuring Devices</b></p> <ul style="list-style-type: none"> <li>• Same</li> </ul>
<b>Test Conditions</b>	<ul style="list-style-type: none"> <li>• Temperature 25 °C</li> <li>• Varying Confining Pressure, <math>\sigma_3</math> = 50, 100, 200 kPa</li> </ul>	<ul style="list-style-type: none"> <li>• Temperature 25 °C</li> <li>• Varying Confining Pressure, <math>\sigma_3</math> = 50, 100, 200 kPa</li> </ul>

Feature	STT	RTT
<b>Loading Conditions</b>	Static or Ramp load applied at a 2.1% mm/min displacement	Static or Ramp load applied at a 2.1% mm/min displacement
<b>Calculation of Principle Stress at Failure</b>	$\sigma_{1,f} = \sigma_{a,f} + \sigma_{dw}$ Where: $\sigma_{1,f}$ = principle stress at failure $\sigma_{a,f}$ = applied failure stress $\sigma_{dw}$ = pressure resulting from dead weight (top cap & loading ram)	$\sigma_{1,f} = \sigma_{a,f} + \sigma_3 + \sigma_{dw}$ Where: $\sigma_{1,f}$ = principle stress at failure $\sigma_{a,f}$ = applied failure stress $\sigma_3$ = confining pressure $\sigma_{dw}$ = pressure resulting from dead weight (top cap & loading ram)
<b>Test Results</b>	Load (Stress) Vs Displacement (Strain)	Load (Stress) Vs Displacement (Strain)
<b>Models Used</b>	$\tau_f = c + \sigma \tan \phi$	$\tau_f = c + \sigma \tan \phi$
<b>Parameters Determined</b>	Shear Strength of Material (cohesion, C and angle of internal friction $\phi$ )	Shear Strength of Material (cohesion, C and angle of internal friction $\phi$ )
<b>Dead Weight</b>	26 kg	33 to 39 kg

### 8.1.2. Disadvantages

The Simple Triaxial Test is not without any disadvantages. The following are some of the limitations of the STT stemming from some features of the Simple Triaxial Cell:

- The latex tube and the steel casing make it impossible to have a transparent cell. Thus you cannot see the specimen while it is being tested;
- The cell does not allow much variability in the sizes of the specimens. This however, is the case with the research triaxial cell.
- The latex tube-like membrane in the case of a research triaxial cell requires replacement after some tests.
- LVDT's cannot be installed on the STT specimen due to the presence of the tube around it, thus limiting the possibility of accurate measurements being made for dynamic tests.

## 8.2. Recommendations

Following the findings of this research project, it is recommended that:

- Now that the Simple Triaxial Test by tube method has been proved to work, a more reliable and quicker method of making this special type of tube is required;
- The development of the Simple Testing System, to go with the Simple Triaxial Cell developed should be undertaken. This can take the form of the CBR loading frame but with the added advantage of computer control;
- Modification in the design, resulting in making the base plate (where the specimen sits) wider than the diameter of the specimen is proposed and filling the space between the tube top and casing to enhance the life of the tube;
- A study to calibrate the pressure obtained on the specimen so as to determine whether or not there is higher pressure on the specimen than that which is set in the tube (tube effect on confinement); and
- This forms just the basis of the Simple Triaxial Test development therefore, more tests by different researchers especially on mixes of known mechanical properties such as G1 materials, are needed to fully understand and verify it and to propose improvements.

## 8.3. Closure

The research reported in this thesis formed part of the tasks of the TGx Project, Updating South Africa's Bituminous Stabilised Materials Guidelines – Mix Design Report, Phase II. The funding was provided by SABITA and Gauteng Department of Transport and Public Works.

## References

- Efron, B., and Tibshirani, R., 1993. **An Introduction to Bootstrap**. London: Chapman and Hall, 1993.
- Jenkins, K.J. and Ebels, L.J, 2007. **Determination of Shear Parameters, Resilient Modulus and Permanent Deformation Behaviour of Unbound and Bound Granular Materials Using Tri-Axial Testing on 150mm Ø x 300mm High Specimens**. Technical Memorandum. Stellenbosch, South Africa, 2007.
- Jooste, F., Long, F., and Hefer, A., 2007. **A Method for Consistent Classification of Materials for Pavement Rehabilitation Design**. Technical Memorandum CSIR, 2007.
- Kelfkens, R.W.C., 2008. **Vibratory Hammer Compaction of Bitumen Stabilised Materials**. MSc.Eng Thesis, Stellenbosch University, South Africa, 2008.
- Nel, D.G., 2008. **Consultation**. Statistical Consultancy Unit at Stellenbosch University, 2008.
- Texas Department of Transport, 2002. **Triaxial Compression for disturbed soils and base materials**, TxDOT Designation: Tex-117-E, August 2002.

## **APPENDIX 1 – TxDOT TRIAXIAL PROCEDURE**

---

**Test Procedure for****TRIAXIAL COMPRESSION FOR DISTURBED SOILS  
AND BASE MATERIALS****TxDOT Designation: Tex-117-E****Effective Date: August 2002**

---

**1. SCOPE**

- 1.1 This method determines the shearing resistance, water absorption, and expansion of soils and/or soil-aggregate mixtures.
  - 1.2 The values given in parentheses (if provided) are not standard and may not be exact mathematical conversions. Use each system of units separately. Combining values from the two systems may result in nonconformance with the standard.
- 

**2. DEFINITIONS**

- 2.1 *Triaxial Test*—The triaxial test is one in which stresses are measured in three mutually perpendicular directions.
  - 2.2 *Axial Load*—Axial load is the sum of the applied load and the dead load (including the weight of the top porous stone, metal block and bell housing) applied along the vertical axis of the test specimen.
  - 2.3 *Lateral Pressure (Minor Principal Stress)*—Lateral pressure is the pressure supplied by air in the triaxial cell, applied in a radial or horizontal direction.
  - 2.4 *Axial (Major Principal Stress)*—The axial load divided by the average area of the cylindrical specimen.
  - 2.5 *Strain*—Strain is the vertical deformation of the specimen divided by the original height, often expressed as a percentage.
  - 2.6 *Mohr's Diagram*—Mohr's diagram is a graphical construction of combined principal stresses in static equilibrium.
  - 2.7 *Mohr's Failure Cycle*—Mohr's failure circle is a stress circle constructed from major and minor principal stresses of the specimen at failure.
  - 2.8 *Mohr's Failure Envelope*—Mohr's failure envelope is the common tangent to a series of failure circles constructed from different pairs of principal stresses required to fail the material. The envelope is generally curved, its curvature depending on the factors related to the characteristics of the material.
-

---

### 3. APPARATUS

- 3.1 *Apparatus*, used in Tex-101-E, Tex-113-E, and Tex-114-E.
- 3.2 *Triaxial cells*, lightweight stainless steel cylinders.
- 3.2.1 *Base Material*, 171.5 mm (6.75 in.) inside diameter (I.D.) and 304.8 mm (12 in.) in height.
- 3.2.2 *Subgrade*, 114.3 mm (4 1/2 in.) I.D. and 228.6 mm (9 in.) in height; fitted with standard air valve and tubular rubber membrane 152.4 mm (6 in.) in diameter.
- 3.3 *Aspirator or other vacuum pump*.
- 3.4 *Air compressor*.
- 3.5 *Load frame and assembly*.
- 3.6 *Pressure regulator, gauges, and valves*, to produce lateral pressure in curing and testing.
- 3.7 *Equipment to measure deformation of specimen*, accurate to 0.025 mm (0.001 in.).
- 3.8 *Axial load measuring device*, calibrated in accordance with Tex-902-K.
- 3.9 *Circumference measuring device*, accurate to 1.0 mm (0.05 in.).
- 3.10 *Lead weights*, for surcharge loads.
- 3.11 *Pans*, curing, at least 51 mm (2 in.) deep, with porous plates.

---

### 4. TEST RECORD FORMS

- 4.1 Record test data on:
- [Form 1964](#), 'Triaxial Compression Test Capillary Wetting Data'
  - [Form 1176](#), 'M/D Triaxial Test Worksheet'
  - [Form 1062](#), 'Triaxial Test Data Sheet'
- 4.2 After tests and calculations are completed, summarize results on:
- [Form 1963](#), 'Triaxial Test Summary Sheet'

---

## PART I—STANDARD TRIAXIAL COMPRESSION TEST

---

### 5. PROCEDURE

- 5.1 Determine optimum water content and maximum dry density of the material and molding of the triaxial test specimens, in accordance with Tex-113-E and Tex-114-E.
- 5.2 Mold seven specimens at optimum moisture and maximum dry density for base and sub-base materials.
- 5.2.1 For fine-grained sub-grade soils, mold six specimens at optimum moisture and maximum dry density.
- 5.2.2 These specimens should be 152.4 mm (6 in.) in diameter and 203.2 mm (8 in.) in height  $\pm$  6.4 mm (0.25 in.) or 101.6 mm (4 in.) in diameter and 152.4 mm (6 in.) in height using a straight edge to strike off the top and bottom.
- 5.2.3 These specimens should be wetted, mixed, molded, and finished as nearly identical as possible.
- 5.2.4 Identify each test specimen by laboratory number and specimen number.
- 5.3 Immediately after extruding the specimens from the molds, enclose the specimens in triaxial cells, with top and bottom porous stones in place, and allow all the specimens to remain undisturbed at room temperature until the entire set of test specimens has been molded. Record data on the 'M/D Triaxial Worksheet,' [Form 1176](#).
- Note 1**—When a different compactive effort is desired, a complete new M/D Curve and test specimens must be molded.
- 5.4 After the entire test set has been completed, remove the triaxial cells. Described below are the appropriate dry curing procedures for various material types. Dry cure the specimens according to the type of material to avoid excessive cracking which will damage the specimen.
- 5.4.1 *For flexible base materials and select granular soils with little or no tendency to shrink:*
- 5.4.1.1 Place specimens in the oven air dryer and remove 1/3 to 1/2 of the molding moisture content at a temperature of 60°C (140°F). (This will require three to six hours, depending on the material, the optimum moisture content, and the load of other wet material in the oven).
- 5.4.1.2 Allow the specimens to return to room temperature before preparation for and subjection to capillarity.
- 5.4.2 *For very plastic clay sub-grade soils that crack badly if subjected to large volume changes during shrinkage:*

- 5.4.2.1 Air dry these soils at room temperature, inspecting specimens frequently by looking at the sides of the specimens and raising the top porous stones to examine the extent of cracking at the top edges of the specimens.
- 5.4.2.2 When these cracks have formed to a depth of approximately 6.4 mm (1/4 in.), replace the triaxial cell and prepare the specimens for capillary wetting.
- 5.4.3 *For moderately active soils that might crack badly if placed in an air dryer for the full curing time:*
  - 5.4.3.1 Dry at 60°C (140°F) and check frequently for the appearance of shrinkage cracks.
  - 5.4.3.2 If cracks appear, examine the extent of cracking as described above, and allow some air-drying at room temperature during the cooling period before enclosing specimens in cells.
- 5.5 The specimens are now ready to be prepared for capillary wetting:
  - 5.5.1 Do not change the porous stones or remove them until the specimens have been tested.
  - 5.5.2 Weigh each specimen and its accompanying stones and record the mass.
  - 5.5.3 Cut a piece of filter paper to 254 x 508 mm (10 x 20 in.), fold into 127 x 508 mm (5 x 20 in.), and make several cuts with scissors (Jack-o-lantern fashion). These cuts will prevent any restriction by the paper.
  - 5.5.4 Unfold the filter paper and wrap it around the specimen and stones so the cuts are parallel with the length of the specimen, allowing the bottom of the paper to be near the bottom of the bottom porous stone, and fasten with a piece of tape.
  - 5.5.5 Replace cell by applying a partial vacuum to the cell, deflating the rubber membrane, then place the cell over the specimen and release the vacuum.
- 5.6 Transfer the specimens to the damp room or temperature controlled environment and place them into the rectangular pans provided for capillary wetting. Adjust the water level on the lower porous stones to approximately 12.5 mm (0.5 in.) below the bottom of the specimens. Add water later to the pans, as necessary, to maintain this level (See Figure 1.)
- 5.7 Connect each cell to an air manifold and open the valve to apply a constant lateral pressure of 6.9 kPa (1 psi). Maintain this constant pressure throughout the period of absorption.
- 5.8 Next, place a suitable vertical surcharge load (which will depend upon the proposed use or location of the material in the roadway) on the top porous stone (See Table 1). When determining the mass for the surcharge, include the mass of the top porous stone as part of the surcharge mass.
- 5.9 Subject all flexible base materials and soils with plasticity index of 15 or less to capillary absorption for ten days. Use a period in days equal to the plasticity index of the material

for sub-grade soils with PI above 15. Keep the specimens at  $25 \pm 5^{\circ}\text{C}$  ( $77 \pm 9^{\circ}\text{F}$ ) during the period of capillary absorption.

- 5.10 Disconnect air hose from cell, remove surcharge weight, and return specimens to laboratory for testing. Use a vacuum and deflate the rubber membrane to aid in removing the cell from specimens and discard filter paper. If any appreciable material clings to paper, carefully press it back into the available holes along the side of the specimen.
- 5.11 Weigh the specimens and record as total mass after capillary absorption. Note that the wet mass of the stones is obtained after the specimens are tested. Record on the 'Triaxial Compression Test Capillary Wetting Data Sheet,' [Form 1964](#).
- 5.12 Measure the circumference of each specimen by means of the metal measuring tape. Measure the height of the specimen including the stones, and enter on the data sheet as height in/out capillarity. Record the height of each stone.
- 5.13 Ready the specimen to be tested by replacing the triaxial cell to eliminate any moisture loss from the specimen and then releasing the vacuum. When a specimen is designated to be tested at zero lateral pressure, remove the cell just before testing. It is important to keep the correct identification on the specimens at all times because weights, measurements, test values, and calculations are determined for each individual specimen.
- 5.14 Test the specimens in compression while they are being subjected to their assigned constant lateral pressure (See Figure 2). The motorized press should compress the sample at a rate of  $2.0 \pm 0.3\%$  strain per minute. Take simultaneous readings of load and deformation at intervals of 0.5 mm (0.02 in.) deformation until specimen fails.
- 5.15 Lower the load frame platen far enough to have room to place the specimen, loading blocks and deformation measuring equipment in the press.
- 5.16 Center the specimen with upper and lower loading blocks in place in the load frame. Determine if the deformation gauge will compress or extend during testing and set the dial stem accordingly. Set the dial of the strain gauge to read zero.
- 5.17 Next, set the bell housing, if used, over the deformation gauge and adjust so that it does not touch the gauge or its mounting.

**Note 2**—The compressive stress will necessarily be applied along a vertical line through the center of the ball that is mounted in the top of the bell housing.
- 5.17.1 Shift the bell housing laterally to bring the ball directly over the axis of the specimen, since it is desirable to apply the compressive force along the vertical axis of the test specimen.
- 5.17.2 Raise the platen by means of the motor, align, and seat the ball on the bell housing into the socket in the proving ring. Then apply just enough pressure to obtain a perceptible reading on the proving ring gauge (not to exceed 5 lbs.).
- 5.17.3 Read the deformation gauge and record as deformation under dead load.

- 5.18 Connect the airline to the triaxial cell and apply lateral pressure to the specimen. The usual lateral pressures used for a series of tests are 0 kPa (0 psi), 20.7 kPa (3 psi), 34.5 kPa (5 psi), 69.0 (10 psi), 103.5 kPa (15 psi) and 138.0 kPa (20 psi).
- 5.18.1 In cases where the load or stress is high, 1207 - 1241 kPa (175 -180 psi), for the specimen tested at 103.5 kPa (15 psi) lateral pressure, use 48.3 kPa (7 psi) instead of 138.0 kPa (20 psi) for the last specimen.
- 5.18.2 The lateral pressure applied by the air will tend to change the initial reading of the gauge. As the air pressure is adjusted, start the motor momentarily to compress the specimen until the deformation gauge reads the same as recorded in Section 5.17.
- 5.18.3 Read the proving ring gauge and enter in load column opposite the initial deformation reading on the 'Triaxial Test Data Sheet,' [Form 1176](#).
- 5.19 The test is ready to be started:
- 5.19.1 Turn on the motor and read the proving ring dial at each 0.5 mm (0.02 in.) deformation of the specimen.
- 5.19.2 Continue readings until 15.2 mm (0.60 in.) of deformation is reached or failure has occurred.
- 5.19.2.1 Failure is reached when the proving ring dial readings remain constant or decrease with further increments of deformation.
- 5.19.2.2 In testing specimens with aggregates, the slipping and shearing of aggregates will cause temporary decreases in proving ring readings.
- 5.19.3 Continue the test until true failure is reached.
- 5.19.4 After 15.2 mm (0.60 in.) of deformation the cross sectional area of the specimen has increased so that the subsequent small increase in load readings is little more than the increase in tension of the membrane acting as lateral pressure.
- 5.20 The above procedure also applies to an unconfined specimen except that no air or axial cell is used. For materials that contain a large amount of aggregate, test two specimens at zero lateral pressure. Use average of test results unless large rocks appear to have created point bearing; in this case use highest value.
- 5.21 Remove the cell and stones from the specimen over a flat, tared drying pan. Use a spatula to clean the material from the inside of cell and stones. Break up the specimen taking care to lose none of the material and place the identification tag in the tray.
- 5.22 Dry material to constant mass at a temperature of 110°C (230°F) and determine the dry mass.
- 5.23 Weigh the damp stones, then dry them at 60°C (140°F) and to constant mass.
- 5.24 Weigh the dry stones.

5.25 Record both the damp and dry masses on the 'Triaxial Test Data Sheet,' [Form 1062](#).

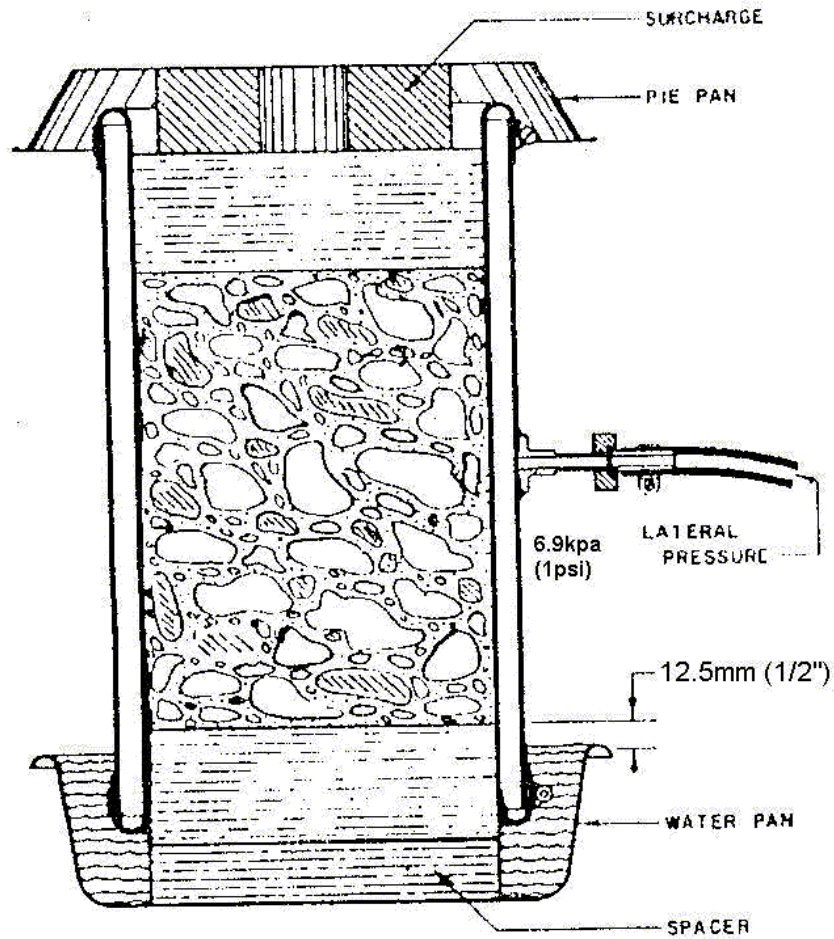


Figure 1—Schematic Arrangement for Capillary Wetting

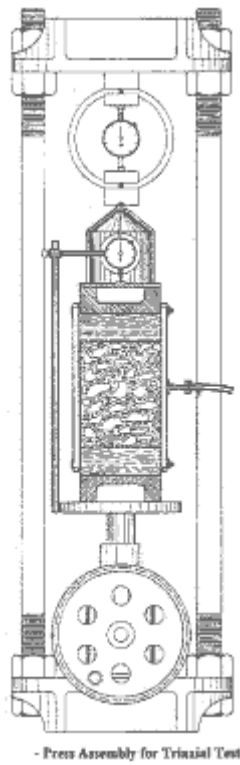


Figure 2—Press Assembly for Triaxial Press

Table 1—Vertical Surcharge Load		
Mold Diameter	Flexible Base	Sub-grade Soil
152 mm (6 in.)	6.4 kg (14.1 lb.)	12.8 kg (28.3 lb.)
102 mm (4 in.)	N/A	5.7 kg (12.6 lb.)

**6. CALCULATIONS**

6.1 Calculate dry density ( $D_D$ ) in  $\text{kg/m}^3$  (pcf):

$$D_D = W_D / V$$

Where:

V = volume of compacted specimen,  $\text{m}^3$  ( $\text{ft}^3$ )

$W_D$  = dry mass of specimen, kg (lbs.).

6.2 Calculate the percent molding moisture ( $M_M$ ):

$$M_M = [ 100(W_w - W_D) / W_D ]$$

Where:

$W_W$  = wet mass of specimen, kg (lbs.).

- 6.3 Calculate the percent of volumetric swell ( $V_S$ ):

$$V_S = 100(V_A - V) / V$$

Where:

$V_A$  = volume of specimen after capillary absorption, m<sup>3</sup> (ft<sup>3</sup>).

- 6.4 Calculate the percent moisture in the specimen after capillarity ( $M_C$ ):

$$M_C = 100(W_A - W_B - W_D) / W$$

Where:

$W_A$  = wet mass of specimen and stones after absorption, kg (lbs.)

$W_B$  = wet mass of stones, kg (lbs.)

$W_D$  = correct oven-dry mass of specimen, kg (lbs.).

- 6.5 Calculate the percent moisture in the specimen before capillarity ( $M_B$ ):

$$M_B = 100(W_C - W_S - W_D) / W_D$$

Where:

$W_S$  = dry mass of stones, kg (lbs.)

$W_C$  = mass of specimen and stones before capillarity, kg (lbs.).

- 6.6 Calculate the corrected vertical unit stress in kPa (psi). A correction is necessary because the area of the cross-section increases as the specimen is reduced in height. Assume that the specimen deforms at constant volume.

$$S = 100(d / h) = \text{percent strain}$$

Where:

d = total vertical deformation at a given instant, mm (in.), by deformation gauge

h = the height of the specimen, mm (in.), measured after specimen is removed from capillarity.

- 6.7 Calculate the corrected vertical unit stress (p):

$$p = 9.81 [ P(1 - S / 100) / A ], \text{ in kPa } \text{ or } p = P[(1 - S / 100) / A ], \text{ in psi}$$

Where:

A = the end area of the cylindrical specimen at the beginning of test, mm<sup>2</sup> (in<sup>2</sup>)

P = the total vertical load on the specimen at any given deformation expressed in g (lbs.). It is the sum of the applied load measured by the proving ring plus the dead mass of the upper stone, loading block, and dial housing.

---

## 7. GRAPHS AND DIAGRAMS

- 7.1 Plot the moisture-density curve shown in Tex-113-E, Figure 1.
- 7.2 Plot the stress-strain diagram as shown in Figure 3, when requested.
- 7.3 Construct the 'Mohr's Diagram' of stress upon coordinate axes in which ordinates represent shear stress and abscissas represent normal stress, both expressed as kPa (psi) to the same scale (See Figure 4).
- L = Minor principal stress which is the constant lateral pressure applied to the specimen during an individual test.
  - V = The major principal stress which is the ultimate compressive strength or the highest value of p determined at the given lateral pressure.
- 7.4 Show each individual test by one stress circle:
- Plot L and V on the base line of normal stress.
  - Locate the center of each circle a distance of  $(V + L)/2$  from the origin and construct a semi-circle with its radius equal to  $(V - L)/2$  intersecting the base line at V and L.
  - Repeat these steps for each specimen tested at different lateral pressures to provide enough stress circles to define the failure envelope on the Mohr's diagram.
- 7.5 Draw the failure envelope tangent to all of the stress circles. Since it is practically impossible to avoid compacting an occasional specimen that is not identical with the other specimens in the same set, disregard any stress circle that is obviously out of line when drawing the tangent line.

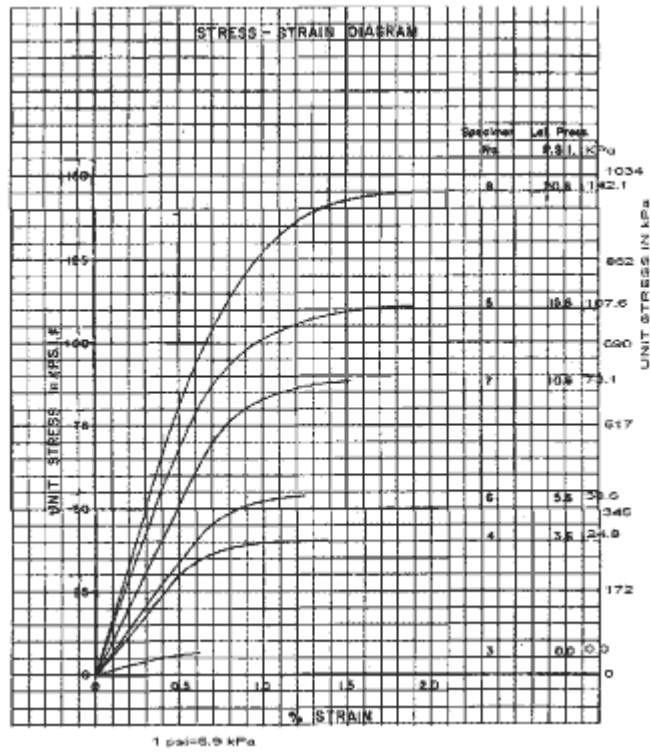


Figure 3—Stress-Strain Diagram

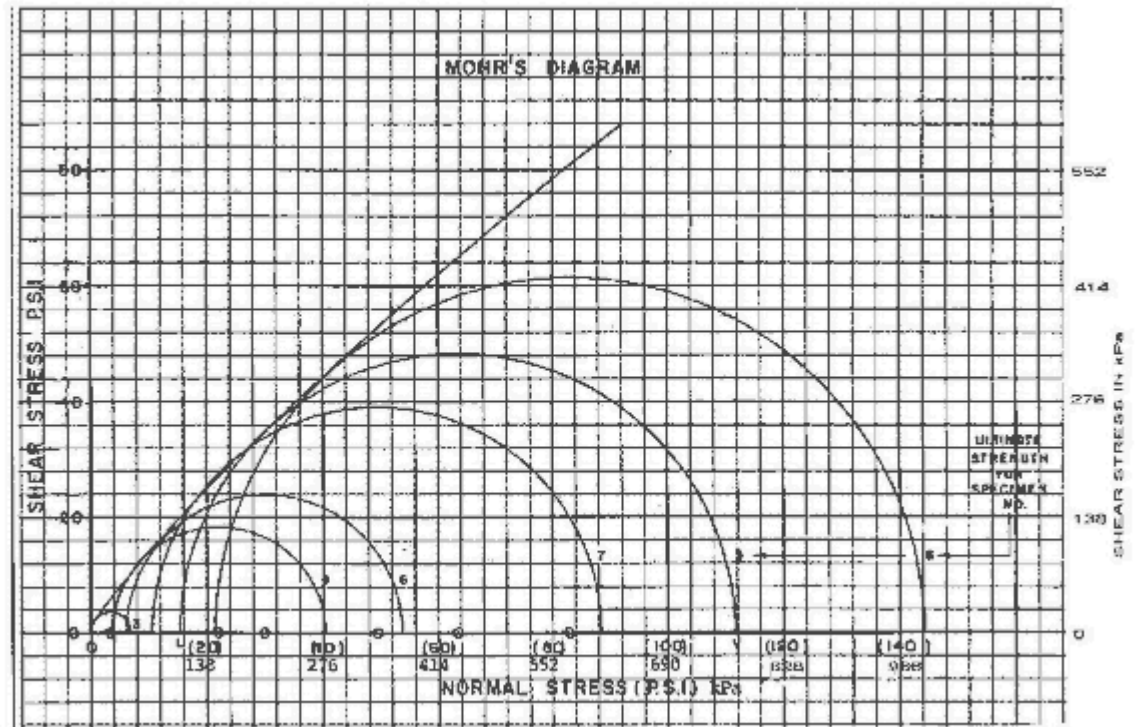
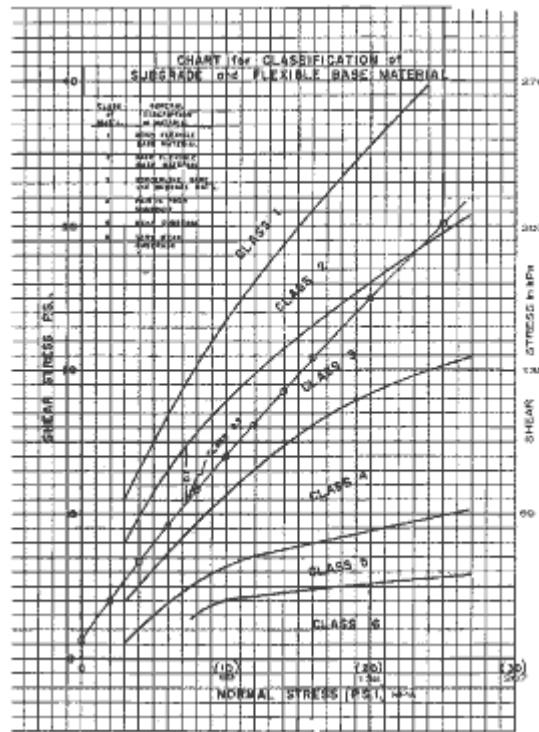


Figure 4—Mohr's Diagram

**8. CLASSIFICATION OF MATERIAL**

- 8.1 Transfer the envelope of failure onto the chart shown in Figure 5 and classify the material to the nearest one-tenth of a class.
- 8.2 When the envelope of failure falls between class limits, select the critical point or weakest condition on the failure envelope.
- 8.3 Measure the vertical distance down from a boundary line to the point to obtain the exact classification (3.7) as shown in Figure 5.



**Figure 5**—Chart for Classification of Sub-Grade and Flexible Base Material

**9. TEST REPORT**

- 9.1 Report the soil constants, grading and wet ball mill value for the base material. Summarize test results on the 'Triaxial Test Summary Sheet,' [Form 1963](#), and strength classification plotted as given in Figure 5.

---

## PART II—ACCELERATED METHOD FOR TRIAXIAL COMPRESSION OF SOILS

---

### 10. SCOPE

- 10.1 This accelerated procedure is based on a correlation with Part I, performed on a large number of different types of soils. Generally, use the accelerated test to control the quality of base materials with low absorption in group (d) during stockpiling. In such cases, roadway samples will not be considered representative.

---

### 11. PROCEDURE

- 11.1 Prepare all materials in accordance with Tex-101-E, Part II.
- 11.2 Determine the optimum moisture and maximum density in accordance with Tex-113-E and Tex-114-E.
- 11.3 Group the soils into five general types of materials:
- A. Fine granular materials with plasticity index less than 5.
  - B. Very low swelling soils with plasticity index of 5 through 11.
  - C. Swelling sub-grade soils, plasticity index of 12 or more.
  - D. Flexible base and sub-base materials with considerable amounts of aggregate.
  - E. Combination soil types.
- Follow the correct procedure for the specimen soil type, as shown below
- 11.3.1 *Group A – Fine Granular Materials with Plasticity Index Less Than 5:*
- 11.3.1.1 Mold six specimens 152.4 mm (6 in.) in diameter and 203.2 mm (8 in.) in height at the optimum moisture and density in accordance with Tex-113-E.
- 11.3.1.2 Cover the specimen (with stones in place) with a triaxial cell immediately after removing from mold and allow to set overnight undisturbed at room temperature.  
**Note 3**—Do not dry cure or subject specimens to capillary absorption.
- 11.3.1.3 Test the specimens at the usual lateral pressures.
- 11.3.1.4 Calculate unit stress, plot diagrams, and classify material.
- 11.3.2 *Group B – Very Low Swelling Soils with Plasticity Index of 5 through 11:*
- 11.3.2.1 Compact a set of six identical specimens at the optimum moisture and density condition in accordance with Tex-113-E.

- 11.3.2.2 Use filter paper, lead surcharge weight, and air pressure for lateral support and subject the specimens to capillary absorption overnight as described in Part I, Sections 5.8 through 5.12.
- 11.3.2.3 The next morning, remove filter paper and test the specimens at the usual lateral pressure shown above. Calculate unit stress, plot diagrams, and classify material.
- 11.3.3 *Group C – Swelling Sub-grade Soils, Plasticity Index of 12 or More:*
- 11.3.3.1 Obtain the plasticity index and hygroscopic moisture of these soils in advance of molding specimens.
- 11.3.3.2 Determine the optimum moisture and dry density of the materials in accordance with Tex-113-E.
- 11.3.3.3 Calculate the Percent Molding Moisture = (1.4 x optimum moisture) – 22.
- 11.3.3.4 Obtain the desired molding density from the following expression:  

$$\text{Molded Dry Density} = \text{Optimum dry density (from Section 11.2)} / [1 + (\% \text{ volumetric swell} / 100)]$$

To determine the percent volumetric swell to be expected, use average condition in chart shown in Figure 6. It is important to modify the percent volumetric swell by multiplying by percent soil binder divided by 100 to obtain the percent volumetric swell to be expected.
- 11.3.3.5 Use the moisture content (Section 11.3.3.3), adjusted if necessary, and adjust the blows per layer to obtain the desired density (Section 11.3.3.4). Where this moisture content is too great to permit the desired density, reduce the molding water slightly (usually about 1%) and continue molding. Mold six specimens, in accordance with Tex-114-E, at the water content established for the desired density. The specimens, being in capillarity overnight, will pick up the moisture that was left out.
- 11.3.3.6 When the six specimens have been molded, put them to capillary absorption (as in Part I ) overnight. Test at the usual lateral pressures and classify.

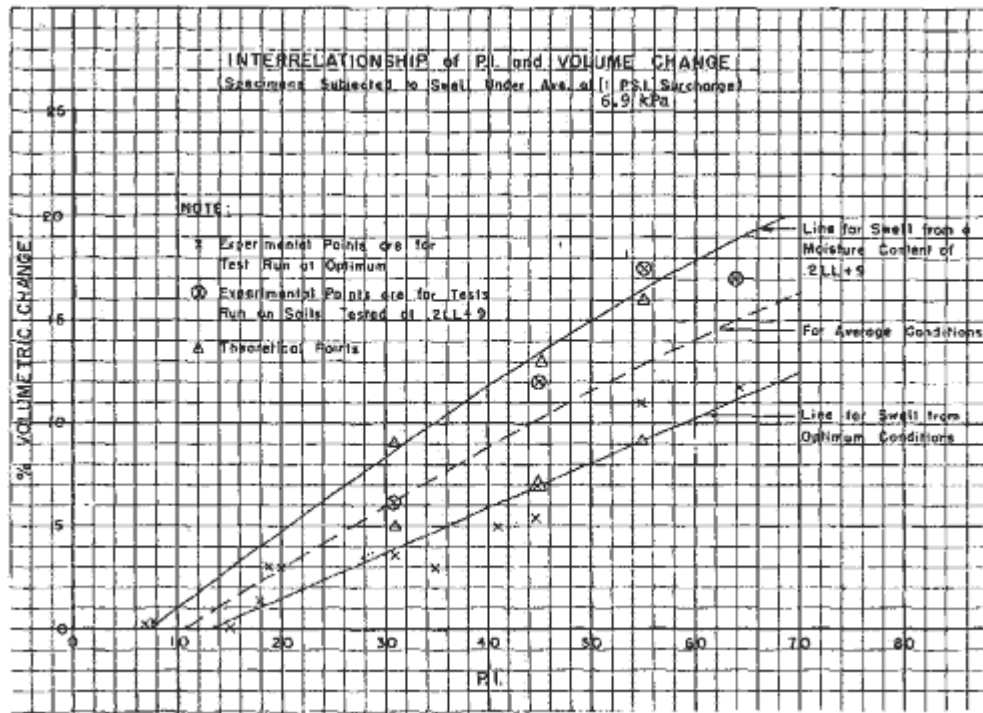


**Figure 6**—Interrelationship of PI and Volume Change

11.3.4 *Group D – Flexible Base and Sub-base Materials with Aggregate:*

11.3.4.1 When classification is required, weigh out enough material to mold seven or more specimens, in individual pans. Sprinkle all the soaking water on the material in the mixing pan and allow to soak for a minimum of 12 hours. The soaking water is the optimum moisture as determined in Tex-113-E, except where a flat top curve exists, then the soaking water would be the amount of the left side or dry side of the flat portion.

11.3.4.2 In testing base and sub-base materials with aggregates, the following procedure may be used where strengths are required.

11.3.4.2.1 Weigh out material for seven specimens in individual pans and sprinkle the water as estimated to be just below optimum moisture on each specimen by adding water in increments while mixing.

11.3.4.2.2 Weigh the contents to obtain the mass of the pan, soil and water, and record upon completion of mixing each sample.

11.3.4.2.3 Cover the specimens for strength or classification, with a lid or suitable cover to reduce moisture loss and let soak overnight with the material weighed out for the M-D curve.

11.3.4.2.4 Begin the M-D curve in accordance with Tex-113-E. Continue molding until the optimum moisture and density are determined.

- 11.3.4.2.5 The difference between optimum moisture and the water the specimens were sprinkled with must be added to the material in the pans. This amount should not exceed 2%. Let soak for at least one hour.
- 11.3.4.2.6 If, in the event the specimens have been wet with slightly more than optimum, not to exceed 1%, they may be dried back at room temperature, by constant stirring, to desired mass.
- 11.3.4.3 Replace any evaporated water, mix, and compact. Mold materials, which can be compacted to the desired density without the addition of more water, at optimum moisture  $\pm 0.1\%$ .
- 11.3.4.3.1 Many materials require the addition of small amounts of moisture to obtain the desired density.
- 11.3.4.3.2 If needed, add in the required amounts of additional water (by trial and error method) until the desired density is obtained, then compact a set of seven specimens using  $1100 \text{ kN}\cdot\text{m}/\text{m}^3$  ( $13.26 \text{ ft}\cdot\text{lbs}/\text{in}^3$ ) effort.
- 11.3.4.3.3 The intent of this technique is to use the minimum amount of moisture equal to or above optimum moisture that will produce a set of accelerated test specimens whose average density is within  $8.0 \text{ kg}/\text{m}^3$  ( $1/2 \text{ pcf}$ ) of the maximum unit dry density of the original moisture density curve.
- Note 4**—Excessive densities can sometimes be obtained in the accelerated set but these are almost always very wet specimens and their resultant strengths can be misleading.
- 11.3.4.4 Subject specimens to overnight capillarity.
- 11.3.4.5 Test, and if required, classify according to Part I. If strengths at zero and  $103.4 \text{ kPa}$  ( $0$  and  $15 \text{ psi}$ ) lateral pressures are specified, test four specimens at zero lateral confinement and three of  $103.4 \text{ kPa}$  ( $15 \text{ psi}$ ) lateral confinement and average the three highest values for each state of confinement of the control values.
- Note 5**—When Grade one or two strength is specified, classification is not required.
- Note 6**—When strengths at zero and  $103.4 \text{ kPa}$  ( $15 \text{ psi}$ ) lateral pressures are specified, it is permitted to run correlation tests on a given source of material. The correlation should be as follows:
- As soon as three satisfactory accelerated test specimens have been molded according to Section 11.3.4.2, test two of them at zero lateral pressure and average the results as one test.
  - Test the third specimen at  $103.4 \text{ kPa}$  ( $15 \text{ psi}$ ) lateral pressure.
  - If these specimens pass, it is safe to assume the set to be tested the next day will pass.
- 11.3.5 *Group E – Combination Soil Types*
- 11.3.5.1 This group includes all materials with enough soil binder to separate the aggregate particles or overfill the voids of the compacted specimen. For example, if the material is a clayey gravel with high plasticity:

- Treat the material as a swelling soil.
- Allow the material to soak a minimum of 12 hours as in the case of aggregate materials.

- 11.3.5.2 Note that the total swelling is figured only for that part passing the 425  $\mu\text{m}$  (No. 40) sieve. Other combinations must be recognized and tested in the proper group.
- 11.3.5.3 Subject all specimens to overnight capillarity, test, and classify.
- 11.3.5.4 When testing aggregate materials under Part II where classification is required:
- 11.3.5.4.1 Test two specimens at 0 kPa (0 psi).
- 11.3.5.4.2 Test the others at 20.7 kPa (3 psi), 34.5 kPa (5 psi), 69.0 kPa (10 psi) and 103.4 kPa (15 psi).
- 11.3.5.4.3 Average the result of the zero lateral pressure tests as one value.
- 11.3.5.4.4 Classify fine grain soils using lateral pressures of 0 kPa (0 psi), 20.7 kPa (3 psi), 34.5 kPa (5 psi), 69.0 kPa (10 psi), 103.4 kPa (15 psi).

## 12. REPORTING TEST RESULTS

- 12.1 The reports and forms are the same as given in Part I of this procedure.

## PAVEMENT DESIGN NOTES

### 13. SCOPE

After materials have been classified according to Part I or Part II, and cohesiometer values for stabilized layers and surfacing have been determined, follow these steps for thickness design.

### 14. PROCEDURE

- 14.1 Obtain the current and projected traffic from the Department’s Transportation Planning and Programming Division.
- 14.2 Select a design wheel load from the traffic data and known local conditions. Use the ‘Flexible Base Design Chart’ (See Figure 7) to calculate total depth of pavement to protect the sub-grade.
- 14.3 Reduce total depth of pavement by using the ‘Thickness Reduction Chart for Stabilized Layers (See Figure 8), whenever stabilized layers are used in the pavement structure.

- 14.3.1 Enter above depth (from two above) on ordinate of Figure 8 and follow across page until intersection of cohesiometer value selected for use is reached, then project to abscissa to read reduction in depth due to bridging effects.
- 14.3.2 Standard cohesiometer values (corrected to represent values from 76 mm [3 in.] height specimens) are used on Figure 8 regardless of thickness of stabilized layer except in the following cases:
  - 14.3.2.1 Consideration should be given to increasing the design wheel load by 30% if traffic is anticipated to have over 50% tandem axles where asphaltic mixtures are used.
  - 14.3.2.2 The modification of cohesiometer values for 76.2 mm (3 in.) high specimens for application to other thickness' of asphaltic mixtures is obtained by the equation:
 
$$C_M = Ct^2 / 9$$
 Where:  
 C<sub>M</sub> = Modified cohesiometer value  
 C = Standard cohesiometer value for a 76.2 mm (3 in.) height specimen  
 t = Proposed thickness of bituminous mixtures, mm (in.).
- 14.4 The load frequency design factor can be obtained from the tabulation in Table 2. The depth obtained from Figure 8 is then multiplied by this factor and used with Figure 7 to design each course of the pavement structure.
- 14.5 Table 3 presents data, which was interpreted from good engineering practice supplemented by utilizing the AASHTO Road Test data and is a suggested method for determining the thickness of surface courses.

Table 2—Criteria for Obtaining the Load - Frequency Design Factor		
Total Equivalent 8.172 mgm (18 Kip) Single Axle Load Applications	Design Wheel Load in Pounds (ADTHWL)	*Load Frequency Design Factor
14,000	6,000	0.65
25,000	6,200	0.70
38,000	6,300	0.75
61,000	6,500	0.80
100,000	6,800	0.85
150,000	7,200	0.90
250,000	7,900	0.95
400,000	8,700	1.00
600,000	9,500	1.05
1,000,000	10,900	1.10
1,500,000	12,000	1.15

Total Equivalent 8.172 mgm (18 Kip) Single Axle Load Applications	Design Wheel Load in Pounds (ADTHWL)	*Load Frequency Design Factor
2,500,000	13,500	1.20
4,000,000	14,900	1.25
10,000,000	17,300	1.35

\*A load-frequency design factor less than 1.0 is not recommended for the design of the main lanes of a controlled access highway.

Total Equivalent 8.172 mgm (18 Kip) Single Axle Load Applications	When Tests Show Materials to be Specifications Grades* of Base Materials (Item 248)		
	Grade 1	Grade 2	Grade 3
14,000	ST	ST	ST
25,000	ST	ST	ST
38,000	ST	ST	ST
61,000	ST	ST	38 mm (1-1/2 in.)
100,000	ST	38 mm (1-1/2 in.)	50 mm (2 in.)
150,000	ST	44 mm (3/4 in.)	64 mm (2-1/2 in.)
250,000	32 mm (1-1/4 in.)	50 mm (2 in.)	76 mm (3 in.)
400,000	38 mm (1-1/2 in.)	57 mm (2-1/4 in.)	89 mm (3-1/2 in.)
600,000	44 mm (1-3/4 in.)	64 mm (2-1/2 in.)	102 mm (4 in.)
1,000,000	50 mm (2 in.)	76 mm (3 in.)	114 mm (4-1/2 in.)
1,500,000	64 mm (2-1/2 in.)	89 mm (3-1/2 in.)	127 mm (5 in.)
2,500,000	76 mm (3 in.)	102 mm (4 in.)	140 mm (5-1/2 in.)
4,000,000	89 mm (3-1/2 in.)	114 mm (4-1/2 in.)	152 mm (6 in.)
10,000,000	114 mm (4-1/2 in.)	140 mm (5-1/2 in.)	178 mm (7 in.)

\*It is assumed that the material in question is no better than the grade shown.

\*\*Exclusive of Cohesionless Materials

**Note 7**—ST denotes surface treatments.

**Note 8**—Stage construction of surfacing permitted if traffic studies indicate slow development of axle load equivalencies.

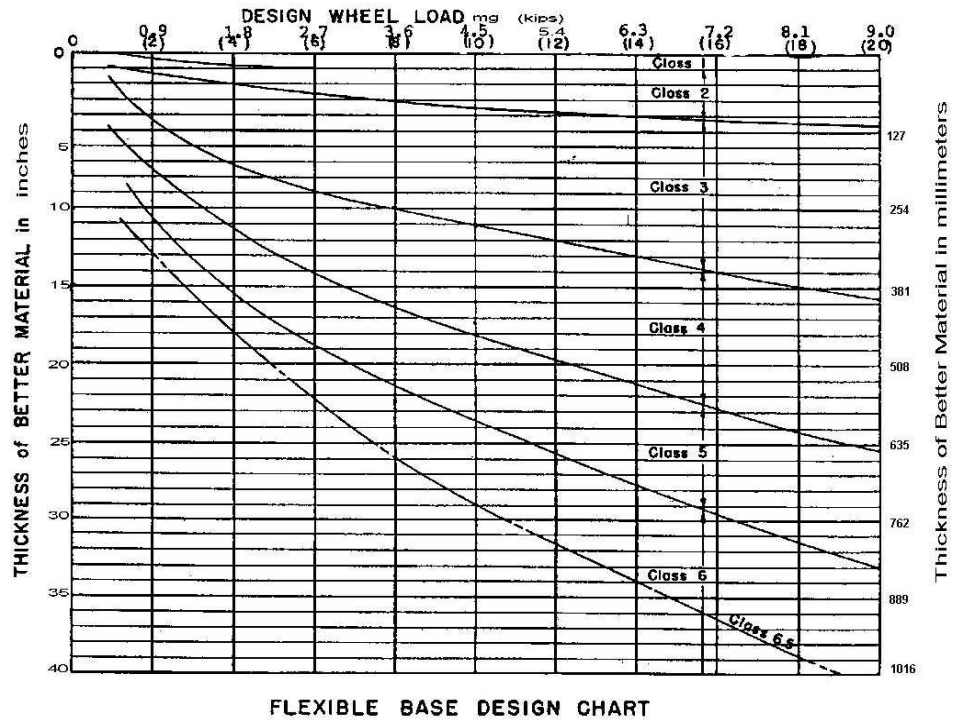


Figure 7—Flexible Base Design Chart

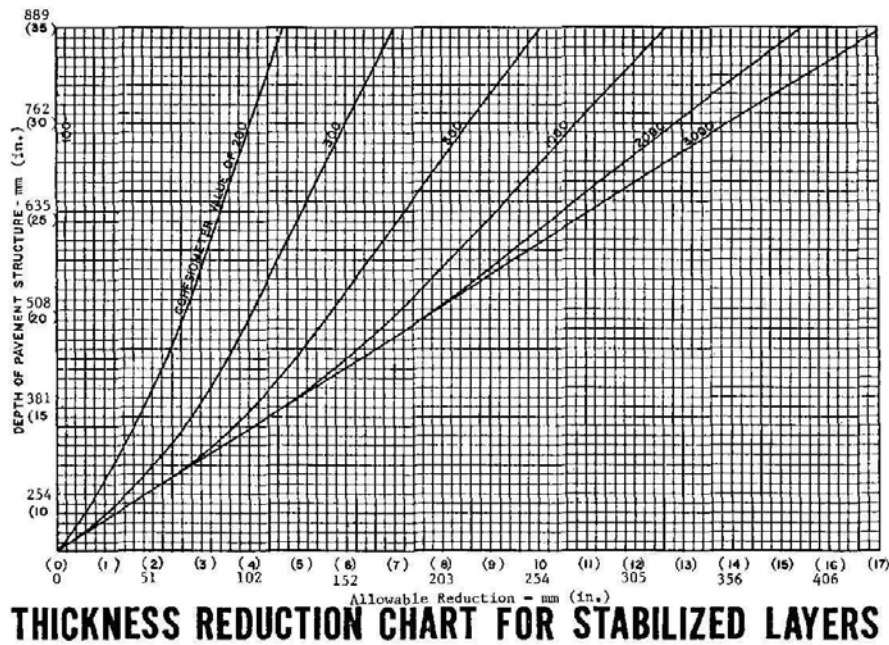


Figure 8—Thickness Reduction Chart for Stabilized Layers

---

**15. LIMITATIONS**

- 15.1 For a 152.6 mm (6 in.) or greater layer thickness, use a value of 152.6 mm (6 in.) in the formula for  $t$ .
- 15.2 When adjacent layers of stabilization and asphaltic concrete are used, the cohesiometer value to be used with the 'Thickness Reduction Chart for Stabilized Layers' should be equal to the sum of the standard cohesiometer value for the stabilized layer and the modified cohesiometer value of the asphaltic concrete.
- 15.2.1 When two adjacent layers of stabilization are used, or if a layer of untreated flexible base material exists between asphaltic concrete and a stabilized layer, only the greater of the two cohesiometer values in Figure 8 should be used.
- 15.2.2 Considerable caution and good engineering judgment should be used in selecting cohesiometer values for use in reduction of base depths. This is especially true in cases where hot mix-cold laid asphaltic concrete is bid as an alternate to hot mix asphaltic concrete laid hot.
- 15.2.3 In the case of stabilized bases, sub-bases and sub-grades, average values rather than highest values should be selected for use in Figure 8.

---

**16. GENERAL NOTES**

- 16.1 Wetted stabilized materials taken from the roadway during construction should be screened over a 6.3 mm (1/4 in.) sieve at the field moisture content without drying.
- 16.1.1 Each of these two sizes is mixed for uniformity and weighed.
- 16.1.2 Specimens are then weighed and recombined to produce multiple identical specimens with the received gradation.
- 16.1.3 Moisture can be adjusted in each specimen by adding water to the material or removing from the material by a fan, as needed.
- 16.2 See the appropriate test method (listed below) for testing wetted stabilized materials taken from the roadway during construction:
- Tex-120-E
  - Tex-121-E
  - Tex-127-E
- 16.3 In any event, the stabilized material should not be completely air-dried.
- 16.4 When molding a set of preliminary specimens for testing lime stabilized sub-grades and base materials, refer to '[Recommended Amounts of Lime for Stabilization of Sub-grades and Bases](#)' in Tex-121-E for the recommended amounts of lime to be used.

**17. ARCHIVED VERSIONS**

17.1 Archived versions are available.

**APPENDIX 2 – CIVIL ENGINEERING LABORATORIES  
QUESTIONNAIRE**



**UNIVERSITY OF STELLENBOSCH**

**DEPARTMENT OF CIVIL ENGINEERING**

**QUESTIONNAIRE**

Dear Respondent,

I am a Master of Science in Engineering student, specialising in Pavement Engineering. Sabita and GDPTRW are currently funding a study, which is the focus of my research, entitled:

**‘DEVELOPMENT OF A SIMPLE TRIAXIAL TEST’**

This study is under the guidance and supervision of Prof Kim Jenkins, SANRAL Chair in Pavement Engineering at Stellenbosch University.

The purpose of the study is to investigate the possibilities of developing a simple, economical, reliable and robust test for characterising granular and bitumen stabilised materials, with a link to performance.

Part of this study therefore, is to distribute questionnaires to civil engineering laboratories in South Africa, in a bid to investigate facilities, testing capacity and resources that are currently available. The response will provide guidance with regard to the nature and sophistication of any new tests to be developed.

Your support with feedback on the questionnaires will be highly appreciated. Please email your response to [wkmulusa@sun.ac.za](mailto:wkmulusa@sun.ac.za) or fax to 021 808 4361. A follow up call will be made to discuss the responses received.

Yours sincerely,

**William K. Mulusa**

MScEng (Pavement Engineering)  
University of Stellenbosch  
Department of Civil Engineering  
Tel: +27 21 808 4938 / Fax: +27 21 808 4361  
E-mail: [wkmulusa@sun.ac.za](mailto:wkmulusa@sun.ac.za)  
P/Bag X1 Matieland 7602  
South Africa

# CIVIL ENGINEERING LABORATORIES QUESTIONNAIRE

## Section A – General Information

1. Name of the Laboratory:

Address:

Tel No:

Fax No:

E-mail:

Contact Person/Representative:

Lab Technical Manager:

*(If different from above)*

2. Establishment

<b>Years since establishment in South Africa</b>	<b>Years since first accreditation with SANAS</b>

**Section B – Technical Information**

<b>Question No.</b>	<b>Can you perform the following tests?</b>	<b>Please say (YES or NO)</b>
1	Determination of CBR for treated and untreated soil or gravel	
2	Determination of Liquid, Plasticity (Atterberg limit)	
3	Determination of UCS for treated soil or gravel	
4	Maximum Dry Density and Optimum Moisture Content	
5	Grading and Sieve Analysis	
<b>6</b>	<b>Compaction Devices</b>	
6.1	Mod AASHTO	
6.2	Proctor	
6.3	Marshall Hammer	
6.3	Gyratory Compactor	
6.4	Vibratory table	

7. If you do perform any CBR tests, is it AUTOMATED CBR (YES / NO) or/and MANUAL CBR (YES / NO). *Please delete or cross out the incorrect answer.*

8. Briefly describe any problems/short comings with the CBR equipment you are using, in the text box below:

9. How many Ovens do you have in your laboratory?

10. If you have any ovens, please give the oven details by filling in the blank cells in the tables below and/or choosing Yes or No options. Please note that if you only have one, just fill in on oven 1 table.

<b>OVEN 1</b>							
<b>Type of Oven</b>		<b>Oven Capacity</b>		<b>Oven Temperature</b>		<b>Relative Humidity (RH)</b>	
Draft Oven	YES/ NO	Capacity in litres		Std Temp settings		RH Gauge?	YES/NO
Static Oven	YES/ NO	No. of specimen, Size (150 x 100) it can accommodate		Temp Range		RH Gauge Range (%)	

OVEN 2							
Type of Oven		Oven Capacity		Oven Temperature		Relative Humidity (RH)	
Draft Oven	YES/ NO	Capacity in litres		Std Temp settings		RH Gauge?	YES/NO
Static Oven	YES/ NO	No. of specimen, Size (150 x 100) it can accommodate		Temp Range		RH Gauge Range (%)	

OVEN 3							
Type of Oven		Oven Capacity		Oven Temperature		Relative Humidity (RH)	
Draft Oven	YES/ NO	Capacity in litres		Std Temp settings		RH Gauge?	YES/NO
Static Oven	YES/ NO	No. of specimen, Size (150 x 100) it can accommodate		Temp Range		RH Gauge Range (%)	

11. Do you carry out curing for Bitumen Stabilised Materials? YES / NO

12. If your answer if YES in Q.11 above, what curing method do you use? Use the text box below to give reference (for standard protocol) or outline the procedure.

## Section C – Loading Frames

The table below lists parameters, features and capabilities of the **Loading Frames** for CBR, UCS and/or Concrete Cube Press machines. You are requested to fill in **YES** or **NO** response in the cells depending on whether you agree or disagree with the listed parameter. Other brief responses are also requested in some cases. Please note that if you only have one (01) loading frame just fill in cells under machine No. 1 column.

Loading Frame Parameters	Machine No.1	Machine No.2	Machine No.3	Machine No.4
<b>1. Load Transmission</b>				
(i) Is it Pneumatic?				
(ii) Is it Hydraulic?				
(iii) Is it Mechanical/fixed gear?				
(iv) Other ( <i>please specify</i> )				
<b>2. Other Features</b>				
(i) Please mark load capacity in kN				
(ii) Static i.e ramp load only? Yes or No				
(iii) Dynamic loading capacity?				
(iv) If your answer is YES to (iii) above, please indicate the range of frequencies that are possible?				
(v) Is it load controlled but not displacement?				

*Continued*

<b>Loading Frame Parameters</b>	<b>Machine No.1</b>	<b>Machine No.2</b>	<b>Machine No.3</b>	<b>Machine No.4</b>
(vi) Is it displacement controlled but not load controlled?				
(vii) Is it both load and displacement controlled?				
(viii) If your answer is YES to (vi) and (vii) above, please indicate the maximum rate in (mm/min)				
(ix) Is it temperature controlled?				
(x) If it is temperature controlled, please indicate the range.				
(xi) Can it capture data electronically?				
(xii) Do you use LVDTs				
(xiii) What is the maximum dimension of specimens including attachments that can fit into the rig on your machine/s (L x B x H)?				
Please give any other relevant details:				

3. Do you have the capabilities of carrying out triaxial testing on 100 to 150 diameter specimens? YES / NO

4. What is your opinion on using triaxial tests as a standard to characterise granular and bitumen stabilised materials for road construction? *Please use the text box below*



**Thank you for answering**

**APPENDIX 3 - LIST OF CIVIL ENGINEERING LABORATORIES**

Item No.	Laboratory	Physical Address	Postal Address	Contact Person/Rep	Telephone	Fax	E-mail
1	Civilab	36, 38 Fourth Street Booyens Reserve 2091 c/o Pretoria Main Road & Marlboro Drive, Eastgate Sandton	P O Box 82223 Southdale 2135	Mr MG Meyers	(011) 835-3117/8/9	(011) 835-2503	<a href="mailto:ihb@civilab.co.za">ihb@civilab.co.za</a>
2	Concrete Testing Services	1225 Michael Brink Street Koedoesport	P O Box 1963 Kelvin 2054	Mr D Tite	(011) 444-9280/2	(011) 444-9283	<a href="mailto:dave@concretetesting.co.za">dave@concretetesting.co.za</a>
3	Dept of Public Transport Roads & Works, Gautrans	993 Park Street, Hartfield Pretoria	Private Bag X3 Lynn East 39	Ms W le Roux	(012) 310-2213	(012) 333-3236	<a href="mailto:wandaq@pgp.gov.za">wandaq@pgp.gov.za</a>
4	Geostrada Engineering Materials	11 Livingstone Road Pinetown 3610 Kwazulu Natal	P O Box 11126, Hartfield 0028	Ms S Dittrich	(012) 427-2548	(012) 427-2650	<a href="mailto:sonjadi@africon.co.za">sonjadi@africon.co.za</a>
5	Geosynthetic Laboratory	Buick street cnr. Chrysler street, Markman Port Elizabeth 6001	P O Box 116, Pinetown 3600 Kwazulu Natal	Mr GM James/ Mr D Julal	(031) 717 2360	(031) 702 3173	<a href="mailto:info@geolaboratory.com">info@geolaboratory.com</a>
6	LABCO Joint Venture	Kelvin Street, Industria West Johannesburg 2042	P O Box 10114 Linton Grange, Port Elizabeth 6015	Mr G Eichbauer	(041) 461 1832	(041) 461 1834	<a href="mailto:eichbauer@telkomsa.net">eichbauer@telkomsa.net</a>
7	Lafarge South Africa	Unit 7 Pennylane Park 64 Ebonyfield avenue Springfield Park, Durban	P O Box 43033 Industria, Johannesburg 2042	Mr J Daly	(011) 474-1323	(011) 474-3110	<a href="mailto:japhta.daly@lafarge.com">japhta.daly@lafarge.com</a>
8	Matrolab Group (Pty) Ltd	Ryneveld Street Eersterivier 7100	P O Box 74663 Rochdale Park, Durban 4034	Mr SL Govender	(031) 579 1220	(031) 579 1344	<a href="mailto:lawrenceg@matrolab.co.za">lawrenceg@matrolab.co.za</a>
9	MUCH ASPHALT (PTY) LTD	Eersterivier 7100	P O Box 49 Eersterivier 7103	Mr AG Rippenaar	(021) 900 4400	(021) 900 4468	<a href="mailto:alec.rippenaar@murrob.com">alec.rippenaar@murrob.com</a>
10	PPC Cement	Technical Support Department Cnr Chain Ave & Montague Drive, Montague Gardens Cape Town 7441	P O Box 268 Milnerton Cape Town 7435	Mr S Crosswell	021 550 2108	021 550 2175	<a href="mailto:scrosswell@ppc.co.za">scrosswell@ppc.co.za</a>
11	Roadlab (Pty) Ltd	168 Rietfontein Road Primrose, Germiston 1402	P O Box 1476 Germiston, 1400	Mr RJ Odendaal	(011) 828 0279	(011) 828 0273	<a href="mailto:info@roadlab.co.za">info@roadlab.co.za</a>
12	SNALAB SAMCOR PARK	191 Vonkprop Road Samcor Park, Lynnwood Ridge 40	PO Box 72727 Lynnwood Ridge 40	HP Diederiks	(012) 842-0060	(012) 803-4630	<a href="mailto:snalabpta@mweb.co.za">snalabpta@mweb.co.za</a>
13	Soilco Materials Investigations (Pty) Ltd	25 Westmead Road, Westmead Pinetown	P O Box 15318 Westmead 3608	Mr L Moodley	031 700 4325	031 700 1909	<a href="mailto:legs@soilco.co.za">legs@soilco.co.za</a>
14	Soilcon cc	279 Mildred Avenue Queenswood 121	P O Box 11361 Queenswood 121	Mr M L B Polluk	(012) 333-7817	(012) 333-7913	<a href="mailto:soilcon@mweb.co.za">soilcon@mweb.co.za</a>
15	SOILLAB (PTY) LTD KRAAIFONTEIN	VKE Centre VKE Centre, 230 Albertus Street, La Montagne Pretoria 184	P O Box 585 Kraaifontein 7570	Mr WA Venter	021 988 7410	021 988 6919	<a href="mailto:venterw@soillab.co.za">venterw@soillab.co.za</a>
16	SOILLAB (Pty) Ltd Pretoria	25 Westmead Road Westmead Pinetown	P O Box 72928 Lynnwood Ridge Pretoria 40	Mr J van Wyk	(012) 481-3813	(012) 481-3812	<a href="mailto:vanwyk@soillab.co.za">vanwyk@soillab.co.za</a>
17	Specialised Road Technologies (Pty) Ltd	25 Westmead Road Westmead Pinetown	P O Box 15324 Westmead 3608	Mr MV Shange	031 700 4510	031 700 3165	<a href="mailto:mangoba@srt.co.za">mangoba@srt.co.za</a>

## **APPENDIX 4 - ANALYSIS OF QUESTIONNAIRE RESPONSES**

## APPENDIX 4 - ANALYSIS OF QUESTIONNAIRE RESPONSES

### A. General Information

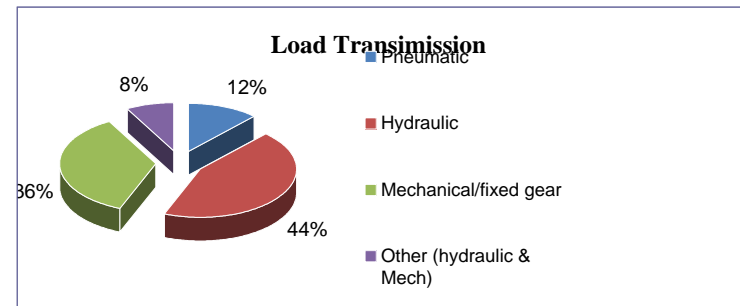
Targeted number of Laboratories      16  
 Number of responses received        8  
**Collection rate**      **50%**

B. Technical Information	Score [8]	%	Reported problems associated with using CBR Machines in industry:
1. Ability to perform CBR of treated and untreated material	5	63%	i) Seating load of 45N; ii) Supplier has monopoly for locally manufactured CBR compaction equipment, imported CBR compactors are slow and double the price; iii) Reliability of test results on extremely soft material is questionable; iv) Electronic problems & poor after sale service from suppliers
2. Ability to perform UCS for treated soil or gravel	5	63%	
3. Type of CBR Machines	<b>Score [5]</b>	<b>%</b>	
i) Using Automated CBR	5	100%	
ii) Using Manual CBR	2	40%	
iii) Using both Automated & Manual	2	40%	

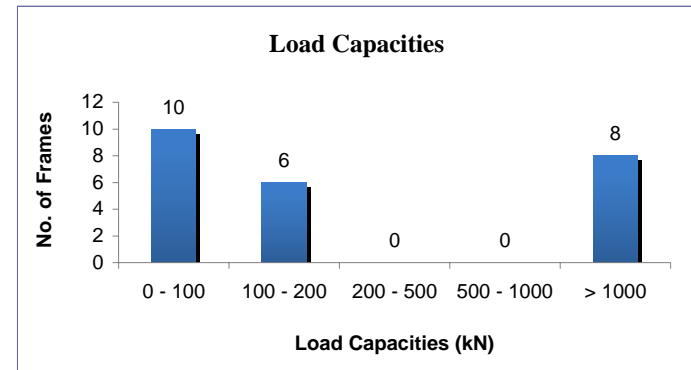
### C. Loading Frames

Total Number of Loading Frames reported      **25**

1. Load transimission	Score [25]	%
Pneumatic	3	12%
Hydraulic	11	44%
Mechanical/fixe gear	9	36%
Other (hydraulic & Mech)	2	8%

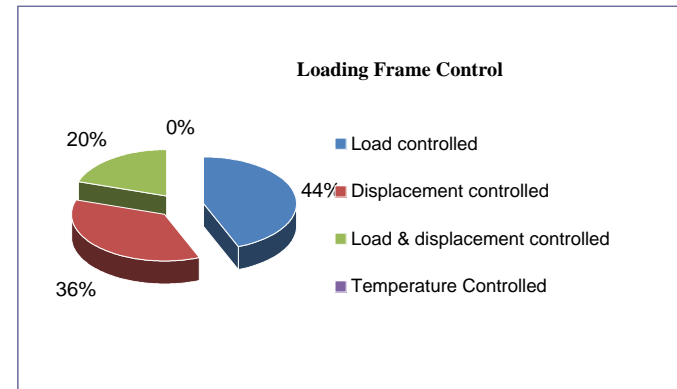


2. Load Capacities (kN)	No. of Frames
0 - 100	10
100 - 200	6
200 - 500	0
500 - 1000	0
> 1000	8



3. Type of loading	Score [25]	%
Static (Ramp load)	16	64%
Dynamic load	0	0%
Not indicated	9	36%

4. Loading Frame Control type	Score [25]	%
Load controlled	11	44%
Displacement controlled	9	36%
Load & displacement controlled	5	20%
Temperature Controlled	0	0%



5. Data Capturing	Score [25]	%
Electronic	16	64%
Manual	9	36%
With LVDTs	3	12%
Without LVDTs	22	88%

6. Dimensions including attachments fitted in the rig

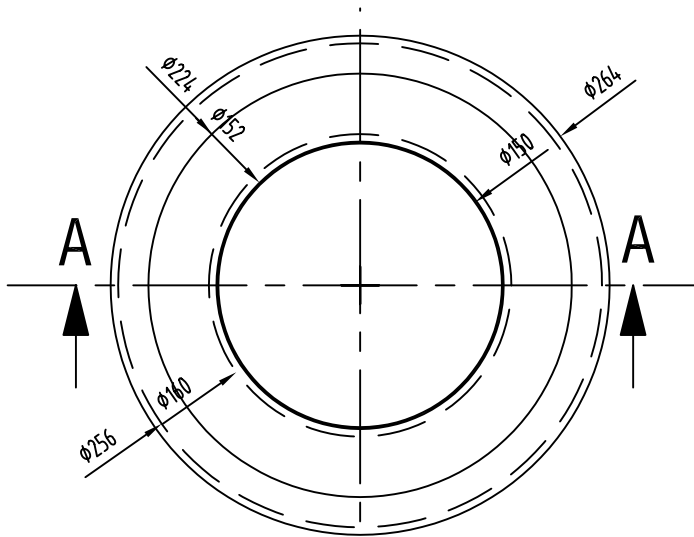
Reported LxBxH	Score
150x150x150	1
150x150x250	1
300x300x1000	1
450x250x300	2
Reported ØxH	Score
101.6x64	1
150x300	2

7. Capacity to carryout triaxial testing on 100 to 150Ø	Score [8]	%
<b>YES</b>	1	13%
<b>NO</b>	7	88%

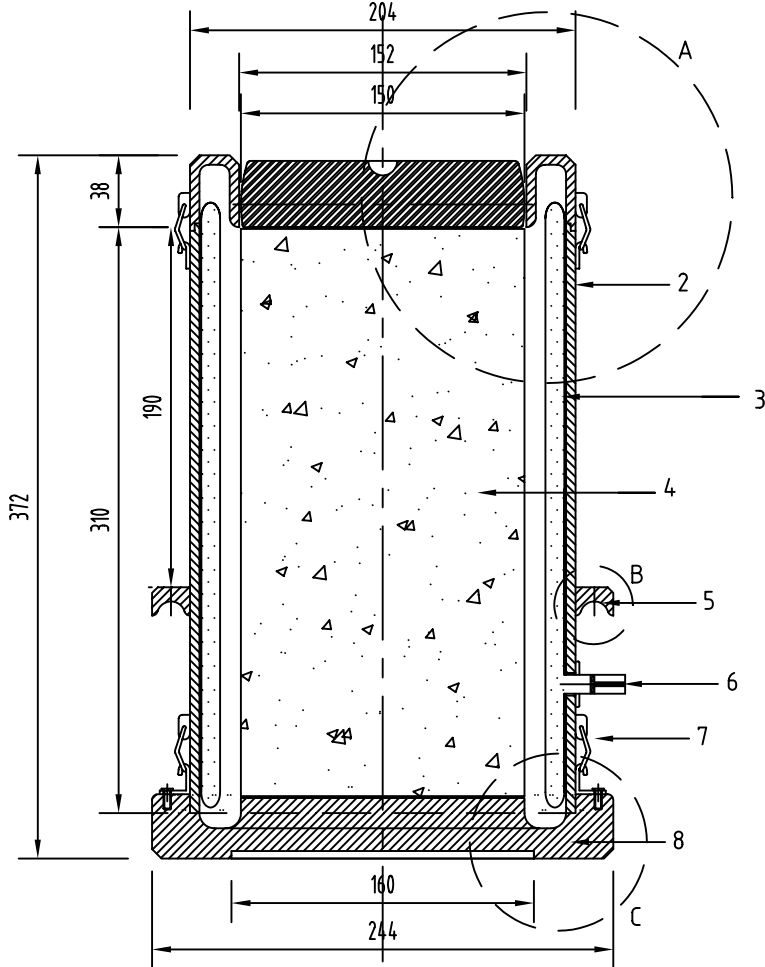
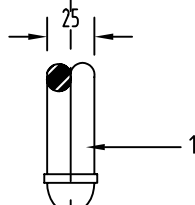
8. Recorded opinions from the industry on using simple triaxial tests as a standard to characterise granular and bitumen stabilised materials:

- i) 'We would welcome this development';
- ii) 'The texas triaxial is a very time consuming test. I do not see it as a routine test. It could be used to confirm parameters after initial UCS/ITS tests have been done to establish type and quantity of additives';
- iii) 'We have never done a triaxial test. Don't you need a shearbox for that?'

## **APPENDIX 5 – STT DRAWINGS**



TOP VIEW OF TRIAXIAL CELL

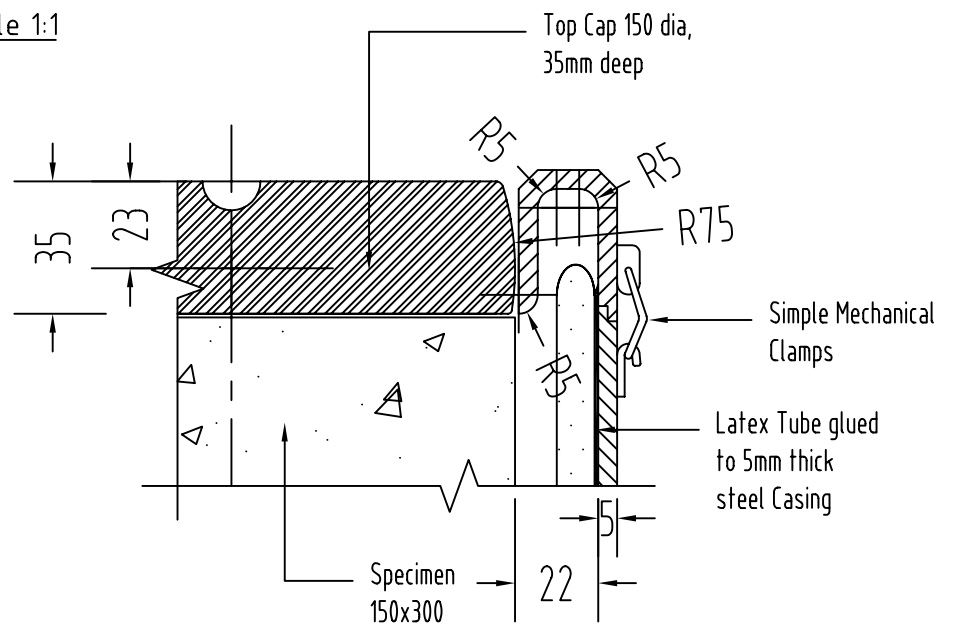
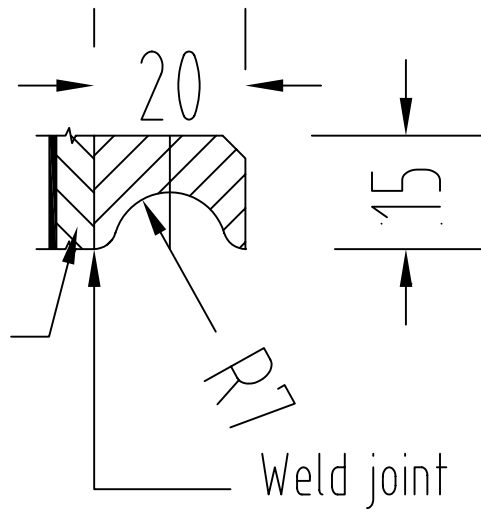
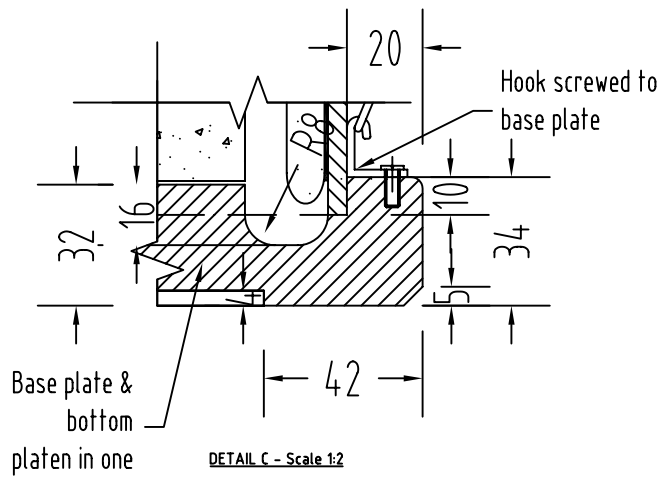


SECTION VIEW A-A (Scale 1:4)

TRIAXIAL CELL ACCESSORIES:

1. Loading ram
2. Galvanised steel casing 5mm thick
3. Latex tube 320 long glued to steel casing
4. Specimen 150x300
5. Steel casing handles (Grooved steel ring handle)
6. Pressure inlet
7. Simple mechanical clamps, 4no@90 degree c/c
8. Base plate and bottom platen in one

N/B: All dimensions in mm



## **APPENDIX 6: ANALYSIS OF VARIANCE**

### 6.1.1 Basic Statistics/Tables

Cross tabulation results dialog as shown in Table 1

**Table 1: Summary frequency table for STT (same as RTT)**

Summary Frequency Table (DATA STTRTT 20081217.sta)					
Marked cells have counts > 10					
(Marginal summaries are not marked)					
SEMENT	AGGREGATE	STTPRESSURE 50	STTPRESSURE 100	STTPRESSURE 200	Row Totals
C	RAP	1	1	1	3
C	G2	1	1	1	3
Total		2	2	2	6
S	RAP	1	3	1	5
S	G2	1	1	1	3
Total		2	4	2	8
Column Total		4	6	4	14

### 6.1.2 ANOVA results with maximum load at failure as dependant variable

**Table 2: Repeated measures ANOVA Table (DV\_1=Load at failure)**

Repeated Measures Analysis of Variance (DATA STTRTT 2)					
Sigma-restricted parameterization					
Effective hypothesis decomposition					
Effect	SS	Degr. of Freedom	MS	F	p
Intercept	17614.17	1	17614.17	152.7673	0.000000
PRESSURE	970.21	2	485.10	4.2073	0.043950
Error	1268.31	11	115.30		
REPEAT	134.00	1	134.00	17.5135	0.001524
REPEAT*PRESSURE	59.47	2	29.74	3.8866	0.052870
Error	84.16	11	7.65		

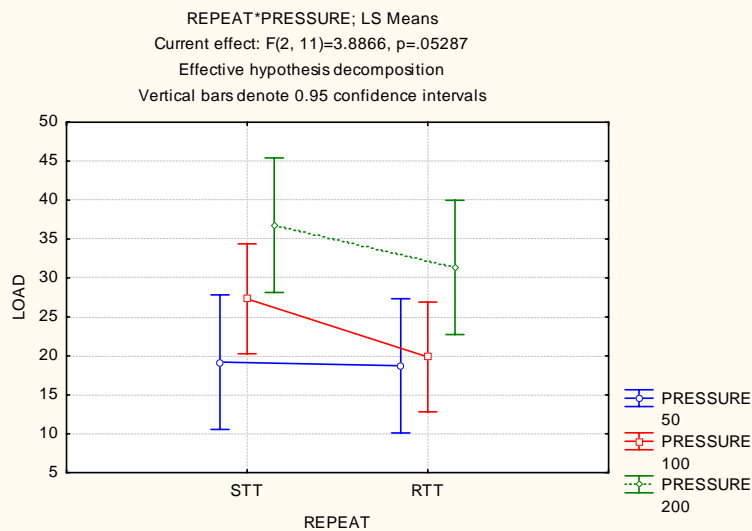


**Figure 1: Variation of load at failure between STT and RTT samples**

**Table 3: Repeat\*Pressure; LS Means**

REPEAT*PRESSURE; LS Means (DATA STTRTT 20081217.sta)							
Current effect: F(2, 11)=3.8866, p=.05287							
Effective hypothesis decomposition							
Cell No.	PRESSURE	REPEAT	DV_1 Mean	DV_1 Std.Err.	DV_1 -95.00%	DV_1 +95.00%	N
1	50	STTLOAD	19.20000	3.926023	10.55888	27.84112	4
2	50	RTTLOAD	18.72500	3.914631	10.10895	27.34105	4
3	100	STTLOAD	27.33333	3.205584	20.27789	34.38878	6
4	100	RTTLOAD	19.86667	3.196283	12.83170	26.90164	6
5	200	STTLOAD	36.77500	3.926023	28.13388	45.41612	4
6	200	RTTLOAD	31.35000	3.914631	22.73395	39.96605	4

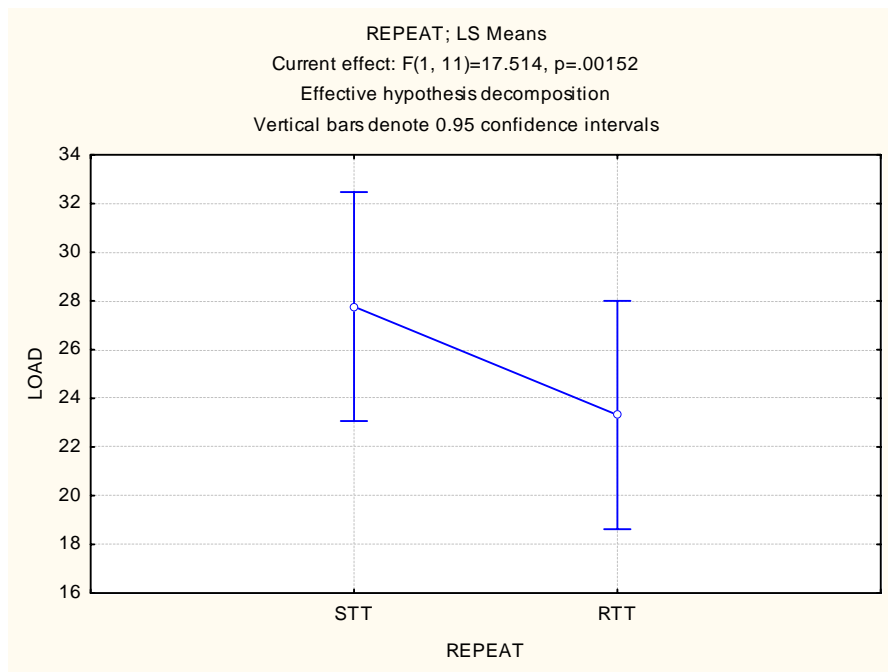


**Figure 2: Variation of load at failure within STT and RTT samples**

**Table 4: Repeat; LS Means**

REPEAT; LS Means (DATA STTRTT 20081217.sta)						
Current effect: F(1, 11)=17.514, p=.00152						
Effective hypothesis decomposition						
Cell No.	REPEAT	DV_1 Mean	DV_1 Std.Err.	DV_1 -95.00%	DV_1 +95.00%	N
1	STTLOAD	27.76944	2.137056	23.06582	32.47307	14
2	RTTLOAD	23.31389	2.130855	18.62391	28.00387	14

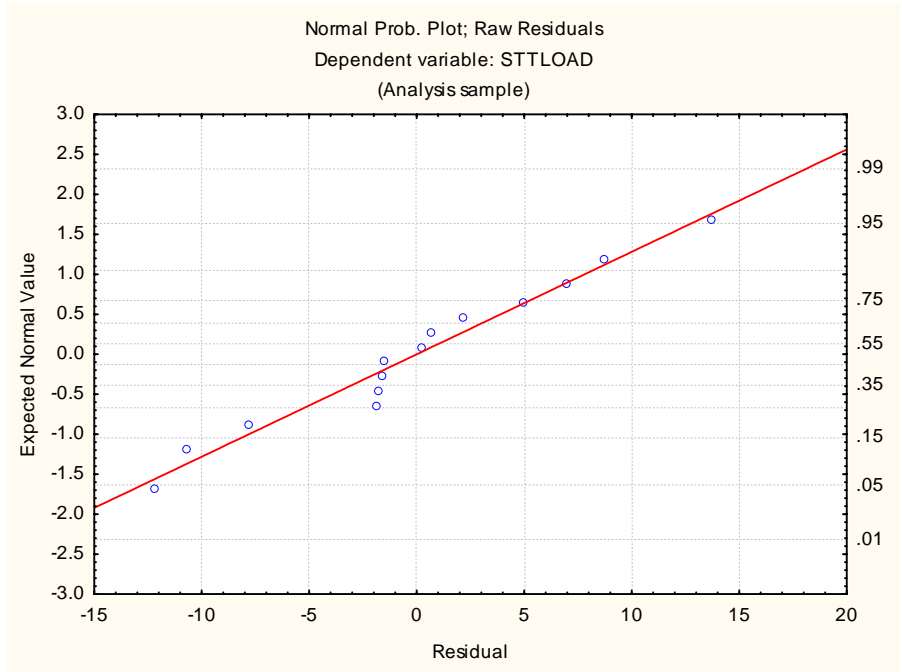


**Figure 3: Normal Probability Plot; DV = STT Load**

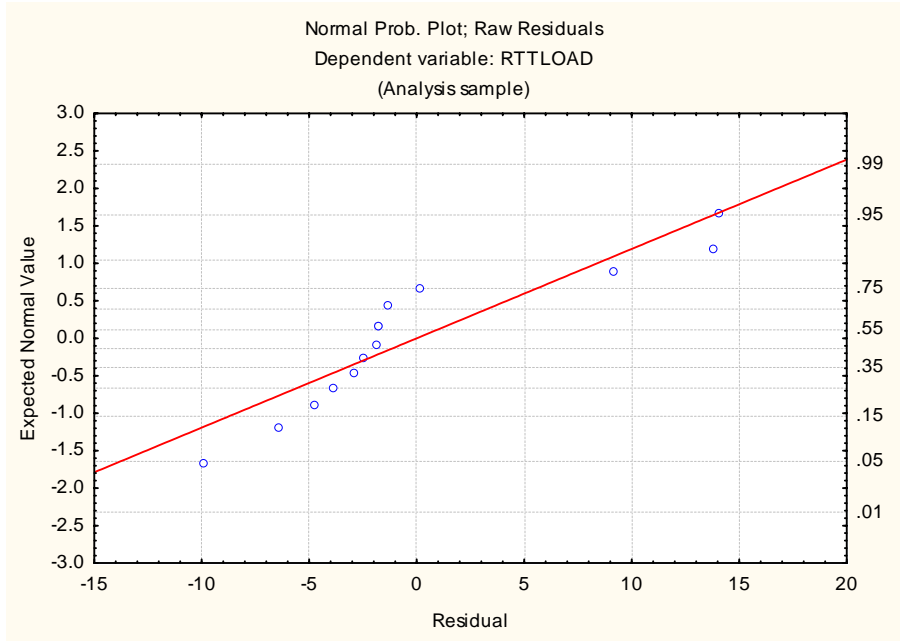


**Figure 4: Normal Probability Plot; DV = RTT Load**

**Table 5: Bonferroni test for variable (DV\_1 = Load)**

Bonferroni test; variable DV_1 (DATA STTRTT 20081217.sta)								
Probabilities for Post Hoc Tests								
Error: Between; Within; Pooled MS = 61.476, df = 12.454								
Cell No.	PRESSURE	REPEAT	{1}	{2}	{3}	{4}	{5}	{6}
			19.200	18.725	27.333	19.867	36.775	31.350
1	50	STTLOAD		1.000000	1.000000	1.000000	0.116110	0.721447
2	50	RTTLOAD	1.000000		1.000000	1.000000	0.098771	0.617274
3	100	STTLOAD	1.000000	1.000000		0.010149	1.000000	1.000000
4	100	RTTLOAD	1.000000	1.000000	0.010149		0.084118	0.626627
5	200	STTLOAD	0.116110	0.098771	1.000000	0.084118		0.271639
6	200	RTTLOAD	0.721447	0.617274	1.000000	0.626627	0.271639	

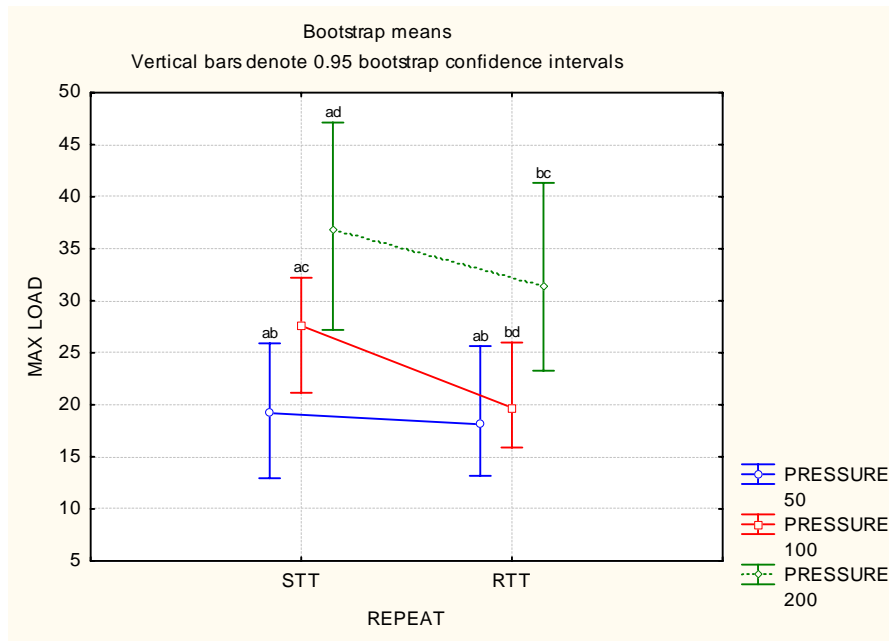


**Figure 5: Bootstrap means**

**Table 6: Bootstrap test; DV\_1 = load**

Bootstrap test; variable DV_1 (DATA STTRTT 20081217.sta)								
Probabilities for Post Hoc Tests								
Cell No.	PRESSURE	REPEAT	{1}	{2}	{3}	{4}	{5}	{6}
			19.200	18.725	27.333	19.867	36.775	31.350
1	50	STTLOAD		1	0.6525	1	0.21	0.51
2	50	RTTLOAD			0.3	1	0.2325	0.3975
3	100	STTLOAD				0	0.5625	1
4	100	RTTLOAD					0.0525	0.2175
5	200	STTLOAD						0
6	200	RTTLOAD						

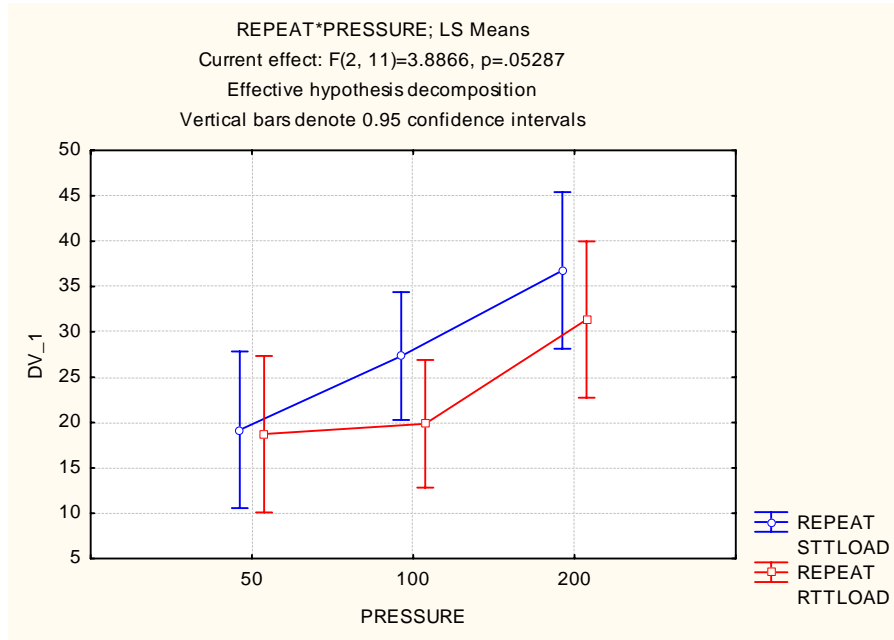


Figure 6: Maximum load at failure vs confinement pressure for STT and RTT

### 6.1.3 ANOVA results with displacement at failure as dependant variable

Table 7: Repeated measures ANOVA Table (DV\_1 = Displ at failure)

Repeated Measures Analysis of Variance (DATA STTRTT 2)					
Sigma-restricted parameterization					
Effective hypothesis decomposition					
Effect	SS	Degr. of Freedom	MS	F	p
Intercept	2900.075	1	2900.075	155.5367	0.000000
PRESSURE	55.665	2	27.833	1.4927	0.266956
Error	205.102	11	18.646		
REPEAT	19.127	1	19.127	1.4720	0.250445
REPEAT*PRESSURE	10.812	2	5.406	0.4160	0.669612
Error	142.935	11	12.994		

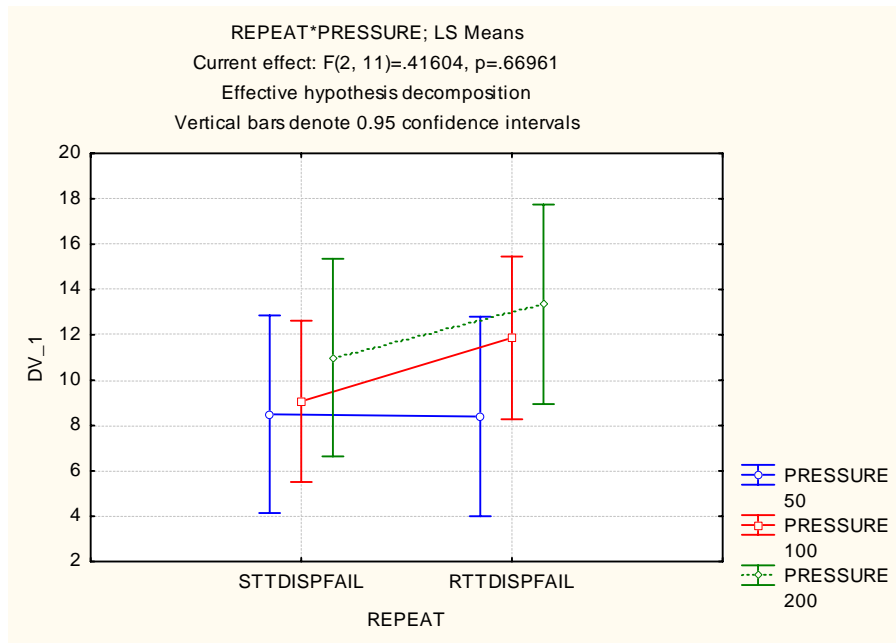


Figure 7: Variation of Displacement at failure between STT and RTT samples

Table 8: Repeat\*Pressure; LS means for Figure 7

REPEAT*PRESSURE; LS Means (DATA STTRTT 20081217.sta)							
Current effect: $F(2, 11) = .41604, p = .66961$							
Effective hypothesis decomposition							
Cell No.	PRESSURE	REPEAT	DV_1 Mean	DV_1 Std.Err.	DV_1 -95.00%	DV_1 +95.00%	N
1	50	STTDISPFAIL	8.50000	1.978598	4.145136	12.85486	4
2	50	RTTDISPFAIL	8.40000	1.998769	4.000740	12.79926	4
3	100	STTDISPFAIL	9.06667	1.615518	5.510935	12.62240	6
4	100	RTTDISPFAIL	11.86667	1.631988	8.274686	15.45865	6
5	200	STTDISPFAIL	11.00000	1.978598	6.645136	15.35486	4
6	200	RTTDISPFAIL	13.35000	1.998769	8.950740	17.74926	4

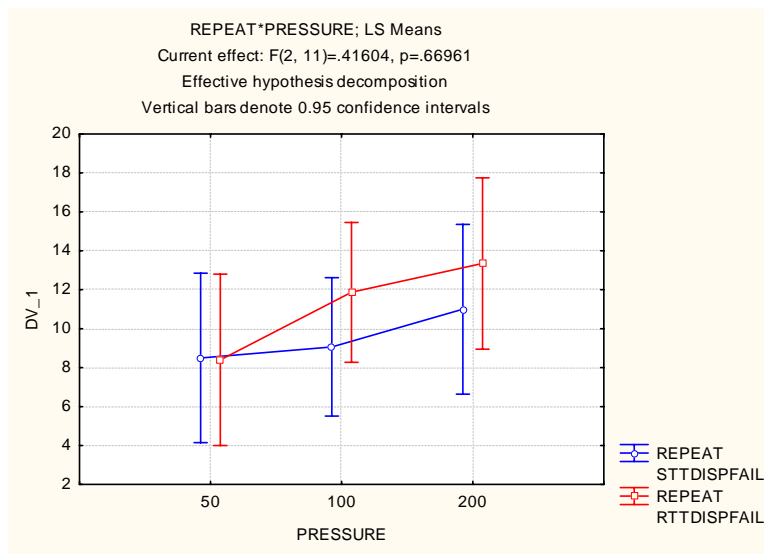
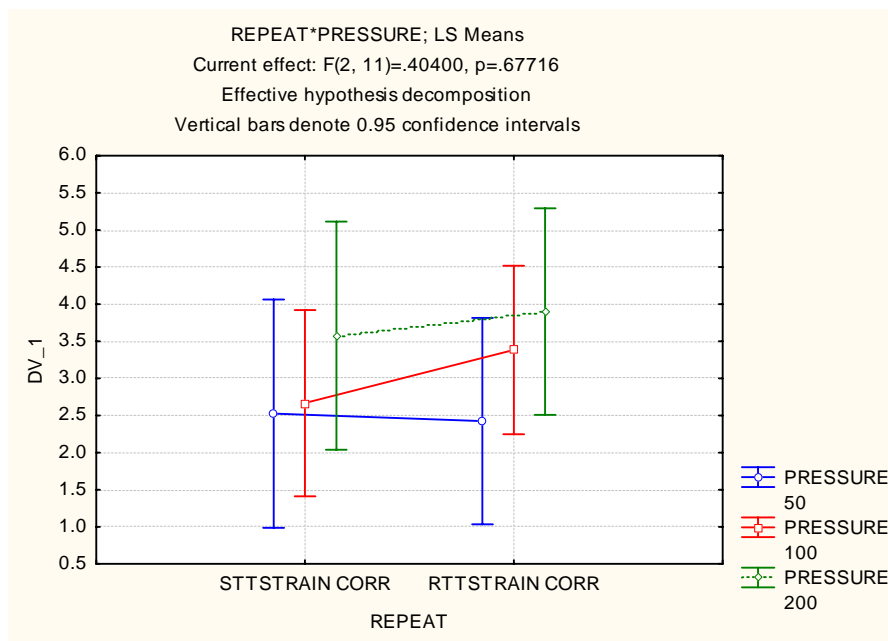


Figure 8: Displacement at failure vs confinement pressure for STT and RTT

### 6.1.4 ANOVA results with corrected strain at failure as dependant variable

**Table 9: Repeated measures ANOVA Table (DV\_1 = Corrected strain)**

Repeated Measures Analysis of Variance (DATA STTRTT 2) Sigma-restricted parameterization Effective hypothesis decomposition					
Effect	SS	Degr. of Freedom	MS	F	p
Intercept	255.9942	1	255.9942	100.4033	0.000001
PRESSURE	6.4209	2	3.2104	1.2592	0.321797
Error	28.0463	11	2.5497		
REPEAT	0.6651	1	0.6651	0.6664	0.431636
REPEAT*PRESSURE	0.8064	2	0.4032	0.4040	0.677161
Error	10.9779	11	0.9980		



**Figure 9: Variation of corrected strain at failure between STT and RTT**

**Table 10: Repeat\*Pressure; LS means for Figure 9**

REPEAT*PRESSURE; LS Means (DATA STTRTT 20081217.sta) Current effect: F(2, 11) = .40400, p = .67716 Effective hypothesis decomposition							
Cell No.	PRESSURE	REPEAT	DV_1 Mean	DV_1 Std.Err.	DV_1 -95.00%	DV_1 +95.00%	N
1	50	STTSTRAIN CORR	2.525000	0.698510	0.987589	4.062411	4
2	50	RTTSTRAIN CORR	2.425000	0.631661	1.034722	3.815278	4
3	100	STTSTRAIN CORR	2.666667	0.570331	1.411376	3.921957	6
4	100	RTTSTRAIN CORR	3.383333	0.515749	2.248176	4.518490	6
5	200	STTSTRAIN CORR	3.575000	0.698510	2.037589	5.112411	4
6	200	RTTSTRAIN CORR	3.900000	0.631661	2.509722	5.290278	4

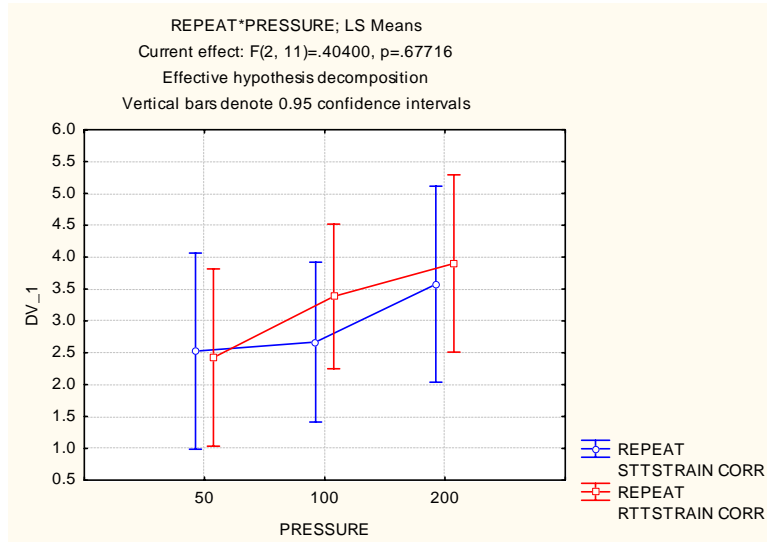


Figure 10: Corrected strain at failure vs confinement pressure for STT and RTT

### 6.1.5 ANOVA results with stress (pressure) at failure as dependant variable

Table 11: Repeated measures ANOVA Table (DV\_1 = Pressure at fail)

Repeated Measures Analysis of Variance (DATA STTRTT 20)					
Sigma-restricted parameterization					
Effective hypothesis decomposition					
Effect	SS	Degr. of Freedom	MS	F	p
Intercept	56474255	1	56474255	152.6160	0.000000
PRESSURE	3101382	2	1550691	4.1906	0.044368
Error	4070458	11	370042		
REPEAT	433390	1	433390	17.5167	0.001523
REPEAT*PRESSURE	186427	2	93213	3.7675	0.056716
Error	272157	11	24742		

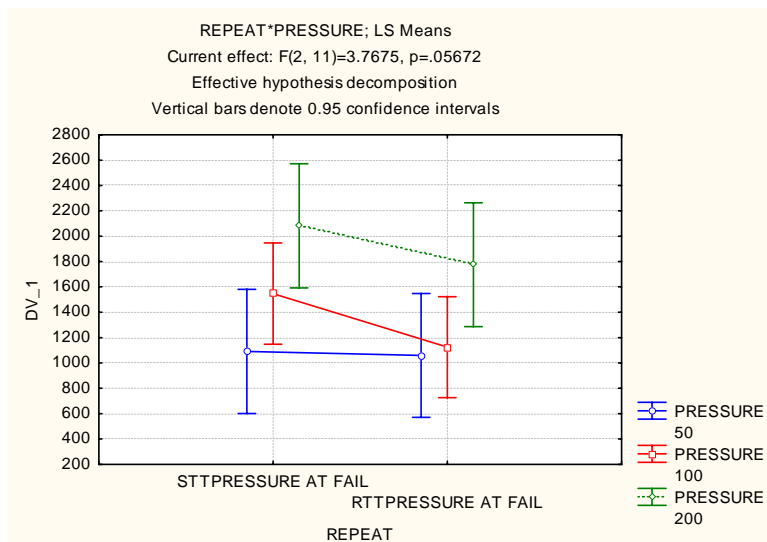


Figure 11: Variation of Pressure at fail between STT and RTT

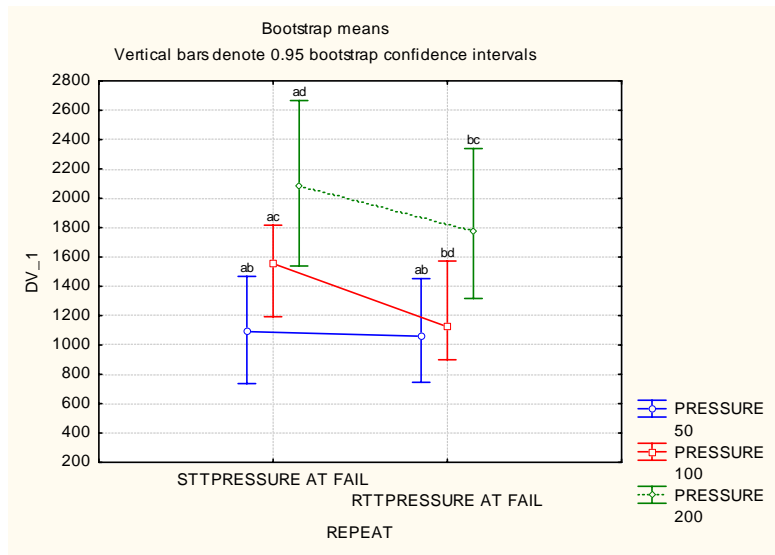


Figure 12: Bootstrap means

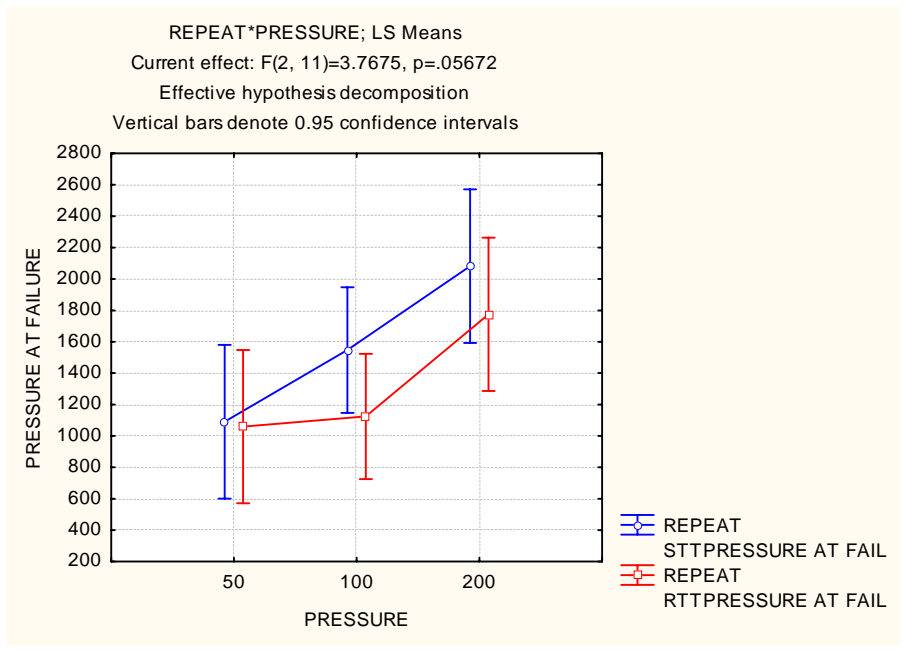


Figure 13: Pressure at failure vs confinement pressure for STT and RTT

**Table 12: Repeat\*Pressure; LS Means**

REPEAT*PRESSURE; LS Means (DATA STTRTT 20081217.sta)							
Current effect: F(2, 11)=3.7675, p=.05672							
Effective hypothesis decomposition							
Cell No.	PRESSURE	REPEAT	DV_1 Mean	DV_1 Std.Err.	DV_1 -95.00%	DV_1 +95.00%	N
1	50	STTPRESSURE AT FAIL	1090.500	222.4364	600.921	1580.079	4
2	50	RTPPRESSURE AT FAIL	1059.500	221.8509	571.209	1547.791	4
3	100	STTPRESSURE AT FAIL	1546.833	181.6186	1147.093	1946.573	6
4	100	RTPPRESSURE AT FAIL	1124.167	181.1405	725.479	1522.854	6
5	200	STTPRESSURE AT FAIL	2081.500	222.4364	1591.921	2571.079	4
6	200	RTPPRESSURE AT FAIL	1775.000	221.8509	1286.709	2263.291	4

**Table 13: Pressure; LS Means**

PRESSURE; LS Means (DATA STTRTT 20081217.sta)						
Current effect: F(2, 11)=4.1906, p=.04437						
Effective hypothesis decomposition						
Cell No.	PRESSURE	DV_1 Mean	DV_1 Std.Err.	DV_1 -95.00%	DV_1 +95.00%	N
1	50	1075.000	215.0702	601.634	1548.366	4
2	100	1335.500	175.6041	948.998	1722.002	6
3	200	1928.250	215.0702	1454.884	2401.616	4

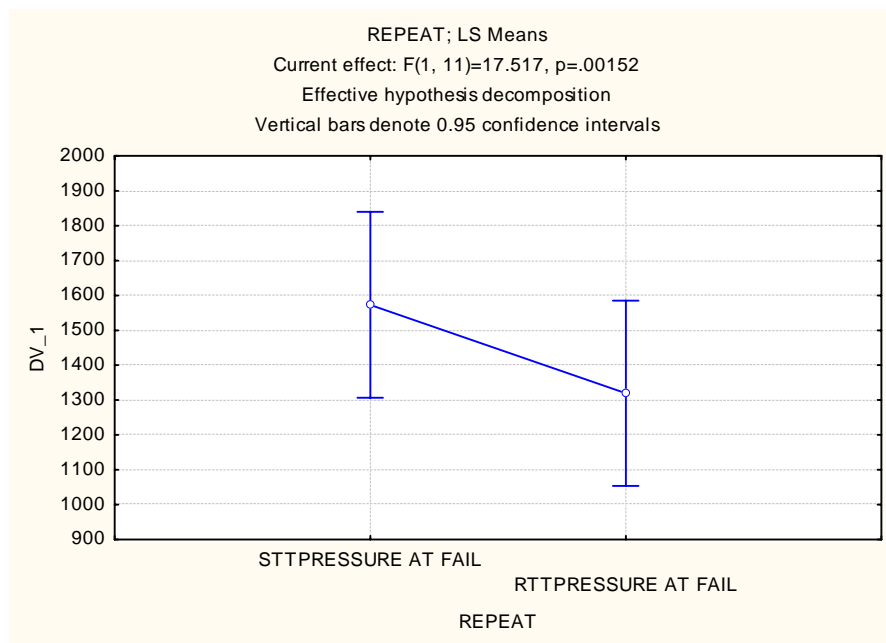


**Figure 14: Variation of pressure at fail within STT and RTT**

**Table 14: Repeat; LS Means**

REPEAT; LS Means (DATA STTRTT 20081217.sta)						
Current effect: F(1, 11)=17.517, p=.00152						
Effective hypothesis decomposition						
Cell No.	REPEAT	DV_1 Mean	DV_1 Std.Err.	DV_1 -95.00%	DV_1 +95.00%	N
1	STTPRESSURE AT FAIL	1572.944	121.0791	1306.451	1839.438	14
2	RTPPRESSURE AT FAIL	1319.556	120.7603	1053.764	1585.347	14

**Table 15: Bonferroni test; variable DV\_1 = Pressure at failure**

Bonferroni test; variable DV_1 (DATA STTRTT 20081217.sta)								
Probabilities for Post Hoc Tests								
Error: Between; Within; Pooled MS = 1974E2, df = 12.464								
Cell No.	PRESSURE	REPEAT	{1} 1090.5	{2} 1059.5	{3} 1546.8	{4} 1124.2	{5} 2081.5	{6} 1775.0
1	50	STTPRESSURE AT FAIL		1.000000	1.000000	1.000000	0.119451	0.737896
2	50	RTPPRESSURE AT FAIL	1.000000		1.000000	1.000000	0.099141	0.616623
3	100	STTPRESSURE AT FAIL	1.000000	1.000000		0.010504	1.000000	1.000000
4	100	RTPPRESSURE AT FAIL	1.000000	1.000000	0.010504		0.084451	0.625830
5	200	STTPRESSURE AT FAIL	0.119451	0.099141	1.000000	0.084451		0.280486
6	200	RTPPRESSURE AT FAIL	0.737896	0.616623	1.000000	0.625830	0.280486	

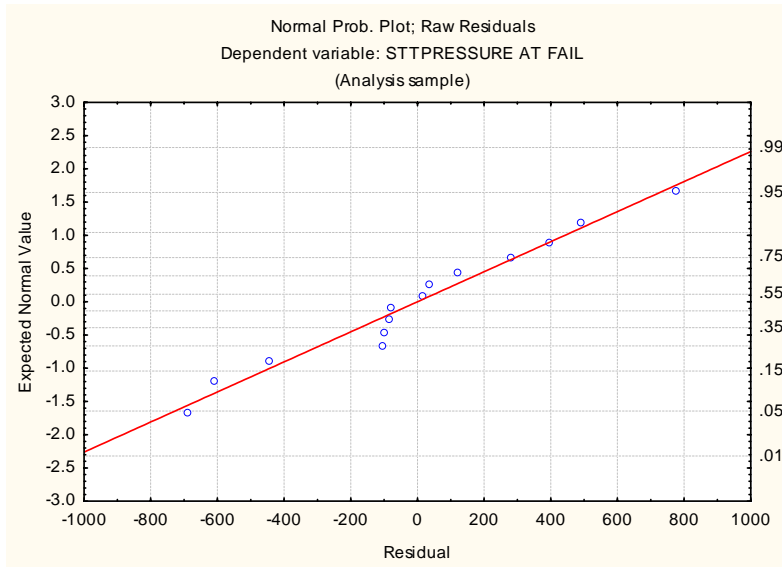


**Figure 15: Normal Probability Plot (DV = STT Pressure at fail)**

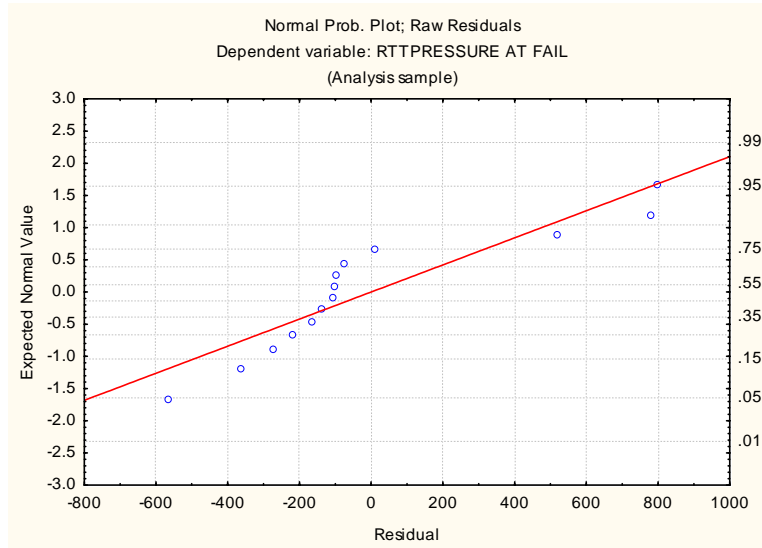


Figure 16: Normal Probability Plot; DV = RTT Pressure at failure

Table 16: Bootstrap test; DV\_1 = Pressure at failure

Bootstrap test; variable DV_1 (DATA STTRTT 20081217.sta) Probabilities for Post Hoc Tests								
Cell No.	PRESSURE	REPEAT	{1} 1090.5	{2} 1059.5	{3} 1546.8	{4} 1124.2	{5} 2081.5	{6} 1775.0
1	50	STTPRESSURE AT FAIL		1	0.5625	1	0.2175	0.5325
2	50	RTTPRESSURE AT FAIL			0.4725	1	0.1575	0.3825
3	100	STTPRESSURE AT FAIL				0	0.8325	1
4	100	RTTPRESSURE AT FAIL					0.0825	0.3975
5	200	STTPRESSURE AT FAIL						0
6	200	RTTPRESSURE AT FAIL						

### 6.1.6 ANOVA results with principal stress at failure as dependant variable

Table 17: Repeated measures ANOVA Table (DV = principal stress at failure)

Repeated Measures Analysis of Variance (DATA STTRTT 20081217.sta) Sigma-restricted parameterization Effective hypothesis decomposition					
Effect	SS	Degr. of Freedom	MS	F	p
Intercept	61351105	1	61351105	165.9261	0.000000
PRESSURE	3666260	2	1833130	4.9578	0.029180
Error	4067246	11	369750		
REPEAT	130052	1	130052	5.2721	0.042321
REPEAT*PRESSURE	149056	2	74528	3.0212	0.089998
Error	271349	11	24668		

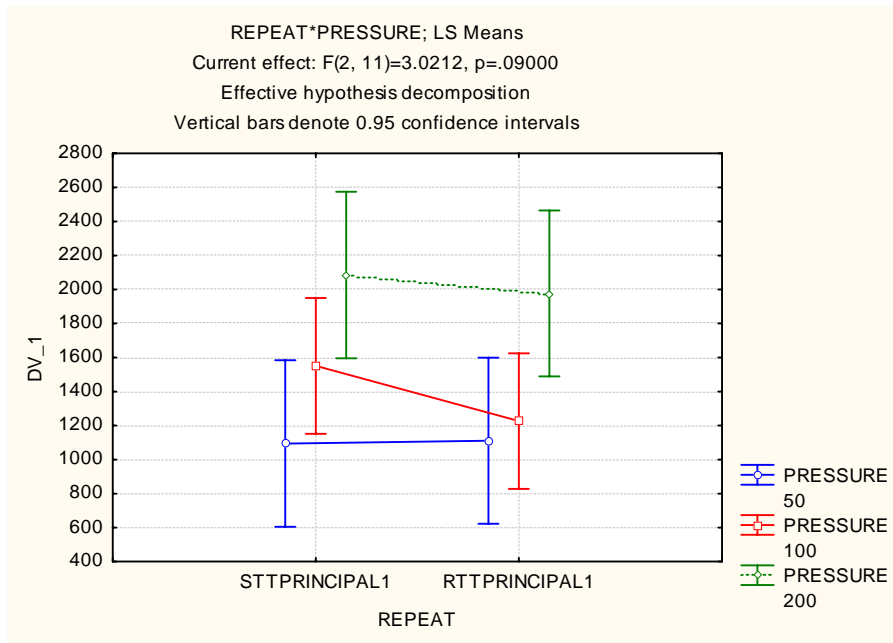


Figure 17: Variation of Principal stress at failure between STT and RTT

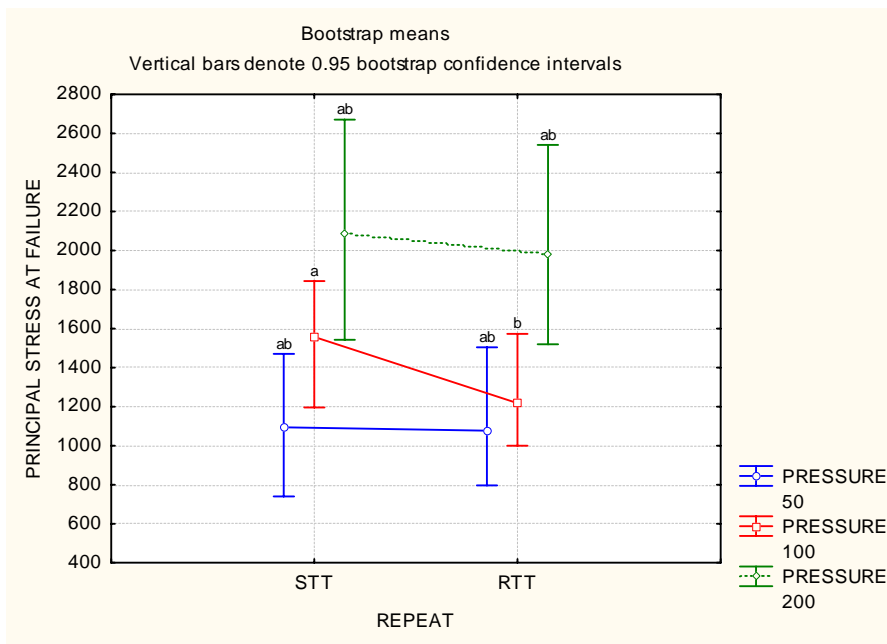


Figure 18: Bootstrap means

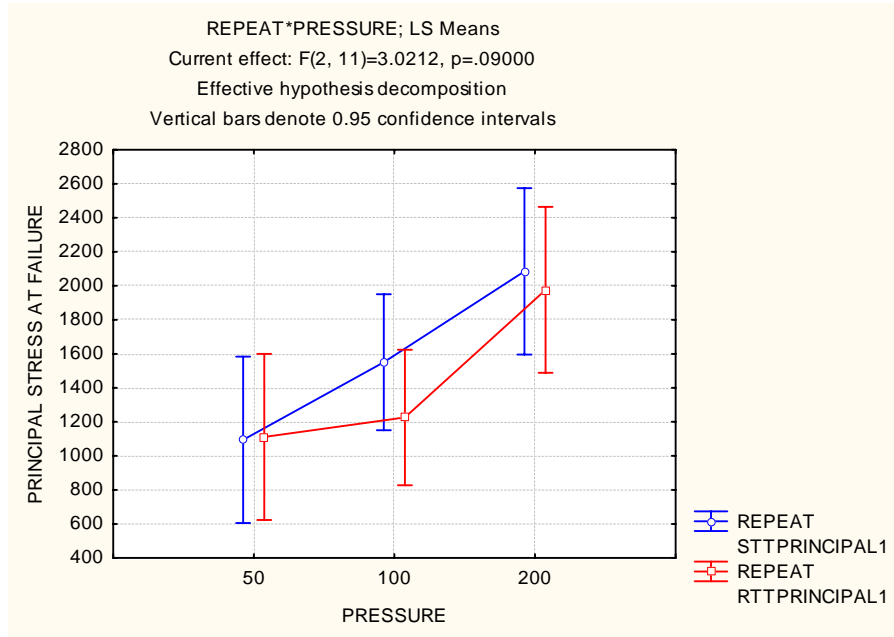


Figure 19: Principal stress at failure vs confinement pressure for STT and RTT

Table 18: Repeat\*Pressure; LS Means (DV = Principal stress at failure)

REPEAT*PRESSURE; LS Means (DATA STTRTT 20081217.sta)							
Current effect: F(2, 11)=3.0212, p=.09000							
Effective hypothesis decomposition							
Cell No.	PRESSURE	REPEAT	DV_1 Mean	DV_1 Std.Err.	DV_1 -95.00%	DV_1 +95.00%	N
1	50	STTPRINCIPAL1	1094.250	222.3576	604.844	1583.656	4
2	50	RTTPRINCIPAL1	1111.250	221.7240	623.239	1599.261	4
3	100	STTPRINCIPAL1	1550.667	181.5542	1151.069	1950.265	6
4	100	RTTPRINCIPAL1	1226.000	181.0369	827.540	1624.460	6
5	200	STTPRINCIPAL1	2085.500	222.3576	1596.094	2574.906	4
6	200	RTTPRINCIPAL1	1976.750	221.7240	1488.739	2464.761	4

Table 19: Pressure; LS Means

PRESSURE; LS Means (DATA STTRTT 20081217.sta)						
Current effect: F(2, 11)=4.9578, p=.02918						
Effective hypothesis decomposition						
Cell No.	PRESSURE	DV_1 Mean	DV_1 Std.Err.	DV_1 -95.00%	DV_1 +95.00%	N
1	50	1102.750	214.9853	629.570	1575.930	4
2	100	1388.333	175.5348	1001.984	1774.683	6
3	200	2031.125	214.9853	1557.945	2504.305	4

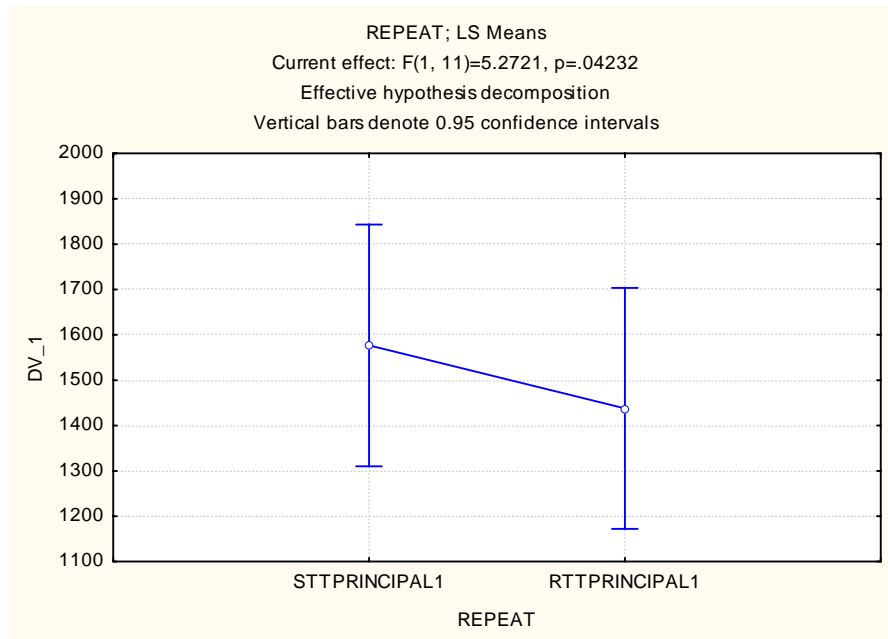


Figure 20: Variation of principal stress at failure within STT and RTT samples

**Table 20: Repeat; LS means**

REPEAT; LS Means (DATA STTRTT 20081217.sta)						
Current effect: F(1, 11)=5.2721, p=.04232						
Effective hypothesis decomposition						
Cell No.	REPEAT	DV_1 Mean	DV_1 Std.Err.	DV_1 -95.00%	DV_1 +95.00%	N
1	STTPRINCIPAL1	1576.806	121.0361	1310.407	1843.204	14
2	RTTPRINCIPAL1	1438.000	120.6913	1172.360	1703.640	14

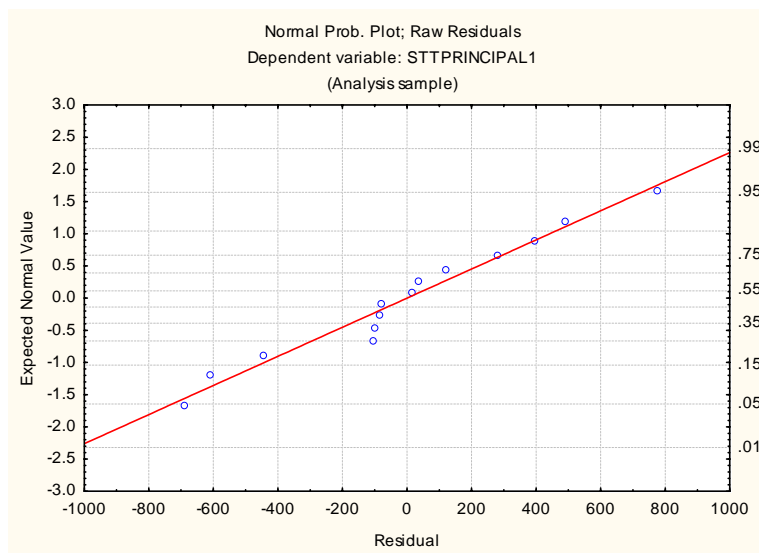
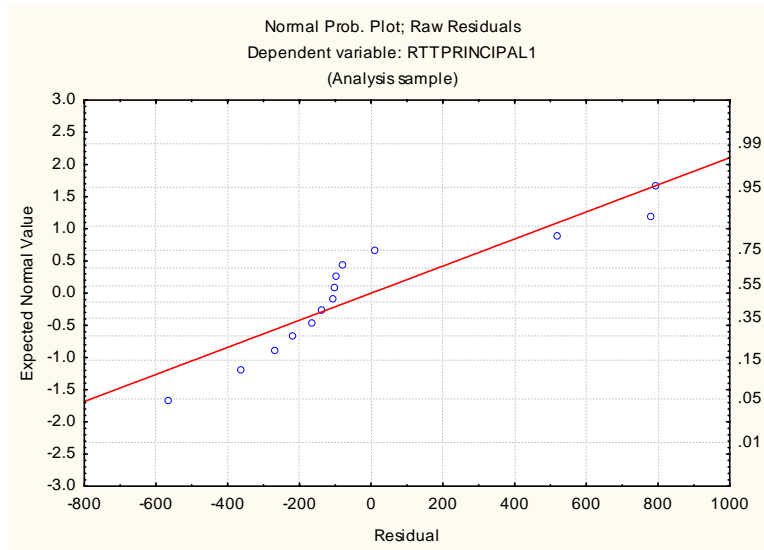


Figure 21: Normal probability plot for STT (DV = Principal stress)



**Figure 22: Normal probability plot for RTT**

**Table 21: Bonferroni test; DV\_1 = principal stress**

Bonferroni test; variable DV_1 (DATA STTRTT 20081217.sta)								
Probabilities for Post Hoc Tests								
Error: Between; Within; Pooled MS = 1972E2, df = 12.461								
Cell No.	PRESSURE	REPEAT	{1}	{2}	{3}	{4}	{5}	{6}
			1094.3	1111.3	1550.7	1226.0	2085.5	1976.8
1	50	STTPRINCIPAL1		1.000000	1.000000	1.000000	0.118976	0.228775
2	50	RTTPrincipal1	1.000000		1.000000	1.000000	0.131790	0.253311
3	100	STTPRINCIPAL1	1.000000	1.000000		0.064735	1.000000	1.000000
4	100	RTTPrincipal1	1.000000	1.000000	0.064735		0.160461	0.327685
5	200	STTPRINCIPAL1	0.118976	0.131790	1.000000	0.160461		1.000000
6	200	RTTPrincipal1	0.228775	0.253311	1.000000	0.327685	1.000000	

**Table 22: Bootstrap test; DV\_1 = Principal stress at failure**

Bootstrap test; variable DV_1 (DATA STTRTT 20081217.sta)								
Probabilities for Post Hoc Tests								
Cell No.	PRESSURE	REPEAT	{1}	{2}	{3}	{4}	{5}	{6}
			1094.3	1111.3	1550.7	1226.0	2085.5	1976.8
1	50	STTPRINCIPAL1		1	0.5775	1	0.1575	0.24
2	50	RTTPrincipal1			0.4875	1	0.2925	0.1875
3	100	STTPRINCIPAL1				0.015	0.6375	1
4	100	RTTPrincipal1					0.2025	0.1275
5	200	STTPRINCIPAL1						0.075
6	200	RTTPrincipal1						

### 6.1.7 ANOVA results with tangent modulus as dependant variable

**Table 23: Repeated measures ANOVA Table; DV = Tangent modulus**

Repeated Measures Analysis of Variance (DATA STTRTT 2) Sigma-restricted parameterization Effective hypothesis decomposition					
Effect	SS	Degr. of Freedom	MS	F	p
Intercept	831738.4	1	831738.4	112.1394	0.000000
PRESSURE	11414.1	2	5707.1	0.7695	0.486665
Error	81587.0	11	7417.0		
REPEAT	11362.1	1	11362.1	4.4978	0.057489
REPEAT*PRESSURE	3057.6	2	1528.8	0.6052	0.563178
Error	27787.5	11	2526.1		

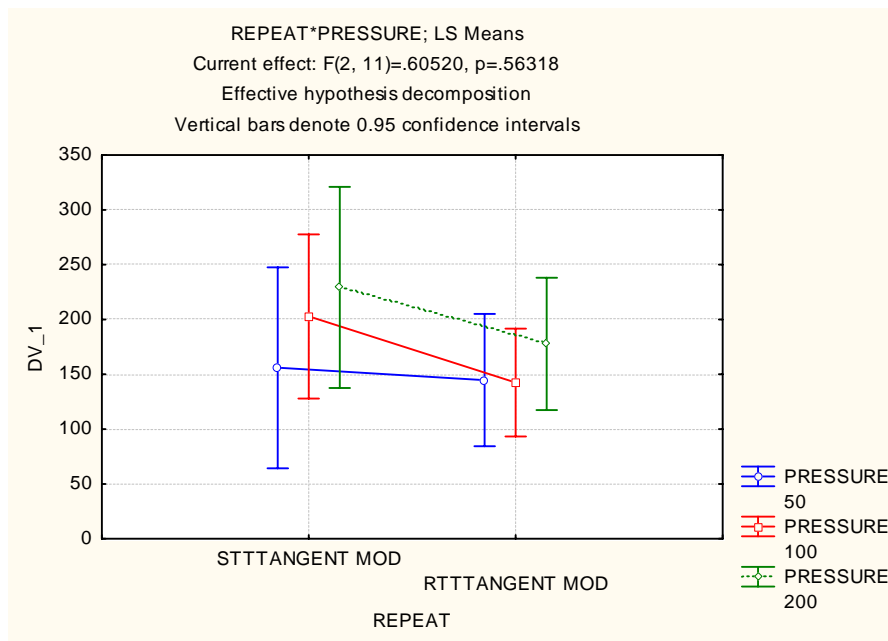


**Figure 23: Variation of Tangent Modulus between STT and RTT**

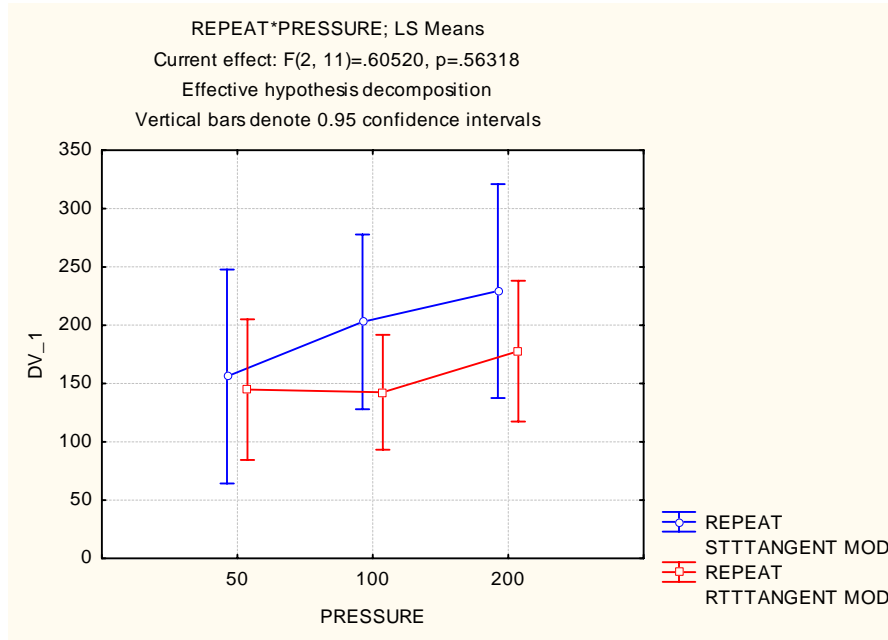
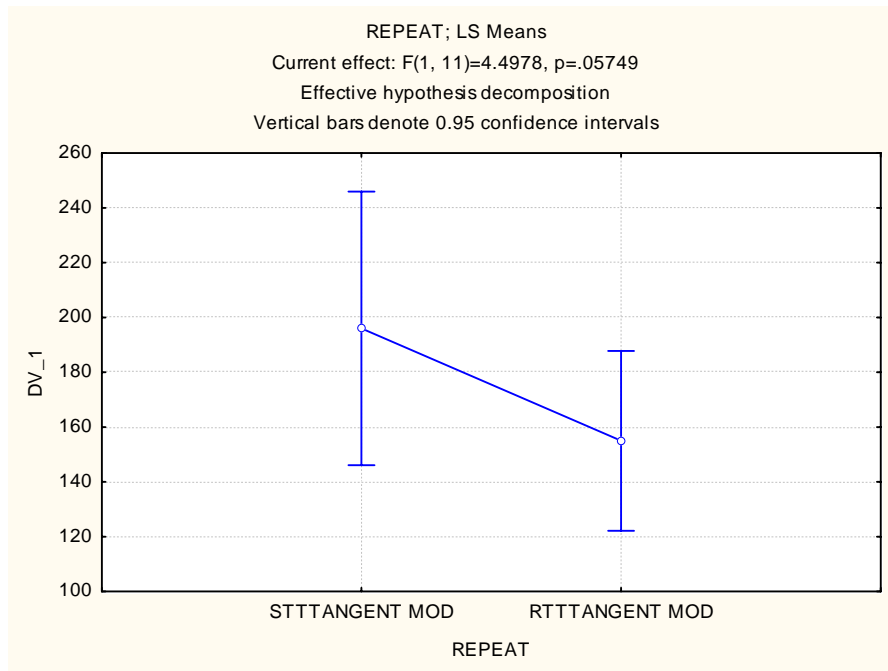


Figure 24: Tangent Modulus vs confinement pressure for STT and RTT

Table 24: Repeat\*Pressure; LS Means

REPEAT*PRESSURE; LS Means (DATA STTRTT 20081217.sta)							
Current effect: F(2, 11)=.60520, p=.56318							
Effective hypothesis decomposition							
Cell No.	PRESSURE	REPEAT	DV_1 Mean	DV_1 Std.Err.	DV_1 -95.00%	DV_1 +95.00%	N
1	50	STTTANGENT MOD	156.0000	41.65376	64.3207	247.6793	4
2	50	RTTTANGENT MOD	144.7500	27.39982	84.4434	205.0566	4
3	100	STTTANGENT MOD	202.8333	34.01016	127.9775	277.6892	6
4	100	RTTTANGENT MOD	142.5000	22.37186	93.2599	191.7401	6
5	200	STTTANGENT MOD	229.2500	41.65376	137.5707	320.9293	4
6	200	RTTTANGENT MOD	177.7500	27.39982	117.4434	238.0566	4



**Figure 25: Variation of tangent modulus within STT and RTT samples**

**Table 25: Repeat; LS Means**

REPEAT; LS Means (DATA STTRTT 20081217.sta) Current effect: F(1, 11)=4.4978, p=.05749 Effective hypothesis decomposition						
Cell No.	REPEAT	DV_1 Mean	DV_1 Std.Err.	DV_1 -95.00%	DV_1 +95.00%	N
1	STTTANGENT MOD	196.0278	22.67344	146.1239	245.9317	14
2	RTTTANGENT MOD	155.0000	14.91457	122.1732	187.8268	14

### 6.1.8 ANOVA results with secant modulus as dependant variable

**Table 26: Repeated measures ANOVA Table; DV = Secant Modulus**

Repeated Measures Analysis of Variance (DATA STTRTT) Sigma-restricted parameterization Effective hypothesis decomposition					
Effect	SS	Degr. of Freedom	MS	F	p
Intercept	98736.02	1	98736.02	37.50667	0.000075
PRESSURE	527.44	2	263.72	0.10018	0.905491
Error	28957.42	11	2632.49		
REPEAT	1740.02	1	1740.02	1.98007	0.187005
REPEAT*PRESSURE	2630.01	2	1315.01	1.49642	0.266180
Error	9666.42	11	878.77		

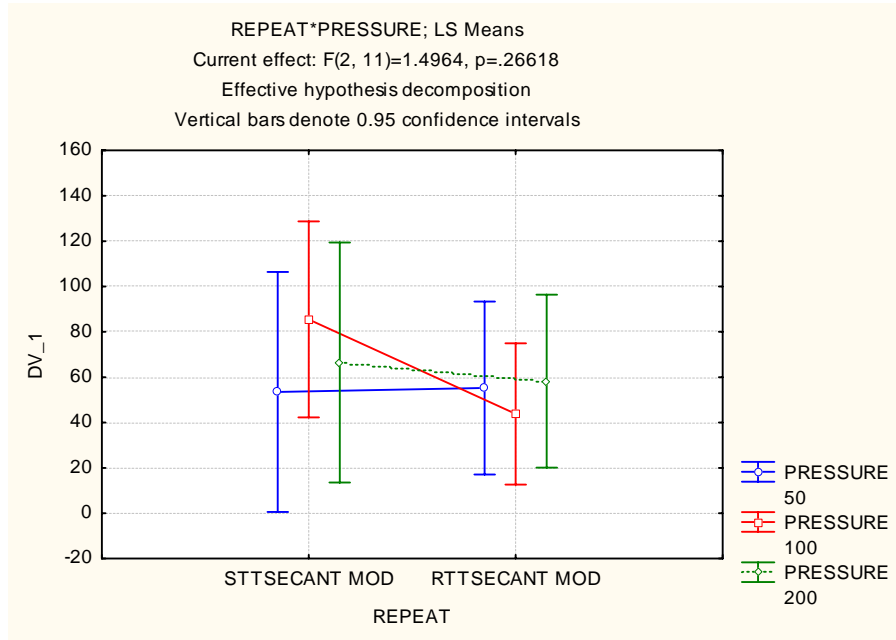


Figure 26: Variation of secant modulus between STT and RTT samples

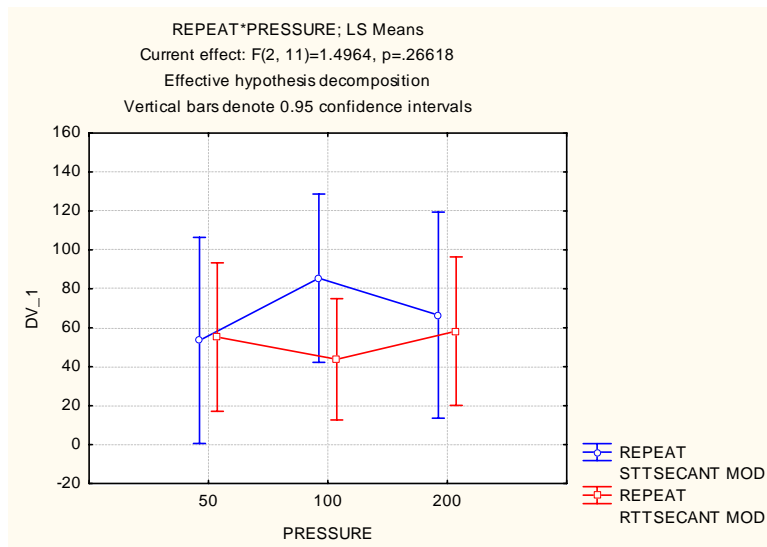
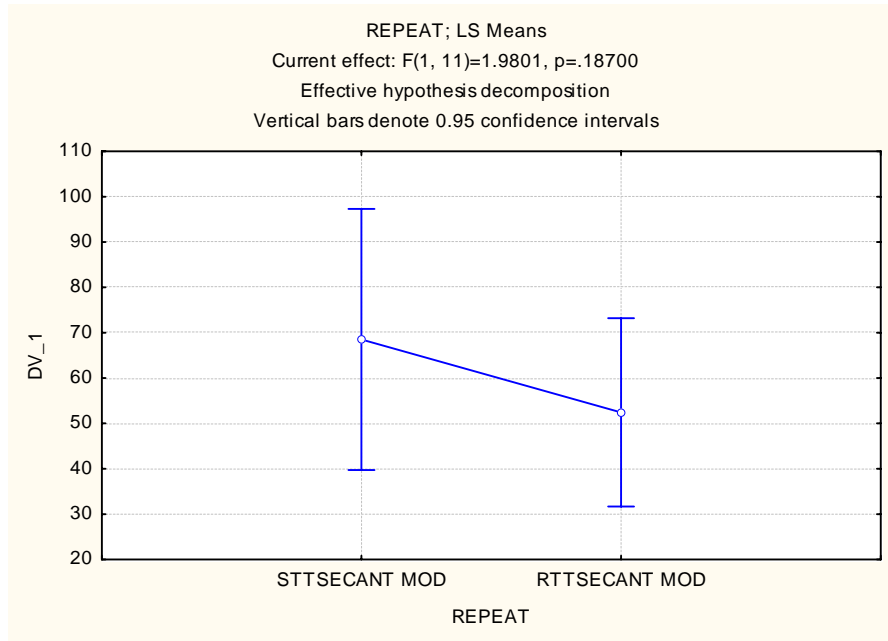


Figure 27: Secant modulus vs confinement pressure for STT and RTT

Table 27: Repeat\*Pressure; LS Means

REPEAT*PRESSURE; LS Means (DATA STTRTT 20081217.sta)							
Current effect: F(2, 11)=1.4964, p=.26618							
Effective hypothesis decomposition							
Cell No.	PRESSURE	REPEAT	DV_1 Mean	DV_1 Std.Err.	DV_1 -95.00%	DV_1 +95.00%	N
1	50	STTSECANT MOD	53.50000	24.03667	0.59565	106.4043	4
2	50	RTTSECANT MOD	55.25000	17.32204	17.12445	93.3756	4
3	100	STTSECANT MOD	85.50000	19.62586	42.30378	128.6962	6
4	100	RTTSECANT MOD	43.83333	14.14339	12.70395	74.9627	6
5	200	STTSECANT MOD	66.50000	24.03667	13.59565	119.4043	4
6	200	RTTSECANT MOD	58.25000	17.32204	20.12445	96.3756	4



**Figure 28: Variation of secant modulus within STT and RTT samples**

**Table 28: Repeat; LS Means**

REPEAT; LS Means (DATA STTRTT 20081217.sta)						
Current effect: F(1, 11)=1.9801, p=.18700						
Effective hypothesis decomposition						
Cell No.	REPEAT	DV_1 Mean	DV_1 Std.Err.	DV_1 -95.00%	DV_1 +95.00%	N
1	STTSECANT MOD	68.50000	13.08390	39.70252	97.29748	14
2	RTTSECANT MOD	52.44444	9.42892	31.69152	73.19737	14

## 6.2 CASE 2 REPEATED MEASURES ANOVA

Case 2 Repeated Measures ANOVA is based on repeated results on RAP (Hornfels) + 3.3 % Emulsion + 1 % Cement mix at 100 kPa confinement. This analysis though with limited data show less

significant variation between STT and RTT samples, however STT samples show significant within sample variability.

### 6.2.1 ANOVA results with principal stress at failure as dependant variable

**Table 29: Repeated measures ANOVA Table; DV = principal stress at failure**

Repeated Measures Analysis of Variance (DATA STTRTT 2) Sigma-restricted parameterization Effective hypothesis decomposition Include condition: V4=100 AND V3="RAP"					
Effect	SS	Degr. of Freedom	MS	F	p
Intercept	12751250	1	12751250	116.1778	0.001708
Error	329269	3	109756		
REPEAT	355324	1	355324	7.3553	0.073037
Error	144926	3	48309		

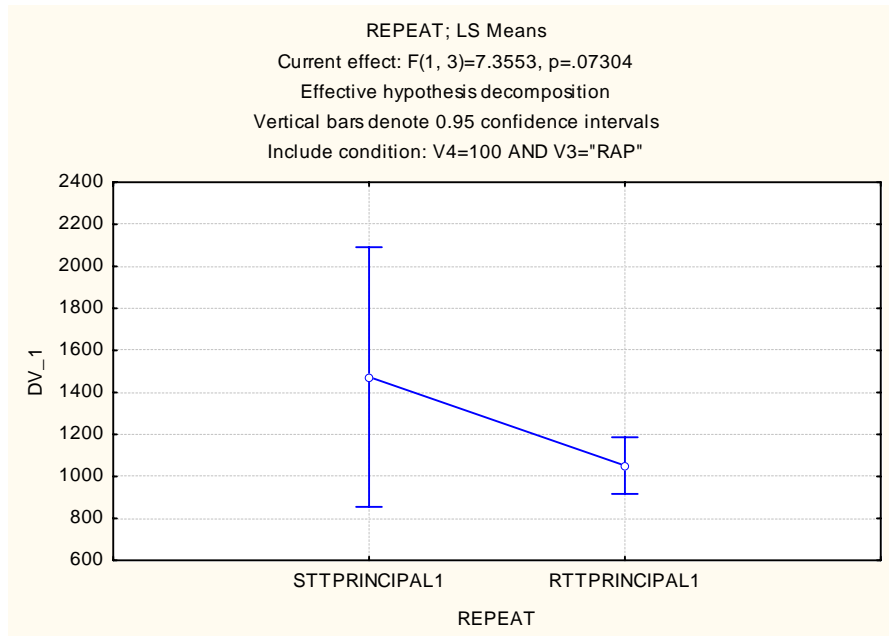


**Figure 29: Variation of Principal stress at failure between and within STT and RTT samples**

**Table 30: Repeat; LS Means**

	REPEAT; LS Means (DATA STTRTT 20081217.sta) Current effect: F(1, 3)=7.3553, p=.07304 Effective hypothesis decomposition Include condition: V4=100 AND V3="RAP"					
Cell No.	REPEAT	DV_1 Mean	DV_1 Std.Err.	DV_1 -95.00%	DV_1 +95.00%	N
1	STTPRINCIPAL	1473.250	194.2037	855.2073	2091.293	4
2	RTTPRINCIPAL	1051.750	42.4409	916.6841	1186.816	4

### 6.2.2 ANOVA results with stress (pressure) at failure as dependant variable

Table 31: Repeated measures ANOVA Table; DV = Applied Pressure at failure

	Repeated Measures Analysis of Variance (DATA STTRTT 2) Sigma-restricted parameterization Effective hypothesis decomposition Include condition: V4=100 AND V3="RAP"				
Effect	SS	Degr. of Freedom	MS	F	p
Intercept	11705541	1	11705541	106.5117	0.001940
Error	329697	3	109899		
REPEAT	540280	1	540280	11.1616	0.044358
Error	145216	3	48405		

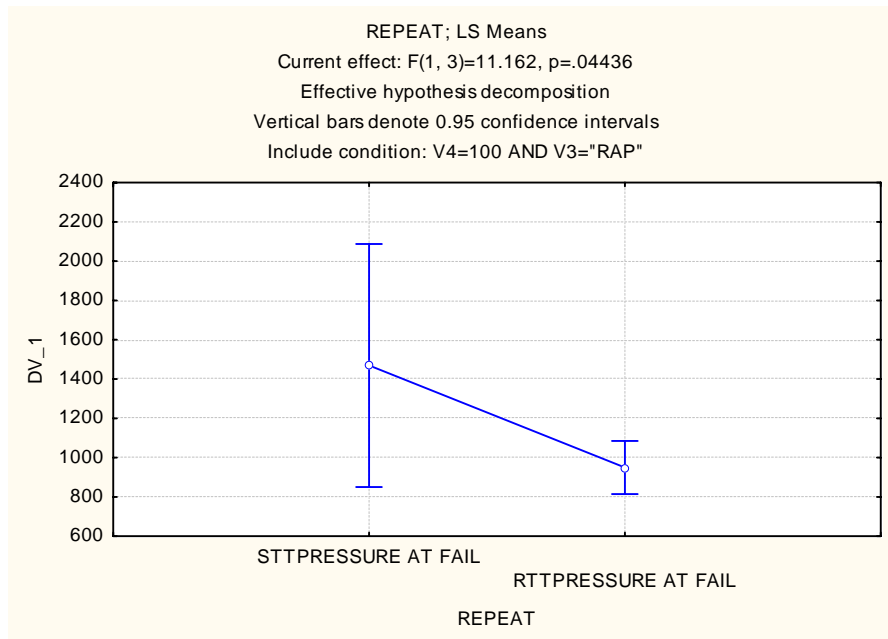


Figure 30: Variation of applied pressure at failure for STT and RTT

**Table 32: Repeated; LS Means**

REPEAT; LS Means (DATA STTRTT 20081217.sta)						
Current effect: F(1, 3)=11.162, p=.04436						
Effective hypothesis decomposition						
Include condition: V4=100 AND V3="RAP"						
Cell No.	REPEAT	DV_1 Mean	DV_1 Std.Err.	DV_1 -95.00%	DV_1 +95.00%	N
1	STTPRESSURE AT FAIL	1469.500	194.3577	850.9670	2088.033	4
2	RTTPRESSURE AT FAIL	949.750	42.4409	814.6841	1084.816	4

**6.2.3 ANOVA results with tangent modulus as dependant variable**

**Table 33: Repeated measures ANOVA Table; DV = Tangent modulus**

Repeated Measures Analysis of Variance (DATA STTRTT)						
Sigma-restricted parameterization						
Effective hypothesis decomposition						
Include condition: V4=100 AND V3="RAP"						
Effect	SS	Degr. of Freedom	MS	F	p	
Intercept	208012.5	1	208012.5	69.29515	0.003633	
Error	9005.5	3	3001.8			
REPEAT	11552.0	1	11552.0	2.14111	0.239592	
Error	16186.0	3	5395.3			

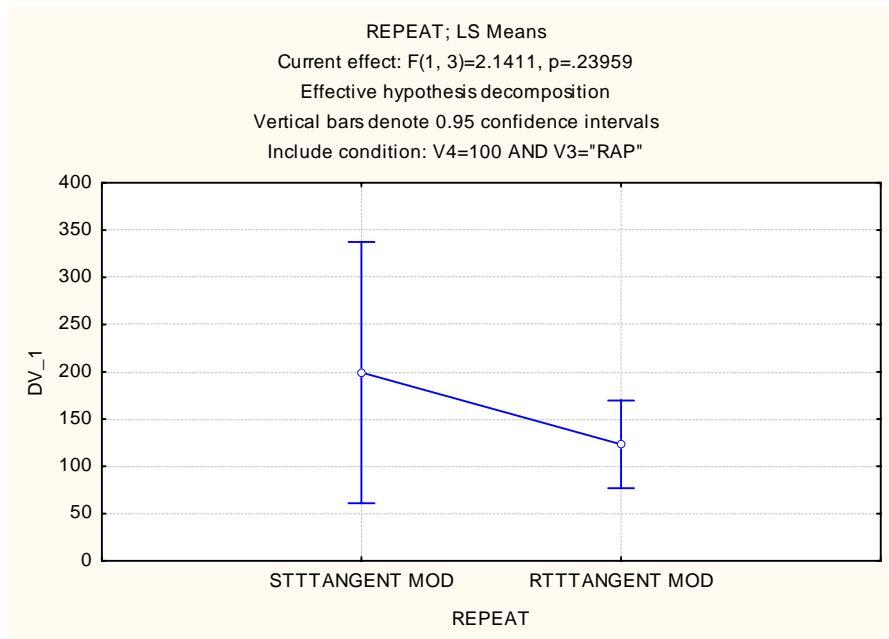


**Figure 31: Variation of tangent modulus between and within STT and RTT samples**

**Table 34: Repeat; LS Means**

REPEAT; LS Means (DATA STTRTT 20081217.sta) Current effect: F(1, 3)=2.1411, p=.23959 Effective hypothesis decomposition Include condition: V4=100 AND V3="RAP"						
Cell No.	REPEAT	DV_1 Mean	DV_1 Std.Err.	DV_1 -95.00%	DV_1 +95.00%	N
1	STTTANGENT MOD	199.2500	43.42882	61.04011	337.4599	4
2	RTTTANGENT MOD	123.2500	14.60237	76.77875	169.7213	4

## **APPENDIX 7: WEIGHT ANALYSIS OF TRIAXIAL CELLS**

**Table 1: Weight comparison of different triaxial cells**

Cell Components	STT Cell for 300 mm specimen [g]	RTT Cell for 300 mm specimen [g]	RTT Cell for 250 mm specimen [g]
Base including bottom disk	9 746.0	7 956.8	11 775.6
Cylinder + tube	11 447.9	n/a	n/a
Cylinder + Six (06) thumb screws + seal + short loading ram	n/a	15 836.0	25 055.0
Top disk	4 746.0	2 567.4	1 968.6
Extension pipe (flanged including 6 bolts)	n/a	6 727.0	n/a
<b>Total Mass</b>	<b>25 939.9</b>	<b>33 087.2</b>	<b>38 799.2</b>

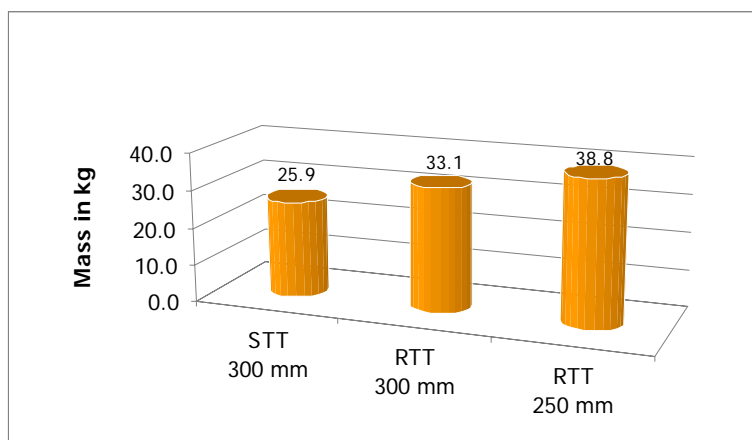


**Figure 1: Weight comparison of STT against RTT**